Title
PERIODIC PHENOMENA IN THE HIGH CURRENT DENSITY ANODIC DISSOLUTION OF COPPER

Author
Cooper, John Frederick.

Publication Date
1975-04-01

PERIODIC PHENOMENA IN THE HIGH CURRENT DENSITY ANODIC DISSOLUTION OF COPPER

John Frederick Cooper
(Ph. D. thesis)

April 1975

Prepared for the U. S. Energy Research and Development Administration under Contract W-7405-ENG-48

DISCLAIMER

A. A violent order is disorder; and
B. A great disorder is an order.
These two things are one. (Pages
of illustrations.)...

--Wallace Stevens
"Connoisseur of Chaos", 1942[57]

Table of Contents

PERIODIC PHENOMENA IN THE HIGH CURRENT DENSITY ANODIC DISSOLUTION OF COPPER

John Frederick Cooper

Inorganic Materials Research Division, Lawrence Berkeley Laboratory
and Department of Chemistry; University of California,
Berkeley, California 94720

ABSTRACT

Uniform and sustained anode potential oscillations were observed during the high rate galvanostatic dissolution of copper in sodium chlorate electrolyte. The phenomenon was investigated under well-defined hydrodynamic conditions from 0.3- to 150 A/cm^2. Over this range, frequency increases with current density from 0.001- to 1000 Hz. Frequency declines by a factor of 0.3 with increase in flow rate (Re=200-7000, channel flow). Weak dependences of frequency on bulk electrolyte temperature (4-80°C) and pH (1.4-11) were noted. Oscillations amplitudes fall in the range, 5- to 20 V.

Large amplitude (> 1V) oscillations with less cycle uniformity were also obtained in a variety of electrolytes containing sulfate, nitrate, or hydroxide in the presence of small concentrations of chloride, bromide, or iodide.

In the chlorate electrolyte, the rise and fall of potential reflects the alternate growth and destruction of a thin, adherent, anode surface film, which was found by X-ray diffraction analysis to consist of cuprous oxide. The apparent valence of the dissolution process is 1.2 above 5 A/cm^2. The predominant net anode reaction may be written,

$$Cu + \frac{1}{2} H_2O = \frac{1}{2} Cu_2O + H^+ + e^- \quad .$$

Reactions occurring in parallel were identified as,

$$Cu = Cu^{+2} + 2e^- \quad ,$$

and

$$\frac{1}{2} Cu_2O + 2H^+ + \frac{1}{6} ClO_3^- = Cu^{+2} + \frac{1}{6} Cl^- + H_2O \quad .$$

Dried samples of surface films produced during the high potential phase of the cycle were found to undergo an electronic insulator to conductor transition upon application of a field strength exceeding about 10^5 V/cm. The duration of the breakdown event was approximately 10^{-6}s. Similar transitions are known to occur with a variety of solids, including bulk samples of cuprous oxide. The transitions characteristically result in the formation of filamentary channels of low electronic resistivity and occur with a probability which increases with field strength and sample thickness.

A model for the oscillations was proposed, based on our observations of resistive transitions. During the potential growth phase of the cycle, current is passed through a uniformly growing cuprous oxide film by ionic conduction. As the films thickens, the incidence of the breakdown transitions increases. The net resistance of the film is lowered by accumulation of channels of low electronic resistance. Eventually the potential falls below the level necessary for continued ionic current and film growth. The potential remains at a low level until the volume of film containing low resistance channels is undermined

or removed by anodic dissolution. Then uniform film growth and potential increase begin anew.

The oscillation phenomena observed with the chlorate electrolyte are evidently the consequence of solid state transformations within the surface films formed during transpassive dissolution. Rigorous proof of this mechanism requires more detailed characterization of film properties and breakdown conditions than is currently available.

I. INTRODUCTION

A. Anode Potential Oscillations in Copper Dissolution

The anodic dissolution of copper in sodium chlorate electrolyte gives rise to a remarkable phenomenon. Upon closing the electrolysis circuit, the anode potential does not assume a steady level; rather, it undergoes a periodic rise and fall of about ten volts. Under constant experimental conditions, the individual potential cycles are impressively uniform in period and amplitude. Sample oscillograph recordings of anode potential against time are shown in Fig. 1.1. Oscillations are found with galvanostatically controlled current densities in the range, 0.3 to over 150 A/cm^2. Frequency increases with current density in this range from 0.003 Hz to over 1000 Hz. In a narrower current density range and with less cycle uniformity, large amplitude oscillations may also be obtained with a variety of mixed electrolytes containing small concentrations of halide ions (See Appendix A).

An investigation of this phenomenon grew out of a wider interest in these laboratories in electrochemical processes involved in high-rate electrolysis.[1-3] An industrial application of particular interest to us is electrochemical machining (ECM)--the technique which employs anodic dissolution at current densities from 5-500 A/cm^2 to cut, shape and polish metals.[4] Kinoshita first encountered the oscillations while investigating the dissolution of copper in electrolytes commonly used in ECM.[5] The chlorate electrolyte is known to provide polished surfaces and close dimensional control in ECM applications,[6] and a desire to understand these properties first motivated further investigation.[7]

Fig. 1.1. Sustained Cell Voltage Oscillations. Electrode-electrolyte system: Cu/2F $NaClO_3$/Cu; stirred electrolyte; current density = 3 A/cm^2. (Cell voltage oscillated continuously for duration of dissolution experiment (1014 s)).

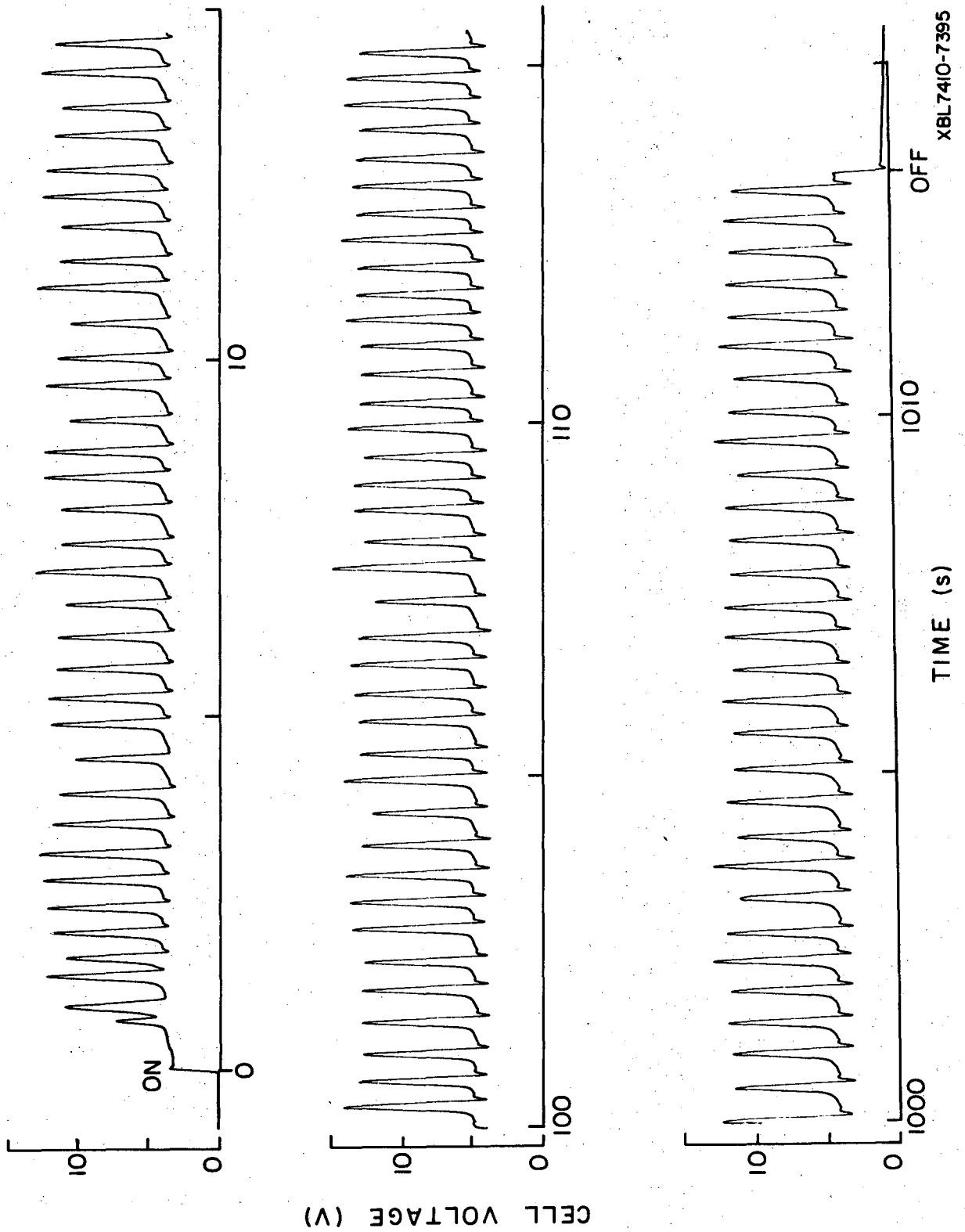
CELL VOLTAGE (V)
10
0
ON
0
10
100
110
1000
1010
OFF
TIME (s)
XBL7410-7395

Fig. 1.1.

The importance of a study of anodic oscillations derives from the close relationship between periodicity and the stability characteristics of anodically formed passive and transpassive films and layers. An understanding of the periodic growth and breakdown of such resistive layers would lend a powerful perspective to the understanding of the passive or transpassive electrode state.

Electrode reactions taking place with periodic changes in current or potential are by no means uncommon. A wealth of descriptive literature dates from the early nineteenth century, though only a few attempts at rational interpretations have been made. A large proportion of the cases of periodicity involve the anodic polarization of metals. Typically, potential oscillations are observed in a narrow, low-lying band of current densities (order of magnitude, 0.1 - 1 A/cm^2). Below the lower limit, a steady electrode process persists (e.g., active dissolution); above the band, continuous transpassive dissolution or oxygen evolution occurs with, at most, only random fluctuations in potential. In the intermediate range, periodic transfers between active and passive (or transpassive) states are effected (it is said) by changes in the electrolyte composition brought about by the ongoing anodic reactions and by diffusion of species to and from the bulk. Period lengths range from seconds to hours, and the oscillations are strongly influenced by the solution-side mass transport situation.

What is exceptional about the oscillations treated in this dissertation is their occurrance over a broad range of current densities lying orders of magnitude above that of familiar cases. Period lengths

are as short as milliseconds and the phenomenon is relatively insensitive to mass transport effects.

B. Objectives of the Research

As a first step to the interpretation of periodic behavior, the physical and chemical processes which take place during each phase of the cycle must be identified. To do so for the oscillations in the chlorate electrolyte is a prime objective of this research. Beyond this, there are more fundamental and challenging questions to be answered. What induces the electrode to progress repeatedly through the same sequence of distinct states rather than approach a single, stable mixed electrode state? What causes the abrupt changes in electrode state to occur at regular time intervals and in phase over extended electrode surfaces, rather than randomly and out of phase on, perhaps, a mosaic of sites with microscopic dimensions? These questions pertain to the so-called "all or nothing" behavior characteristic of a broad class of periodic electrode phenomena, including the case at hand.

In Chapter II, the background of the problem of periodic electrochemical phenomena will be discussed. Particular attention will be given to general approaches to the rational interpretation of periodicity, as well as to specific cases of anode oscillations and their experimental basis and qualitative explanations.

In Chapter III, the experimental difficulties encountered in high current density regime will be surveyed together with the general aspects of our experimental design. Experimental apparatus and materials will be discussed in detail.

Chapter IV presents the bulk of our experimental results concerning the electrical, chemical, and morphological aspects of the anodic dissolution of copper in the chlorate electrolyte. Results of our investigation of breakdown characteristics of the transpassive films will be presented.

In Chapter V, experimental results will be interpreted and a model for the periodic growth and breakdown of electrode resistance will be proposed.

II. PERIODIC ELECTRODE PHENOMENA: BACKGROUND AND FUNDAMENTALS

A. Introduction

Periodic chemical and physical phenomena occur in widely different classes of reacting systems including multiple as well as single phase systems. A striking example of spatial and temporal periodicity in a single phase system may be found with the Zhabotinsky-Zaikin reagent.[8,9] Diffusion processes and the kinetics of the bromination of malonate interact to generate three-dimensional, expanding and rotating spiral waves of reactivity. This and other examples of periodic chemical reactions are of special biological interest and serve as models for complex biological cycles found within organisms and on ecological levels.[10-13] For example, the classic study of Lotka[14] on periodicity derived from the law of mass action has been applied to explain the cyclic variation in the populations of predators and prey[15] as well as to electrochemical oscillations observed during the oxidation of organic fuels.[16]

The earliest observation of periodic phenomena in an electrochemical system was reported by Fechner (1828), who observed alternate deposition and dissolution of silver on iron electrodes.[17] Since then, hundreds of cases have been reported where electrode reactions proceed periodically in a spatial or temporal sense. Most cases involve fluctuations in current or potential at electrodes undergoing anodic polarization. Cathodic current/potential oscillations are also common,[18-22,80] as are oscillations in the rest potential of corroding "single" electrodes.[23-26]

In recent years many cases have been reported involving periodic reactions at "inert" noble metals during the anodic oxidation of hydrogen or hydrocarbons.[27-29] Oscillations observed in the potential drop across membranes represent a class of electrochemical oscillations not involving electrodes.[31-34]

B. Periodic Phenomena Associated with the Anodic Dissolution of Metals

Potential oscillations observed with the chlorate electrolyte belong to a restricted class of periodic electrochemical reactions. The class is characterized by the alternate production and destruction of current restricting layers of reaction products on electrodes undergoing anodic dissolution. With galvanostatic dissolution, the growth and destruction of resistive layers is reflected in the periodic rise and fall of potential. If the electrode is polarized by an external voltage source of finite impedance, both anode potential and current will oscillate.

The preponderance of cases of periodic electrode phenomena involve such active-passive or active-transpassive transitions.[38] Older literature has been reviewed by Hedges and Meyers,[35,76] and Indira, et al.[37] Wojtowicz reviewed recent experimental and theoretical work in the general field of electrochemical periodicity.[38] Some case studies of periodic reactions involving passivating electrodes are tabulated in Appendix B.

The low resistance phase of the cycle is generally attributed to active dissolution, whereby the metal cation passes directly from a site on the metal surface to an aqueous complex. The high resistance

phase is variously attributed to: (1) thin oxidic films such as those held responsible for passivation phenomena; (2) porous layers resulting from the precipitation of sparingly soluble salts of the metal cation; (3) precipitates from relatively soluble aqueous complexes; and (4) "electropolishing films" showing a higher ionic conductivity than passivating films.

Virtually every conceivable scheme has been adduced to account for the periodic growth and breakdown of resistance. The more reasonable models include: (1) shifts in the Flade potential for active/passive transitions resulting from changes in anolyte pH; (2) sequential deposition, oxidation, and chemical dissolution of a salt or oxide layer; (3) exhaustion followed by diffusion controlled replenishment of an acceptor anion necessary for maintaining active dissolution; (4) dielectric or mechanical disruption of the resistive layer; and (5) solid state transformations within the resistive layer, such as recrystalization, insulator-conductor transitions, transport and accumulation of aggressive anions within the lattice, etc. We shall discuss a few of the models below.

1. Franck's Model for Oscillations at Passivating Electrodes

U. F. Franck's theory applies to oscillations observed with electrodes capable of anodic passivation and exhibiting characteristic N-shaped steady state polarization curves.[39,40] (See Fig. 2.1). In the idealized model, transfers between active and passive states occurs at a single critical potential, the Flade potential. Oscillations result from the pH dependence of the Flade potential, which, for the

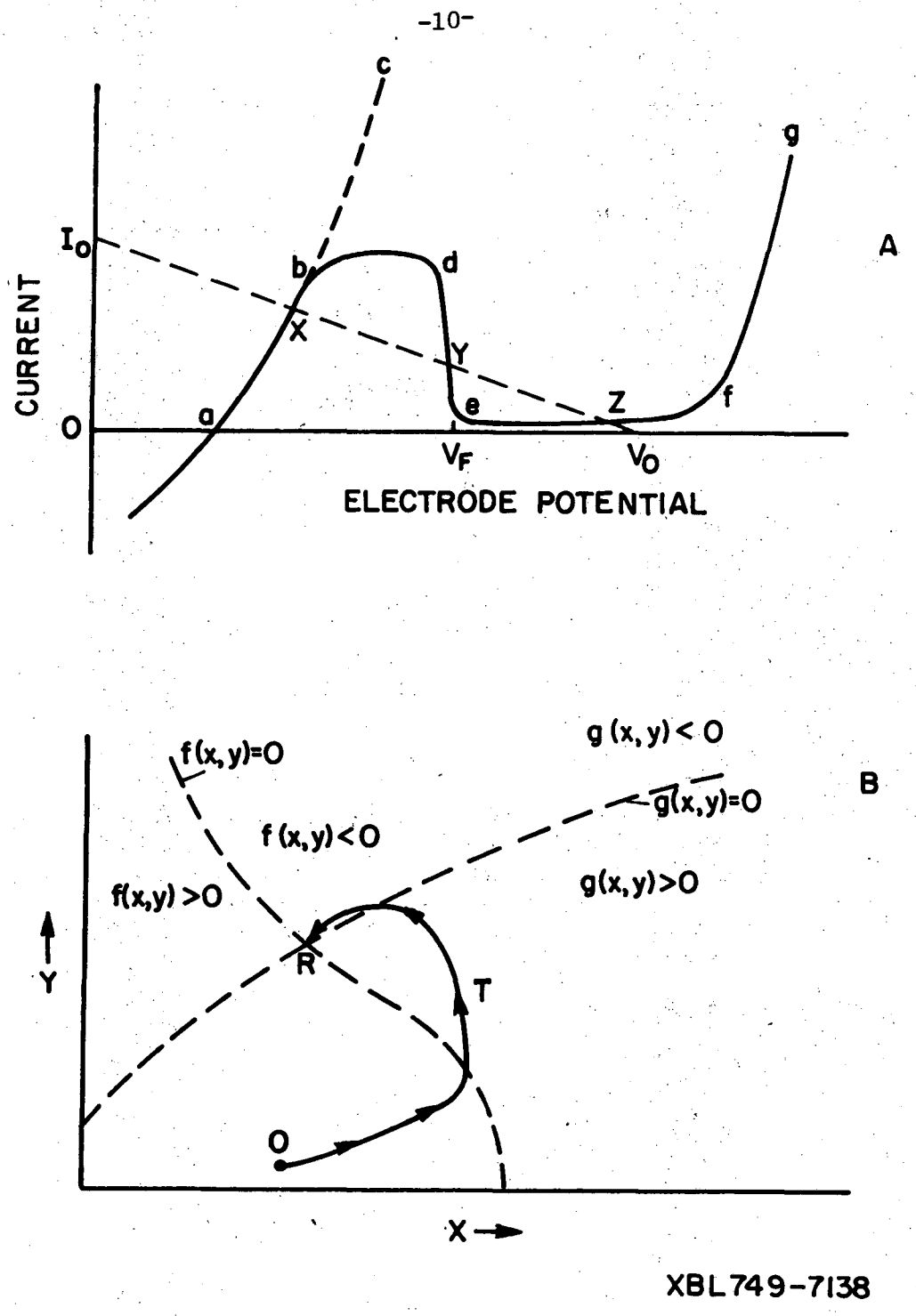

Fig. 2.1. (A) Idealized polarization curve for a passivating electrode. I_o-V_o, load line; abc, active dissolution; bd, porous film formation; ef, passive state; fg, transpassive dissolution; V_F Flade potential. (B) Phase plane representation of reaction described by two variables. dy/dt = g(x,y); dx/dt = f(x,y). OTR, reaction trajectory; R, quasi-stationary point.

Fe/H_2SO_4 system, is given by:[41]

$$E_F = 0.58 - 0.058\ pH\ (Volts\ vs.\ 0.1N\ Calomel\ Electrode).$$

For an electrode initially in the active state, hydrogen ion is progressively depleted from the anodic diffusion layer because of its high mobility relative to that of the metal cation. The local pH consequently rises until the Flade potential drops below the electrode potential. The passive state is established and the current drops by many orders of magnitude. Gradually the concentration of the hydrogen ion is restored to bulk levels by diffusion. The passive film is then destroyed by reduction (via local cell action) and by dissolution. Active dissolution again predominates and the cycle begins anew.

Franck showed that no stable, mixed electrode (with coexisting active and passive sites) is accessible to the system. A mixed electrode state would be represented by a point on the falling portion of the polarization curve at the Flade potential. A slight displacement of electorde potential positive or negative of the Flade potential would give rise to self-accelerating passivation or activation, respectively. Franck and Fitzhugh tested the theory using computer simulation of film growth kinetics and mass transport; the periodic behavior of electorde potential was accurately predicted.[41]

2. Model Involving Sequential Deposition, Oxidation, and Dissolution of Film

Shams el Din and Abd el Wahab reported anode potential oscillations during the galvanostatic dissolution of tin in sodium hydroxide solutions at current densities between 1.5 and 3 mA/cm^2.[42] The potential cycled between equilibrium potentials of the two couples, $Sn/Sn(OH)_2$ and $Sn(OH)_2/Sn(OH)_4$. Above 3 mA/cm^2, stannic hydroxide and oxygen were produced continuously. The following reaction sequence was hypothesized: (1) after application of current, $Sn(OH)_2$ is deposited on the anode surface; (2) the $Sn(OH)_2$ is oxidized to $Sn(OH)_4$; (3) the latter product readily dissolves to form the stannate complex, restoring the initial active state.

The interpretation does not account for the failure of the dissolution processes to reach a steady state, whereby the stannous and stannic hydroxides are produced simultaneously at the higher potential and the distribution between products is controlled by kinetic factors.

3. Models Involving Exhaustion and Replenishment of Acceptor Anions

During the dissolution of silver in cyanide solutions, oscillations in current and potential occur over a narrow range of current densities just below those required for electropolishing.[43,44] The following sequence was hypothesized: (1) silver initially dissolves to form a soluble argentocyanide ($AgCN_2^-$) complex; (2) free cyanide is depleted from the diffusion layer to form the complex and solid AgCN precipitates; (3) access to the metal is restricted by the solid layer and the current

falls to a low level; (4) the initial concentration of cyanide is restored by diffusion from the bulk; (5) the precipitate dissolves and the cycle begins anew. Cooper and Bartlett advanced a similar model to explain oscillations in the copper/hydrochloric acid system, where only $CuCl_2^-$ and CuCl were produced.[45,46] A common objection is that the models assume rather than explain the inaccessibility of a stable mixed electrode state.

4. Film Disruption Models

Pointu attempted to explain potential oscillations observed during the dissolution of copper in phosphoric acid by postulating the alternate formation and electrical discharge breakdown of a Cu/CuO/viscous layer condenser.[47] Lal et al. reported oscillations in the anodic dissolution of silver in chloride solutions.[48] The phenomenon was attributed to the alternate growth and mechanical disruption of a thin silver chloride film. In both cases, the authors do not explain why electrical or mechanical breakdown should occur periodically and in phase over extended electrode surfaces rather than randomly and out of phase at discrete sites. Electrical and mechanical breakdown are generally localized events and are followed by rapid local repair, as in the cases of the valve metals.[49]

5. Insulator-Conductor Transitions

Indira and coworkers proposed that oscillations in certain instances arise from subtle changes in the stoichiometry of anodically formed layers.[37,50] The model assumes the existence of a thin, non-porous film on the metal surface through which current flows by cation migration

through lattice defects. The authors proposed a gradient of cation concentration across the film causing a stoichiometric excess near the metal/film interface and a deficit near the film/electrolyte interface. In the intervening region lies a relatively defect-free zone--the stoichiometric region (SR). For a wide class of solids, ionic conductivity is proportional to defect concentration. Hence, the SR separates two higher conductivity layers,and thus the ensemble is analogous to a parallel plate condenser. As the film thickens during anodic dissolution, the field strength increases in the SR until it is destroyed by an electrical discharge between the two extreme regions. The discharge leaves behind filaments of highly defective and hence highly conductive material. The buildup or repair of the stoichiometric region then begins anew. The mechanism for restoring the high resistance state is not identified by the authors.

Indira and coworkers offered no quantitative predictions based on their model; nor was the existence of the conducting filaments verified experimentally. Nevertheless, the basic assumption of a concentration gradient and conductivity profile within the solid film has sound theoretical basis. Calculations of mobile ion concentration profiles have been made by Fromhold and Kruger.[51] Field-induced insulator to conductor transitions occur in a variety of metal oxides and often involve the formation of high conductivity filaments. (See Chapter IV-D) We shall return to a discussion of non-stoichiometry and conductivity in Chapter V.

C. Problems in the Elucidation of Periodic Electrode Reactions

The elucidation of periodic electrode reactions requires an identification of the processes dominant during each phase of the cycle. The models described above present reasonable mechanisms for the growth and destruction of current-restricting layers. With the exception of Franck's scheme, the models assume rather than explain why growth and breakdown should occur in sequence and in phase over an extended electrode surface. The authors do not rule out the possibility that the growth and breakdown processes could occur simultaneously but out of phase on discrete sites on the electrode surface. With a sufficiently large number of sites, the current and potential might approach steady levels which reflect the average effect of sites in different stages of growth and breakdown.

Franck showed explicitly why a stable mixed electrode state could not be attained with the processes he hypothesized for the iron/acid systems under the experimental conditions where oscillations were observed. However, proof of the inaccessibility of a stable mixed electrode state is not sufficient to explain the observed periodicity. In many other situations, stability is clearly not obtained, yet the consequent fluctuations are random. Examples include: (1) the high frequency (10^5 Hz) fluctuations in the Ag/AgCl/HCl system, which are attributed to alternate charge and discharge of a PN junction in the silver chloride layer;[37,50] and (2) the random potential fluctuations observed during the anodization of zinc and cadmium resuling from localized breakdown and repair of an oxide film.[61]

The oscillations observed with the copper/chlorate system as well as the electrode/electrolyte combinations reviewed above are not random but show a high degree of "regularity": successive cycles are of similar (and often identical) amplitude, period, and waveform. The regularity of the oscillations is at once the most striking and most difficult feature to explain. To account for the regularity, dynamics of the hypothesized processes may be represented by a set of differential equations; solutions to the equations (if obtainable) can be examined for periodic behavior. (See Section II-D)

We summarized the problem of periodicity as follows:

(1) The mechanisms involved in the growth and destruction of resistive layers must be identified.

(2) The mechanisms must be shown to be incompatible with the attainment of a stable mixed electrode state.

(3) The instability must be shown to cause regularly periodic changes between electrode states.

D. Approaches to the Quantitative Interpretation of Periodicity

The interpretations for oscillating systems described in Section II-B were limited (Franck's model excepted) to hypothetical descriptions of the sequence of events during individual oscillation cycles. Such interpretations do not constitute proof that the proposed mechanisms should lead to oscillatory behavior.

1. Mathematical Modeling of Reaction Kinetics

A stronger argument for a hypothetical scheme can be made if the processes can be accurately described in a mathematical model and if the resulting equations exhibit oscillatory behavior. Higgins[52] and Frank-Kamenetskii[53] treated the general problem of oscillations derived from reaction kinetics. The kinetics of a complex chemical reaction can be described in principle by a set of kinetic equations of the form

$$dx_i/dt = F_i(x_1, x_2, \ldots, x_i, \ldots, x_k) \qquad i = 1,2,\ldots k \qquad (1)$$

where subscripted x represents the activities of the reacting species. The Eq. (1) will in general involve non-linear terms and analytical solutions may be unobtainable.

The interpretation of oscillations in the Cu/HCl system by Bonhoeffer[54,55] exemplifies the use of graphical solutions to equations of the form (1). Bonhoeffer considered the periodicity to result from cross-coupling between the processes of growth and dissolution of solid cuprous oxide and cuprous chloride. Accordingly, Eq. (1) take the simple form:

$$dx/dt = f(x,y) \qquad (2)$$

$$dy/dt = g(x,y) \qquad (3)$$

where x and y refer to the quantities (in units, moles/cm^2) of cuprous oxide and cuprous chloride adhering to the metal substrate.

Solutions of Eqs. (2) and (3) may be represented as a family of curves, or reaction trajectories, on a phase plane with axes x and y. (See Fig. 21b). On the trajectories, time may be indicated as a parameter. With given initial conditions, the course of the reaction is predicted by solving the equation,

$$dy/dx = g(x,y)/f(x,y) \tag{4}$$

Bonhoeffer evaluated the functions g and f for combinations of three experimentally determined values of x and y. A closed-loop trajectory was constructed by the method of isoclines.[56]

Mathematical modeling allows the identification of possible stable electrode states. In phase plane representation, it is convenient to depict the curves

$$f(x,y) = 0 \tag{5}$$

and

$$g(x,y) = 0 \tag{6}$$

Points of intersection represent system compositions where the time rates of change of x and y both vanish. Such intersections, called "quasi-stationary points," may correspond to either stable or unstable electrode states. Stability may be determined by examining the behavior of Eqs. (2) and (3) in the region immediately surrounding the intersection. For a reacting system where no sustained oscillations are observed, all trajectories lying within a region surrounding the quasi-stationary

point will tend toward this point. The reaction trajectory may be monotonic, or it may pass through a number of maxima and minima in x and y (damped oscillations). Otherwise the intersection will be unstable. A family of trajectories will then lead away from the point and may approach a stable limiting cycle. The necessary conditions for the existence of a stable cycle are discussed by Higgins.[52]

Mathematical modeling of reaction kinetics is of limited practical value in the quantitative interpretation of periodicity at passivating electrodes. Small errors in the magnitude of kinetic parameters or the inadvertant exclusion of terms in formulating the equations may lead to mathematical solutions of drastically different character. The approach is chiefly useful in the elimination of certain hypothetical mechanisms which predict only stable stationary points or which fail to fulfill the necessary conditions for stable limiting cycles.

Finally it should be mentioned that mathematical modeling is not restricted to oscillations derived from mass action; models of Franck and Fitzhugh[41] and Degn[30] include explicit representation of mass transport effects.

2. Modeling of Relaxation Oscillations

The implicit assumption of the previous discussion was that a set of kinetic equations could be found which would describe the course of an oscillating system. This is rarely possible in electrode oscillations involving passivating films. The majority of cases of anodic oscillations are of the so-called "relaxation" type. Relaxation oscillations are

characterized by abrupt changes in the state of the reacting system, when the ongoing processes bring the system beyond some sharply defined stability limit.

A clear example of a relaxation oscillation (in a non-electrochemical system) is given by Frank-Kamenetskii:[53] (1) a vessel is subjected to a constant rate of influx of reactants; (2) when a critical concentration is reached, and explosion takes place and the reactants in the vessel are rapidly consumed; (3) the build up of reactants toward the critical level begins anew.

Many cases of oscillations involving passivating electrodes follow an analogous sequence in the buildup and abrupt destruction of resistive surface layers. While the growth kinetics of the layers may be mathematically described, the propagation of the relaxation is often of a complex nature, and a precise mathematical description may not be known. Therefore the relaxation process is treated as a discontinuity. Relaxation oscillations are conveniently represented on a phase plane as a series of analytical curves (for growth kinetics) connected by lines signifying quasi-discontinuous jumps (for relaxation processes).

In the model of Franck and Fitzhugh, rapid processes of short duration occur at the Flade potential and involve the nucleation of the passive film and its destruction via local cell action. Explicit representation of the processes are substituted in the computer simulation by a discontinous change between two sets of equations, one of which is operative above the Flade potential and the other, below the Flade potential.

In the interpretation of relaxation oscillations, it is not necessary to fulfill the conditions required for limiting cycles derived for kinetic oscillations. Nor is it required to determine the stability of quasi-stationary points in the phase plane diagram. It is only necessary to prove that, because of the intervention of the relaxation event, no stable system states are accessible.

III. EXPERIMENTAL DESIGN AND APPARATUS

A. Considerations in Experimental System Design

Potential oscillations observed during copper dissolution in the chlorate electrolyte occur only at high current densities, in the range of 1 to 150 A/cm^2. Experimental studies at such elevated current densities present technical difficulties in the design of electrolysis cells. The problems encountered in the high current density regime were reviewed by Landolt, et al.[90] In our investigation, the primary factors considered were: (1) provision of high rates of solution-side mass transport; (2) prevention of excessive ohmic heating of the electrolyte; (3) the choice of electrical variable (current and/or potential) to be measured and practical limits of the accuracy of electrical measurements; and (4) problems arising from the continuous recession and changes in topography of the anode surface during anodic dissolution.

1. Mass Transport Considerations

Anodic dissolution processes involve the transport of reactants to-- and reaction products away from the anode/electrolyte interface. If reactants and products are in the form of dissolved ions, transport may be effected by a combination of molecular diffusion, ion migration in the electric field of the electrolysis cell, and natural or forced convection of the electrolyte. Solid reaction products may be transported by entrainment in the electrolyte flow.

The electrolytic cells and flow systems used in this research provide for forced convection of the electrolyte under well-defined hydrodynamic conditions. The mass transfer capabilities of these systems may be characterized by certain dimensionless correlations. These correlations express a dimensionless mass transfer rate, the Nusselt number, as a function of Reynolds number and Schmidt number. In Table III-1, mass transfer equations for the various flow systems used in our research are presented together with ranges of applicability and definitions of symbols.

For our purposes, the mass transfer correlations are useful (1) for estimating the limiting transport rate under given hydrodynamic conditions; (2) for predicting the dependence of the limiting rate on system parameters (e.g., flow rate, transport properties, and characteristic dimensions); and (3) for comparing the mass transport capabilities of different flow systems. To facilitate the comparison of different flow systems, we may calculate the Nernst diffusion boundary layer thickness, δ, from the equation

$$\delta = X/Nu \qquad (1)$$

where X is the characteristic dimension used in the Nusselt number formulation.

The complex problem of mass transport in electrolyte solutions is not pertinent to the problem of periodic phenomena at hand, and the subject will not be treated further at this point. Discussions of transport phenomena in electrochemical systems may be found in Newman[91,92] and Selman.[93]

Table III-1. Mass transfer correlation of experimental flow systems.

System	Mass Transfer Correlation	Characteristic Quantities	Comments	References
Channel Flow Systems	$Nu = 1.85(ReSc\ D_h/L)^{1/3}$ $Nu = kD_h/D$ $Re = VD_h/\nu$ $Sc = \nu/D$	D_h = hydraulic diameter L = electrode length in direction of flow V = average linear flow rate	Laminar flow (Re<2000) (Average mass transfer rate)	Newman (91,92)
	$Nu = 0.28Re^{0.58}(ScD_h/L)^{1/3}$ $Nu = kD_h/D$ $Re = VD_h/\nu$ $Sc = \nu/D$	(same as above)	Mass transfer enentry region in fully developed turbulent flow $D_h/L<Re^{7/8}2(10^{-4})$ (Average mass transfer rate)	Von Shaw, et al.(96)
Rotating Disk	$Nu = 0.62\ Re^{1/2}Sc^{1/3}$ $Nu = kr/D$ $Re = \omega r^2/\nu$ $Sc = \nu/D$	r = disk radius ω = rotation rate (radians/s)	Laminar flow; $Re<2.7(10^5)$	Newman (91,92)
Stagnation Point Flow (Jet)	$Nu = 0.78\ Re^{1/2}Sc^{1/3}$ $Nu = kR/D$ $Re = UR/\nu$	R = radius of entrance tube U = potential flow rate; approximated by average linear flow rate of impingeing jet		Arvia and Marchiano (97)

Definition of Symbols
k = mass transfer coefficient = $N/\Delta C$
D = diffusion coefficient
ν = kinematic viscosity
N = flux
ΔC = difference between concentration at interface and concentration in bulk

2. Ohmic Heating of the Electrolyte Solution

At high current densities, considerable ohmic heat may be generated in the interelectrode gap. The rate of temperature increase at a point within the electrolyte solution may be estimated from the equation:

$$dT/dt = I^2/(c_p d k_e) \qquad (2)$$

where T = temperature; t = time; I = current density; c_p = electrolyte heat capacity; d = density; and k_e = electrical conductivity. In writing Eq. (2) we have neglected heat losses and have ignored the temperature dependence of material constants. For a pair of plane parallel electrodes Eq. (2) predicts that a stagnant 2F $NaClO_3$ electrolyte in the interelectrode gap would boil within 0.4 s after the application of a current density of 10 A/cm^2.

The temperature rise could be kept within reasonable limits by limiting experimental times, but this would not be feasible for an investigation of periodic, time dependent phenomena. It is therefore necessary to limit the residence time of the electrolyte in the region of high ohmic dissipation by providing for a large volume flow rate through the interelectrode gap. For the flow channel systems used in this research, the steady state temperature increase in the electrode gap may be estimated from the equation:

$$\Delta T = (I^2 s A)/(c_p d k_e Q) \qquad (3)$$

where Q = volume flow rate; s = electrode separation; and A = electrode area. For the channel flow system no. 1 (see Section III-B.1),

$A = 0.09\ cm^2$ and $s = 0.1$ cm. At a volume flow rate of 15 cm^3/s (Re=7000) the steady state temperature increase for 2F $NaClO_3$ solutions would be only 0.05°C at 10 A/cm^2 and 5°C at 100 A/cm^2, assuming no heat losses.

3. Measurement of Electrical Variables

The periodic phenomena in the copper/chlorate system are manifested by fluctuations in current and potential when the electrolytic cell is connected in series with an external voltage source of finite impedance. For simplicity, we may consider this voltage source to consist of a battery placed in series with a resistor. Constant cell voltage would be obtained in the limit of zero external resistance. On the other hand, constant current would be delivered by a voltage source with an infinitely high resistance.

We have chosen to investigate the oscillatory phenomena under galvanostatic (i.e., constant current) conditions, using electronically controlled constant current sources. This approach allows one electrical quantity (the current) to be accurately fixed and treated as a system parameter. Anode potential fluctuations may then be measured against a reference electrode immersed in the electrolyte.

The classical procedure for the measurement of electrode potential employs a so-called "Luggin capillary".[95] The tip of a capillary tube is positioned close to the solution side of the electrode/electrolyte interface. The other end of the tube opens into a vessel containing a reference electrode. Electrical contact is obtained by filling the connecting tubes and capillary with a suitable electrolyte.

In the channel flow system no. 1, the capillary tube is replaced by a small hole drilled in the wall of the flow channel just upstream from the electrode.

Errors in anode potential measurements due to ohmic potential drop in the electrolyte are proportional to the current density and to the separation between the capillary opening and the anode surface. For a current density of 30 A/cm^2 and a separation distance of 0.01 cm, the error in anode potential resulting from the ohmic potential contribution is roughly 3 volts in 2F $NaClO_3$. The problem of estimating this error is compounded by the continuous recession of the anode surface during dissolution; by changes in local current distribution during the potential cycle; and by distortion of the current distribution in the electrolyte by the capillary opening.

An alternate approach to anode potential measurement employs a reference electrode "at infinity," i.e., far from both the anode and cathode. The reference electrode is then situated in an environment of low current density, and the measured anode potential is no longer sensitive to small errors in electrode position. Such a configuration is useful in the rotating disk electrode system, where the ohmic contribution may be accurately calculated.

Finally, once it has been experimentally established that the cathode potential fluctuations are small in comparison with the amplitude of the anode potential oscillations, useful information on oscillation waveform, amplitude, and period may be derived from cell voltage measurements alone:

4. Changes in the Position and Topography of the Anode Surface

Anodic dissolution involves the continuous removal of the metal surface. As a result, the position of the metal/electrolyte interface recedes--at a rate given by the equation:

$$dx/dt = eIM/(zFd) \qquad (4)$$

where x = interface position; t = time; e = current efficiency for metal removal; I = current density; M = atomic weight of the metal; z = valence change of the metal; F = the Faraday constant; and d = density of the metal. At 100 A/cm^2, the rate of recession is approximately 0.007 cm/s, assuming a current efficiency of 1.0 and a valence change of 1.0.

In the channel flow systems and rotating disk system, the hydrodynamic situation is well-defined only when the electrode surface lies in the plane of the surrounding insulation. The rotating hemispherical electrode has been suggested for anodic dissolution studies because the system maintains a similar geometry and fluid flow pattern after extended metal removal.[94] The stagnation point flow system used in our work has a similar advantage.

Extended periods of anodic dissolution also lead to changes in surface topography and area. Uncertainties in surface area introduce errors in calculated current density.

The effects of electrode recession and shape change were minimized in our work by limiting the duration of experimental runs. The recession of the anode surface was generally limited to 3% of the electrode width or diameter.

B. Experimental Apparatus

1. Channel Flow System No. 1 ("Channel #1")

The channel flow system no. 1 was designed by Kinoshita for his investigation of high current density copper dissolution in a variety of electrolytes.[5,89] The flow system was designed to provide forced convection of the electrolyte under well defined hydrodynamic conditions at Reynolds numbers up to 10,000.

A schematic of the flow system is shown in Fig. 3.1a. Electrolyte is circulated through the system by means of a positive displacement pump (B).* The electrolyte flow rate may be adjusted with the stainless steel needle valve on the by-pass pipe line (D) or with the variable speed control on the pump motor. Flow rate is measured with a Rotameter (E).** The Rotameter was calibrated by measuring the volume of electrolyte displaced through the cell in a measured time interval.

The electrolyte supply tank (A) and the drain tank (B) were constructed of polyethylene and polyvinyl chloride (PVC), respectively. Pipe lines and valves were constructed of stainless steel.

The rectangular duct flow channel (F) was constructed of PVC. The entrance length provided by the flow channel is 30 cm (200 hydraulic diameters). This entrance length is sufficient to establish the stable parabolic velocity profiles of laminar flow.[99]

---

*Constametric Controlled Volume Chemical Pump, Milton Roy Co., Philadelphia, Pa.

**Safeguard Rotameter Type 3RB, Shutte and Koerting Co., Cornwall Heights, Pa.

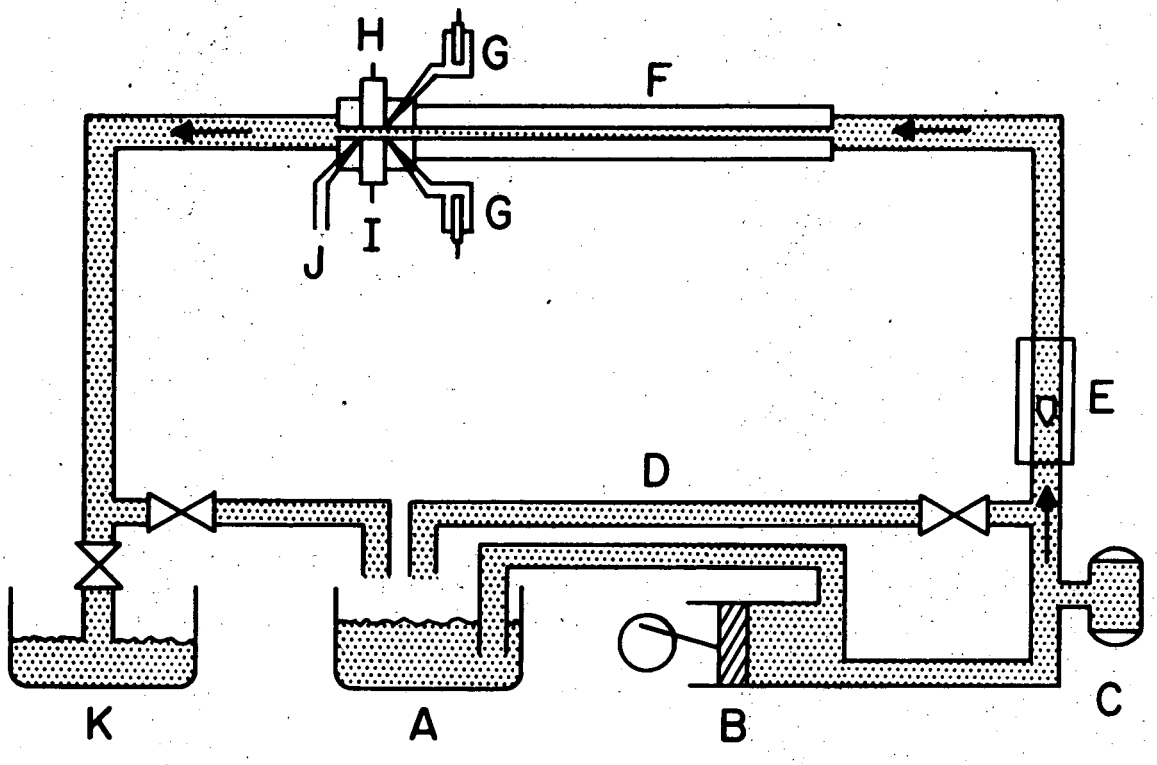

XBL704-2707

Fig. 3.1a. Schematic of Channel Flow System No. 1.(A) Fresh electrolyte reservoir; (B) piston pump; (C) accumulator; (D) bypass line; (E) Rotameter; (F) entrance channel; (G) reference electrodes; (H) cathode; (I) anode; (J) capillary for sample collection; (K) spent electrolyte reservoir.

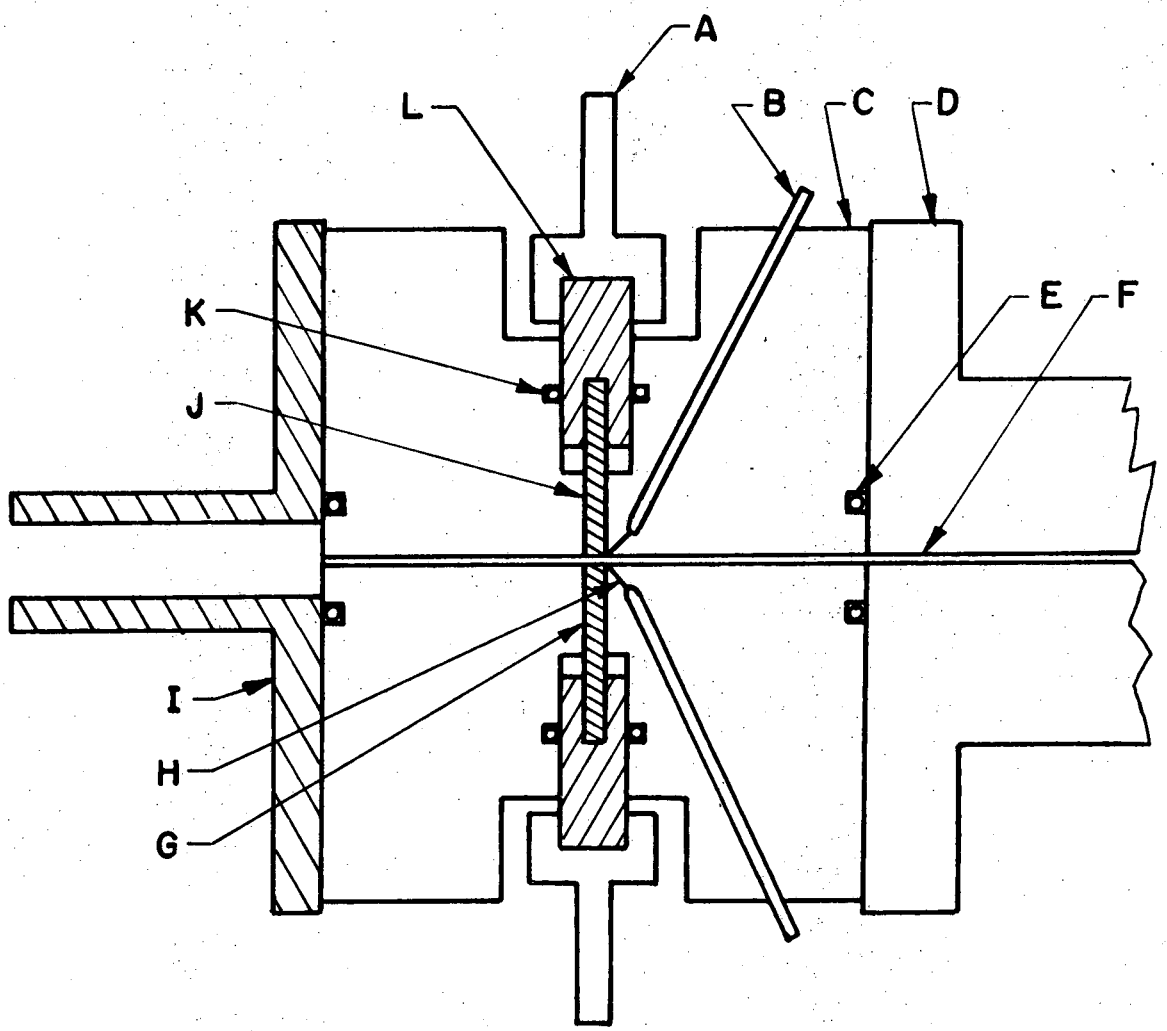

XBL 747-6812

Fig. 3.1b. Electrolysis cell of channel flow system no. 1. (A) electrode current connector; (B) capillary tube; (C) Epoxy cell body; (D) PVC entrance channel; (E) O-ring seal; (F) rectangular duct; (G) anode; (H) capillary; (I) stainless steel flange. (J) cathode; (K) O-ring seal; (L) electrode holder.

The flow system was modified for our experimental work as follows: (1) the grease-packed piston bearings were replaced by Teflon bearings; (2) the accumulator (C) was found unnecessary and was removed.

A schematic of the channel flow cell no. 1 is shown in Fig. 3.1b. The rectangular duct channel (F) is 0.3 cm wide and 0.1 cm deep. The anode (G) and cathode (J) are rectangular bars with dimensions 0.3 cm × 0.3 cm × 3 cm. The square ends of the electrodes are the active surfaces and are positioned flush with the horizontal walls of the flow channel. The anode surface faces upwards in all experiments with the channel flow system 1.

A gap of roughly 5 mils existed between the long sides of the electrodes and the epoxy resin cell body (C). To prevent stray dissolution along the sides of the anodes, a coating of insulating varnish was applied. (See Section IV-A.1) Leakage of electrolyte around the cylindrical electrode holders (L) was prevented by Teflon O-ring seals (K).

Capillary holes (H) were drilled into the cell body just upstream of the electrodes. The capillaries opened into stainless steel tubes (B). The tubes were connected with Tygon tubing to glass vessels containing commercial saturated calomel reference electrodes.* The vessels and connecting tubing were filled with 2F $NaClO_3$ to establish electrical contact between the reference electrodes and the anode or cathode.

---

*Beckman Fiber Junction Reference Electrode No. 39270; Beckman Instruments, Inc., Fullerton, Ca.

The vertical walls of the flow channel (not shown in Fig. 3.1b) were constructed with optically flat glass. A telescope was provided for positioning the electrodes and for viewing the development of reaction product layers during dissolution.

The constant current source employed with all the flow systems was an Electronic Measurements Power Supply, Model C618.* The power supply delivered a maximum of 3A at 200 V. The rise time of the instrument is approximately 10^{-3} s.

Electrical measurements were recorded with a Brush Light Beam Oscillograph.** The instrument has six separate input amplifiers, the outputs of which are fed to separate galvanometers in a photographic recording component. The galvanometers are mechanically linked to mirrors which deflect light beams onto a moving strip of photosensitive paper. The photographic records are then developed by exposure to ambient room light. The system response frequency is 10^3 Hz. The frequency of the potential oscillations is of the same order of magnitude at current densities above 50 A/cm^2; hence the use of the oscillograph was limited to lower current densities.

In work with the channel flow system no. 1, cell voltage, anode potential, and cathode potential, as well as the voltage drop across a low resistance current measuring shunt, were recorded.

---

*Electronic Measurements, Inc., Eatontown, N.J.

**Series 2300, Brush Instruments, Division of Clevite Corporation, Cleveland, Ohio

2. Channel Flow System No. 2 ("Channel #2")

Our investigation of the effects of bulk electrolyte temperature and composition (including pH) on the anode potential oscillations required a flow system of low heat capacity and low electrolyte "dead volume." The channel flow system no. 2, designed by D. Landolt,[3] was used in this work.

A photograph of the system is shown in Fig. 3.2a. Electrolyte is forced through the channel flow cell (E) by a piston pump (C). A dial indicator (B) is attached to the speed control lever of the motor. The capacity of the piston pump is 400 ml.

The pump cylinder was constructed of PVC, and connecting tubes and fittings were made of Tygon, Nylon, or Pyrex. The electrolysis cell (E) was constructed of Teflon and Epoxy. Hence, no metal parts were in contact with the electrolyte other than the electrodes.

A schematic of the flow channel cell no. 2 is shown in Fig. 3.2b. Rectangular electrodes, 0.05 cm × 0.3 cm, were cast into epoxy cylinders, (C) and (K). The cylinders were separated by a Teflon sheet of thickness, 0.05 cm. A slot 0.3 cm wide was cut into the Teflon sheet to form the flow channel. The anode (H) and cathode (A) were positioned on opposite walls of the flow channel, with the anode surface facing upwards. The short length of the electrodes was parallel to the direction of flow. The anode cylinder was pressed against the Teflon seal by means of four knurled screws (G).

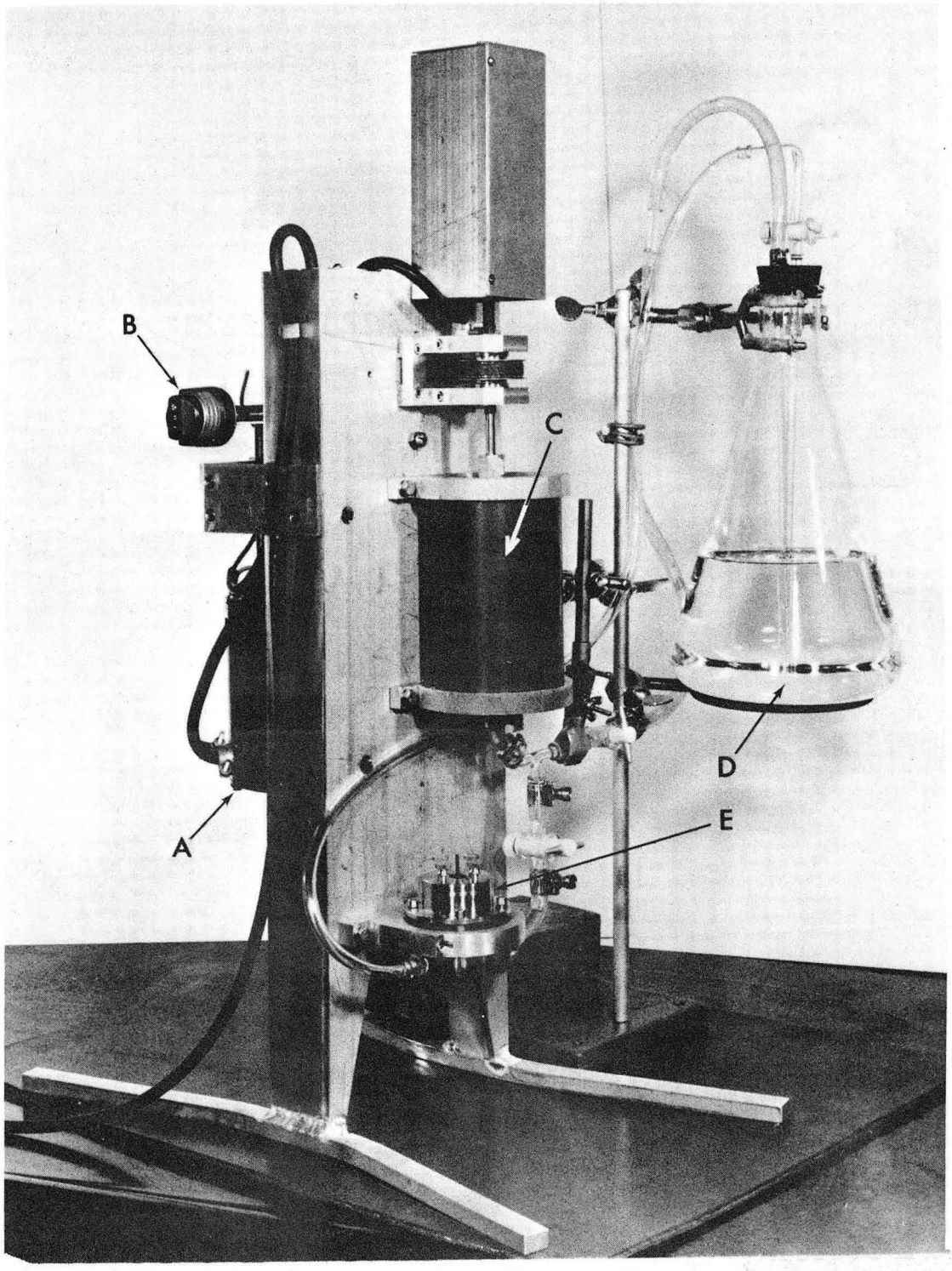

CBB 681-213A

Fig. 3.2a. Channel flow system no. 2. (A) electric motor; (B) dial indicator of motor speed control; (C) piston pump; (D) electrolyte reservoir; (E) flow channel.

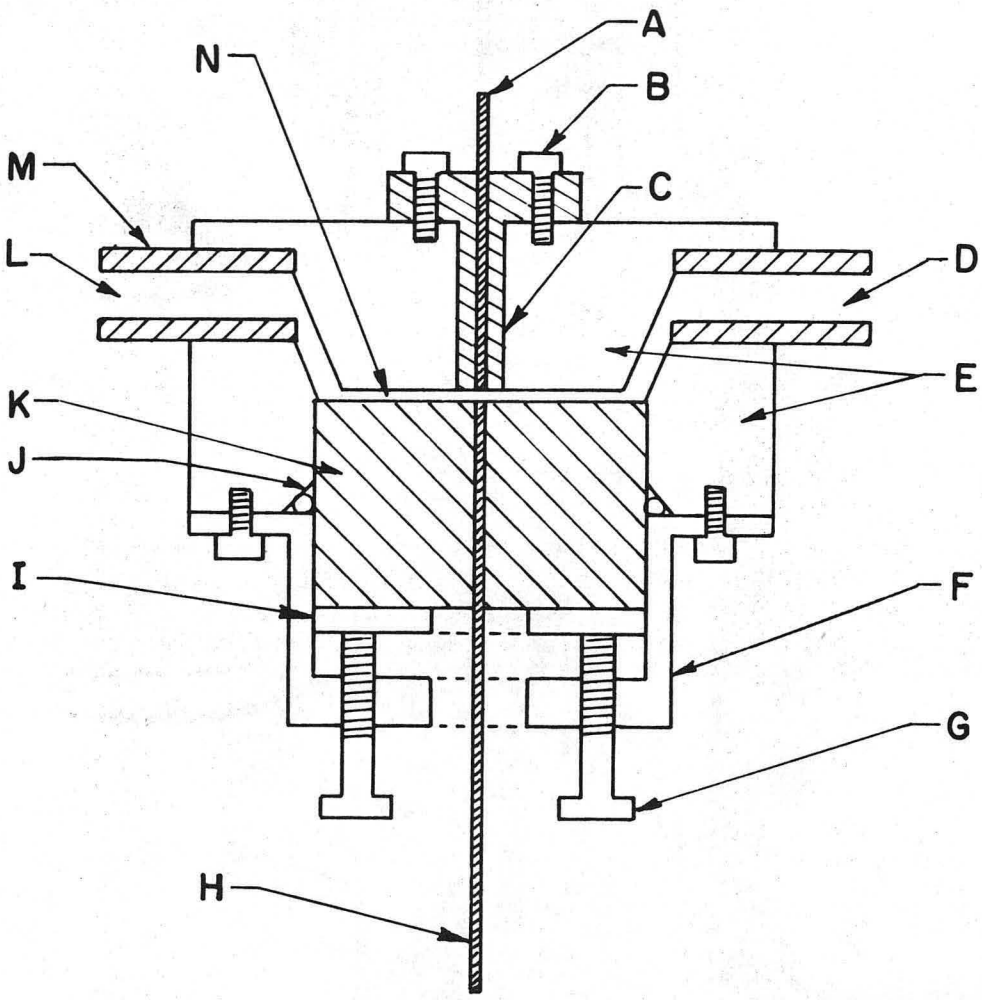

XBL747-6811

Fig. 3.2b. Flow channel no. 2. (A) cathode; (B) machine screws; (C) Epoxy cathode holder; (D) entrance tube; (E) Epoxy cell body; (F) stainless steel flange; (G) machine screws; (H) anode; (I) stainless steel ring; (J) O-ring seal; (K) anode holder; (L) exit tube; (M) Nylon tube; (N) flow channel.

The hydrodynamic entrance length of 1.3 cm (15 hydraulic diameters) is insufficient for the establishment of stable velocity profiles.

3. Rotating Disk Electrode System ("Rotating Disk")

The electrolyte is contained in a 1.5 L glass beaker (14 cm diameter, 10 cm deep). A copper wire mesh (total geometric area, 250 cm^2) was pressed against the bottom of the beaker to serve as cathode. The rotating anode surface was positioned on the central axis of the beaker, 6-8 cm above the cathode. With this configuration, the anode surface faces down.

The rotating anode unit is shown schematically in Fig. 3.3. To construct the anodes, brass rods were tapered and threaded for attachment to the motor driven spindle (A). Cylinders of OFHC copper (C) were silver soldered to brass connectors (D). With the use of a dummy spindle mounted in a precision lathe, the brass and copper stocks were trued and turned to a diameter of 0.564 ± 0.001 cm. An Epoxy casting (B) provided an insulating plane surrounding the anode surface. The anode surface area is 0.250 cm^2.

The rotating disk assembly was powered by a $\frac{1}{4}$ h.p. variable speed DC motor.

4. Stagnation Point Flow System ("Jet")

A stagnation point flow system was designed to allow the investigation of periodic phenomena at high current densities under well defined hydrodynamic conditions. The anodes used in this system have small active surface areas (0.02 cm^2). Current densities as high as 150 A/cm^2

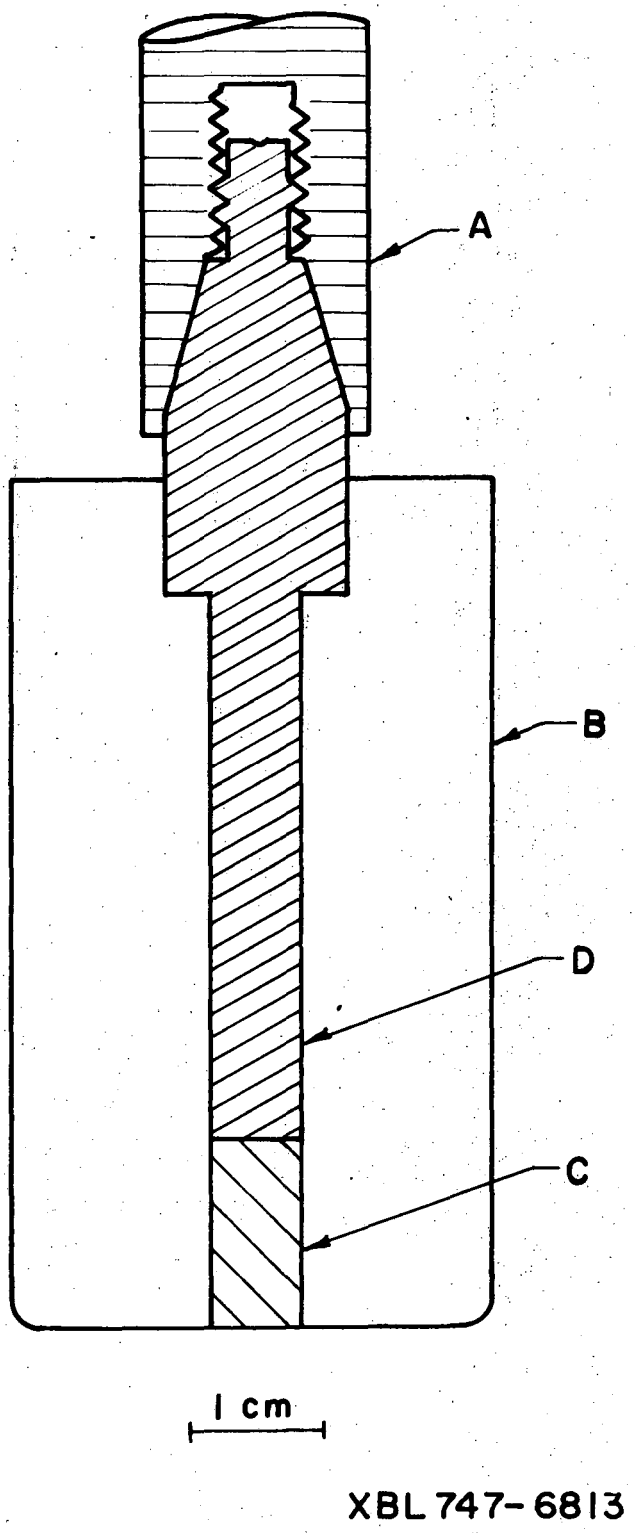

Fig. 3.3. Rotating disk electrode. (A) Spindle; (B) Epoxy anode holder; (C) copper cylinder anode; (D) brass cylinder connector.

may be attained with the Electronic Measurements Power Supply delivering a current of 3 A. The low total capacitance of the electrolyte cell, the low total power dissipation, and the rapid (10^{-3} s) rise time of the power supply give this system distinct advantages over systems of larger scale. Finally, the low weight of the individual anodes (0.7 g) allow weight loss measurements to be made with a precision of 0.01 mg.

A cross section view of the stagnation point flow cell is shown in Fig. 3.4. A jet of electrolyte flows through the entrance tube (A) of diameter 0.32 cm and impinges on the surface of the anode (H). The electrolyte flows radially over the cathode (J) and up through six, 1 - cm diameter holes (D) to fill the spent electrolyte reservoir (B). The anode wire is press-fit into the Teflon plug (G), which provides the plane of impingement of the electrolyte jet. Electrical contact is made to the cathode by means of an insulated copper rod (L). To allow adjustment of the position of the entrance tube, the tube and the floor of the Lucite cell body are threaded. A retaining nut (K) locks the tube in place. The upper (C) and lower (I) halves of the Lucite cell body are held together with screws (F), and a ring of Teflon (E) seals the joint.

The piston pump used with channel no. 2 provides a controlled electrolyte flow to 450 cm/s (average linear flow rate in the entrance tube).

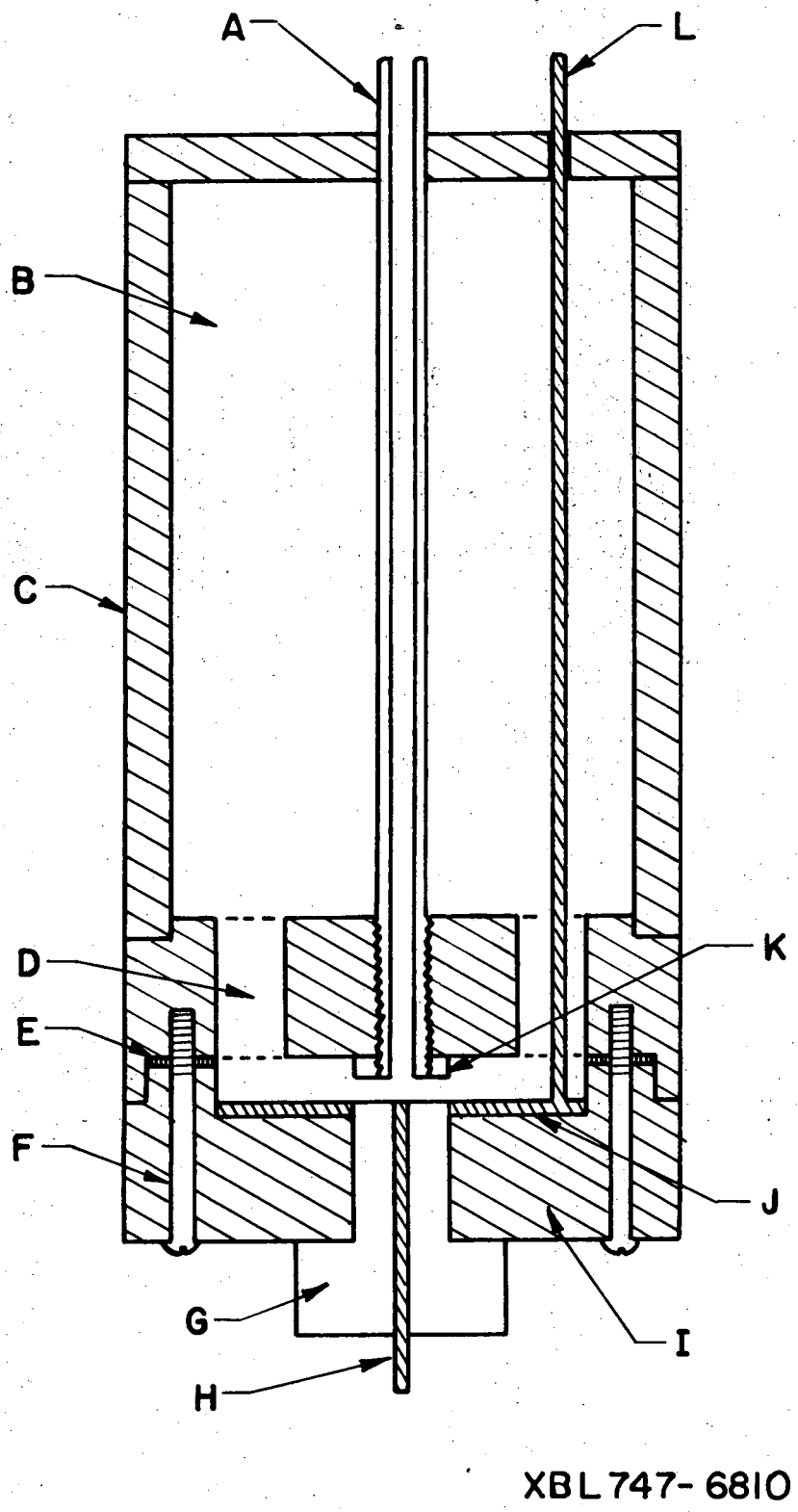

Fig. 3.4. Stagnation point flow cell. (A) Lucite entrance tube; (B) used electrolyte reservoir; (C) Lucite cell body; (D) drain holes; (E) Teflon seal; (F) machine screws; (G) Teflon anode holder; (H) copper wire anode; (I) Lucite cell body; (J) copper ring cathode; (K) retaining nut (Nylon); (L) copper rod current collector.

5. Stationary Electrolyte Cell

The time scale of the periodic phenomena is greatly expanded at low current densities: at 1 A/cm^2, the oscillation cycle lasts roughly 5 seconds, and therefore changes in dissolution chemistry and electrode morphology within the cycle may be resolved. However, the charge passed in each cycle is small ($4(10^{-5})$ eq/cm^2 at 1 A/cm^2) as is the weight lost by the copper anode (3 mg/cm^2). An electrolytic cell was designed to provide: (1) a large anode area--to provide for measureable weightlosses; (2) a small anolyte volume--to bring concentration changes up to measureable levels; (3) a uniform primary current distribution; and (4) suppressed mixing of anolyte and catholyte.

The cell is shown in Fig. 3.5. The anolyte chamber (H) has a volume of 20 cm^3 and is separated from the catholyte chamber (K) by filter paper diaphragms (I). The anode is a disk of OFHC copper, 5 cm in diameter and 0.1 cm thick; the "active" anode has an area of 9.6 cm^2. The cathode is a copper wire mesh of total surface area, 25 cm^2. The two halves of the Lucite cell body are held together by bolts (A), which clamp the anode disk firmly to a large brass heat sink and electrical connector (G).

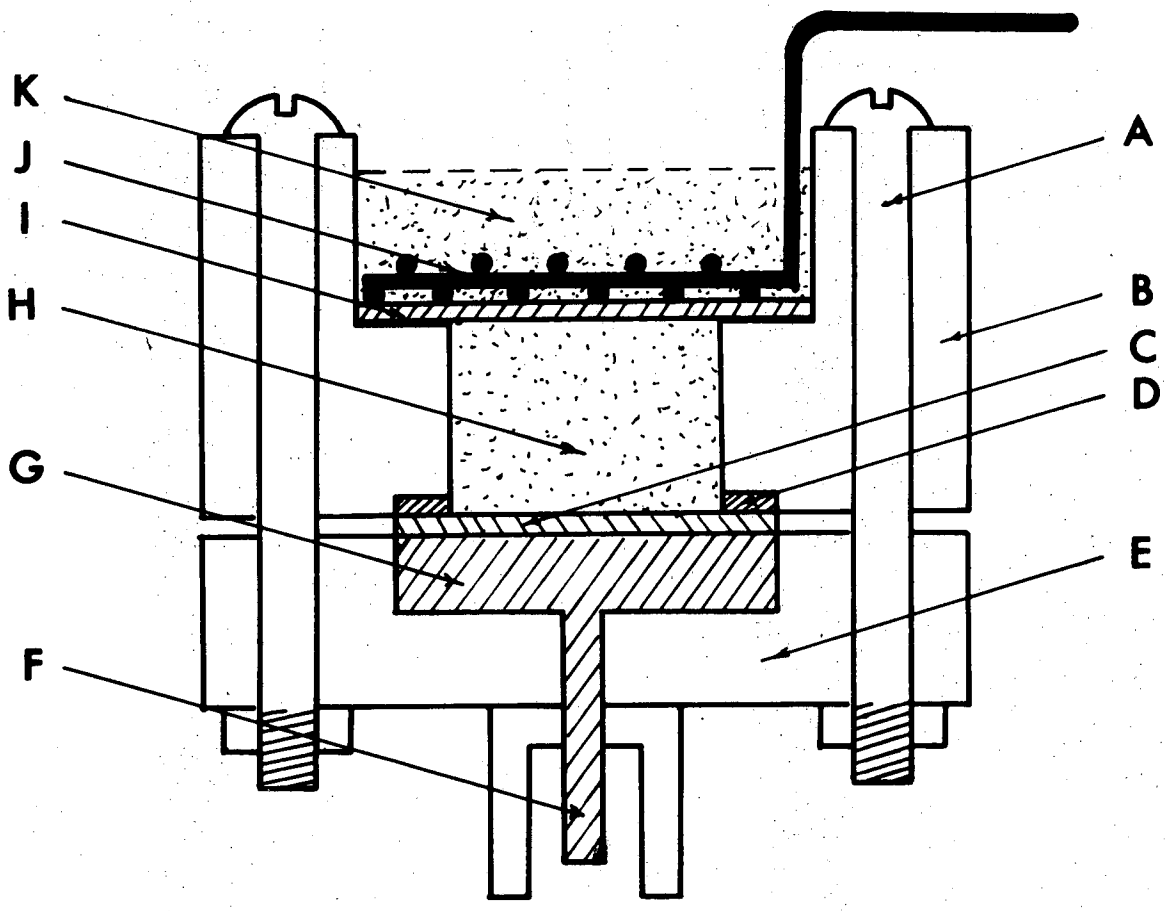

XBL 709-6605

Fig. 3.5. Stationary electrolyte cell. (A) Machine screws; (B) Lucite cell body; (C) copper disk anode; (D) Teflon ring seal; (E) Lucite cell body; (F) anode connector; (G) brass heat sink; (H) anode chamber; (I) filter paper separator; (J) wire mesh cathode; (K) cathode chamber.

C. Chemicals

1. Copper

The copper wire used with the stagnation point flow system was zone refined by the manufacturer to a high purity; 99.999+% Cu.* Quoted impurities, in parts per million by weight, were as follows: Zn<5; Sn<1; Ni, P, Pb<1; O<2; Mo<5; rare earths < 1; Cl<0.01.

In all other flow systems and in the stationary electrolyte cell oxygen free, high conductivity copper (OFHC) was used. The purity of the OFHC copper was 99.99+%. No impurity specifications were quoted by the manufacturer.**

2. Sodium Chlorate

Electrolyte solutions in all cases were prepared with "Baker Analyzed" Reagent grade sodium chlorate;*** or Baker and Adamson Reagent Grade sodium chlorate.**** Chloride content of the salt was below 50 p.p.m. in both cases.

---

*Stock No. 29-29-199-062; lot 29-16543; grade Marz; Materials Research, Inc., Orangeburg, N.Y.

**OFHC, Alloy 101; American Brass and Copper Co., Inc., Emergyville, Ca.

***J. T. Baker Chemical Co., Phillipsburg, N.J.

****Allied Chemical, General Chemical Division, Morristown, N.J.

IV. EXPERIMENTAL STUDY OF THE ANODE POTENTIAL OSCILLATIONS

In the preceding chapter, the experimental apparatus, instrumentation, and chemicals were described in detail.

In this chapter, we shall report the procedures and results of an experimental investigation of periodic phenomena in the high current density anodic dissolution of copper in the chlorate electrolyte. The experimental study falls into four main categories: (1) electrical properties of the oscillation (i.e., period, amplitude, waveform); (2) chemical aspects of the dissolution processes; (3) morphology of the anodic reaction products and of the copper substrate; and (4) electrical breakdown of the thin films on copper. Certain observations will be analyzed and interpreted in this chapter. In chapter V, the different aspects of the phenomenon will be integrated into a comprehensive picture of the periodicity.

A. Electrical Properties of the Oscillations

1. Experimental Procedures

a. Procedures with Channel Flow System #1

Experiments were conducted with this channel for the purpose of determining: (1) electrical properties of the oscillations (i.e., waveform, amplitude, and period length), and (2) apparent valence of the dissolution processes. Apparent valence is defined as the ratio of the equivalents of charge passed to the moles of copper dissolved. The experimentally determined values of apparent valence will be presented in Section IV-B.

Electrode Preparation. A sheet of OFHC copper was cut into rectangular bars with dimensions, 0.3 cm by 0.3 cm square and 3 cm long. The long sides of the electrodes were coated with insulating varnish (General Electric Adhesive and Insulating Varnish No. 7031), allowed to dry, and bake-hardened for 4 hours at 100°C. The coating served to prevent stray dissolution along the sides of electrodes.

The electrodes were prepared for dissolution as follows:

(1) Electrode ends were ground flat against water-wetted, #600 carborundum paper;

(2) electrodes were washed in Labtone detergent and rinsed in distilled water;

(3) rinsed in 10%/vol. nitric acid followed by a rinse in distilled water;

(4) weighed to a precision of ± 0.01 mg.*

Experimental Procedure. Prior to each dissolution run the current delivered by the Electronics Measurements Power Supply was determined from the potential drop across a low resistance shunt.** Potential drop was measured with a balancing potentiometer.***

Dissolution times were measured with a stopwatch. Dissolution times were chosen to allow the passage of 10-25 coulombs, corresponding to a weightloss of approximately 6-15 mg. Electrode position was not readjusted during dissolution; as a consequence of dissolution, anode

---

*Mettler Mode H20T, Greifensee-Zurich, Switzerland.

**Daystrom, Inc., Weston Instruments Division, NEwark, N.J.

***Leeds and Northrup, Inc.; Model 8667, Philadelphia, Penn.

surfaces retracted from 0.007 to 0.017 cm. Anode potential, cathode potential, cell voltage, and potential drop across the current measuring shunt were simultaneously recorded on the light beam oscillograph.

Following dissolution, anodes were removed from the cell and:

(1) washed in distilled water;

(2) rinsed in 10%/vol HNO_3 to remove adherent layers of reaction products;

(3) rinsed in distilled water;

(4) rinsed in reagent grade acetone and allowed to dry.

The anodes were then re-weighed.

In control experiments, in which the same procedure was followed without anodic dissolution, weightlosses were less than 0.10 mg--a quantity small compared to the weightlosses resulting from anodic dissolution.

In all experiments conducted with channel #1, the electrolyte was passed through the cell only once and was then discarded. This assured a uniform electrolyte composition and pH for all dissolution experiments.

No provisions were made for the deaeration of the electrolyte or for temperature control. The pH of stock solutions of 2F $NaClO_3$ was 4.6, the slight acidity possibly the consequence of hydrolysis dissolved carbon dioxide.

b. Procedures with Channel Flow System #2

The channel flow system #2 was used in the investigation of the effect of electrolyte temperature and pH on oscillation frequency.

The electrodes were prepared for dissolution as follows: (1) Electrodes were ground flat against water wetted #600 carborundum paper; (2) washed in Labtone detergent and distilled water; (3) rinsed in dilute nitric acid (10%/vol); and (4) rinsed thoroughly in distilled water.

With the electrodes inserted in the cell, the flow rate was adjusted to the required value using the speed control on the piston pump motor.

pH Variation Procedure. The pH of prepared solutions was measured before dissolution experiments with a Corning pH meter.* Stock solutions of 2F $NaClO_3$ prepared with distilled water had a pH of 4.6. Alkaline solutions were prepared by the addition of reagent grade sodium hydroxide to the stock solution. Acidic solutions were prepared by the addition of aliquots of concentrated reagent grade perchloric acid.

Temperature Variation Procedure. A liter of 2F $NaClO_3$, contained in a Pyrex beaker, was heated on an electric hot plate, or chilled in an ice bath, until the required temperature was attained. Immediately after the conclusion of a dissolution experiment, the temperature of the collected effluent from the electrolytic cell was measured. The temperature of the effluent was assumed to be a good approximation of the electrolyte temperature between the electrodes. As no significant

*Corning Scientific Instruments, pH Meter Model 7, Corning, N.Y.

dependence of oscillation frequency on electrolyte temperature was found, a more precise determination of temperature was deemed unnecessary.

In these experiments, only cell voltage was recorded on the oscillograph.

c. Procedures with the Stagnation Point Flow System (Jet)

The Jet was employed in the investigation of potential oscillations at high current densities (8-150 A/cm^2).

The high purity (99.999% Cu) anodes were prepared for dissolution following the procedure described in the preceding section. A wire electrode was inserted into the Teflon plug which provided the plane of impingement of the electrolyte jet. Using a strip of 2 mil copper shim stock as a guage, the end of the copper wire serving as anode surface was positioned 0.005 cm beyond the surface of the Teflon plug. With this configuration, the anode surface had a total geometric area of 0.022 cm^2. The protrusion allowed the passage of 1.5 coulombs (corresponding to roughly 100 oscillation cycles) before the anode surface would recede into the plug.

The speed control on the piston pump motor was calibrated by measuring the volume of electrolyte displaced through the cell in a measured time period. The current level control on the Electronic Measurements power supply was calibrated with the use of the low resistance shunt and balancing potentiometer described earlier. Cell voltage was measured using the Brush Oscillograph (for current densities up to 31 A/cm^2), or the Tektronix Model 502 Oscilloscope (for current densities up to 150 A/cm^2).

The electrolyte was passed twice through the cell before being discarded. No measureable differences in oscillation parameters were found for the fresh and recycled electrolyte at the current densities employed.

d. Procedures with the Rotating Disk Electrode System (Disk)

The disk was used in the investigation of the anode potential oscillations at low current densities. In a first set of experiments, rotational velocity was held constant and current density was set at various values between about 0.3 and 12 A/cm^2. In a second set of experiments, the effect of different mass transfer rates (different rotational rates) was investigated at 0.8 and 1.6 A/cm^2.

Electrode Preparation. In the first set of experiments, the anodes were prepared as follows: (1) Electrodes were ground flat against water wetted #600 carborundum paper; (2) washed in Labtone detergent and water; (3) rinsed in distilled water; (4) preanodized in 2F $NaClO_3$ at 4 A/cm^2 for 5 seconds; (5) rinsed in dilute HNO_3 to remove surface films; and (6) thoroughly rinsed in distilled water. The preanodization treatment served to remove cold worked metal to a depth of 15 micrometers.

In the second set of experiments (current density held constant, rotational rate varied) it was desirable to provide an anode surface with a maximum degree of flatness and polish. The electrodes in their cast epoxy shields were polished on a 1-micron diamond abrasive wheel. The preanodization step was replaced by a cathodic treatment in 0.5M NaOH at roughly 1 A/cm^2 for 5 seconds.

Electrolyte Preparation. Because of the small volume of the electrolyte cell (1.5 liters), continuous changes in the electrolyte composition during the course of a single dissolution experiment were expected. For example for a dissolution run lasting 1000 seconds at 0.4 A/cm^2, the cathodic evolution of hydrogen would produce a hydroxyl ion concentration of $10^{-3}M$. Comparable increases in aqueous chloride and copper concentrations were also expected. To buffer the electrolyte against small changes in composition, small quantities of reagent grade $CuCl_2$ and NaOH were added to stock solutions prior to dissolution to make the following composition: 2F $NaClO_3$ + 1 mF NaOH + 1mF $CuCl_2$. Results obtained with this composition will be compared with results with 2F $NaClO_3$.

e. Procedures in Stationary Electrolyte

Preliminary investigations of the oscillations were conducted in stationary electrolyte under conditions where natural convection was suppressed. The anodes used were resin insulated copper wire of cross sectional area, 0.02 cm^2. The wire ends serving as anode surfaces were (1) ground flat against #600 carborundum paper; (2) preanodized in 2F $NaClO_3$ at 5 A/cm^2 for 15 seconds; (3) rinsed in dilute HNO_3; and (4) rinsed thoroughly in distilled water. The preanodization treatment left a shield of insulation 0.004 cm high at the periphery of the anode surface.

The wires were bent into U-shapes and positioned with surfaces face upwards in the center of a 600 ml beaker filled with electrolyte.

A copper wire mesh, pressed against the vertical walls of the beaker, served as cathode. Cell voltage was measured during dissolution as in experiments with the flow systems.

2. Range of Experimental Study

Table IV-1 summarizes the range of experimental conditions investigated for each experimental system. Periodic phenomena were studied over wide ranges of four experimental parameters: (1) current density; (2) electrolyte flow rate; (3) bulk electrolyte pH; and (4) bulk electrolyte temperature.

The range of current densities investigated include the upper and lower limits for sustained oscillations under the experimental conditions employed. The lowest current density at which oscillations were clearly obtained with the rotating disk was 0.28 A/cm^2 at Re = 280 (360 r.p.m.). In channel #1, the lowest current density at which oscillations were observed was 0.61 A/cm^2 at Re = 200 (14.2 cm/s).

The highest current density investigated was 146 A/cm^2, using the stagnation point flow system. At this current density, only a few oscillation cycles could be recorded after current switch-on before the cell potential rose to the limiting voltage of the constant current supply (200V) and a continuous "anode effect" (gas evolution and spark discharges) occurred.

No upper limit of flow velocity has been established for the oscillatory phenomena, although at low current densities (2.5 A/cm^2), the regularity of waveform was lost at Re = 10200 (600 cm/s) in

Table IV-1. Experimental Conditions Investigated in the Determination of Oscillation Period and Amplitude

System	Current Density Range (A/cm^2)	Flow Conditions		Bulk Electrolyte pH	Bulk Electrolyte Temperature (°C)	Bulk Electrolyte Composition
Channel Flow System #1	0.606-5.40	14.2 cm/s;[a]	Re= 200	neutral	26	2F $NaClO_3$
	0.24 -5.28	20	425		23	
	0.05-33.04	50	708		20	
	0.6 - 5.2	115	1630		20	
	0.89- 5.3	280	3990		26	
	0.91-33.4	478	6810		25-26	
	2.53, 2.55	600	8490		26	
Channel Flow System #2	7.1 -32.7	50 cm/s;[a]	Re= 400	1.4,2.4,4.6, 10.6,11.2	ambient	2F $NaClO_3$
	7.1 -32.7	50 cm/s	400	neutral	4,24,48,80	2F $NaClO_3$
Stagnation Point Flow System	8.5 -31.5	28 - 510 cm/s[b] Re = 210-3800		neutral	ambient	2F $NaClO_3$
	8.5 -146	94, 194 cm/s Re = 704, 1450		neutral	ambient	2F $NaClO_3$
Rotating Disk Electrode System	0.28-12	360 r.p.m.[c] Re = 283			23	2F $NaClO_3$ + 10^{-3}F NaOH + 10^{-3}F $CuCl_2$; or 2F $NaClO_3$
	0.8, 1.6	110 to 2920 r.p.m. Re = 86-2293			ambient	
Stationary Electrolyte	5 - 35	----		10 - 11	ambient	2F $NaClO_3$ + 10^{-4} to 10^{-3}F NaOH

[a] Linear flow velocity

[b] Linear flow velocity of impinging jet

[c] Rotation frequency, revolutions per minute

channel #1. Sustained oscillations have been observed over the range of electrolyte temperatures 4-80°C, and over of bulk electrolyte pH from 1.4 to 11.2.

3. Periodic Phenomena Associated with the Anodic Dissolution Processes

The large amplitude (1 to 50 volts) voltage oscillations are associated with the anodic dissolution processes and not with cathodic reactions. This was established (with the use of channel #1) by the simultaneous measurements of (1) cell voltage; (2) potential of the anode relative to a saturated calomel electrode (SCE); and (3) potential of the cathode relative to a second SCE. A tracing of a typical oscillograph record is shown in Fig. (4.1). The fluctuations of cell voltage were congruent with the fluctuations in anode potential, while the cathode showed no comparable time dependence.

Once it had been established that fluctuations in cathode potential were small compared to the periodic changes in anode potential, oscillation amplitude and frequency were obtained directly from the relative changes in cell voltage.

4. Characteristic Oscillation Waveforms: Qualitative Descriptions

The waveform of the potential oscillation cycles depends on current density and electrolyte flow rate. The current density range in which sustained oscillations are observed may be divided into four regions on the basis of waveform type. There are no clear boundaries between these regions, as one waveform changes continuously into another as current density is increased. The transition between waveform types occurs at higher current densities, the higher the flow rates employed.

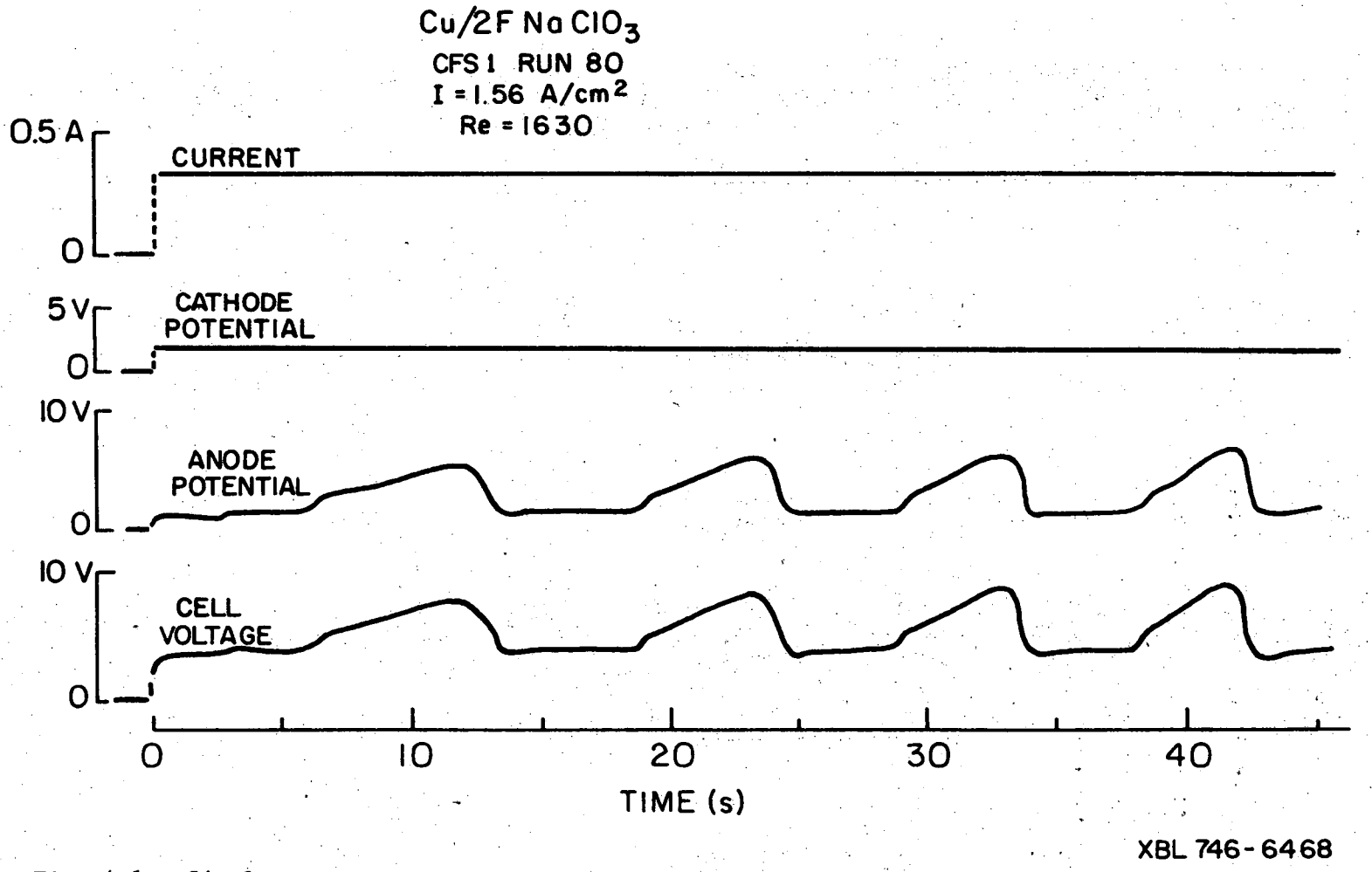

Fig. 4.1. Simultaneous electrical measurements. Tracings of oscillograph recording. Cu/2F $NaClO_3$; channel flow system no. 1.; current density = 1.56 A/cm^2. Anode and cathode potentials measured relative to saturated calomel electrode.

(a) Anode Potential Behavior below 1 A/cm^2 in Channel No. 1.

Below 0.5 A/cm^2, no periodic variations in potential were observed in channel #1 at flow rates from 14.2 to 479 cm/s. In the current density range from 0.5 to 0.8 A/cm^2, the first evidence of periodicity was observed: rectangular waves of non-uniform period and amplitude, 0.5 V (Fig. 4.2a).

(b) Low Current Density Range, 1-5 A/cm^2. With Current densities in the range 0.7 to 1 A/cm^2, the high plateau of the rectangular wave may persist and develope into a peak of several volts magnitude. Above 1 A/cm^2, the characteristic waveform for dissolution in channel #1 is shown in Fig. 4.2b. Waveforms in this range are characterized by an interval of low potential dissolution followed by a step to a potential plateau; the plateau then gradually slopes upward into a potential peak.

(c) High Current Density Range, 5-100 A/cm^2. With experiments conducted at current densities increasing in the range of 1 to 5 A/cm^2, the plateau and step structure becomes increasingly indistinct. At about 5 A/cm^2, the potential cycle is resolvable only into an upward sweeping curve followed by a relatively abrupt (but smooth) drop to the lowest potential of the cycle (Traces c,d). This sawtooth waveform is characteristic of the potential oscillations observed with channel #1 (to 33 A/cm^2) and with the jet (to 70-100 A/cm^2).

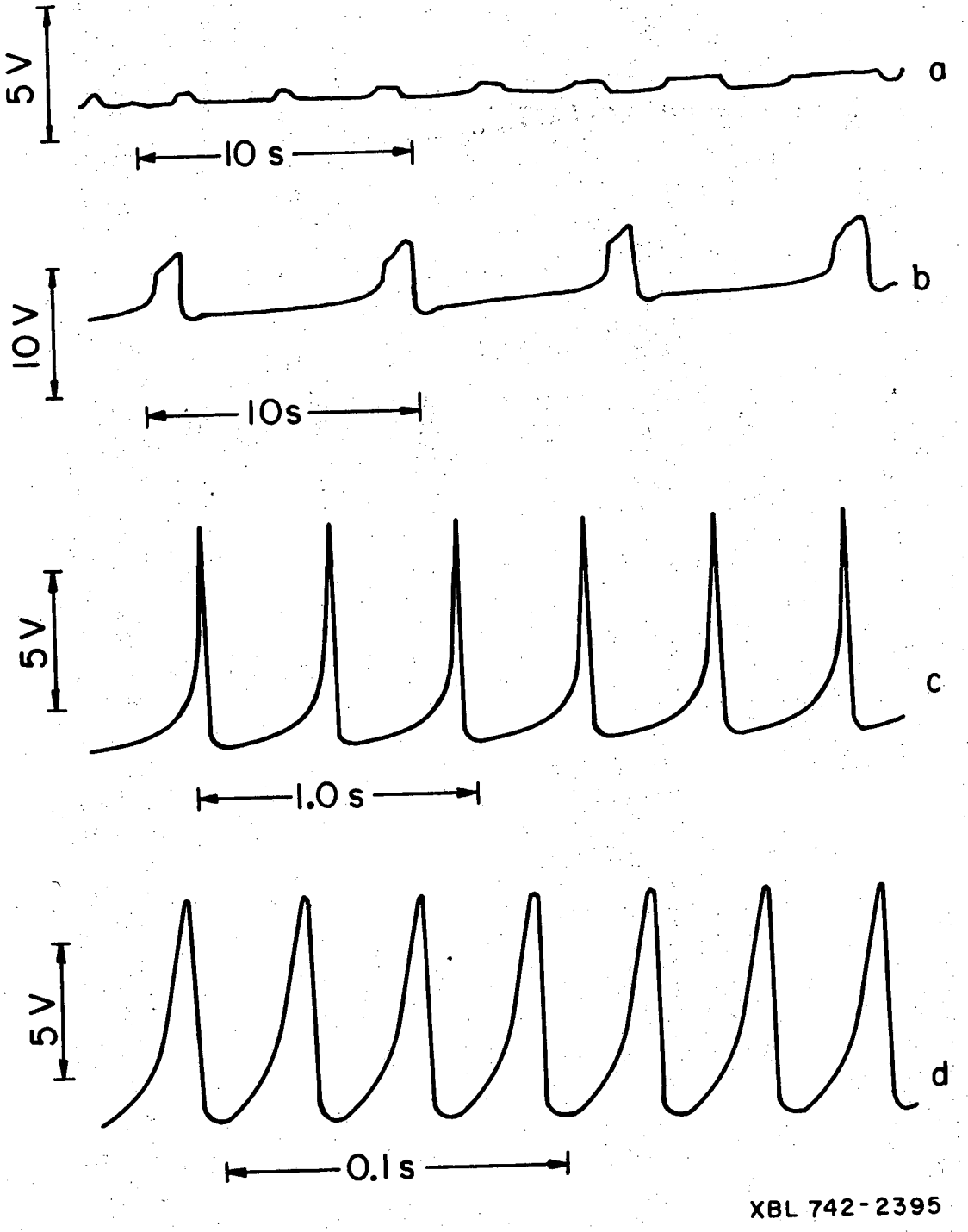

Fig. 4.2. Characteristic Oscillation Waveforms. Cell voltage tracings. Cu/2F $NaClO_3$; channel flow system no. 1. (a) current density = 0.61 A/cm^2, Re = 425; (b) 1.83 A/cm^2, Re= 6810; (c) 6.57 A/cm^2, Re = 6810; (d) 22.4 A/cm^2, Re = 6810.

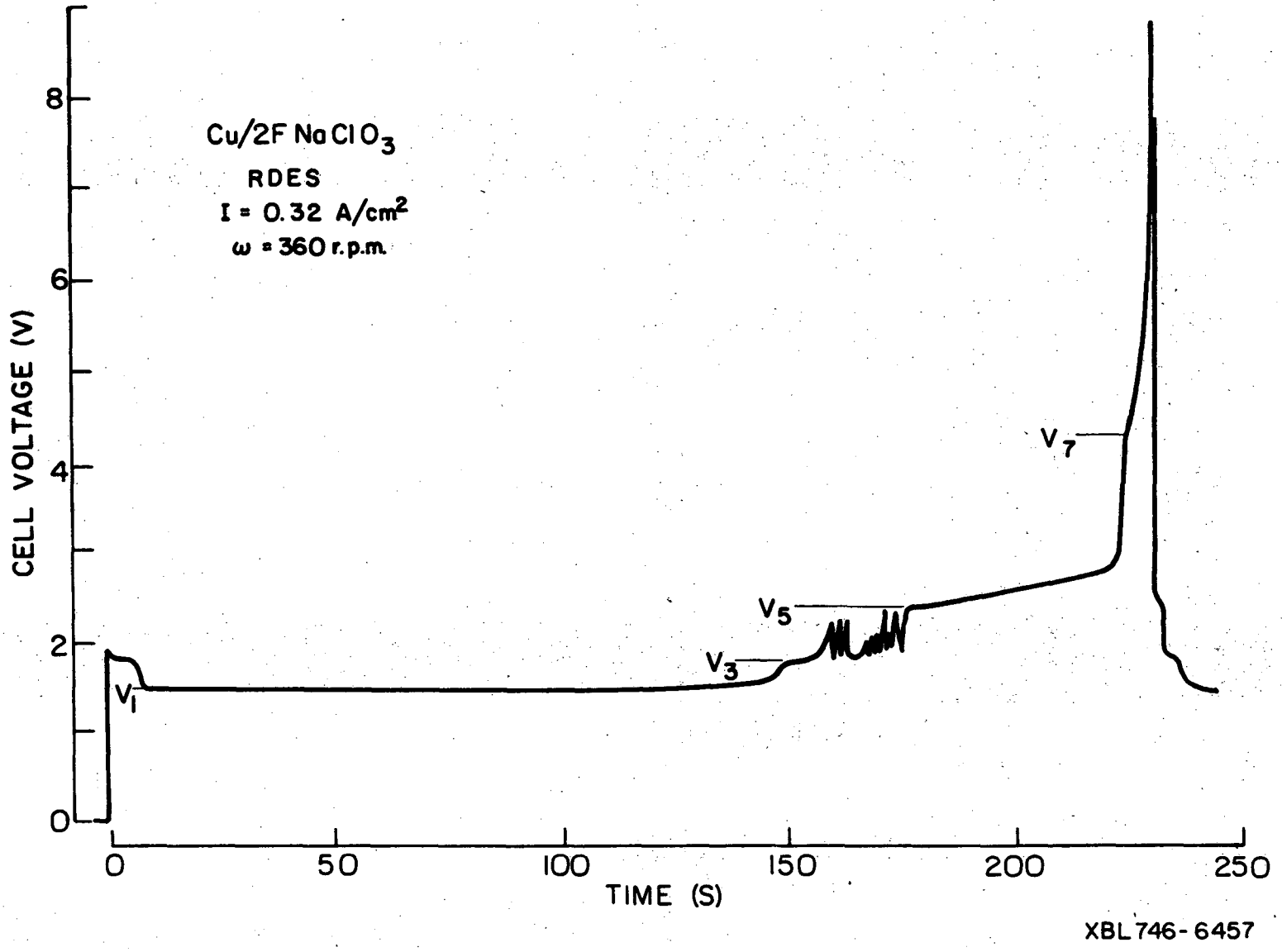

Fig. 4.3. Low Current Density Oscillation Waveform. Rotating disk electrode system.

Fig. 4.4. Oscillation Waveforms at High Current Densities. Cu/2F $NaClO_3$; Jet; ordinate; cell voltage; abscissa; time. Coordinates of lower left edge of photos, (cell voltage, time): photos A-F, K, L, (0 V, 0 s); photos G. H, I, J, (40 V, 0 s).

Photo	Current Density (A/cm^2)	Flow Rate (cm/s)	Time Scale (10^{-3}s/large division)	Voltage Scale (V/large division)	Comments
A	27	0	10	10	12 volt amplitude
B	27	94	10	10	12 volt amplitude
C	27	355	10	10	12 volt amplitude
D	75	0	10	20	
E	75	94	10	20	Dual waveform
F	75	355	10	20	
G	133	0	1.0	20	
H	133	94	1.0	20	
I	133	355	1.0	20	
J	133	0	0.2	20	Detail of h.c.d. wave
K	95	94	1.0	20	Detail of dual wave
L	95	355	1.0	20	Detail of dual wave

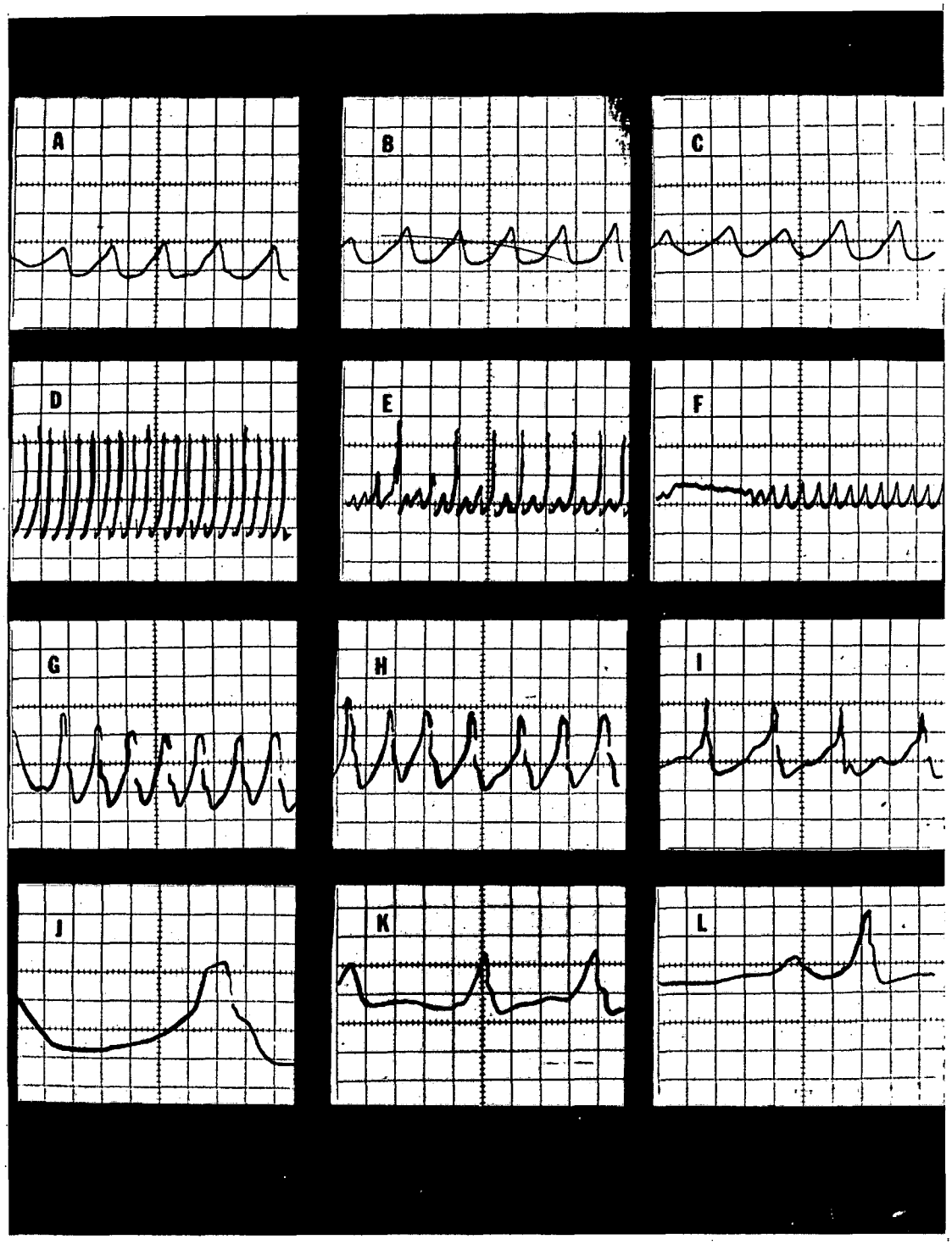

XBB 745-3288

Fig. 4.4. High Current Density Oscillation Waveform. (See caption on preceding page.)

(d) Anode Potential Behavior above 100 A/cm^2. From 70- to 100 A/cm^2, cycle amplitude undergoes an increase from about 15 to 50 volts. In the high amplitude waveform, the fall from peak potentials may be resolved into a rapid drop (duration, 10^{-5}s) followed by a slower drop to the lowest potential of the cycle. The high amplitude and transitional waveforms, shown in Fig. 4.4, were observed in the channel #2 (to Re=1220) and with the jet (up to 190 cm/s).

With the rotating disk, the same sequence is observed in the development of the low current density waveform at increasing current densities. However, the low amplitude potential peaks were observed at current densities down to 0.28 A/cm^2, at a rotational velocity of 360 r.p.m. From 0.28- to 0.5 A/cm^2, the unit cycle shows considerable structure: a succession of potential plateaus and rapid, non-uniform fluctuations in potential occur before the peak develops. (See Fig. 4.3)

5. Regularity of Waveform and Anomalous Behavior

The term "regularity of waveform" is used to refer to the degree of similarity between consecutive potential cycles observed during the course of a single dissolution experiment. For example, an extremely high degree of regularity was attained with one run (channel #1, 2F $NaClO_3$, Re=200, I=4.16 A/cm^2) after 25 s of dissolution. For a sampling of 20 consecutive cycles, the standard deviations of amplitude and period were each less than 2%. Such a high degree of regularity is exceptional: changes in period length or amplitude of 5% or more are commonly found for a single dissolution run. Sample tracings are shown in Figs. 4.5 and 4.7.

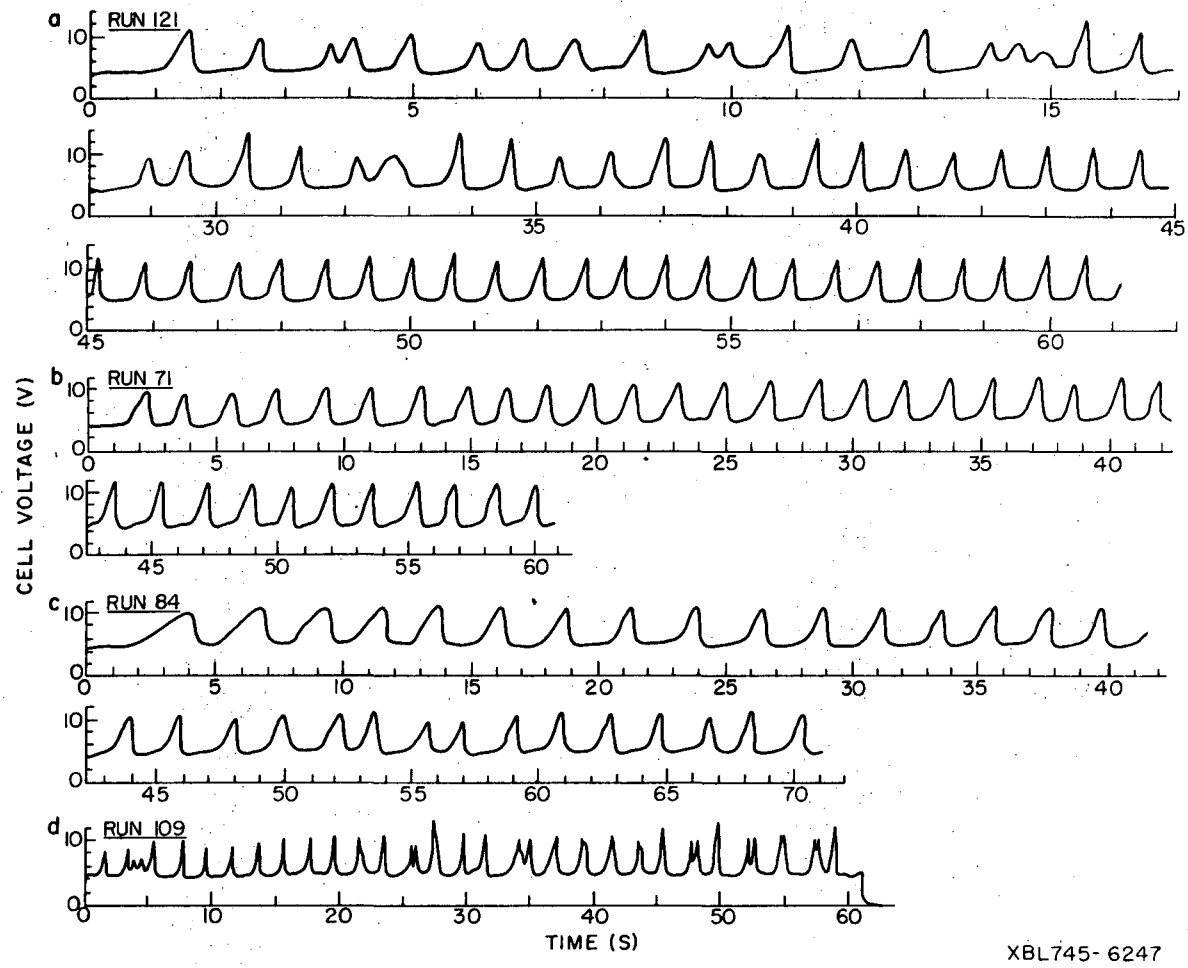

Fig. 4.5. Regular Oscillation Waveforms: Cell Voltage Tracings. Cu/2F $NaClO_3$; channel flow system no. 1; current density = 3 A/cm^2; (a) Re = 200; (b) Re = 708; (c) Re = 1630; Re = 6810.

At current densities below about 5 A/cm^2, the degree of regularity may change considerably during the course of a single dissolution run. Figure 4.5 shows cell voltage traces for dissolution at 3 A/cm^2 using the channel #1 at Re=200, 708, 1630, 6810. In trace (a), an interval of highly regular cycles began after 40 seconds of dissolution. In trace (b), cycles were similar throughout the course of the experiment. Trace (d) contains only a short interval in which consecutive cycles are of uniform amplitude and period. As a general rule, the first few oscillation cycles were longer by a factor of two or three than the steady state cycles. Except for the initial lengthening of the cycles, the variations of regularity during an experiment were unpredictable. No correlations were found between deviations of regularity and current density, flow rate, or experimental times.

On occasion, highly irregular and unreproducible waveforms arose under experimental conditions which normally produced regular waveforms. Samples of anomalous waveforms are shown in Fig. 4.6. In trace (a), alternate cycles were similar in waveform. Traces (b) and (c) show repeating patterns with three and four peaks, respectively. Trace (c) demonstrates that an initially regular pattern may degenerate into random fluctuations, which, in turn, may be followed by periods of greater regularity. In other experiments, an anomalous pattern might develope after many regular cycles, persist for a time, and, finally, revert to a regular waveform. Anomalous waveforms predominated in no more than 15% of dissolution experiments below 5 A/cm^2.

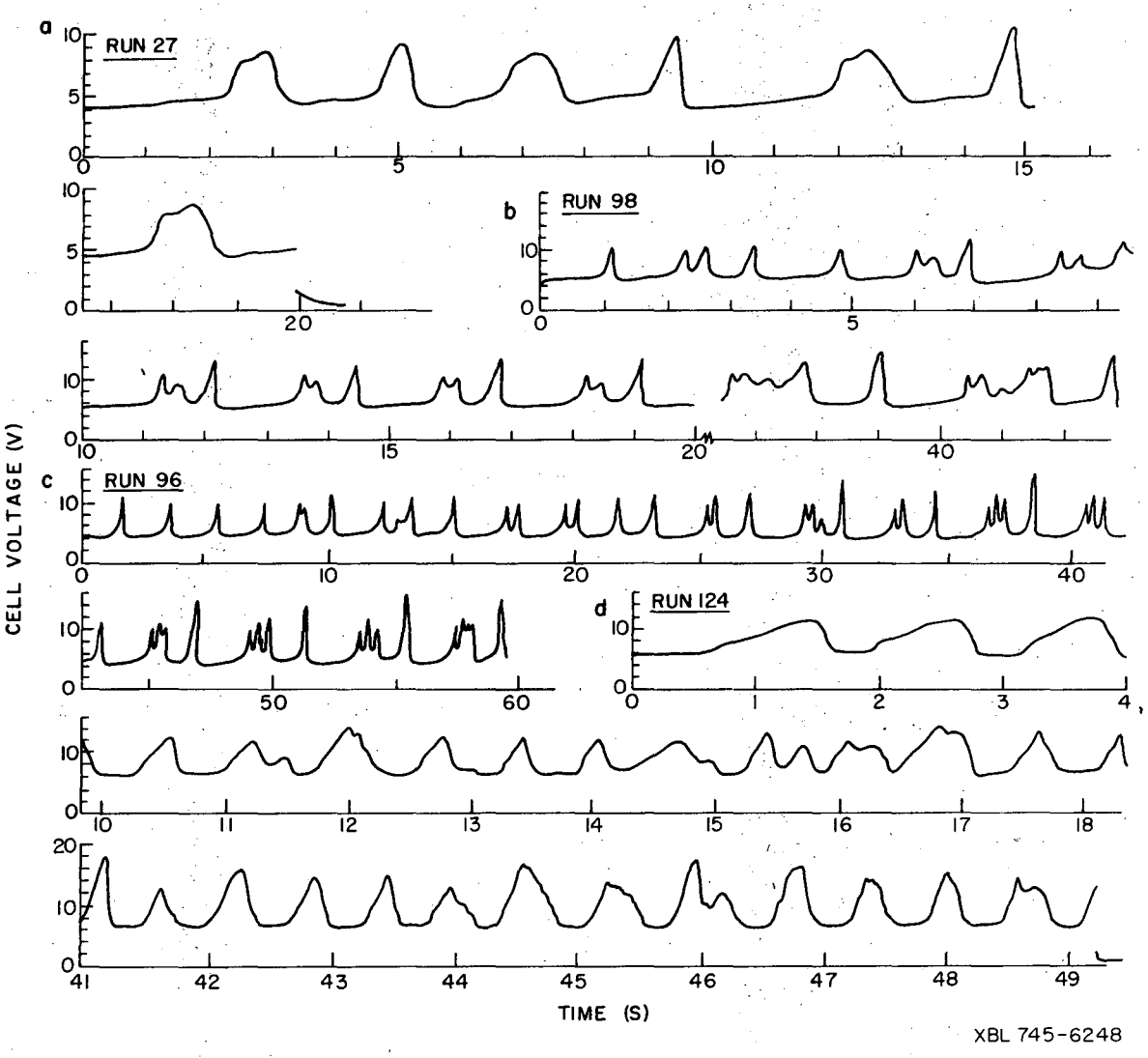

Fig. 4.6. Anomalous waveforms: cell voltage tracings. Cu/2F $NaClO_3$; channel flow system no. 1; (a) current density = 2.42 A/cm^2, Re = 708; (b) 4.17 A/cm^2, Re = 3990; (c) 3.05 A/cm^2, Re = 3990; (d) 4.67 A/cm^2, Re = 200.

Such anomalous behavior may reflect "out-of-phase" oscillations sustained on different portions of the same anode surface. This conclusion is based on the following observations: During experiments exhibiting regular waveforms, a red, porous layer of solid reaction products (found by X-ray diffraction analysis to consist of Cu_2O*) was observed to detach from the entire anode surface immediately following the fall from peak potentials. During Run 27 (Fig. 4.6a), similar red layers were observed to detach alternately from the upstream 1/3 and the downstream 2/3 of the anode surface. After the experiment, the anode was removed from the cell and examined. The upstream 1/3 of the anode surface was covered with an adherent layer of Cu_2O while the downstream end was free of any visible layers and had a polished appearance. The demarcation between the two portions of the anode was sharp, linear, and perpendicular to the direction of electrolyte flow. Alternate cycles on the two distinct portions of the anode thus resulted in alternating waveforms.

It is a likely deduction that the anomalous waveforms showing three-peaked, four-peaked, and random fluctuations result from out-of-phase oscillations on, respectively, three, four, and many distinct areas of the anode surface.

---

*See Chapter IV-B.3.

As with the variations of regularity within a single run, the occurence of the irregular waveforms could not be predicted. Irregularities in waveform may be the consequence of spacial non-uniformity of the cold-working or cleaning of the copper surface prior to dissolutions. Also, the accidential retention of resistive solid reaction products on one portion of the anode after a given cycle may temporarily change the current distribution for the following cycles. Different portions of the surface would then be subjected to different local current densities and, hence, different characteristic oscillation frequencies.

In the remainder of this dissertation we will confine our discussion to the more reproducible, regular, saw-tooth waveforms.

6. Persistence of the Oscillations

It is important to determine whether the anode potential oscillations represent: (1) a sustained mode of dissolution, in which the cycling continues as long as experimental conditions are maintained; or (2) a transient mode of dissolution, in which the oscillations dampen with continued dissolution until a steady potential is attained. The question concerning the persistence of the oscillations may be answered within the context of the experimental dissolution times.

Dissolution times were chosen to maintain the surface of the anode within 0.02 cm of the plane of the channel floor. This constraint allowed experimental times sufficient to produce hundreds of cycles at current densities above 10 A/cm^2. (The anodes could not be advanced during dissolution because of the undissolving insulation coating on the electrode sides.)

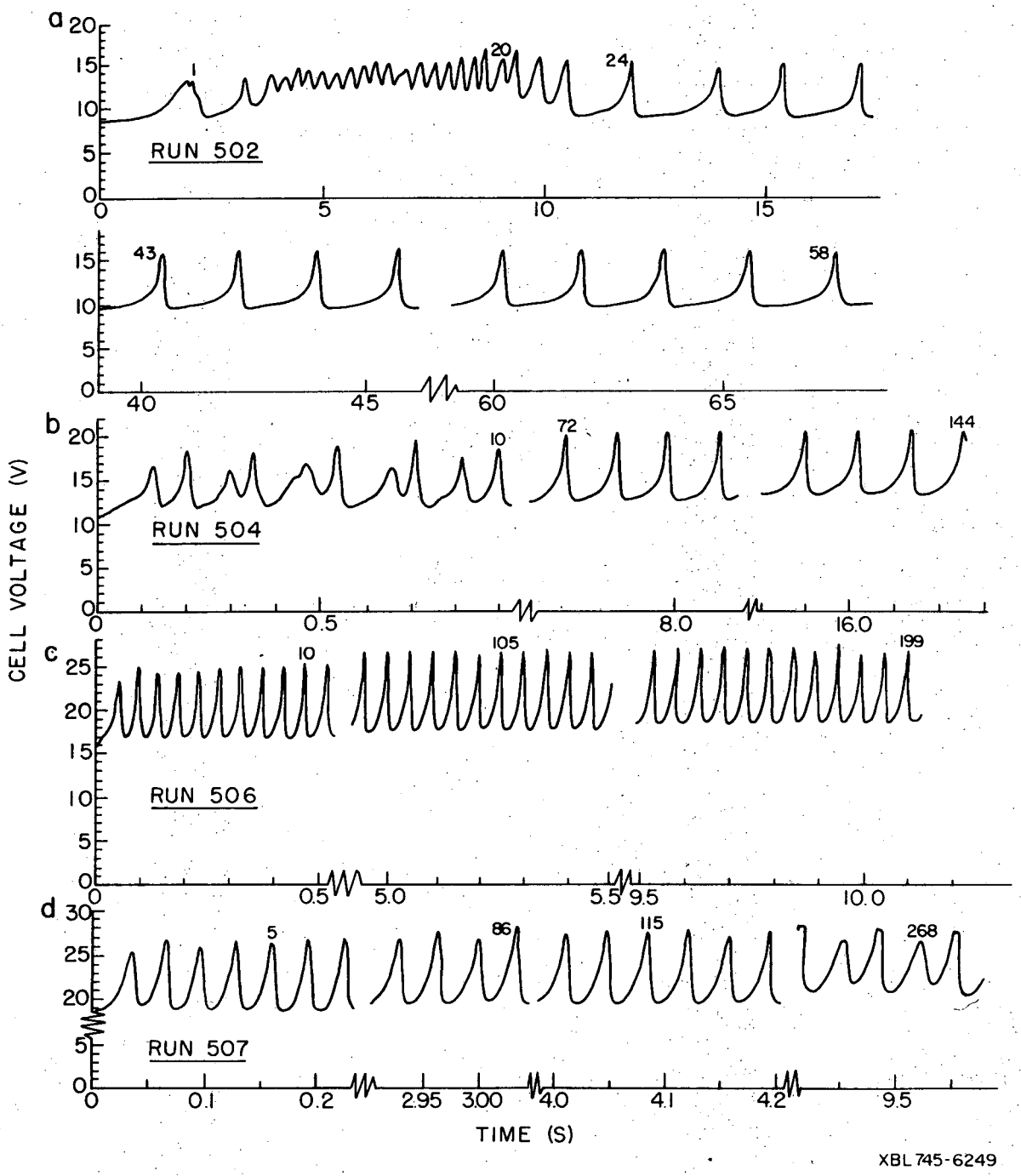

Fig. 4.7. Oscillation waveforms at different intervals of dissolution. Cu/2F $NaClO_3$; channel flow system no. 1; Re = 6810. (a) 8.3 A/cm^2; (b) 12.2 A/cm^2; (c) 17.3 A/cm^2; (d) 19.9 A/cm^2.

In Fig. 4.7, sample cell voltage tracings are shown for dissolution at Re=708 and current densities of 8-20 A/cm^2. Cycle numbers (counting from the first cycle after beginning of dissolution) are shown on the traces. In trace (a), initial cycles dampened rapidly, then developed into highly regular cycles. In trace (b), initially irregular cycles became uniform in amplitude and period after about ten cycles; the remaining 134 cycles showed little change in form. Trace (c) shows sawtooth cycles persisting for 199 cycles. In trace (d) intervals of different degrees of regularity alternate, but no trend toward a dampening is evident after 270 cycles. These traces are typical of the many-cycled dissolution runs in channel #1.

In conclusion, no dampening-out of oscillations to a permanent steady state potential was observed with channel #1. Irregular patterns or random fluctuations of potential, when then arose, tended to evolve into sustained oscillations of more uniform character. Apparently, the oscillations represent a persisting mode of dissolution under the experimental conditions investigated.

7. Dependence of Oscillation Period on Experimental Parameters

a. Dependence of Oscillation Period on Current Density.

Oscillation period decreases with increasing (galvanostatic) current density, for experiments conducted under fixed conditions of electrolyte flow rate, composition (including pH), and temperature. The logarithm of oscillation period is plotted against the logarithm of current density in Figs. 4.8-4.16. Each data point represents the results of a single dissolution experiment. "Oscillation period" is

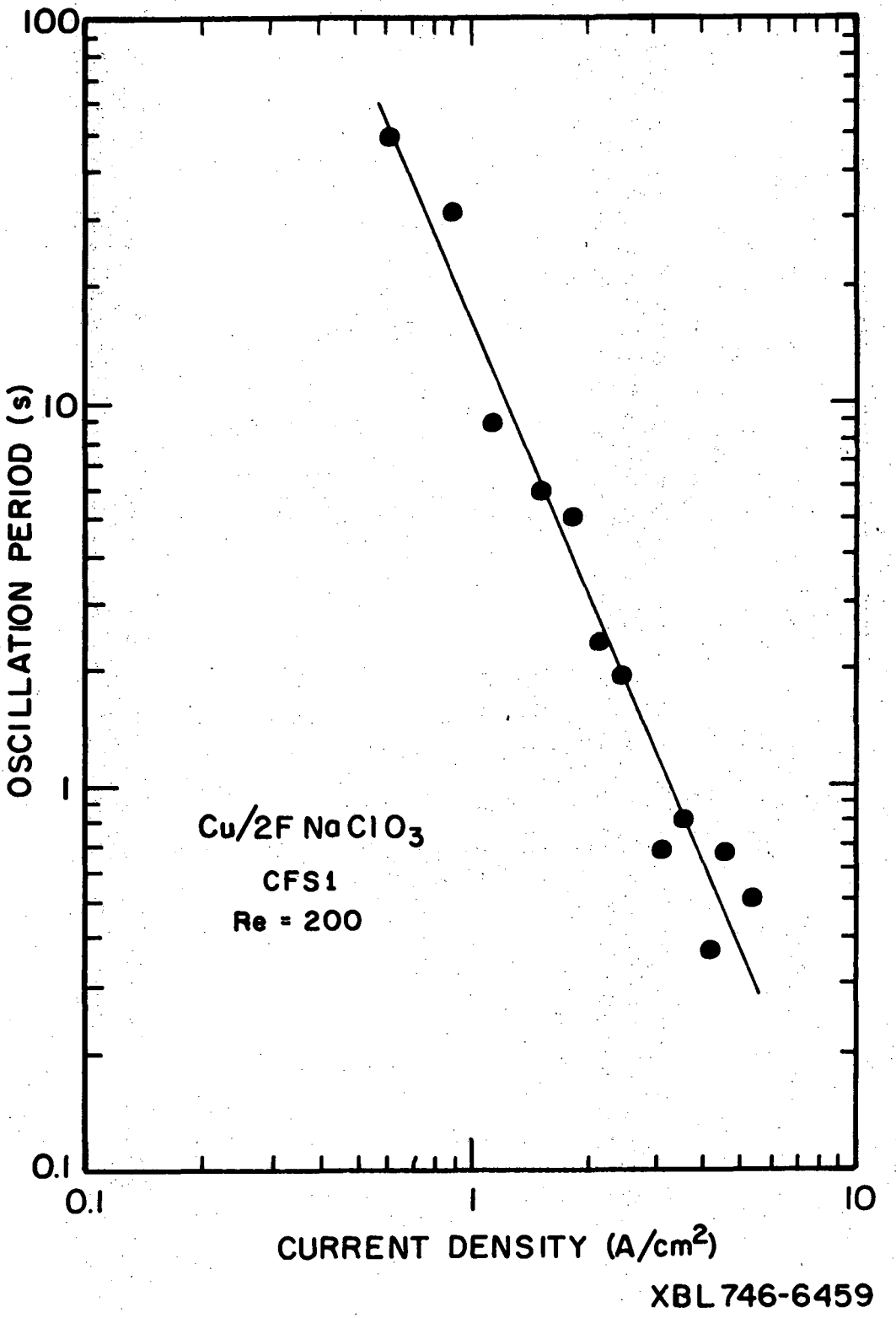

Fig. 4.8. Dependence of average oscillation period on current density. Channel flow system no. 1.

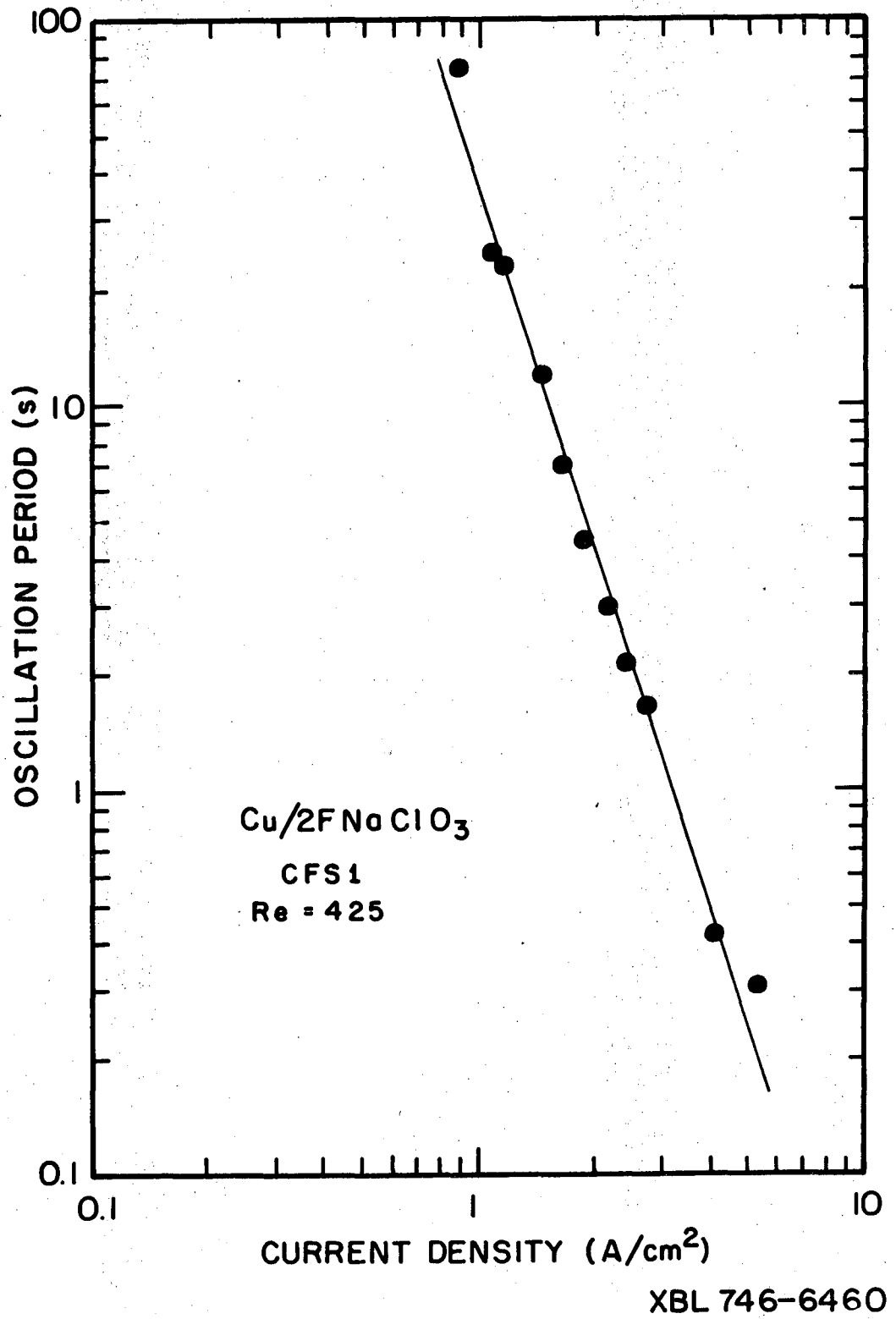

Fig. 4.9. Dependence of average oscillation period on current density. Uncoated electrodes.

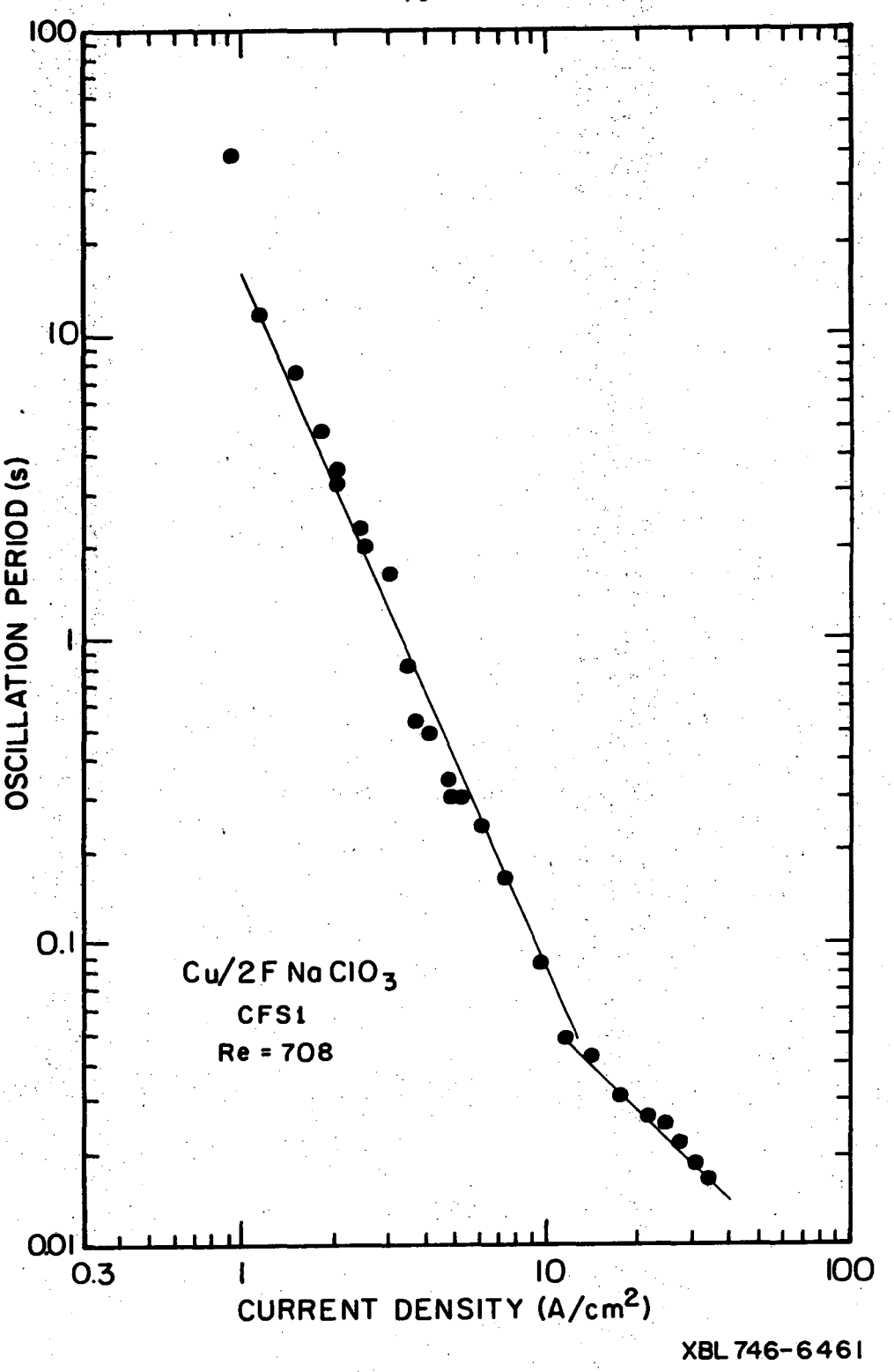

Fig. 4.10. Dependence of average oscillation period on current density.

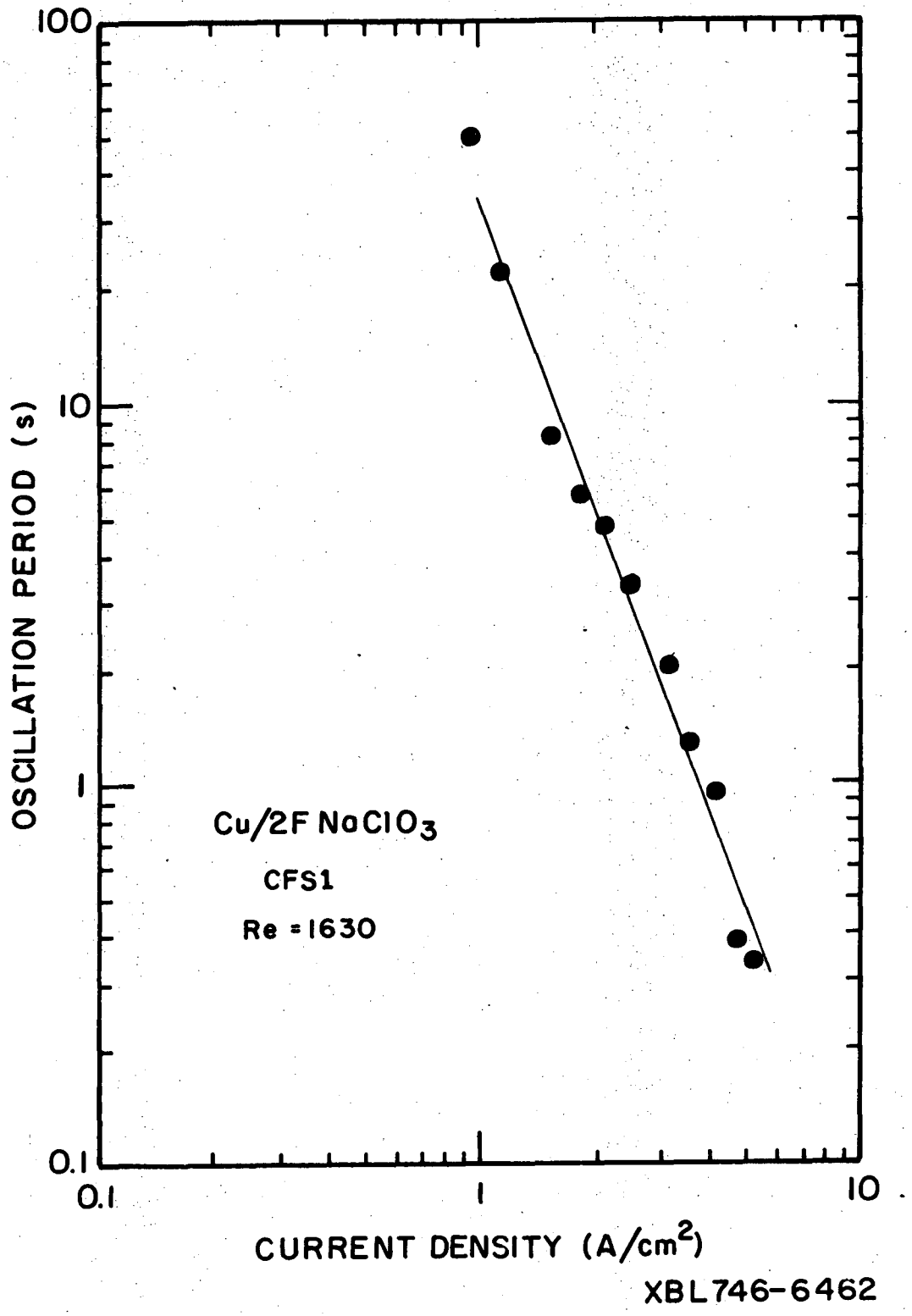

Fig. 4.11. Dependence of average oscillation period on current density.

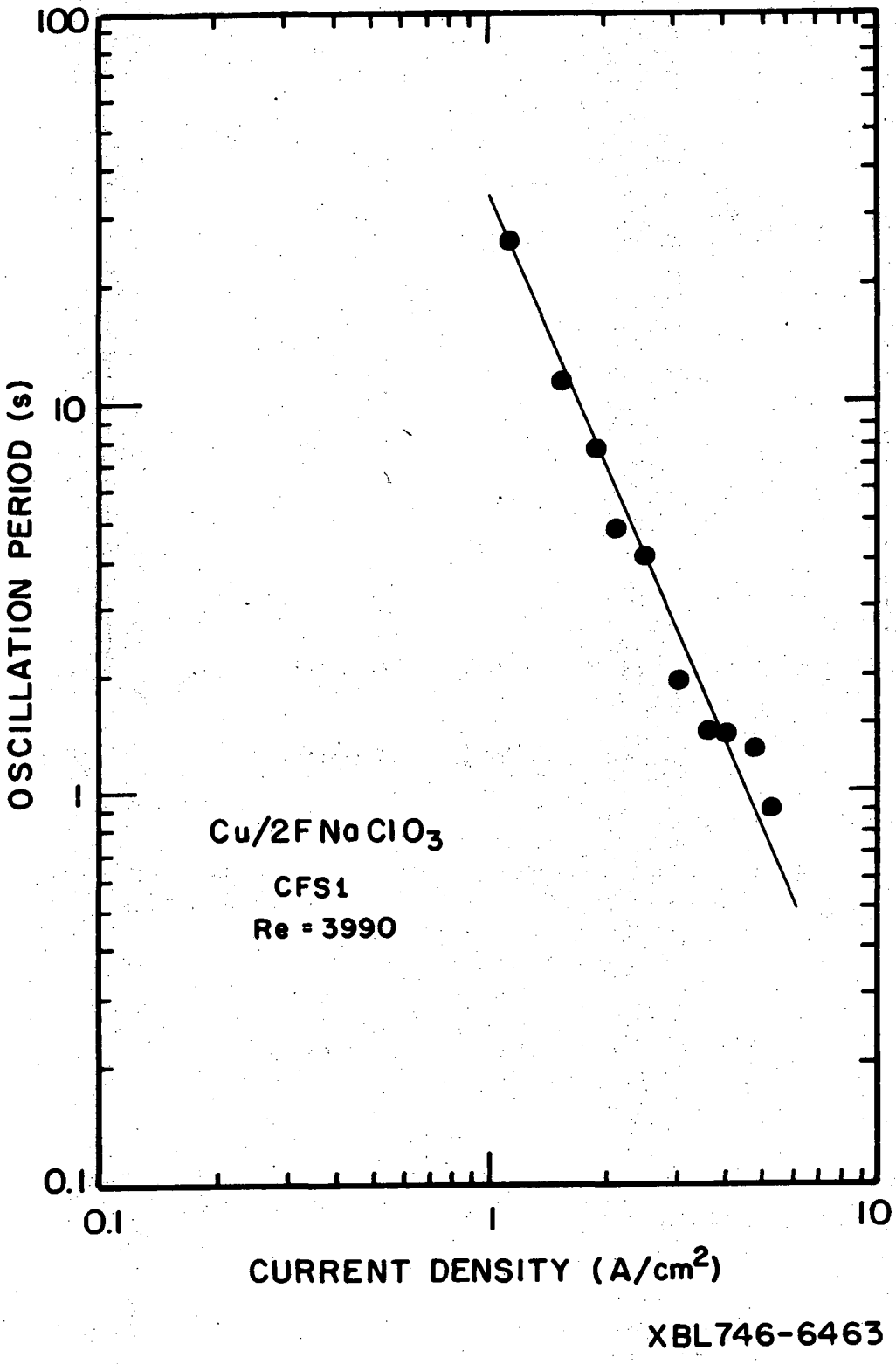

Fig. 4.12. Dependence of average oscillation period on current density.

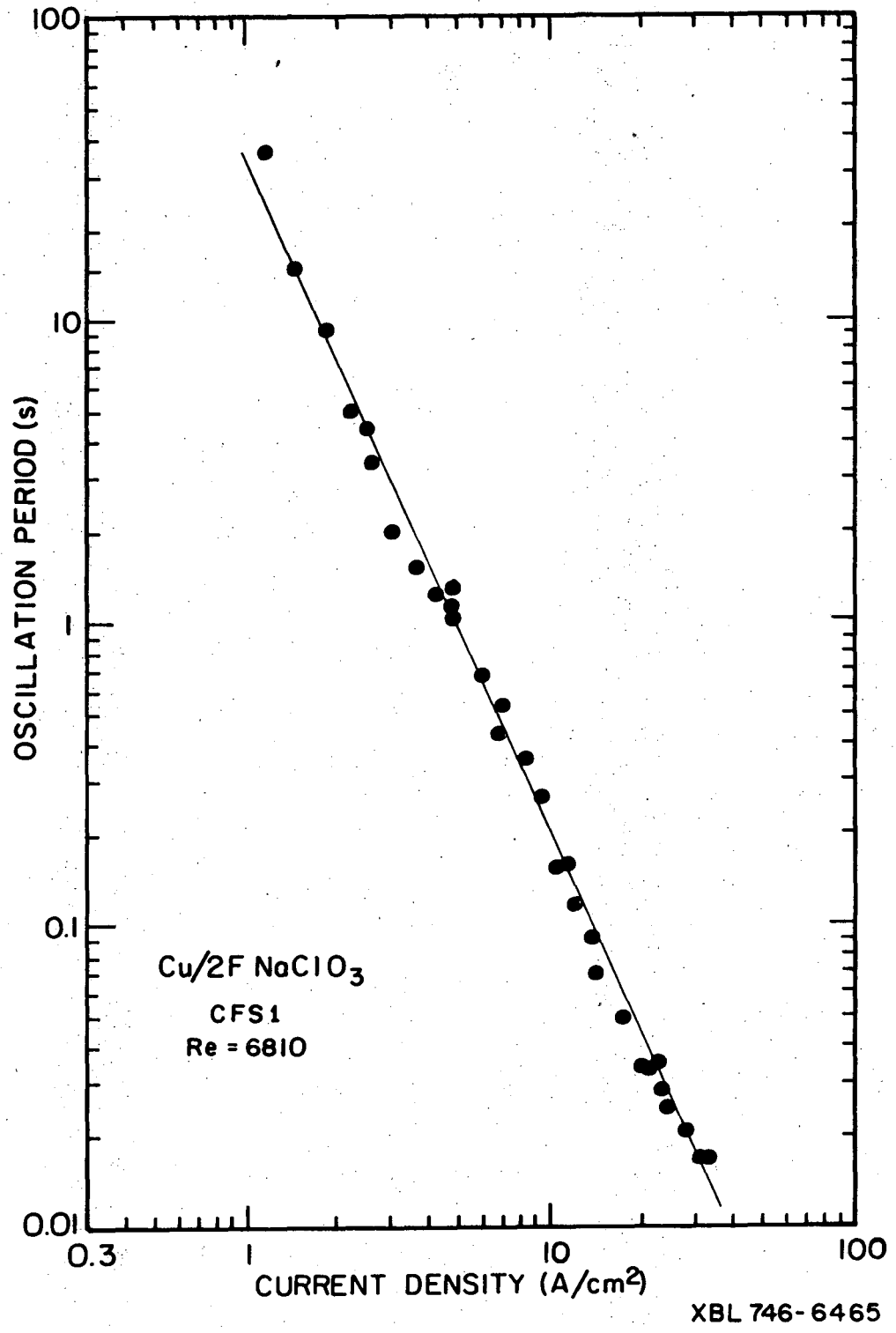

Fig. 4.13. Dependence of average oscillation period on current density.

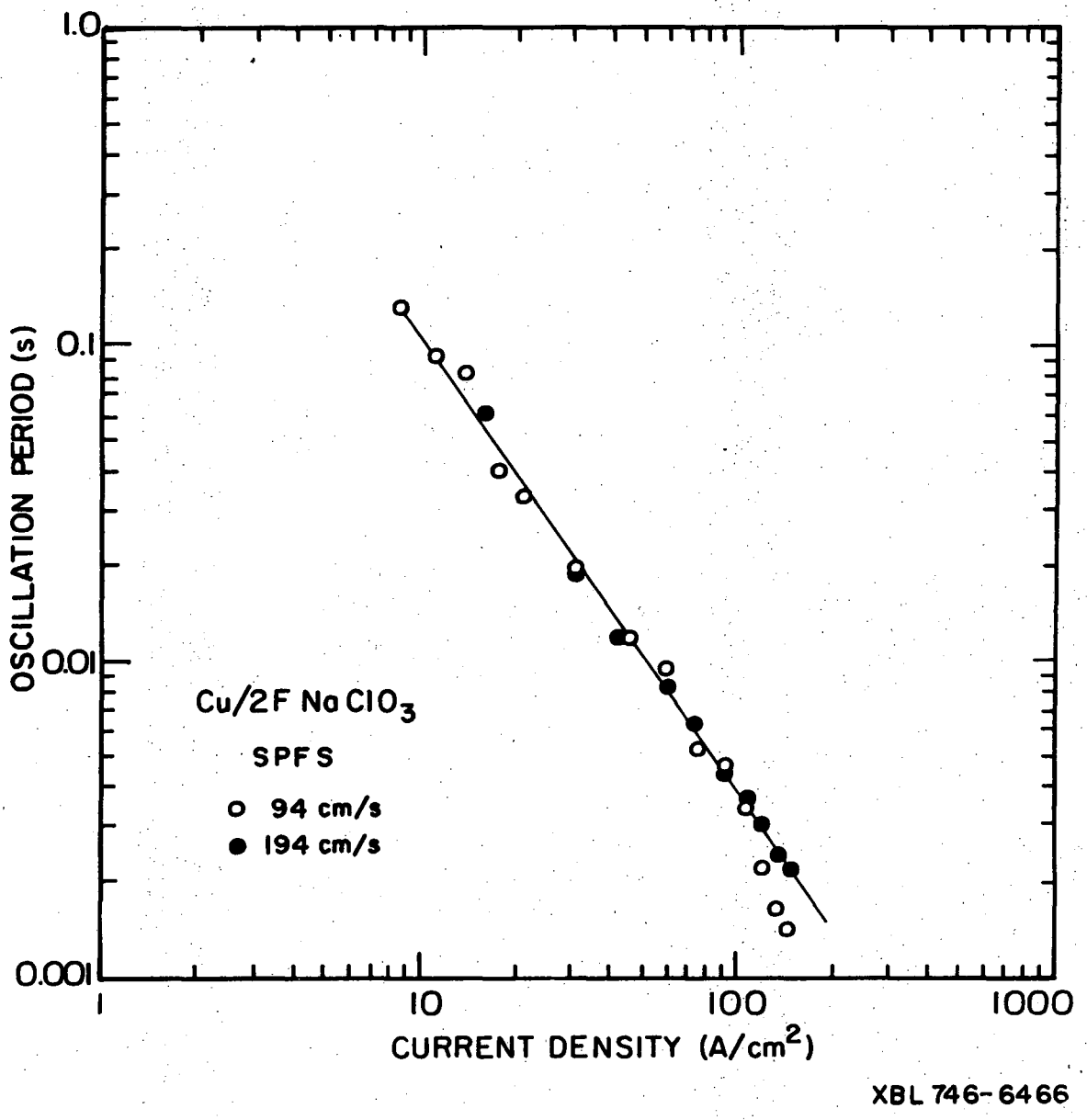

Fig. 4.14. Dependence of average oscillation period on current density. Stagnation point flow system.

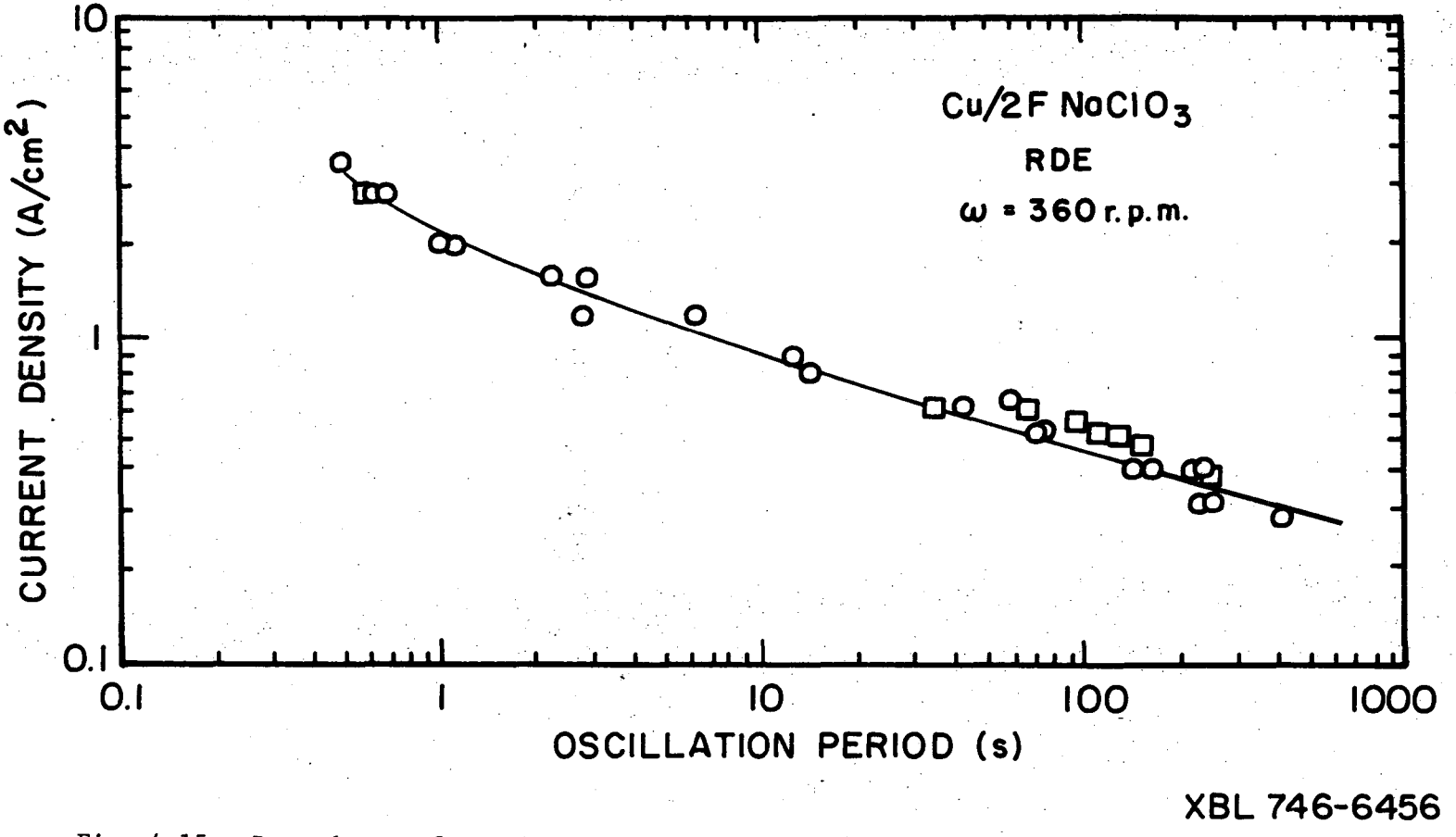

Fig. 4.15. Dependence of oscillation period on current density at low current densities rotating disk electrode system.

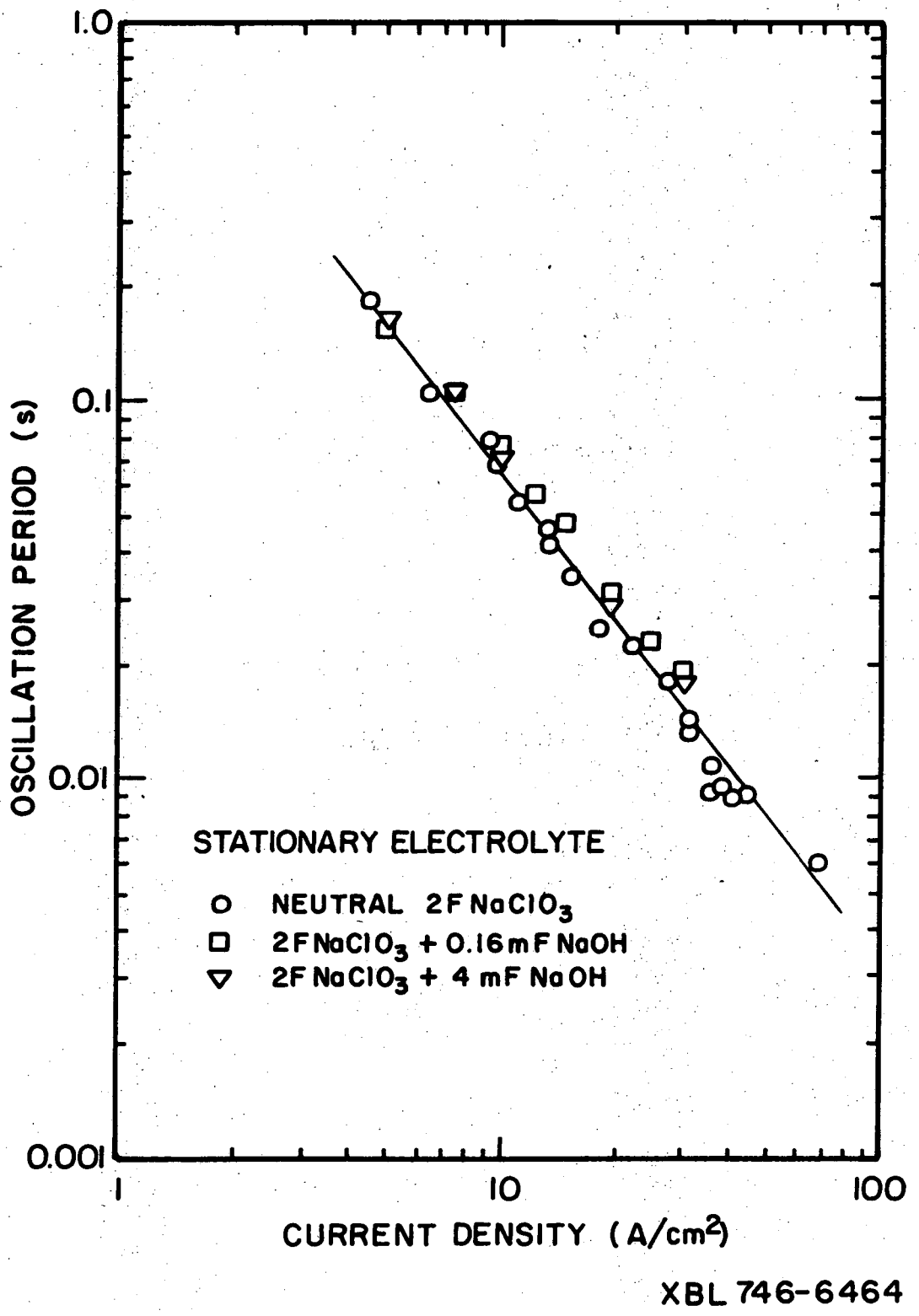

Fig. 4.16. Dependence of average oscillation period on current density in natural convection. Shielded anode surfaces facing upwards.

taken as the average cycle length of at least five consecutive cycles chosen from those portions of the potential-time recording showing greatest regularity of waveform. (Any irregular waveforms were thus excluded from the average). At the lower end of the current density range investigated with the rotating disk, only one or two potential cycles could be obtained within reasonable experimental times. Therefore the oscillation periods reported in Fig. 4.15 do not represent averages.

In all experiments reported in this section, current density was calculated by dividing the value of current by the geometrical area of the anode. In calculating current density, no attempt was made to correct for surface irregularities or for changes in area resulting from changes in surface topography during dissolution.

The double-logarithmic plots of Figs. 4.8-16 are seen to be linear. For both flowing and stationary electrolyte, the relation between period and current density may be represented by an empirical equation of the form:

$$\log(T/T_o) = -a \log(I/I_o) \qquad (1)$$

or, equivalently,

$$T = T_o(I/I_o)^{-a} \qquad (2)$$

where T = oscillation period; I = current density; and (-a) is the slope of the double-logarithmic plot. The quantity T_o is the oscillation period at an arbitrary current density, I_o. Values of (a) and T_o (at I_o = 1 A/cm^2) are presented in Table IV-2, together with the

Table IV-2. Parameters of an Empirical Equation Describing the Dependence of Oscillation Period on Current Density.[a]

System	Current Density Range (A/cm^2)	Flow Rate	(a)	T_o (I_o=1A/cm^2) (s)	Comments
Channel No.1	0.61- 5.4	14.2 cm/s	2.32	15.9	
"	0.88- 5.28	30	3.06	35.6	Uncoated electrodes
"	0.67-11.4	50	2.30	15.4	
"	0.90- 5.21	115	2.70	33.8	
"	1.15- 5.3	280	2.25	30.1	
"	1.14-33.4	479	2.25	34.8	
"	11.4 -33.4	50	0.96	0.50	
Jet	8.6 - 146	94,194 cm/s	1.4	2.5	
Stationary Electrolyte	1 - 100	----	1.3	1.2	pH neutral, 10.2; 11.6
Rotating disk	0.28-1	360 r.p.m.	3.5	7	

[a] Data fit by an equation of the form, $\log(T/T_o) = -a\log(I/I_o)$. For channel flow system no. 1, parameters a and T_o (at I_o=1 A/cm^2) were obtained by the method of least squares.

experimental conditions and the ranges of current densities over which Eq. (1) applies.

The linearity of the plots is evident for as many as three orders of magnitude of period, corresponding to two orders of magnitude of current density. It is remarkable that so complex a phenomenon is represented by a simple empirical equation over so broad a range of current densities and with so great a degree of reproducibility. Data points deviate from the fitted line by at most ± 30%, and a comparable maximum deviation in average period was obtained for different dissolution experiments conducted under the same experimental conditions. The scatter is likely to be the consequence of the disparity between calculated (geometric) current density and true current density, which is a function of the changing anode surface area. Because of the power relation between current density and period, fluctuations in true area introduce even greater fluctuations in true area introduce even greater fluctuations in period.

An explanation for the dependence of oscillation period on current density requires experimental results to be presented in later sections. We shall return to a discussion of these results in Chapter V.

b. Dependence of Oscillation Period on Electrolyte Flow Rate

At fixed values of current density, oscillation period increases with increasing flow rate. The logarithm of oscillation period is plotted against the logarithm of a measure of electrolyte flow rate in Figs. 4.17,18,19 for low, intermediate, and high current densities, respectively. The dependence of period on flow rate is relatively weak compared to the dependence of period on current density.

At this point, a qualitative explanation is offered for the dependence of period on flow rate. The effect of increased electrolyte flow is to enhance the transport of dissolved reaction products away from the anode surface by convection. Solid reaction products formed by precipitation near the anode surface may also be transported by entrainment in the flow. It will be shown in Sections IV-B, C that the increase of anode potential during the cycle reflects the growth of resistive layers of solid reaction products at the anode electrolyte interface. To a first approximation, breakdown of anode potential occurs upon attaining a critical potential. The buildup of solid layers and of potential toward the critical level is slower at higher flow rates because of the increased removal rate of reaction products into the electrolyte stream. Consequently cycle lengths should increase with increasing mass transport rates.

With the disk electrode, at a low current density (0.8 A/cm^2), oscillation period is found proportional to the square root of rotational rate. However, already at 1.6 A/cm^2, the oscillation period is only weakly dependent on rotation rate over the same range of rotation rate. The relative independence of oscillation period from rotation rate at this current density may reflect a large contribution of free convection to the total convective transport. In this system the anode surface faces downwards. During anodic dissolution, a saturated solution of cupric chlorate should develope near the anode surface at a sufficiently high current density for

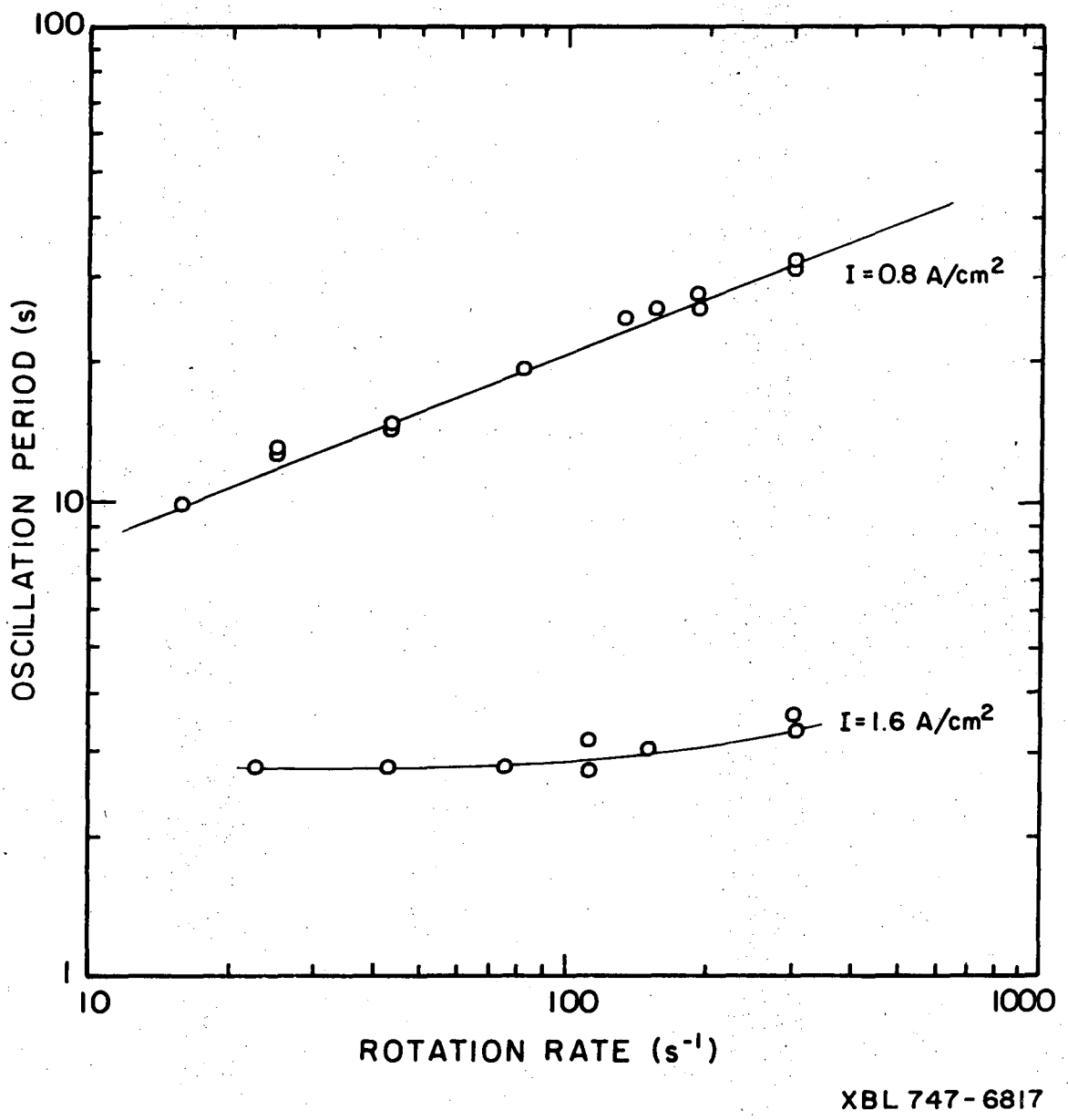

Fig. 4.17. Dependence of oscillation period on mass transport rate (disk rotation rate). Cu/2F $NaClO_3$; rotating disk electrode system.

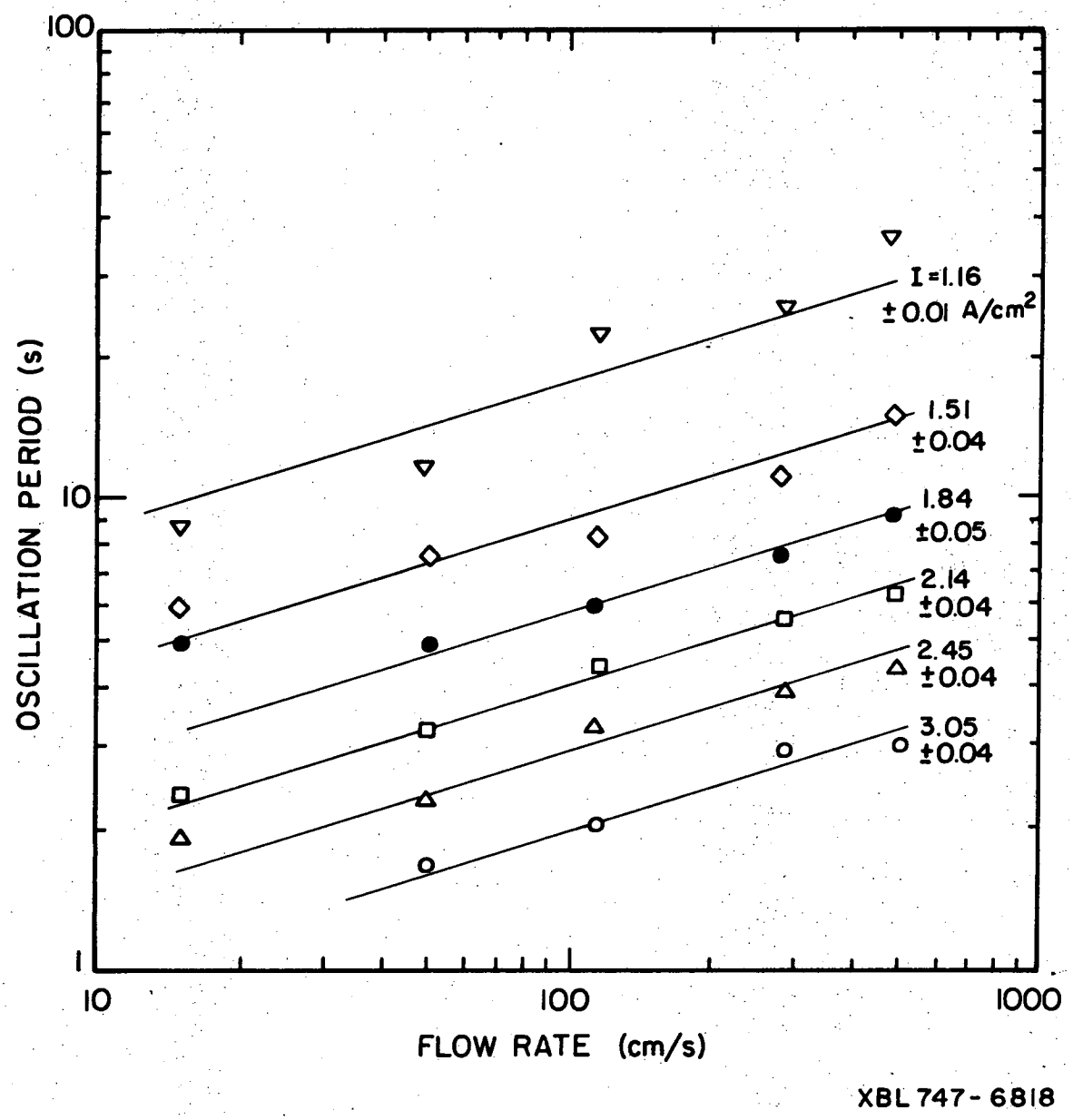

Fig. 4.18. Dependence of oscillation period on electrolyte flow rate flow rate = volume flow rate/(cross sectional area of flow channel. Channel flow system no. 1. Cu/2F $NaClO_3$; current density indicated on the plot.

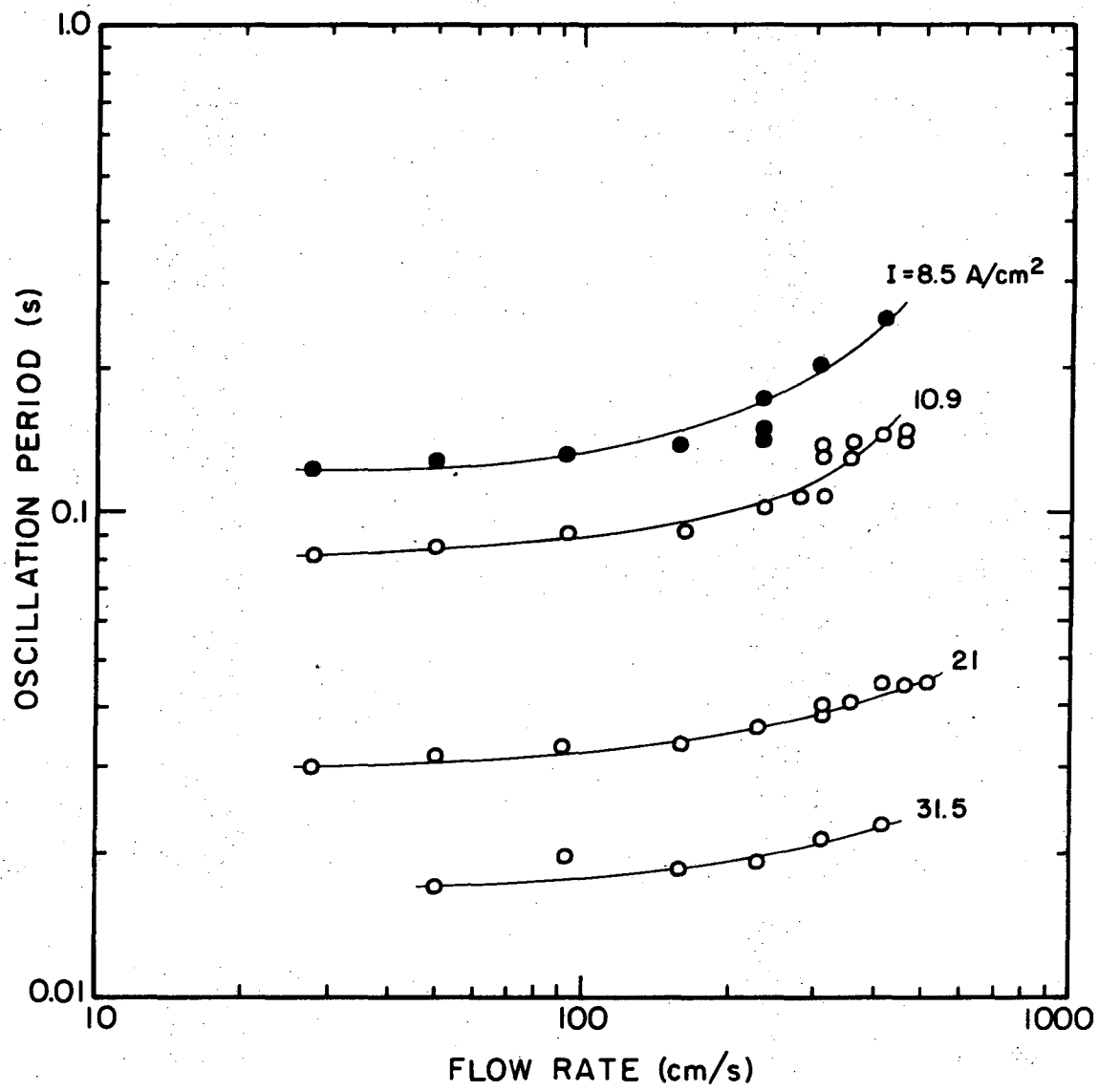

Fig. 4.19. Dependence of oscillation period on flow rate under stagnation point flow. Current density as shown on the plot.

each rotational rate. This solution, being more dense than the bulk electrolyte, will tend to stream downward from a stationary anode surface, being displaced by the less dense bulk electrolyte. With a rotating disk, such free convection may predominate at low rotation rates, leading to a flattening of the log(period)-log(rotational rate) plots. As the rotation rate is increased, the slope should increase to reflect the enhanced contribution of forced convection (See Fig. 4.17, I=1.6 A/cm^2).

With the Channel #1, the logarithm of period is proportional to the logarithm of linear flow rate, with a slope of 0.3 ± 0.05. Figure 4.18 represents a cross-plot of Figs. 4.8, 10-13. Data for a linear velocity of 30 cm/s are not included in Fig. 4.18, as the true electrode area of the uncoated anodes used in that set of experiments is not well defined.

For the Jet system, the data in the double logarithmic plots (Fig. 4.19) are non-linear, but slope upwards at increasing flow rates. The velocity of impingeing jet affects the oscillation period only at velocities higher than about 100 cm/s. The relative constancy of oscillation period at flow rates below 100 cm/s may be the consequence of the retention of solid reaction products on the anode surface. At the high current densities and low flow rates, a porous layer of solid reaction products representing many cycles may accumulate on the anode surface, partially isolating the reacting surface from the influence of the flowing electrolyte.

It is interesting that the power dependence of period on flow rate (or rotation rate) is nearly the same as the power dependence of limiting current density on flow rate (or rotation rate) for the channel #1 and rotating disk results. We have not been able to determine that the correspondence is anything but coincidental.

c. Dependence of Oscillation Period on Bulk Electrolyte pH

Oscillation period decreases with increasing pH of the bulk electrolyte, the effect being strongest at low current densities (Fig. 4.20). The relationship between logarithm of period and logarithm of current density is linear at each value of pH investigated, but there is considerable scatter of the data in the more acidic solutions. The increase in period with increasing hydrogen ion concentration is consistent with the effects of pH on the rate of accumulation of solid cuprous oxide. Increased hydrogen ion concentration enhances the driving force for the oxidation of cuprous oxide by the chlorate ion,

$$2H^+ + \frac{1}{2}\,Cu_2O + \frac{1}{6}\,ClO_3^- = Cu^{++} + \frac{1}{6}\,Cl^- + H_2O$$

We will return to a discussion of this hypothesis in Section IV-B.2, and in Appendix D.

d. Dependence of Oscillation Period on Electrolyte Temperature

Oscillation period is only weakly dependent on electrolyte temperature over a wide range of current densities (7-30 A/cm^2). In Fig. 4.21, oscillation period is plotted against current density on double logarithmic axes for sets of experiments conducted at 4, 24,

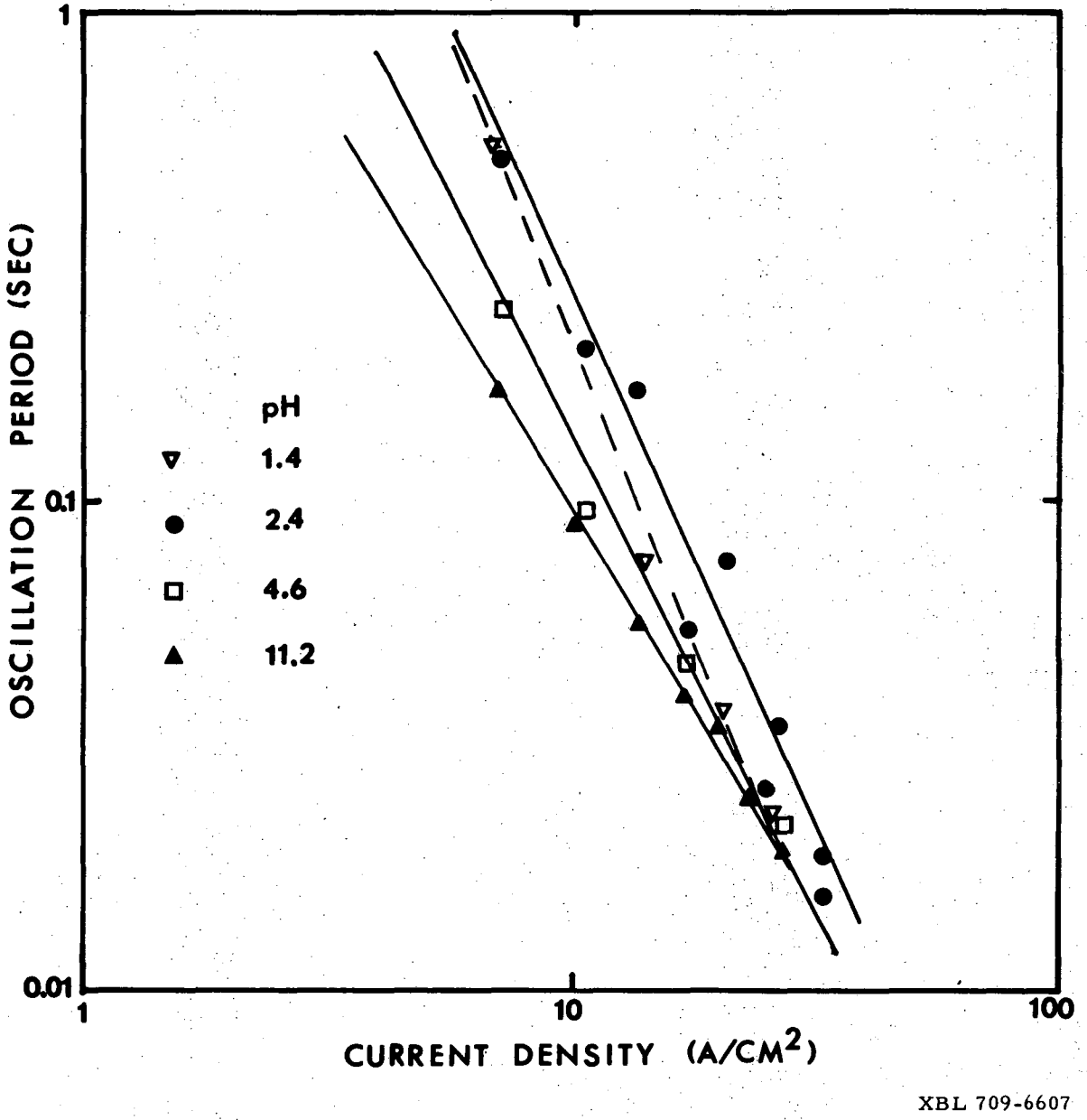

Fig. 4.20. Dependence of oscillation period on bulk electrolyte pH. Cu/2F $NaClO_3$; channel flow system no. 2; Re = 400.

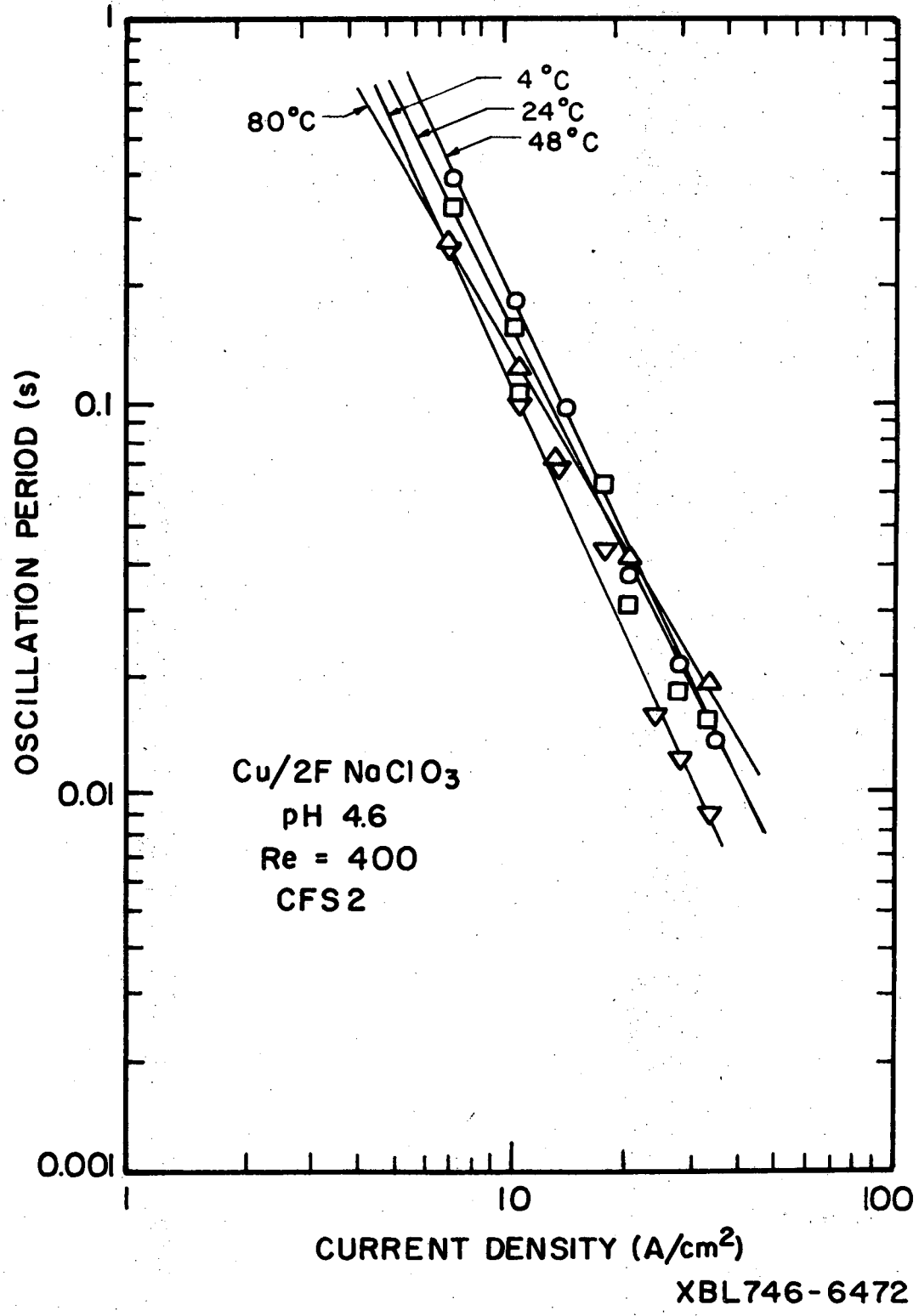

Fig. 4.21. Dependence of oscillation period on bulk electrolyte temperature. Cu/2F $NaClO_3$; channel flow system no. 2; Re = 400.

48, and 80°C. Oscillation period tends to increase with electrolyte temperature, although the effect is not significantly greater than experimental scatter. Earlier it was noted that oscillation period is roughly proportional to limiting mass transport rate. The limiting mass transport rate may be increased by increasing temperature, because of the temperature dependence of the diffusion coefficient and viscosity. For the channel #2, limiting current is proportional to $D^{2/3}$ (See Table III-1). As the quantity $D\mu/T$ is approximately constant, $D^{2/3}$ is roughly proportional to $\mu^{-2/3}$ over a limited temperature range. Between 4 and 48°C, water viscosity decreases by a factor of 2.8 (from 1.56 cp to 0.57 cp). Therefore, limiting current density should increase by a factor of $(1/2.8)^{-2/3} = 2.0$. This is in rough agreement with the observed doubling of period between 4- and 48°C. However the period length at 80°C is not explainable by viscosity effects alone. There are many other possible causes of the temperature dependence of oscillation period. Ionic and electronic conductivity of the transpassive film, chemical and electrochemical reaction rates, and reaction product solubility are all strong functions of temperature.

8. Cell Voltage Measurements and Oscillation Amplitude

In this section, we shall report measurements of cell voltage (or anode potential) of characteristic points on the oscillation cycle. Cell voltage measurements are plotted against current density in Figs. 4.22-4.24. The data points labeled V_1 represent the lowest ("trough") potentials of the oscillation cycle. The points labeled V_p represent peak potentials of the cycle. These plots show the typical

behavior of the cell voltage at low, intermediate, and high current densities as investigated with the disk, channel #1, and Jet, respectively.

In Figs. 4.25-4.28, the average oscillation amplitude is plotted against current density for experiments conducted under specified hydrodynamic conditions. "Oscillation amplitude" is defined as the difference between the highest and lowest potentials of the oscillation cycle. Amplitude may be determined from recordings of either cell voltage or anode potential measured against a reference electrode.

a. Cell Voltage Behavior at Low Current Densities. At the low current densities employed with the disk, peak potentials varied considerably from cycle to cycle. In Fig. 4.22, individual measurements of peak cell voltage are shown. At current densities below 2 A/cm^2, at a rotational rate of 360 r.p.m., oscillation amplitudes ranged from 4-14 volts. At higher current densities, peak voltages were reproducible within a range of ±1 volt.

In addition to peak and trough potentials, two other characteristic potentials of the low current density waveform are shown in Fig. 4.22. The curve labeled "5" represents the lowest potential of the plateau phase of the cycle, which is depicted in Figs. 4.2 and 4.3. The onset of this plateau marks a transition from active to transpassive dissolution and the formation of a thin, non-porous film which was found by X-ray diffraction analysis to consist of cuprous oxide. The characteristics of active and transpassive dissolution and the nature of the film will be treated in Sections IV-B and IV-C.

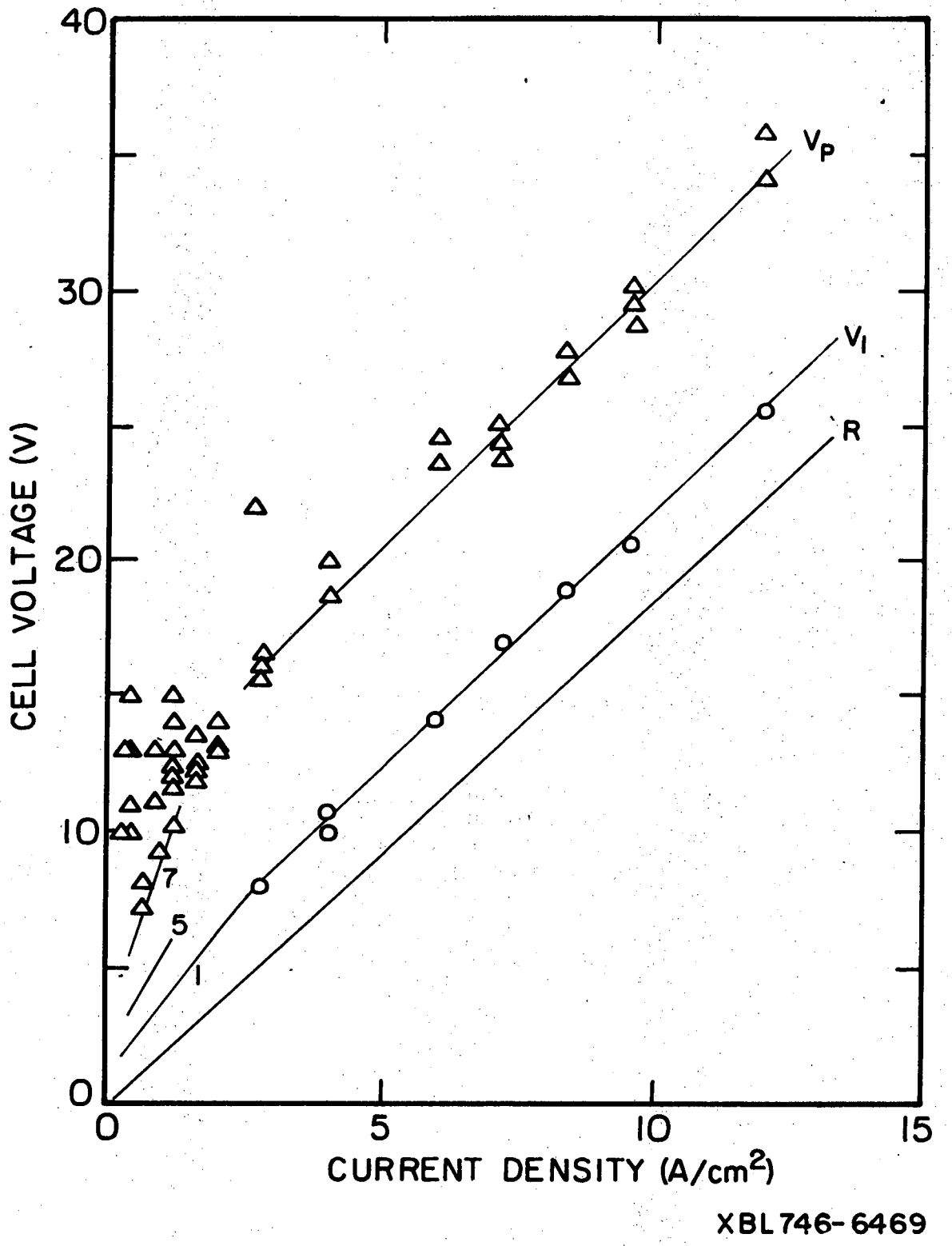

Fig. 4.22. Cell voltage measurements for copper dissolution at low current densities. Cu/2F $NaClO_3$; rotating disk electrode system; 360 r.p.m. V_p = peak voltage; V_1 = trough voltage; R shows ohmic drop through electrolyte assuming primary current distribution.

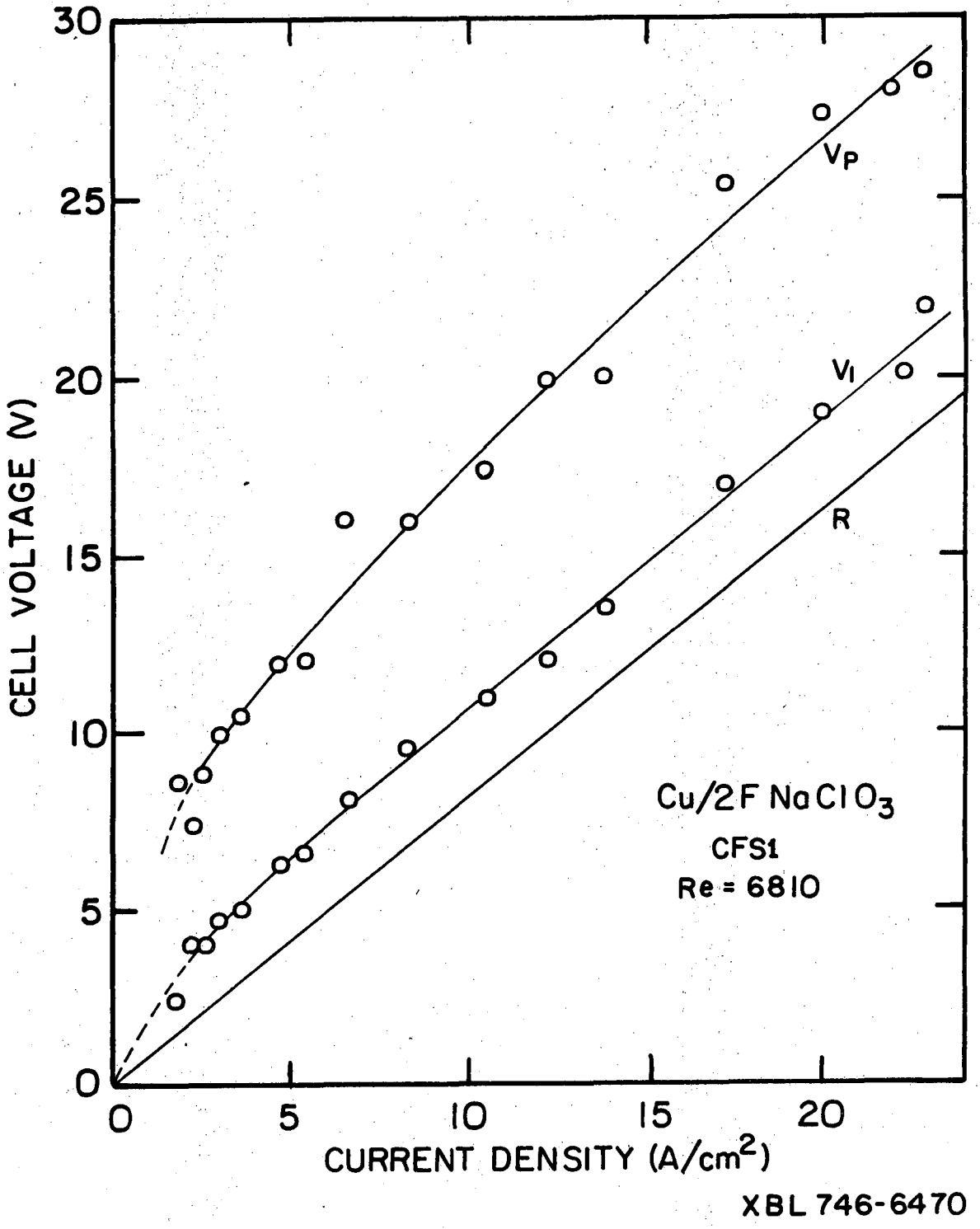

Fig. 4.23. Cell voltage measurements for copper dissolution at intermediate current densities. V_p, peak voltage; V_l, trough voltage; R indicates ohmic potential drop through the electrolyte assuming primary current distribution. Channel flow system no. 1.

The curve labeled "7" represents the potential of a shoulder, or inflection point, on the upward sweeping portion of the low current density oscillation cycle, as identified in Figs. 4.2b and 4.3. The inflections mark a slowing in the rate of growth of the anode surface films. The abrupt drop in potential from peak to trough levels was invariably found to occur at potentials equal to or greater than the potential of this inflection. Both the onset of the potential plateau and the inflection point were clearly distinguishable only to about 1 A/cm^2 in the disk at a rotational frequency of 360 r.p.m. In the channel #1, at Reynolds numbers corresponding to much higher rates of mass transfer, these details in the waveform structure were observed up to about 5 A/cm^2.

b. Cell Voltage Behavior at High Current Densities. As shown in Figs. 4.24 and 4.27, oscillation peak voltage and amplitude undergo a step increase of 35 volts at a current density of the order of 100 A/cm^2. At current densities lower than the transition current density, amplitude varies continuously with current density over the range 4-17 volts. Above the transition current density, amplitudes lie in the range, 45-55 volts. The enhancement of amplitude at high current densities was observed with the stagnation point flow system at flow rates from 0 to 193 cm/s (Re=1450) and with the Channel #2 at flow rates to 1220 cm/s (Re=12,500).

Photographs of the oscilloscope traces in Fig. 4.4 show the developement of the high amplitude waveform as observed with the Jet. At transition current densities, both low and high amplitude waveforms

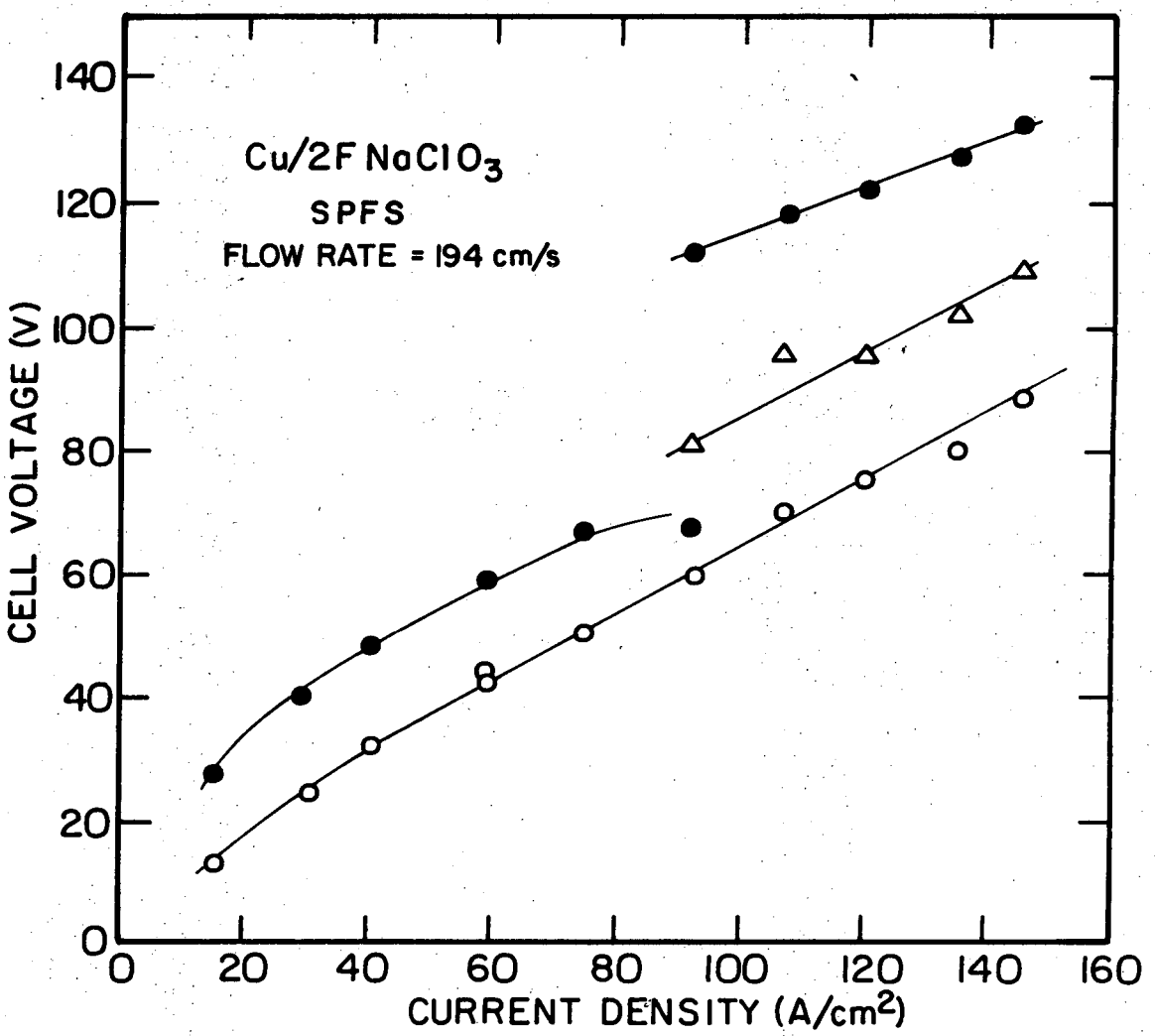

Fig. 4.24. Cell voltage measurements for copper dissolution at high current densities. Stagnation point flow system. Re = 1450 closed circles, peak potential; open circles, trough potentials; triangles, potential of arrest upon voltage breakdown.

occur in the same experiment. The low and high amplitude forms may alternate, as shown in Fig. 4.4e. No cycles with amplitudes in the intermediate range (about 20-40 volts) were recorded. The transition from low to high amplitudes occurs over a narrow range of current densities which shifts to higher current densities as the flow rate is increased. The dependence of oscillation period on current density is the same in the high amplitude range as in the low amplitude range, as is evident from Fig. 4.14.

The fine structure of the high amplitude and transition waveforms are shown in Fig. 4.4 j,k,l. While the potential fall from peak potential is smooth and continuous for the low amplitude waveforms, the potential breakdown of the high amplitude cycles occurs in two distinct steps: (1) a rapid drop to about 20 volts above trough potential occurs in an interval of about 10^{-5}s at 133 A/cm^2; (2) this is followed by a slower drop to trough potentials (about 10^{-4}s at 133 A/cm^2).

Unlike the low amplitude waveforms, the high amplitude oscillations were accompanied by gas evolution and clearly visible (and audible) spark discharges at the anode surface. A similar association between high amplitude oscillations and gas evolution with spark discharges was found for anodic dissolution of copper in a variety of halide containing electrolytes (See Appendix A). The increase in amplitude may be the consequence of the growth of bubbles of anodically evolved oxygen on the surface of the anode by the following reaction:

$$H_2O = \frac{1}{2} O_2 + 2H^+ + 2e^-$$

Bubbles might restrict the passage of current, causing the potential to rise until the observed spark discharge occurs. We shall return to a discussion of the high amplitude waveforms in Chapter V.

c. Dependence of Trough and Peak Potential on Current Density. The increase of cell voltage during the oscillation cycle is a consequence of the growth of resistive layers of solid reaction products on the surface of the anode. The fall from peak potentials reflects changes in either the electrical conductivity of the layers or in the extent of their coverage of the metal substrate. The dependence of peak and trough potentials on current density provides an insight into the nature of the anode surface during the transpassive dissolution and potential breakdown phases of the oscillation cycle.

To a first approximation, trough potentials increase linearly with current density. The linearity is to be expected if, at the lowest potential of the cycle, the electroly resistance is the predominant resistance of the electrolytic cell or if other sources of potential drop vary slowly with current density. As shown in Table IV-3, the measured slopes of the trough potential vs. current density plots (Figs. 4.22, 4.23) are in close agreement with the resistances calculated with the assumption of primary current distribution. The calculated contribution of ohmic potential drop is plotted in Figs. 4.22 and 4.23.

Table IV-3. Measured Slopes and Intercepts of Trough Cell Voltage Curves. Dissolution of Copper in 2F $NaClO_3$

System	Flow Condition	Temperature (°C)	Measured Slope ($Ohm-cm^2$)	Calculated Slope ($Ohm-cm^2$)	Measured Intercept (Volts)	Current Density Range (A/cm^2)
Channel No. 1	479 cm/s (Re=6810)	25±1	0.80	0.78[a]	2.5	5-25
Disk	360 r.p.m. (Re=280)	23±1	1.9	1.9[b]	3	3-13
Jet	194 cm/s (Re=1450)	23±1	0.53	---	10	40-150

[a] Primary current distribution assumed. Resistance given by the equation $RA = AK(1/\cosh^2 e)/(\kappa WK(\tanh^2 e))$ where A = electrode area; K = value of elliptic integral of the first kind; κ = electrolyte conductivity; W = width of electrodes perpendicular to flow direction; and $e = \pi L/2h$, where L and h are electrode length and separation, respectively. (See Newman,[91] p. 343).

[b] Primary current distribution assumed. Resistance of a disk electrode embedded in an infinite insulating plane with the counter electrode far away is given by

$$RA = A/(4r\kappa)$$

where r = electrode disk radius, A = electrode area, and κ = electrolyte conductivity. (Newman[91])

The linear segments of the trough potential curves do not extrapolate to zero potential at zero current density. The positive intercepts reported in Table IV-3 indicate the sum of anode and cathode potentials. The 2.5 volt intercepts found for dissolution at high flow rates (Re=6800) in the channel flow system no. 1 are comparable to the intercepts obtained by Kinoshita for active dissolution of copper in sulfate and nitrate electrolytes using the same flow system at equal flow rates.[5]

This 2.5 volt intercept is close to the sum of the estimated equilibrium cell voltage and anode and cathode overpotentials for the electrode reactions. Assuming a net cell reaction,

$$Cu + 2H_2O = Cu^{++} + 2OH^- + H_2$$

the equilibrium potential difference is approximately 1.2 volts for unit Cu^{++} activity in the anolyte and a local catholyte pH of 12. Landolt et al.[98] measured the charge transfer overpotentials for active dissolution of copper ($Cu = Cu^{++} + 2e^-$) in acidified 0.1F $CuSO_4$: the Tafel relation obtained up to approximately 100 A/cm^2, where the overpotential was about 0.4 V. We expect a charge transfer overpotential of the same order for the active dissolution of copper in the chlorate electrolyte. At the copper cathode, the reduction of water ($2H_2O + 2e^- = H_2 + 2OH^-$) should proceed with an overpotential of about 0.7 volts.[140] The sum of the estimated equilibrium cell voltage and anode and cathode overpotentials is 1.2 + 0.4 + 0.7 = 2.3 volts--in close agreement with the residual cell voltages at low current densities investigated with the disk and channel flow systems.

At the high current densities investigated with the stagnation point flow system, the ten volt intercepts at zero current density are much too large to be explained by familiar sources of electrode polarization. The large anode potential drop is indicative of the presence of a resistive film on the anode surface after the fall from peak potential. We conclude that the periodic rise and fall of potential at high current densities reflects, not alternating states of active and transpassive dissolution, but alternating degrees of anode film resistance.

d. Dependence of Oscillation Amplitude on Current Density and Flow Rate. In Figs. 4.22-4.24, the curves representing peak potentials run roughly parallel to the curves for trough potentials, indicating a weak dependence of oscillation amplitude on current density. The dependence of amplitude on current density is shown more directly in the plots of Figs. 4.25-4.28. Amplitudes range from 2 to 19 volts for current densities up to 100 A/cm^2. A high current density waveform characterized by amplitudes in the range 45-55 volts has been discussed above. In contrast to the relatively weak dependence of amplitude on current density, oscillation frequency increased by a factor of 10^5 over the same current density range (0-100 A/cm^2).

The relative independence of amplitude and current density can be expected from the nature of ionic conduction through thin solid films. If charge is carried through the anode surface films by ionic conduction at field strengths of 10^5 V/cm or greater, then we should expect the current-voltage relationship to be of the form:[49,121]

$$V_f = (S/B)\ln(I/A)$$

where V_f is the voltage drop through the film; S is film thickness; I is current density; and A and B are empirical constants. If film thickness at peak potentials is independent of current density, then amplitude should vary only as the logarithm of current density.

The dependence of amplitude on flow rate was studied with the channel flow system no. 1 and with the stagnation point flow system (jet). Over the range of current densities, 8-33 A/cm^2, neither system show a strong dependence of amplitude on current density. The average amplitudes obtained with the channel no. 1 are shown in Figs. 4.25 and 4.26. At current densities below 5 A/cm^2 and for Reynolds numbers of 200, 708, and 6810, no trend is clearly distinguishable from the experimental scatter of ± 0.5 volts. In Fig. 4.26 a curve representing the amplitudes obtained with the rotating disk system (Re-283) are also shown with scatter indicated by broken lines. At such low current densities, the results may be expected to show considerable scatter: here experimental conditions are close to the regime where stable active dissolution may occur.

With the stagnation point flow system, amplitude increased with flow rate as shown in Fig. 4.28. Amplitudes were greater in the jet system than in the channel flow system. At 33 A/cm^2, amplitudes obtained with the jet averaged 17 volts--twice the magnitude of amplitudes obtained with the channel flow system for comparable mass transport rates. A fundamental difference exists between the jet and channel flow systems which may account for the disparity in the results for oscillation amplitude and the dependence of amplitude on flow rate.

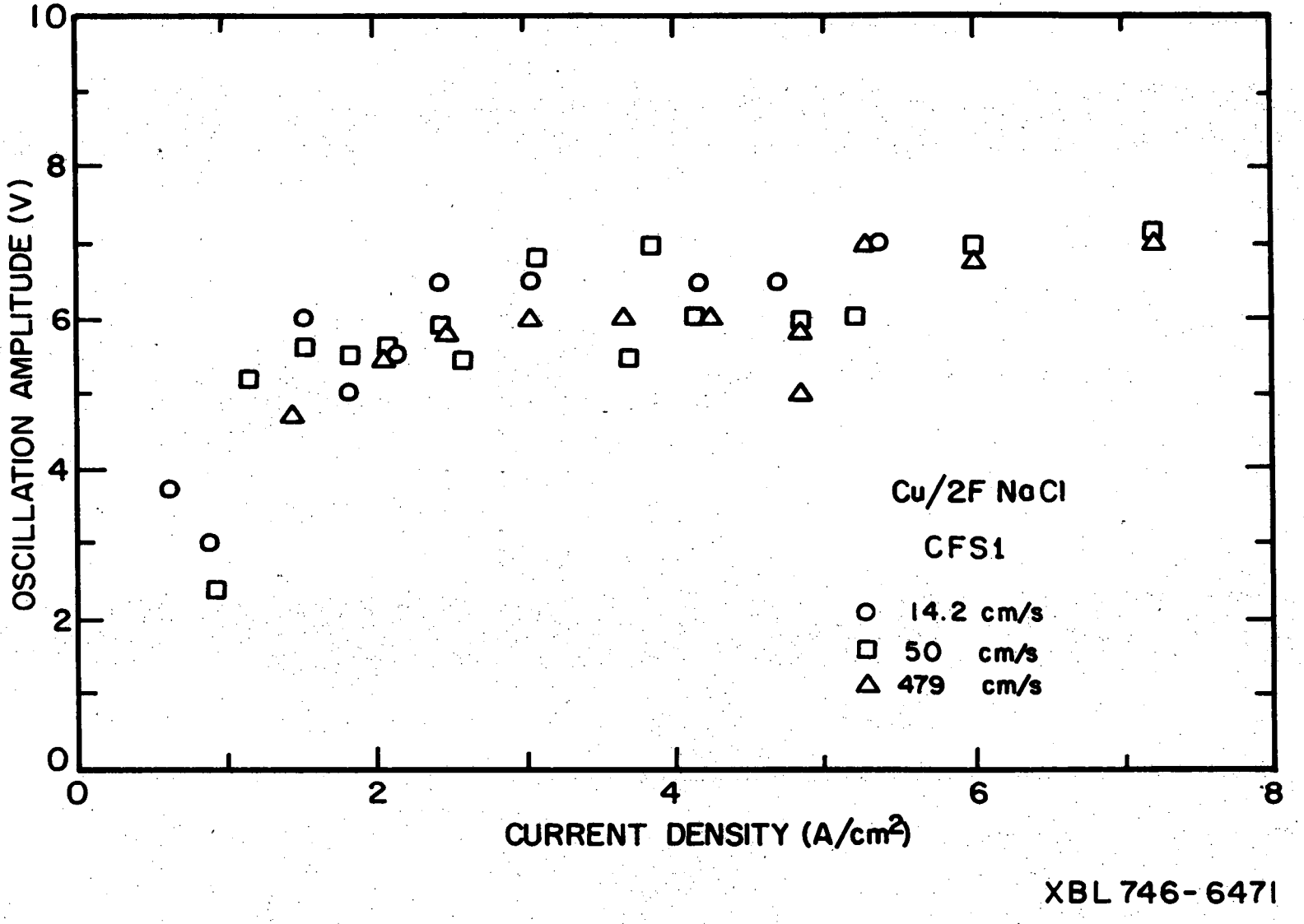

Fig. 4.25. Cell voltage amplitudes at low current densities. Open circles, Re = 200; squares, Re = 708; triangles, Re = 681C.

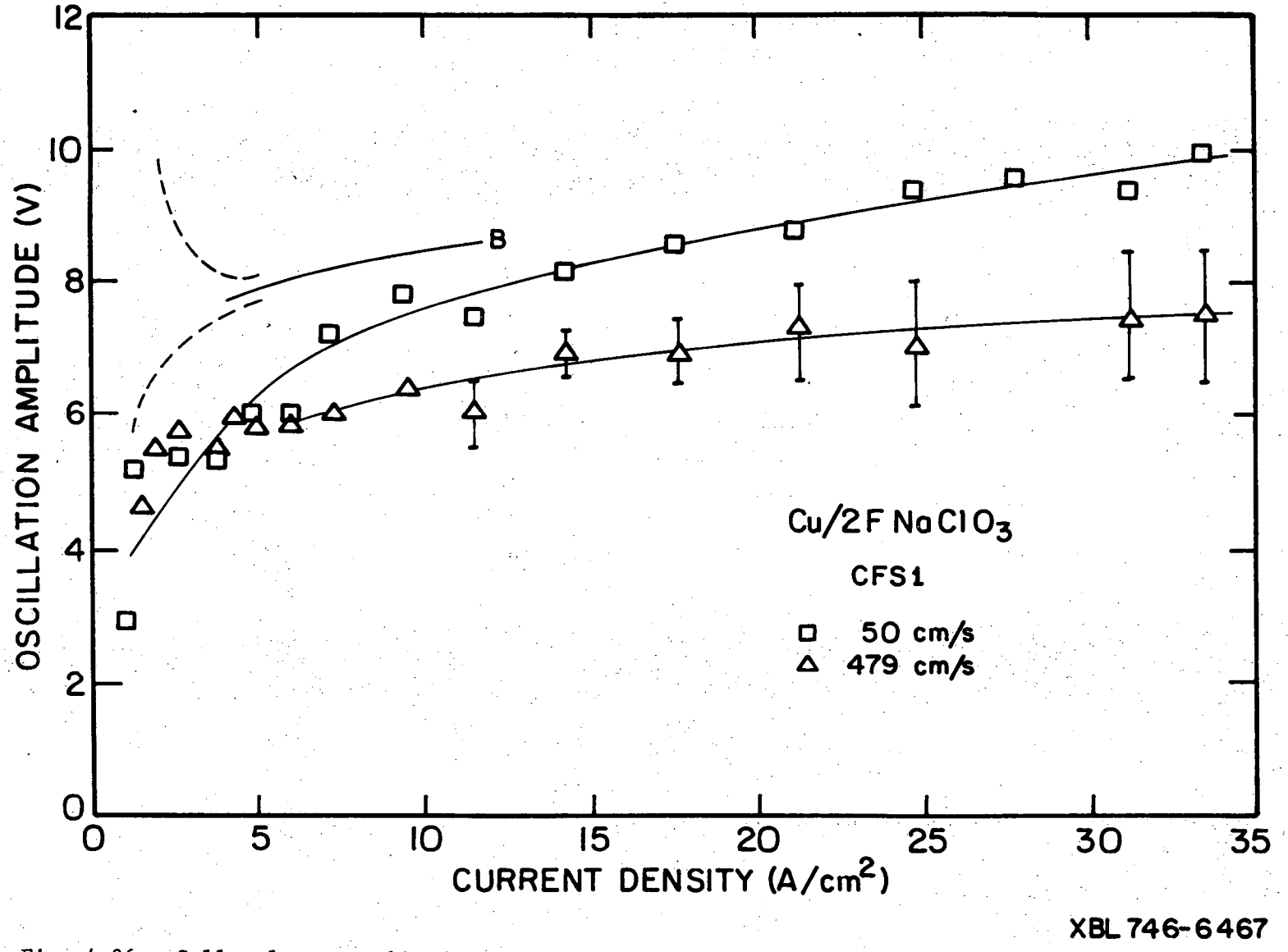

Fig. 4.26. Cell voltage amplitudes at intermediate current densities. Line B shows amplitudes obtained with rotating disk electrode system at 360 r.p.m.; broken segments indicate experimental scatter; squares, Re = 708; triangles, Re = 6810.

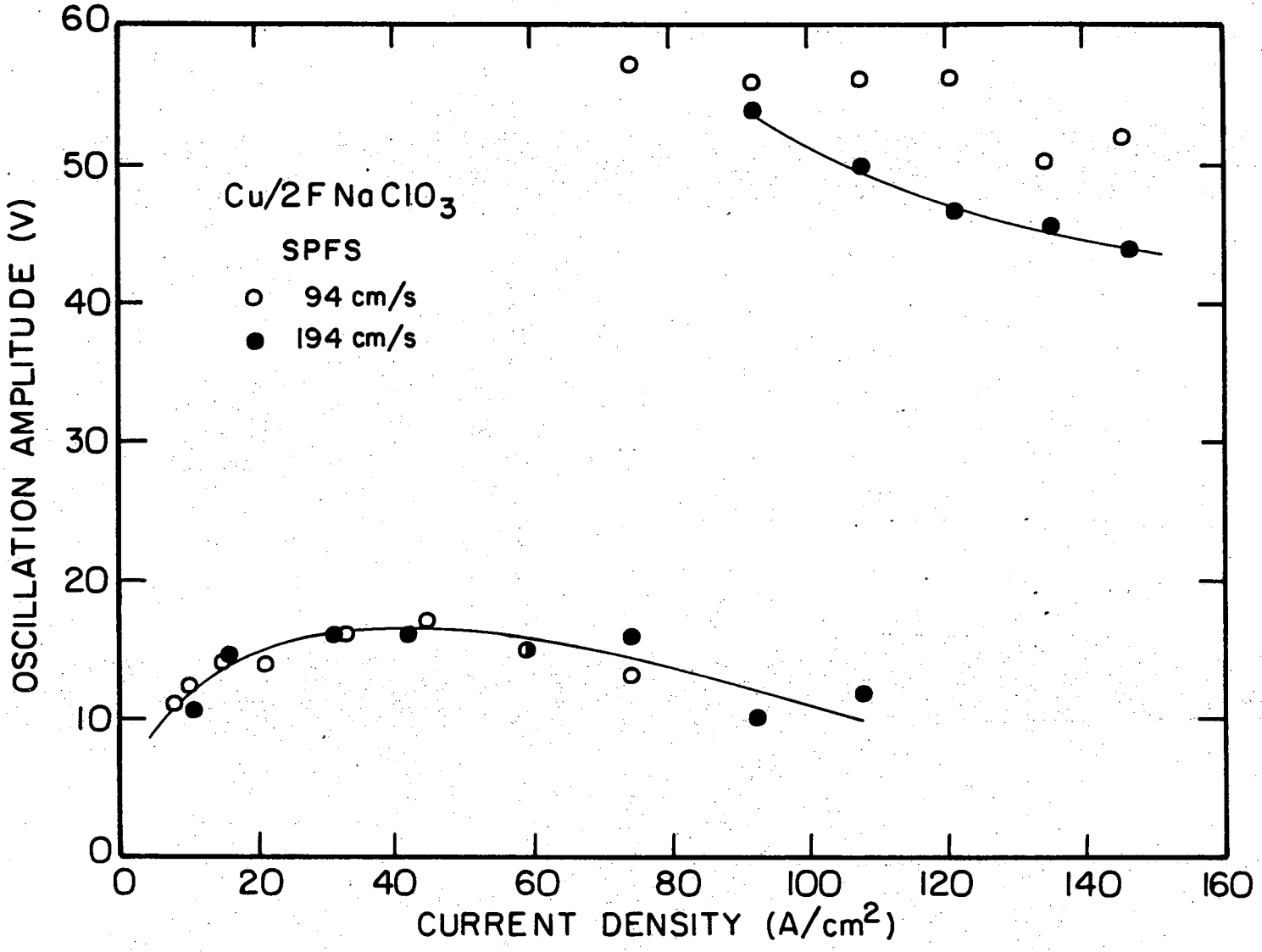

Fig. 4.27. Cell voltage amplitudes at high current densities. Stagnation point flow system; open circles, Re = 704; closed circles, Re = 1450.

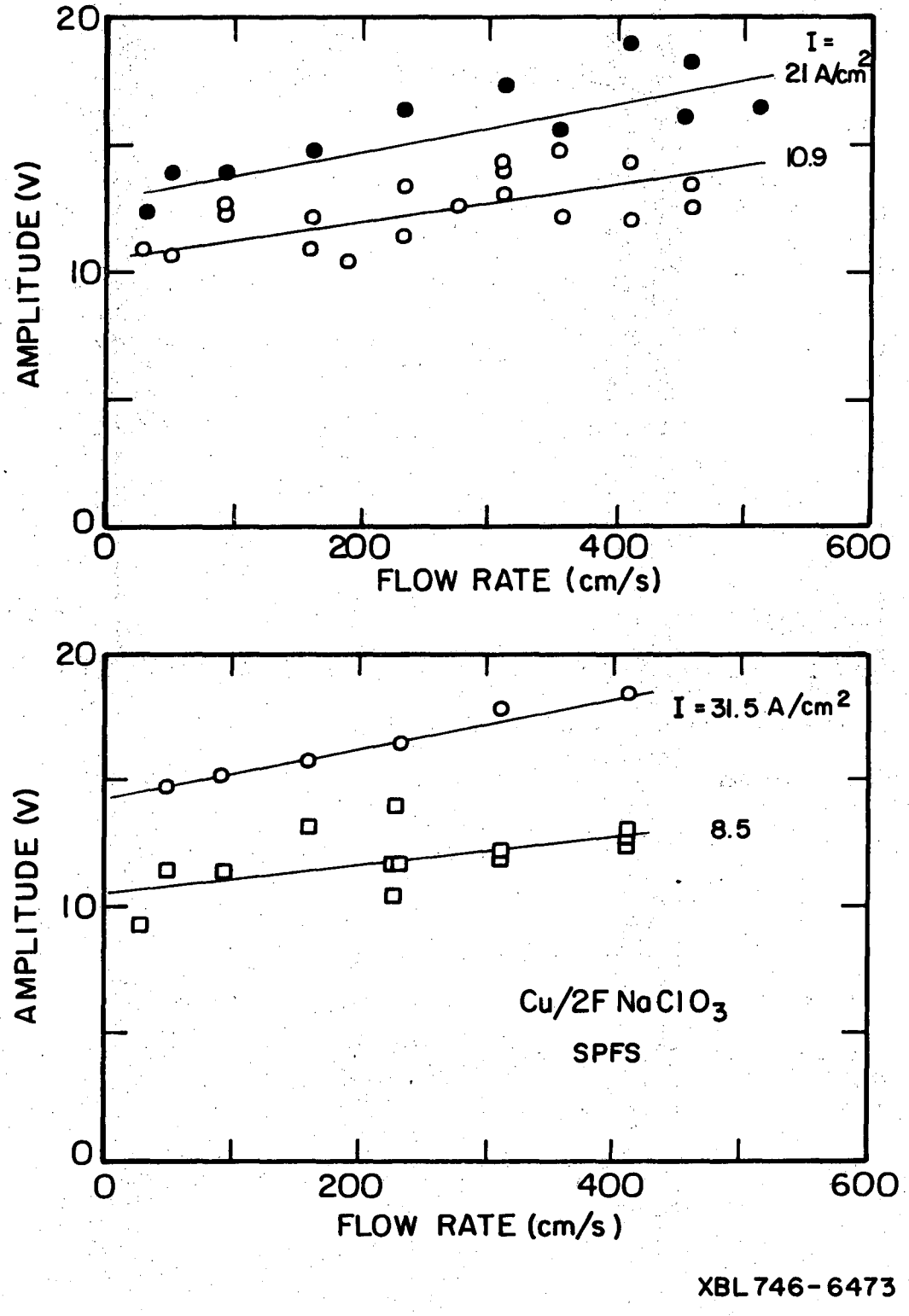

Fig. 4.28. Dependence of cell voltage amplitude on flow rate. Stagnation point flow system.

The primary current distribution for the jet is more strongly non-uniform than the primary current distribution for the channel flow system. The enhancement of current at the edges of the anode of the jet system may give rise to accelerated film growth near the edges and a film of non-uniform thickness and resistance to electrical breakdown.

B. Chemical Aspects of the Anodic Dissolution Processes

At current densities below about 1 A/cm^2, the oscillation period length is sufficiently long to allow the resolution of chemical processes occurring at different phases of the cycle. The chemical basis of the oscillations was investigated by (1) determining the apparent valence of the dissolution process, (2) measuring the quantity of chloride ion produced during dissolution; and (3) analyzing X-ray diffraction spectra.

1. Apparent Valence

a. Introduction and definitions. The passage of electric current across a metal/electrolyte interface is always accompanied by a chemical reaction. The amount of electricity passed through the interface may be directly related to the amount of chemical reaction products by Faraday's laws, which may be expressed in the following equation:

$$q = F \sum_i S_i \qquad (1)$$

Here, q is the quantity of charge (coulombs); S_i is the quantity of reaction product (i) (gram-equivalents); and F is the Faraday constant (96,500 coulombs/gram-equivalent).

The simplest case of anodic dissolution of a metal might involve the production of a single metal ion species of valence, z:

$$Me = Me^{+z} + ze^{-}$$

With knowledge of the stoichiometry of the dissolution reaction, weight loss of the metal could be predicted from the current and time of dissolution, using a form of Eq. (1):

$$it = F(zW/M) \qquad (2)$$

where

i = current
t = time of dissolution
W = weight loss of metal
M = atomic weight of metal

Alternatively, the stoichiometry could be verified from weight loss and charge data.

In general, more than one simple electrochemical reaction will take place simultaneously during the anodic dissolution of a metal, and the quantity z calculated from Eq. (2) may assume non-integral values. In the case of copper, mono-, di-, and trivalent oxydation states may be produced under certain conditions of anodic polarization and electrolyte composition. The anodic decomposition of water may occur, and the copper may corrode in the presence of any oxydizing electrolyte. Finally, the number and relative importance of the different anodic dissolution processes may change progressively during the course of dissolution.

For purposes of investigating the stoichiometry of the anodic dissolution of copper in chlorate electrolytes, we have measured the average apparent valence of the dissolution process. "Average apparent valence", n_a, is defined by an equation analogous to Eq. (2):

$$n_a = \frac{it/F}{W/M} \tag{3}$$

Dissolution times are chosen to be many times longer than the period length of the oscillation cycle at the experimental current density.

The investigation of possible changes of stoichiometry during the course of a single oscillation cycle requires the measurement of an "instantaneous apparent valence," n, defined by:

$$(1/n) = (F/iM)(\delta W/\delta t) \tag{4}$$

Here, the quantity $\delta W/\delta t$ is the increment of weight loss divided by an increment of time. In practice, the weight loss (W/M) is plotted against the charge passed (it/F); each point represents the weight-loss-charge data for a dissolution experiment terminated after a time, t. The slope of the plot is just (1/n). In all the calculations reported in this section, the atomic weight of copper is taken as 63.54.

b. Average apparent valence. Average apparent valence was determined (1) with Channel Flow System No. 1 at current densities from 0.1 to 23 A/cm^2; and (2) with the Stagnation Point Flow System (Jet) from 10 to 100 A/cm^2.

Procedures. Experimental procedures followed with the Channel #1 are described in Section IV-A.1.

For the Jet, electrode preparation was as follows: (1) Anode surfaces were ground flat against #600 carborundum paper; (2) approximately 2 mg of copper (corresponding to a layer 0.01 cm thick) was removed by anodic dissolution (2F $NaClO_3$, 10 A/cm^2, 15 s); (3) anode surface films were removed by rinsing in the solution,[133]

4 g $SnCl_2 \cdot 2H_2O$
4 ml conc. HCl(sp.g., 1.19)
100 ml ethanol

(4) anodes were rinsed in distilled water and reagent grade acetone; and (5) weighed to a precision of 0.01 mg.

Dissolution times were sufficient to allow weight losses of 1.5-3 mg. After dissolution, anodes were rinsed in distilled water and steps (3) to (5) were followed. The electrolyte was discarded after every six dissolution experiments, when $4\times(10^{-4})$ equivalents of charge had been passed per liter of solution. Spurious weight losses resulting from the cleaning procedure were determined in control experiments, in which the same procedure was followed but without anodic dissolution. Such weight losses were less than 0.04 mg.

Results. Average apparent valence (n_a) is plotted against current density in Figs. 4.30a,b. In Fig. 4.30a, each data point represents results of a single weight loss determination, using Channel #1; in Fig. 4.30b, the average of three separate determinations using the Jet are plotted, with the data spread indicated by bars. The average

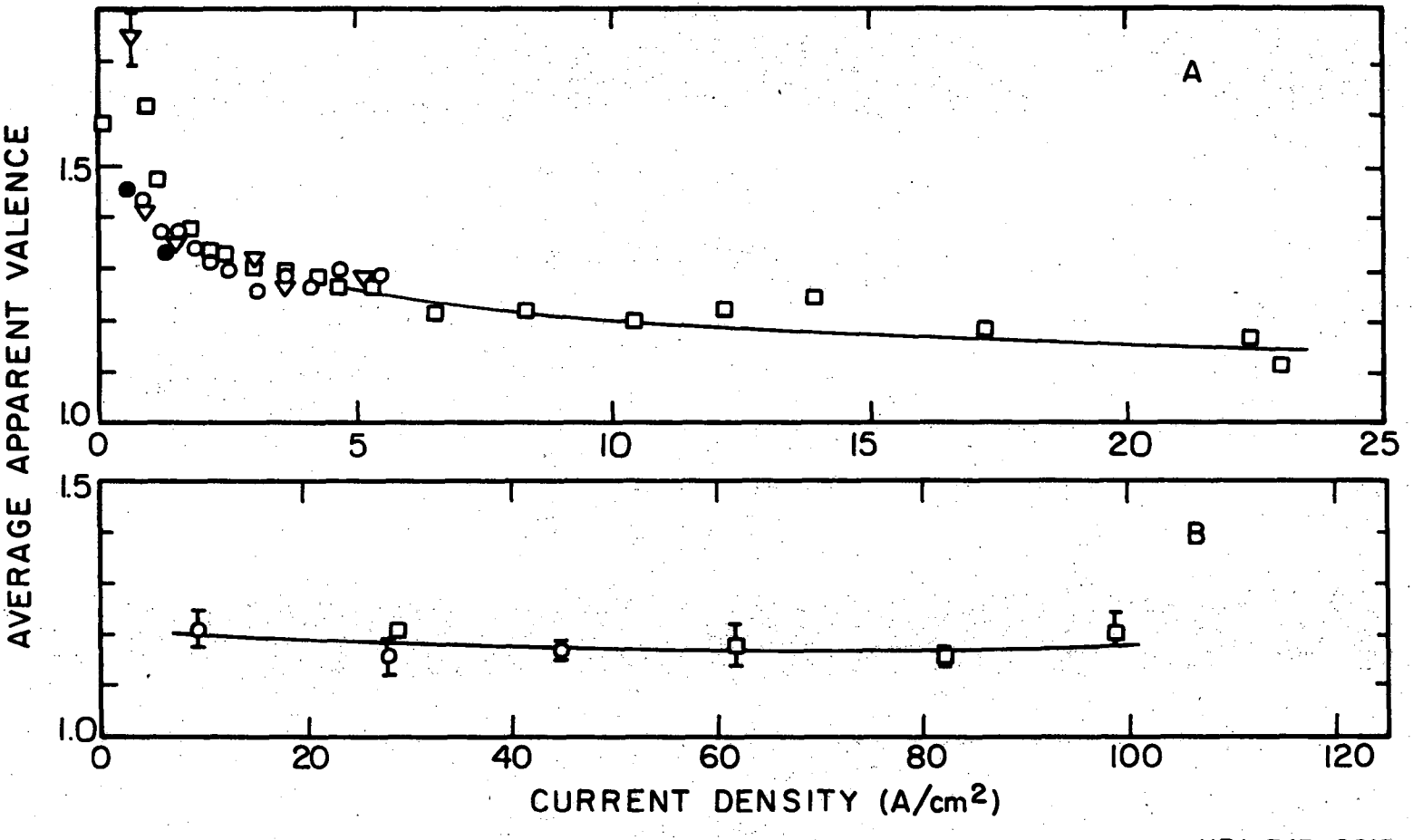

Fig. 4.30. Average apparent valence. Cu/2F $NaClO_3$; (A) channel flow system no. 1; triangles, Re=200; squares, Re=708; circles (open), Re=6810. Closed circles, average apparent valence in first cycle; experiments in stationary electrolyte cell. (B) Stagnation point flow system; squares, Re=700; circles, Re=2600.

apparent valence decreased from 1.6 to 1.2 as the current density was raised from 0.1 to 10 A/cm^2. Apparent valence remained virtually independent of current density above 10 A/cm^2. Above 2 A/cm^2, n_a showed no marked dependence on electrolyte flow rate.

c. Instantaneous apparent valence. Instantaneous apparent valence was determined at points within the first and second oscillation cycles to develope after the application of current. The stationary electrolyte cell used in this research was described in Chapter III. Current densities of 0.54 and 1.33 A/cm^2 were employed in the experiments to be described. At such low current densities, the different phases of the oscillation cycles (active dissolution, potential plateau, peak) were clearly distinguishable in the cell voltage recording.

Procedure. The 9.6 cm^2 OFHC copper disk electrodes were polished on kerosene-wetted emergy paper to 4/0 grade. The disks were then washed in labtone detergent and distilled water. The electrodes were then rinsed sequentially in: (1) concentrated, reagent grade NH_4OH, (2) distilled water, and (3) reagent grade acetone. The rinse in ammonia served to remove grease films and tarnish. Following the cleaning treatment, the electrodes were weighed to a precision of 0.01 mg on the Mettler balance.* Just prior to dissolution, the electrodes were treated cathodically at a current density of 0.1 A/cm^2, for 30 seconds, in 1F NaOH. Cell voltage and potential drop through a low resistance shunt were recorded simultaneously on the Brush Oscillograph as for the experiments conducted with Channel #1. After dissolution, the electrodes were quickly removed from the cell and

*Mettler Model H20T, Greifensee-Zurich, Switzerland.

rinsed sequentially in (1) distilled water; (2) 10% NH_4Cl; (3) distilled water; and (4) reagent grade acetone. The anodes were then re-weighed. The treatment in 10% NH_4Cl served to remove adherent layers of anodically formed Cu_2O from the surface of the anode.

The constant current source used in these experiments was a Perkin Electronics DC Power Supply.* The current was measured with the use of a low resistance shunt and a balancing potentiometer following the procedure of Section IV-A1.

To determine the magnitude of spurious weight losses introduced by electrode preparation procedures, control experiments were conducted, i.e., the same procedure was followed without anodic dissolution. Weight losses in the control experiments were on the order of 0.1 mg, while weight losses resulting from anodic dissolution ranged from 5 to 30 mg. Weight loss determinations are therefore expected to be accurate to within 2%. Time and current were each measured with an estimated precision of ± 1%.

Results. In Figs. 4.31 and 4.32, cell voltage and weight loss (W/M) are plotted against charge passed (it/F). Instantaneous apparent valence, determined from the inverse slopes of the linear segments of the plots, are tabulated in Table IV-4.

*Model TV040-15, Perkin Electronics, Inc., El Segundo, California

Table IV-4. Instantaneous and Average Apparent Valence for Copper Dissolution in 2F $NaClO_3$. Natural Convection.

Apparent Valence	Active Phase	Transpassive Phase	Average in First Cycle
Current Density = 0.54 A/cm^2	1.59	1.22	1.45
1.33 A/cm^2	1.15	1.33	1.33

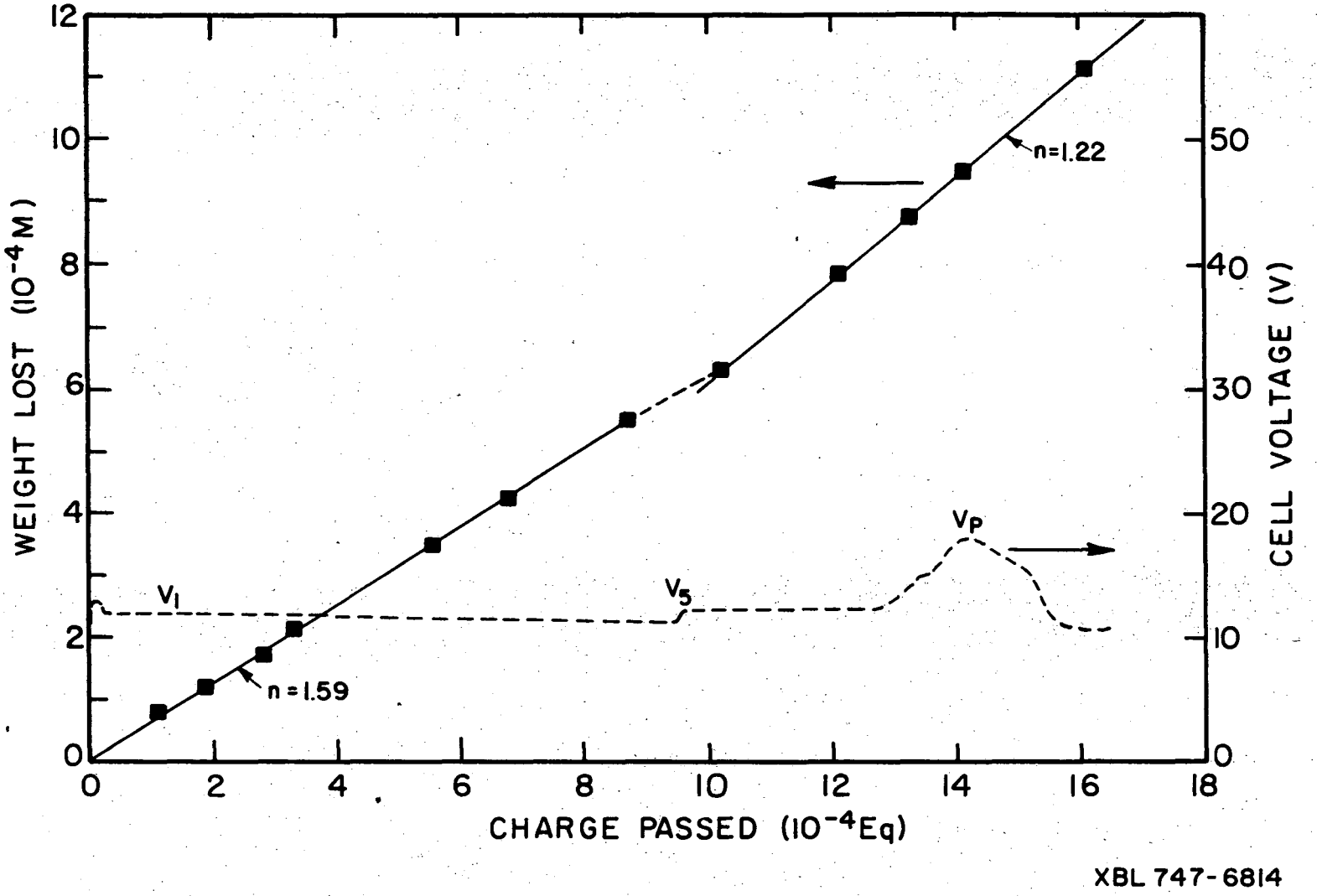

XBL 747-6814

Fig. 4.31. Integral apparent valence. Stationary electrolyte cell; Cu/2F $NaClO_3$; current density 0.54 A/cm^2. Instantaneous apparent valence is indicated on the graph. Anode area = 9.6 cm^2.

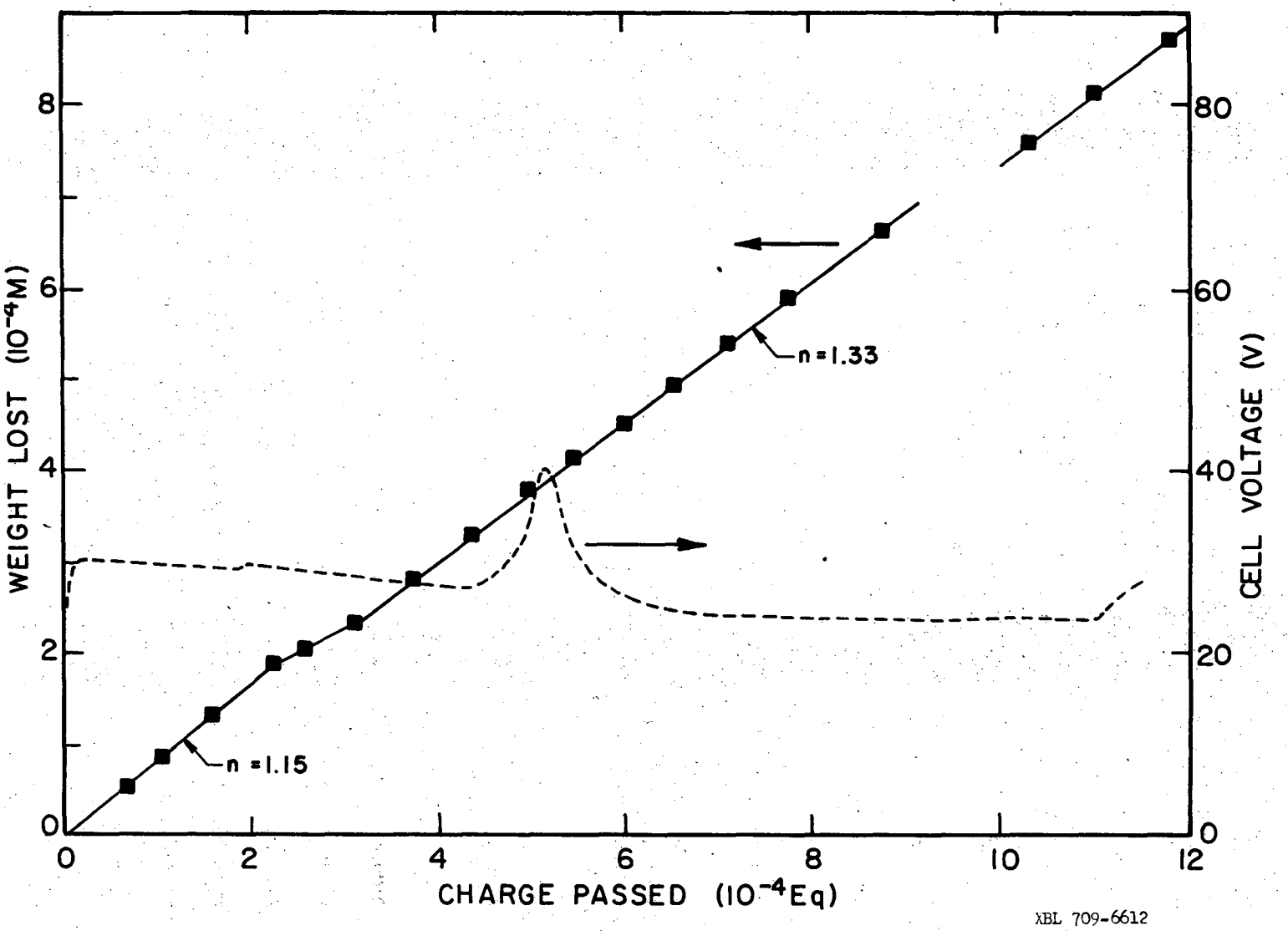

XBL 709-6612

Fig. 4.32. Integral apparent valence. Stationary electrolyte cell; Cu/2F $NaClO_3$; current density = 1.33 A/cm^2. Instantaneous apparent valence is indicated on the graph. Anode area = 9.6 cm^2.

Several important observations may be made at this point:

(1) At a given current density, instantaneous apparent valence is constant within the active phase of the oscillation cycle.

(2) At a given current density, the instantaneous apparent valence remains constant throughout the transpassive phase of the dissolution cycle, which includes the potential plateau and ascending and descending portions of the peak.*

(3) For a given phase of the cycle (active or transpassive), apparent valence depends on current density.

In these experiments no oxygen evolution was observed throughout the active and transpassive phases of the first oscillation cycle. During potential breakdown a few gas bubbles developed on the anode surface with a total volume estimated to be less than 0.1 cm^3. This volume corresponds to roughly $0.2\times(10^{-4})$ equivalents, or less than 3% of the charge passed during the cycle. If no charge transfer reactions occur other than those involved in oxygen evolution and copper dissolution, then the instantaneous apparent valence is an indication of the net stoichiometry of the copper dissolution process. An important conclusion is thus possible: no gross change in the stoichiometry of copper dissolution occurs as the oxide film responsible for the potential increase developes and ultimately breakdown.

---

*At the onset of transpassive dissolution, a short-lived increase in n may be detected; the technique is not sufficiently sensitive to ascertain the value of n in so short an interval.

2. Chloride Production

The solution in the anolyte compartment of the stationary electrolyte cell was analyzed for chloride ion after dissolution at a current density of 1.33 A/cm^2.

Procedure. The disk electrodes of the Stationary Electrolyte Cell were prepared for dissolution as in the apparent valence determination experiments described in the previous section. For each experimental run, the current was shut off at a different point within the first or second oscillation cycle. The entire anolyte, including all loose precipitates, was transferred to a centrifuge test tube. Solid reaction products adhering to the copper surface were removed with a rubber stick and added to the anolyte mixture. The anolyte was centrifuged and the supernatent liquid was transferred to a beaker. The solid residue was leached with distilled water and again centrifuged; the supernatent was decanted into the first beaker.

The liquid phase thus collected was acidified with dilute nitric acid. An aliquot of standardized $AgNO_3$ was added, and the solution was backtitrated with a standardized NaCl solution. The extent of titration was monitored by recording the potential between a silver wire electrode and a saturated calomel electrode immersed in the titration beaker. (Leakage of Cl^- from the calomel electrode was determined in a control experiment and was found to be negligible.) The silver nitrate solution was standardized by titration against a stock solution of sodium chloride. The sodium chloride solution was prepared by the solution of a weighed quantity of the heat desiccated salt.

The solid phase of the anolyte mixture was dissolved in dilute nitric acid and similarly back-titrated.

Results. The quantity of chloride determined in the liquid phase and the total quantity of chloride (liquid plus solid phases) are plotted against charge passed in Fig. 4.33. Cell voltage is also plotted against charge passed.

The chloride ion present in the liquid phase is presumed to be a product of the chemical reduction of chlorate by cuprous ion. The chloride determination for the solid phase represents an upper limit to the quantity of chlorine present in the solid phase in the minus one oxidation state. The analytical technique used did not distinguish between free chloride and oxychlorides which might have been reduced by any cuprous compounds present when the solid mixture was dissolved.

To account for the production of the chloride ion, we hypothesize the following net reaction:

$$Cu^{+} + 1/6\ ClO_3^{-} + 1/2\ H_2O = Cu^{++} + 1/6\ Cl^{-} + OH^{-} \qquad (A)$$

On the basis of this reaction, the maximum rate of production of chloride may be calculated. If one mole of copper dissolved to form Cu^{++} and Cu^{+} according to the net reaction,

$$Cu = x\ Cu^{+} + y\ Cu^{++} + ne^{-} \qquad (B)$$

then mass and charge balances may be written as follows:

$$x + y = 1$$
$$x + 2y = n$$

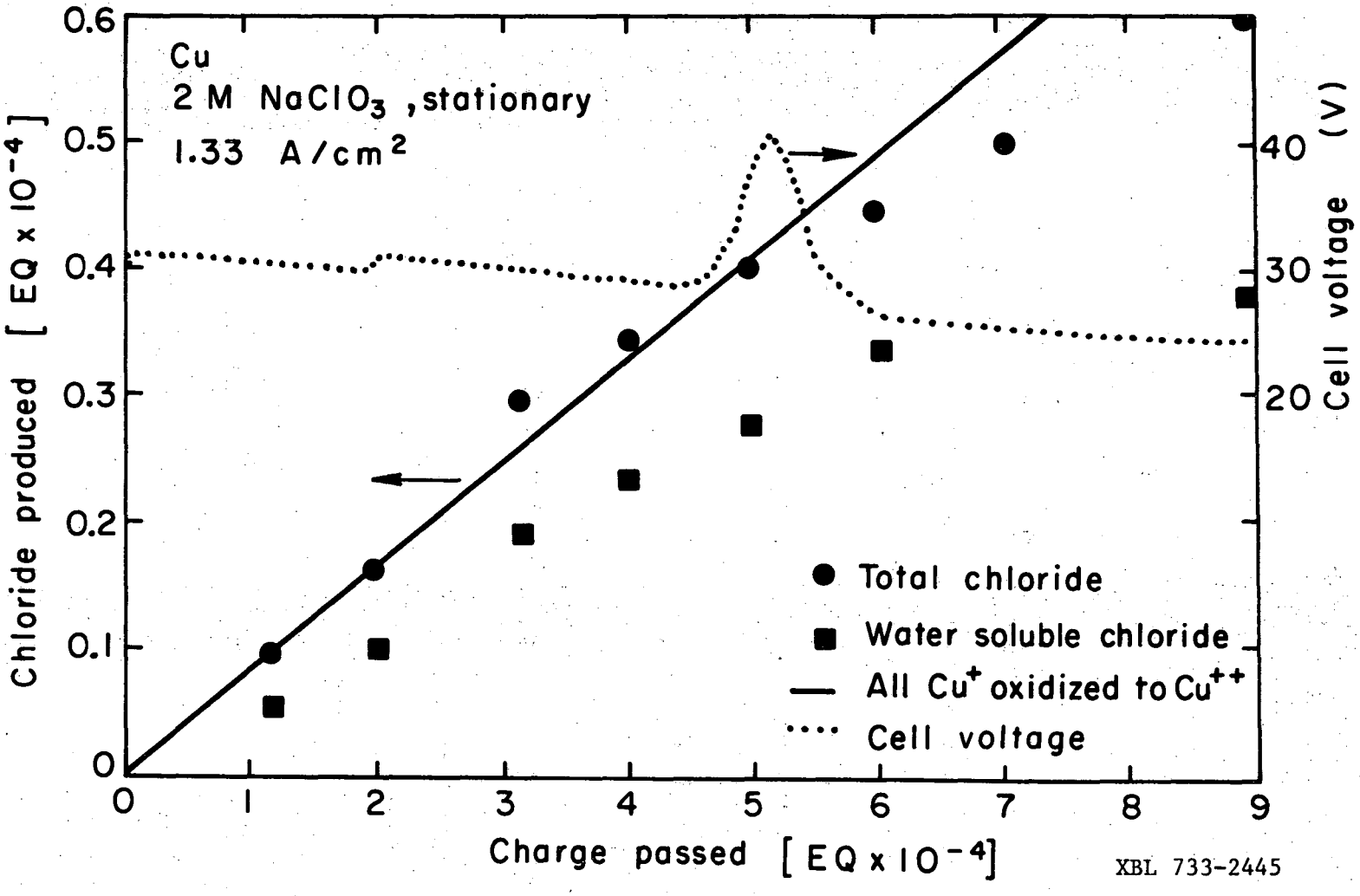

Fig. 4.33. Chloride production during the potential oscillation cycle Cu/2F $NaClO_3$; stationary electrolyte cell; 1.33 A/cm^2. Anode area = 9.6 cm^2.

Therefore,

$$x = 2 - n ,$$

and the fraction of charge consumed in the production of Cu^+ is

$$f_{Cu^+} = (2-n)/n$$

The average apparent valence under the experimental conditions at hand was 1.33. Hence the passage of one equivalent of charge should result in the production of 0.5 equavelents of Cu^+ and a maximum of 0.083 equivalents of Cl^- via reaction (A). As shown in Fig. 4.33, the total measured chloride is close to that predicted on the basis of our model.

These results are also consistent with those of Royer, et al.,[139] who studied the anodic dissolution of copper in 1.2 m $NaClO_3$ at a constant current density of 0.015 A/cm^2 and at temperatures between 25°C and 100°C. Above 70°C, the apparent valence was 1.0 and the amount of chloride determined in the anolyte after dissolution was within 1% of that expected on the basis of reaction (A).

3. X-Ray Diffraction Analysis of Solid Dissolution Products

Solid reaction products formed during various phases of the oscillation cycle were analyzed by X-ray diffractometry. Nickel filtered copper radiation at 40 kV and 14 mA was used in the X-ray apparatus.* Samples were prepared using the stationary electrolyte or the rotating disk electrode system.

*X-ray Diffractometer, Model 3488K, Picker X-ray Corporation, Waite Manufacturing Division, Inc., Cleveland, Ohio.

a. Procedure with stationary electrolyte cell. Electrodes of the stationary electrolyte cell were prepared for dissolution as in the case of the instantaneous apparent valence experiments. Dissolution, at a constant current density of 1.33 A/cm^2 or 0.54 A/cm^2, was terminated at points within the first or second oscillation cycle. The anodes were then quickly removed from the cell.

The anode specimens for which dissolution had been terminated during the active phase of the first cycle were covered with an adherent, red-orange, granular deposit. The anodes with active phase solid products were rinsed in distilled water and dried in a vacuum desiccator. The X-ray beam was allowed to impinge directly on the anode surface and the copper substrate was used as an internal reference.

The anode specimens for which dissolution had been terminated during the transpassive phase of the cycle or immediately following the fall from peak potential were covered with a loose precipitate. The precipitate could be readily removed from the surface in a jet of distilled water. In one set of experiments the solids were collected with a sintered glass filter and washed with distilled water. The insoluble residue was placed in a Lucite holder for diffraction analysis. In a second set of analyses, the anodes with transpassive phase products on the surface were carefully removed from the cell and desiccated under vacuum. The solid products thus prepared were analyzed on the copper substrate.

b. Procedure with rotating disk electrode system. The removal of the loose precipitates formed on the anode surface during transpassive dissolution revealed a smooth, polished copper surface. Interference patterns on the surface were taken as evidence for the presence of a thin solid film. The disk was used to produce samples of the thin, transpassive film for X-ray diffraction analysis. Dissolution (at 0.64 A/cm^2 and 360 r.p.m.) was terminated at a series of points between the onset of the potential plateau of the first cycle and the beginning of the active phase of the second cycle. The anodes were then removed from the electrolyte, rinsed in a jet of distilled water, and allowed to dry.

c. Results. Cuprous oxide was found to be a constituent of the solid phase of the anodic reaction products formed during each phase of the oscillation cycle. Absent from the spectra in all cases were lines attributable to CuCl, CuO, $Cu(OH)_2$, and basic cupric chloride salts. Table IV-5 is a summary of the diffraction analysis results.

The red-orange, granular, adherent deposit formed during active dissolution in stationary electrolyte was identified as Cu_2O. Figure 4.34 shows tracings of spectra of active phase, water insoluble products (traces A,B); of the copper anode prior to dissolution (C); and of a sample of Cu_2O (Baker Reagent Grade). No peaks were found other than those attributable to Cu_2O or to the copper substrate. Similarly, only peaks due to Cu_2O and Cu were found in the spectra of active phase products produced with the disk.

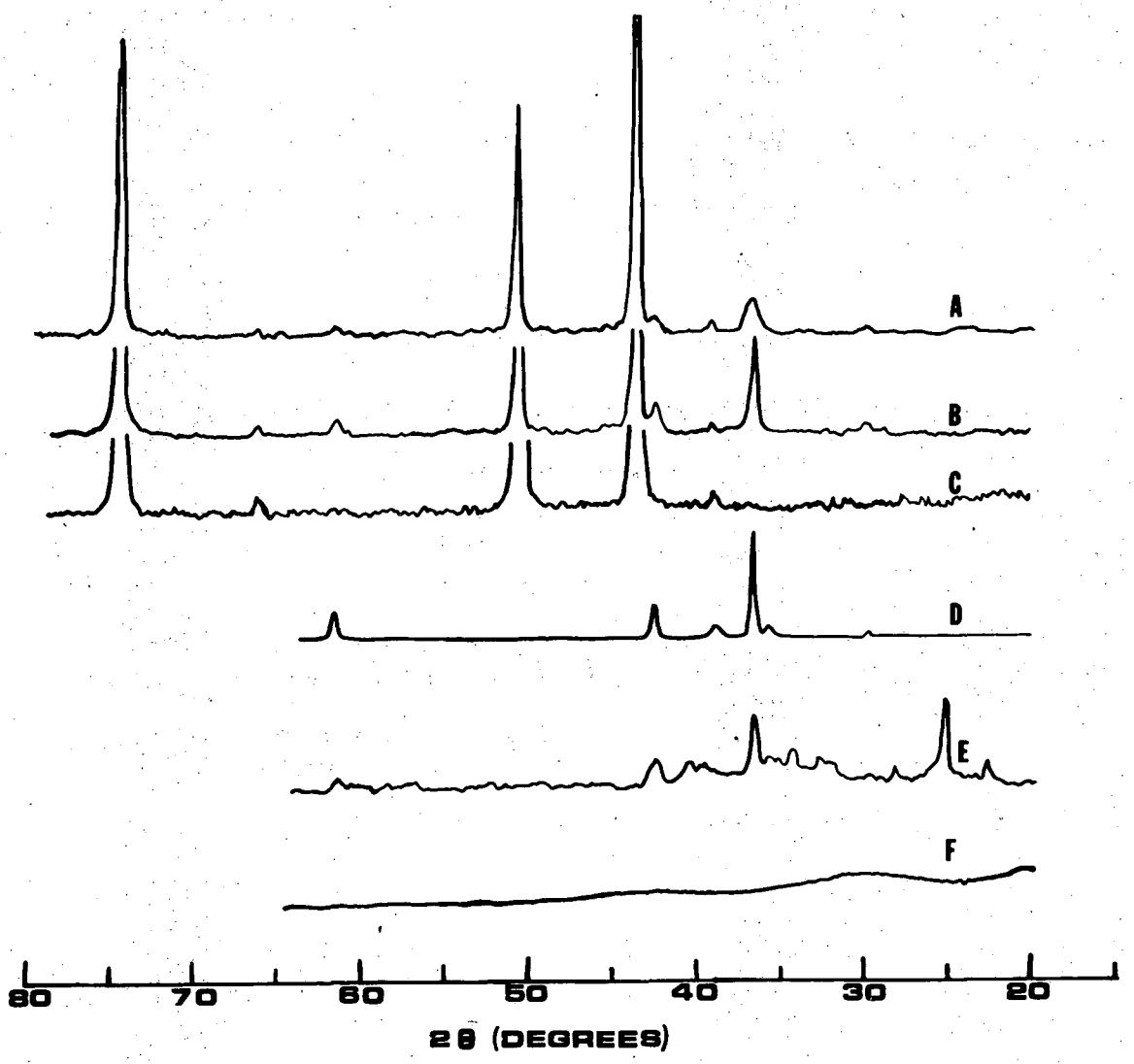

Fig. 4.34. X-ray diffraction patterns of anode precipitates compared to known samples of Cu_2O and Cu. (A) stationary electrolyte cell products from active dissolution at 1.33 A/cm^2; (B) stationary electrolyte cell products from active dissolution 0.457 A/cm^2; (C) copper anode before dissolution; (D) reagent grade Cu2O in Lucite holder; (E) insoluble transpassive phase dissolution products, stationary electrolyte cell, 1.33 A/cm^2; (F) Lucite holder.

Table IV-5. Summary of Results of X-Ray Diffraction Analyses: Water Insoluble Reaction Products. Cu/2F $NaClO_3$

System	Experimental Conditions	Point of Cycle of Current Interruption	Sample Support	Compounds Identified	Unidentified Peaks?
STAT.*	1.33 A/cm^2	Active dissolution	Cu	Cu, Cu_2O	No
STAT.	0.457A/cm^2	Active dissolution	Cu	Cu, Cu_2O	No
STAT.	1.33 A/cm^2	Peak	Lucite	Cu_2O	Yes
Disk	0.64 A/cm^2, 360 r.p.m.	Active, 1st cycle	Cu	Cu, Cu_2O	No
Disk	"	Transpassive, 1st Cycle: V_5/V_7	Cu	Cu, Cu_2O	No
Disk	"	Transpassive, 1st Cycle: V_7/peak	Cu	Cu, Cu_2O	No
Disk	"	Active, 2nd cycle	Cu	Cu, Cu_2O	No

*Stationary electrolyte cell.

The spectrum of the insoluble phase of the loosely adherent, transpassive products is shown in Fig. 4.34-E. Peaks due to cuprous oxide are evident. In addition, several unidentified peaks were found, including a strong peak at $2\theta = 25.0 \pm 0.1$ degrees (corresponding to a diffraction plane spacing of 3.559 ± 0.014Å). It is likely that at least part of the cuprous oxide found in the transpassive region had been produced in the active phase of the cycle.

Analyses were made of the films adhering to the copper substrate at the following points within the oscillation cycle: (1) between the onset of transpassive dissolution and the shoulder on the potential peak; (2) between the shoulder and peak potential; and (3) one second after the fall from peak potential to the trough potential of the second oscillation cycle. In all cases, the X-ray diffraction spectra showed only peaks corresponding to copper and cuprous oxide.

C. Morphology of Anodic Reaction Products and Copper Substrate

1. Introduction

In Section IV-A, it was noted that the oscillation cycle produced at low current densities could be resolved into a succession of distinct potential plateaus and a potential peak. The term "active phase" was given to the lowest potential phase of the cycle, between points V_1 and V_3 in Figs. 4.3 and 4.36. The remaining, higher potential portions of the oscillation cycle were called the transpassive phase.

The active phase is associated with a dull, etched appearance of the copper substrate. During active dissolution, an adherent, porous layer of a red-orange substance (identified as cuprous oxide) was observed to accumulate on the surface. Beginning with the onset of transpassive dissolution, the copper substrate becomes progressively smoothed and polished. Solid reaction products are found in two distinct layers: (1) a thin layer of submicron thickness (containing cuprous oxide); and (2) a thick precipitate (order of magnitude, 10-100 microns) containing cuprous oxide and a dark blue, water soluble substance (presumably cupric chlorate). Active and transpassive phases were further distinguished on the basis of instantaneous apparent valence.

At low current densities, the separate portions of the oxcillation cycle may occupy intervals of tens or hundreds of seconds, and the morphology of solid reaction products and of metal substrate characteristic of each phase may be clearly identified. In Chapter V, morphological aspects will be correlated with electrical and chemical results in order to develope a comprehensive picture of the oscillation cycle.

2. The Growth and Removal of the Precipitate Layer

One of the most striking features of the oscillation phenomenon is the abrupt outward displacement of solid reaction product layers which occurs during each cycle. In the channel flow system (No. 1), the periodic detachment and removal of solids from the anode surface was viewed through the glass walls of the channel with the use of a telescope. At low flow rates and current densities below about 5 A/cm^2,

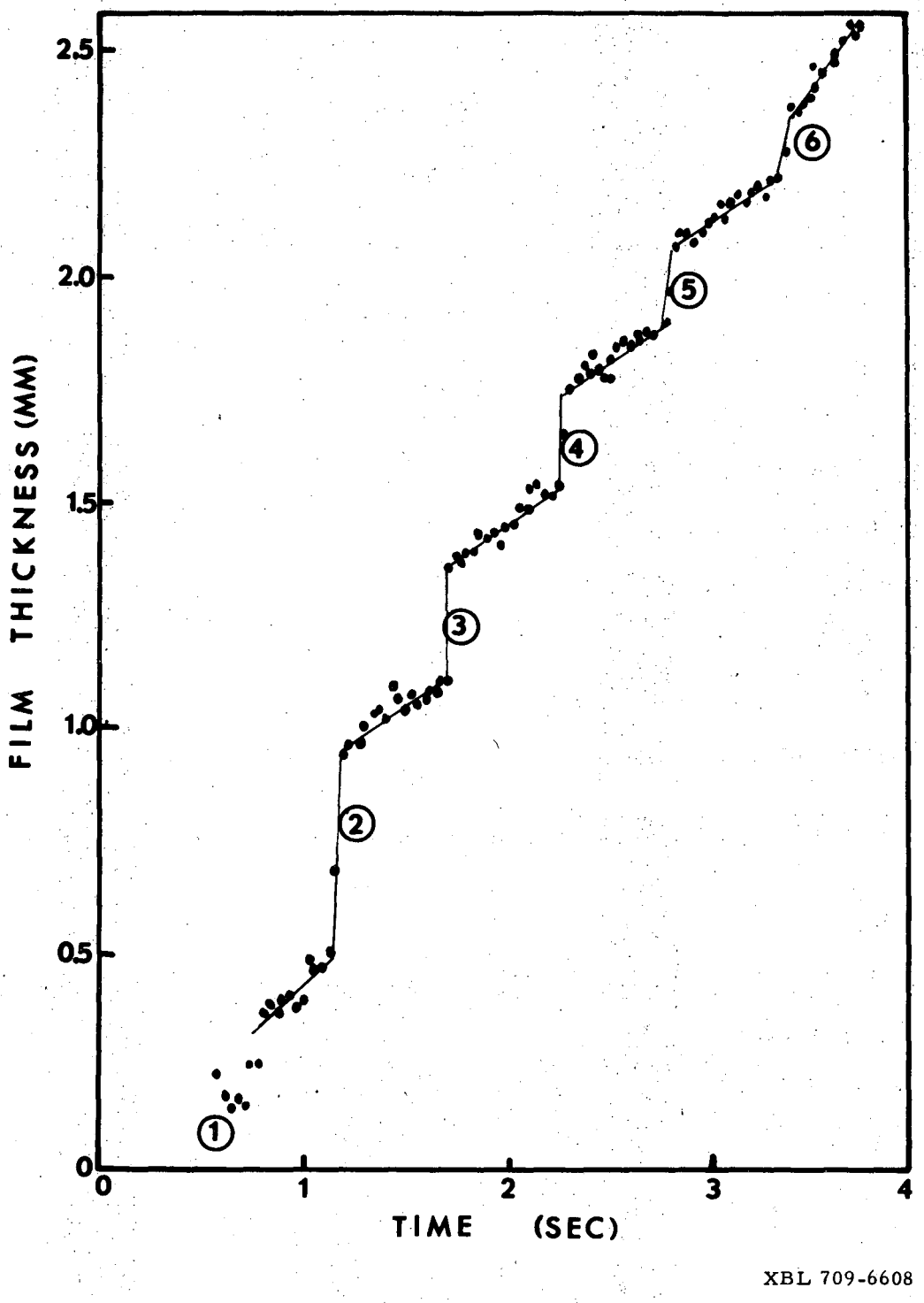

XBL 709-6608

Fig. 4.35. Plot of relative film displacement during anodic dissolution of Cu in 3F $NaClO_3$ at current density, 3.12 A/cm^2.

a surface film was observed to detach as a unit from the copper substrate at a frequency equal to that of the potential oscillations. With the rotating disk electrode system, at 0.32 A/cm^2, the detachment was observed to occur a few seconds after the abrupt drop from peak potentials, when the potential had settled to the active level of the following cycle.

An analysis was made of a motion picture of the growth and removal of reaction products during dissolution in stationary 3F $NaClO_3$.* The anode was machined from a 0.61 cm diameter rod of OFHC copper, which had been cast in Epoxy. The circular cross section of the rod served as the anode surface. The current density was 3.12 A/cm^2. The motion picture was filmed from a line of sight lying in the plane of the vertical anode surface.

The distance between the images of the electrode surface and a particle lodged in the center of a thick layer of accumulated products was measured frame by frame. The measurements were converted to a plot of film displacement against time (Fig. 4.35). It was assumed that the displacement of the bulk of the precipitate reflects the thickening and outward displacement of a layer adjacent to the anode/electrolyte interface.

Until the drop from peak potential, the precipitate layer thickens linearly with time. The outward movement near the fall from peak potential is comparatively rapid, occurring in less than 0.33 seconds

*The motion picture was filmed by K. Kinoshita as part of his doctoral research.[5]

(the time resolution limit for a 32 frame/second camera speed). An order of magnitude estimate of the solid fraction of the precipitate layer may be obtained by dividing the thickness of a hypothetical Cu_2O layer (grown at 100% current efficiency) by the measured change in thickness of the precipitate layer during the same cycle. For the experimental conditions at hand, solids comprised a small fraction (less than 2%) of the total volume of the observed layer.

3. Optical Microphotography of the Anode Surfaces

a. Preparation of electrodes for microphotography. The rotating disk anodes were prepared for dissolution as follows: (1) electrodes were ground flat against kerosene-wetted 4/0 emergy paper; (2) polished on a 1 micrometer diamond abrasive wheel; (3) washed in Labtone detergent and distilled water; (4) rinsed in ethanol and then acetone; and (5) dipped in dilute (10%/vol) nitric acid. After the interruption of current, the anode was immediately withdrawn from the electrolyte and washed in a jet of distilled water. The ellapsed time between current interruption and completion of washing was less than 5 seconds.

b. Results. The electrode surfaces were examined and photographed with the use of a Carl Zeiss Metallograph microscope.* Table IV-6 summarized the experimental conditions under which the anode specimens were prepared. Figure 4.36 is intended as a key for the correlation of the photographs in Figs. 4.37-38 with points on the oscillation cycle. Dark field illumination was generally used to heighten contrast between the etched and polished surface textures. With dark field illumination, polished surfaces appear dark.

*Carl Zeiss, Oberkochen, West Germany

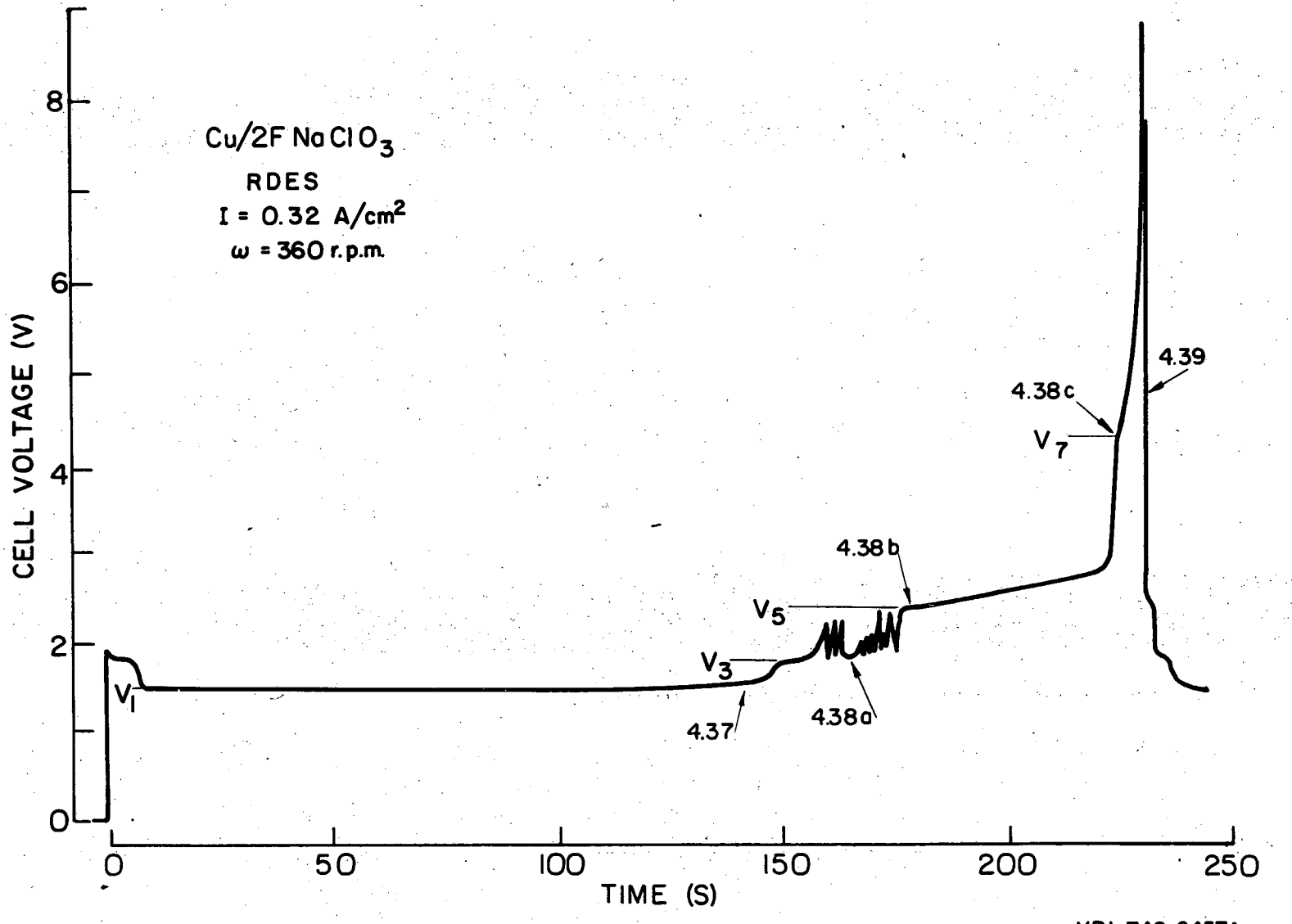

Fig. 4.36. Key to anode surface microphotographs, Figs. 4.37-4.39.

The surface preparation (including polishing with 1-micrometer diamond) is not expected to influence the surface textures obtained after prolonged dissolution. For example, at a current density of 0.32 A/cm^2, a layer of copper 32 micrometers is removed by dissolution before the completion of the active phase of the first dissolution cycle.

Figure 4.37 shows the active surface before and after removal of the porous cuprous oxide layer.

The term "active phase" was given to this portion of the cycle as an interpretation of the etched appearance of the copper substrate and the low overpotentials for dissolution. Active dissolution involves mechanism whereby the metal cation is believed to pass from a position in the metal lattice (or from a position adsorbed on the crystal surface) directly to a complex in the aqueous phase. Certain defect sites (such as grain boundaries, kink sites, or edges of incomplete planes) have lower free energies of activation for dissolution. Continued removal of cations from such sites gives rise to fine pits, the walls of which often consist of planes of low index numbers. Light scattered from the pitted surface accounts for the dull, matt appearance of the electrode surfaces produced during active dissolution.

The transition from active to transpassive dissolution is accompanied (at low current densities) by random fluctuations in potential (Fig. 4.36). Figure 4.38a shows a surface obtained by the interruption of current at the V_3 potential level during the trough phase of the low amplitude fluctuations. The surface at this stage of

Table IV-6. Key to Microphotographs of Anode Surface

Figure Number	Current Density (A/cm^2)	Phase of Cycle	Cycle Number	Illumination	Comments
4.37a	0.32	active dissolution	1	Dark Field	Thick phase of Cu_2O, and copper substrate
b	0.32	active dissolution	1	Dark Field	Detail of active phase copper substrate
4.38a	0.32	onset of transpassive	1	Dark Field	Thick phase of Cu_2O (x)
b	0.32	V_5 potential plateau	1	Dark Field	Thin transpassive film of Cu_2O spreads from right to left in photo
c	0.32	Inflection point (V_7)	1	Dark Field	Etching of Cu Substrate
d	0.60	active, 1 s after breakdown	2	Dark Field	Transpassive thin film detached from surface; growth of second thick phase of Cu_2O
4.39a	0.32	During breakdown of potential	1	Bright Field	Interface (arrow) between pre-breakdown and post-breakdown transpassive film.
b	0.32	"	1	Dark Field	Interface (arrow) between pre-breakdown and post-breakdown transpassive film.

Table IV-6. Key to Microphotographs of Anode Surface (Continued)

Figure Number	Current Density (A/cm^2)	Phase of Cycle	Cycle Number	Illumination	Comments
c	0.32	During breakdown of potential	1	Dark Field	Detail of post-breakdown film, showing detachment of film from substrate
d	0.32	"	1	Dark Field	Detail of post-breakdown film showing growth of thick, porous phase of Cu_2O
4.40a	4.0	Trough potential after prolonged dissolution	--	Dark Field	Etch patterns
4.40b	4.0	"	--	Dark Field	Detail of etch pattern

All samples were produced in 2F $NaClO_3$ with an anode rotation frequency of 360 rpm.

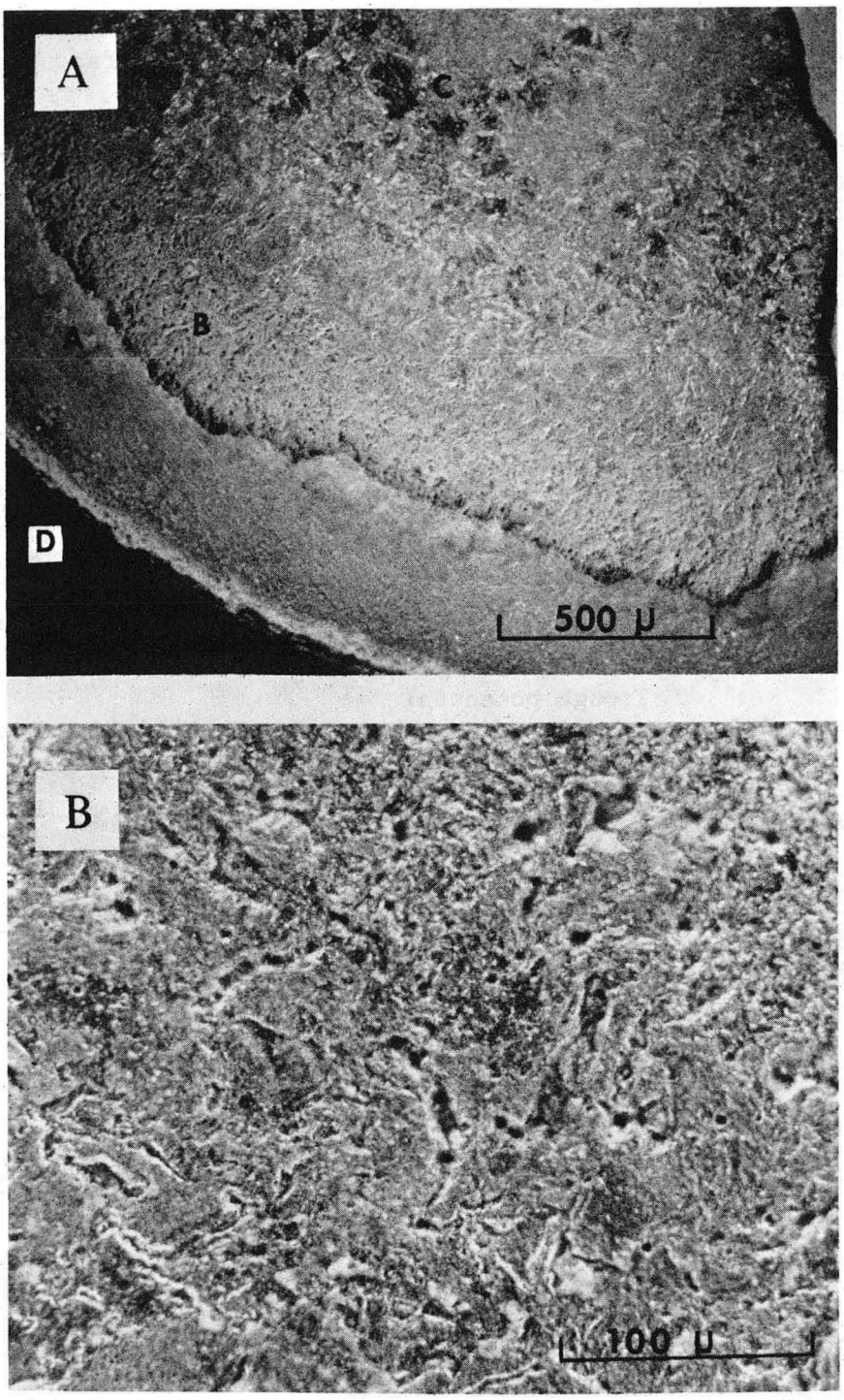

XBB 7401-7512

Fig. 4.37. Anode surface during active dissolution. (See Table IV-7). (A) Porous layer of Cu_2O--A; pitted substrate--B; initial passive film formation--C; Epoxy electrode holder--D; (B) Detail of pitted substrate.

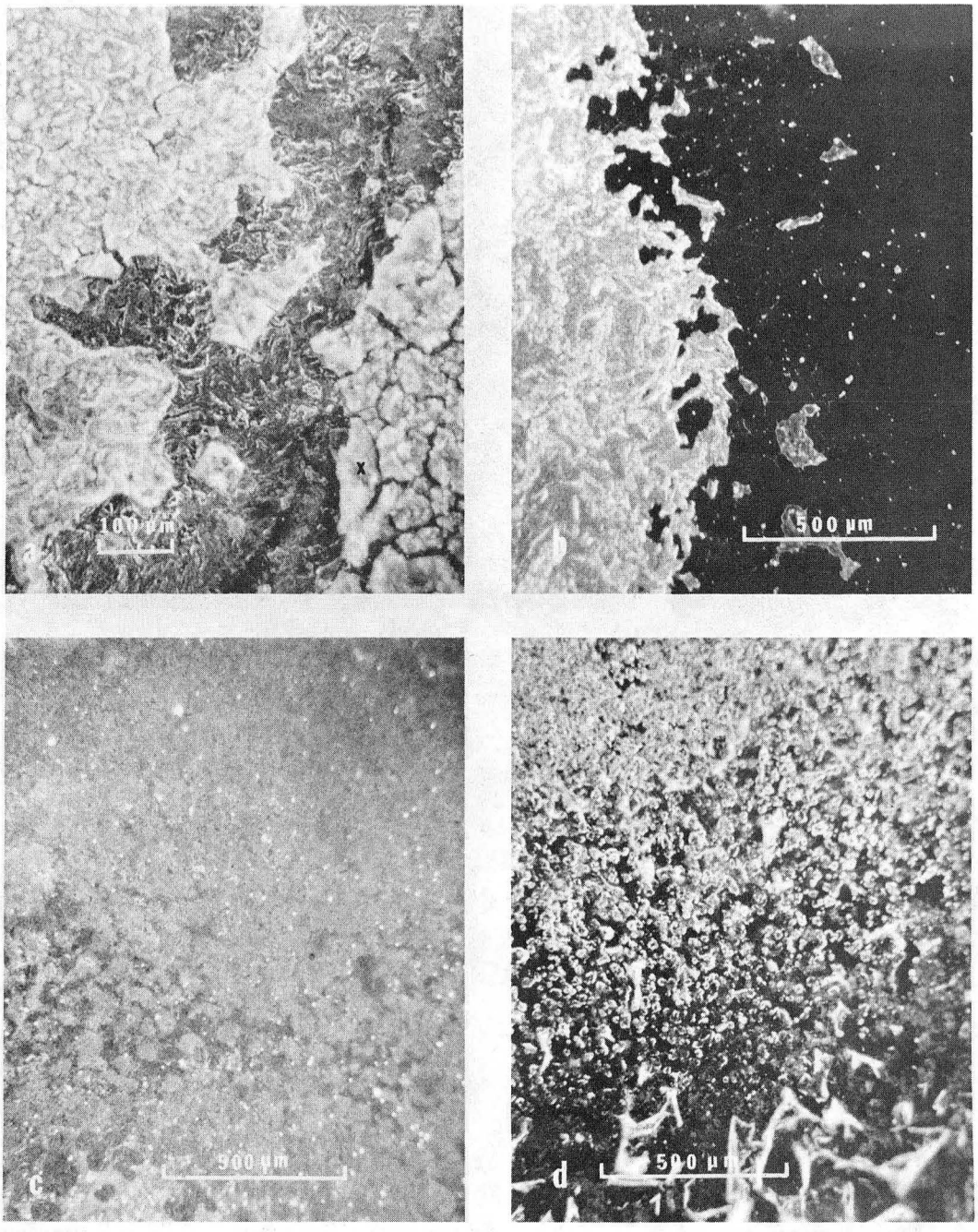

XBB 742-1071

Fig. 4.38. Anode surface during transpassive dissolution phases.
(a) onset of transpassive dissolution; thick Cu_2O phase indicated by X;
(b) thin transpassive film spreads from right;
(c) inflection point;
(d) breakup of thin transpassive film following potential breadkown.

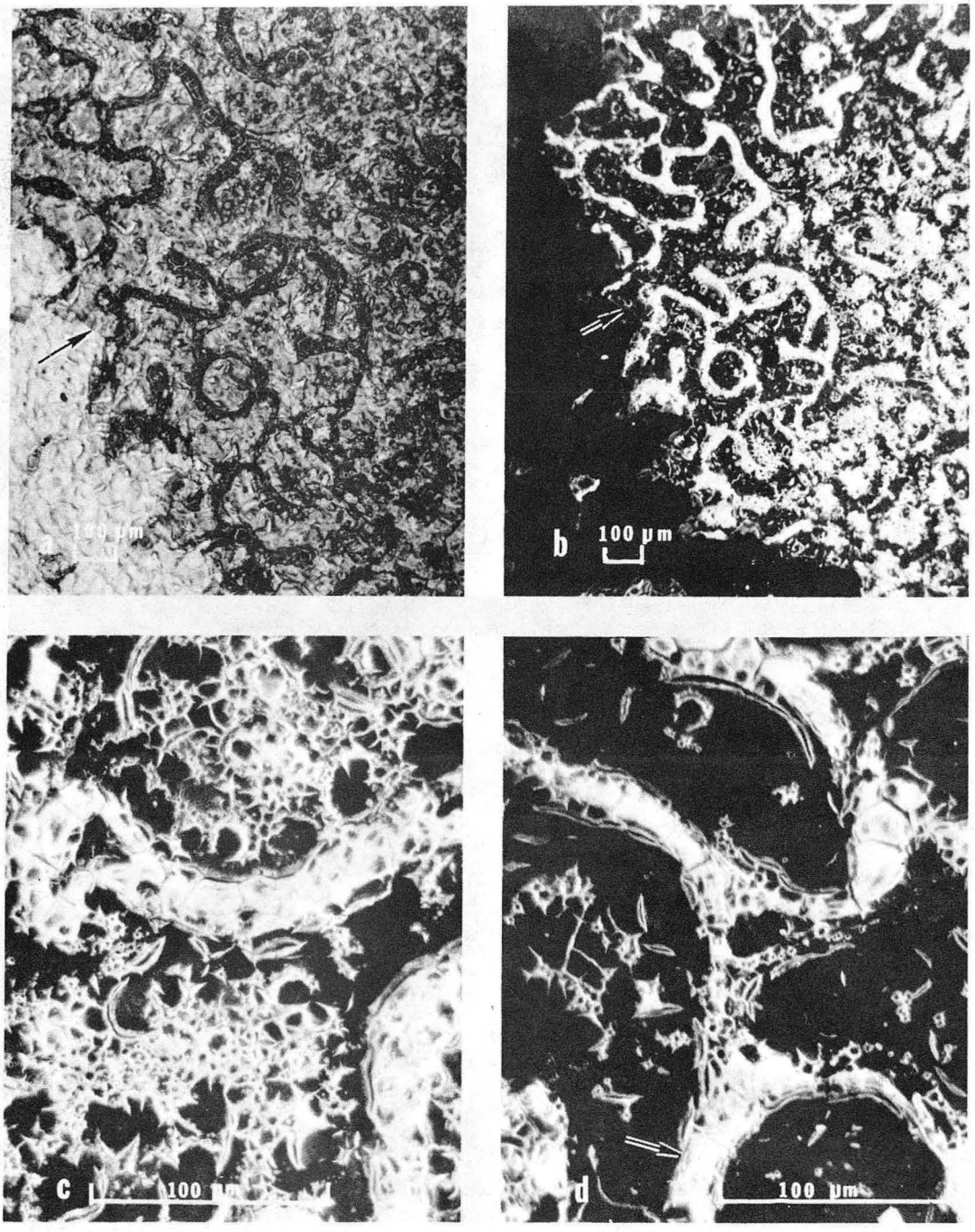

XBB 742-1070

Fig. 4.39. Anode surface during potential breakdown. In photographs (a) and (b), interface between broken and unbroken portions of film indicated by an arrow.

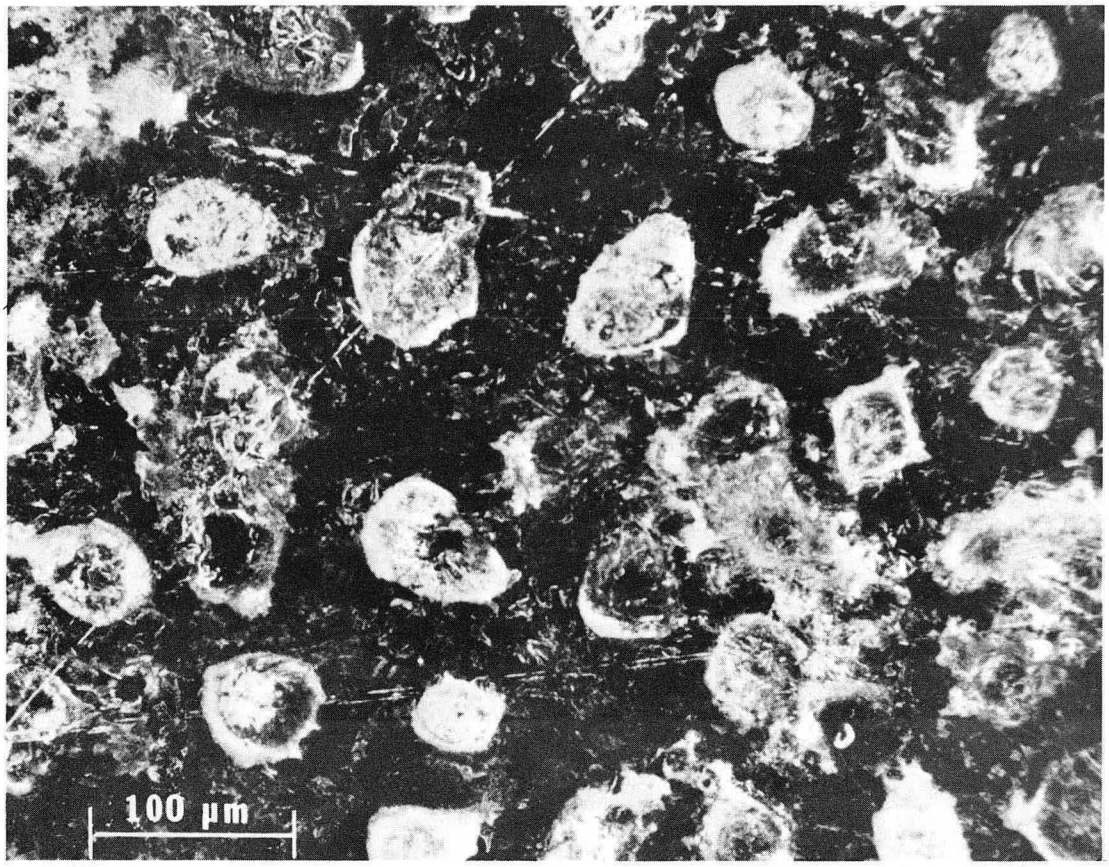

CBB 754-1801

Fig. 4.40. a. Etch patterns obtained after prolonged dissolution.

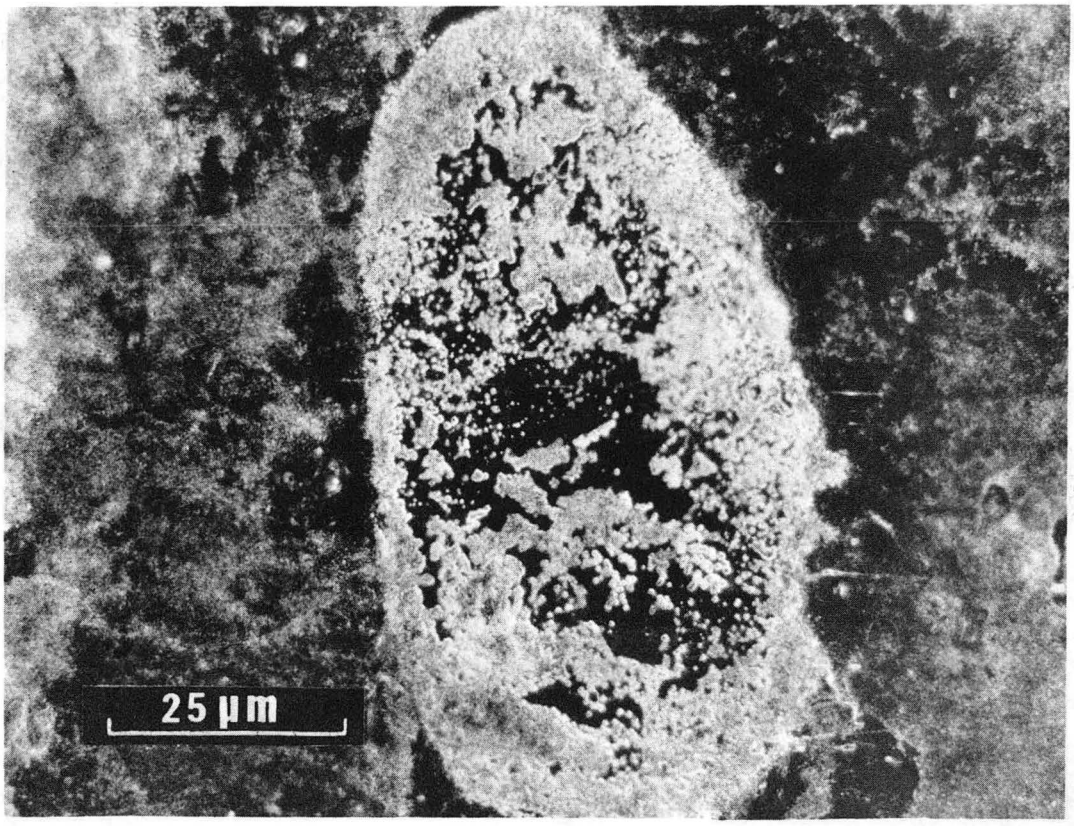

XBB 746-4065

Fig. 4.40b Detail of etch pattern obtained with prolonged dissolution.

the cycle is partially covered with the thick layer of cuprous oxide. The thick layer is marked with an "x" in Fig. 4.38a. The layer is less strongly adherent to the metal substrate at this point in the cycle than during the active phase. The layer is 10-20 micrometers thick, as determined by measurements with a stylus surfanalyzer.

From the onset of transpassive dissolution, a thin film spreads progressively from the circumference of the anode disk toward the center. At the same time, the copper substrate beneath the film becomes progressively flattened and polished. The thin film undermines the thicker layer such that, with the rise in potential to V_7, the thick layer may be entirely removed from the substrate in a jet of distilled water. In stationary electrolyte experiments the thick layer has been found to entrap an intensely blue fluid. As cuprous complexes are pale blue or colorless, the blue substance undoubtedly contains a mixture of cupric chlorate and chloride.

Figure 4.38b shows a boundary between a polished annular ring and a rough central area during the potential plateau following V_5. The sharpness of the boundary is likely to be enhanced as a result of local corrosion currents flowing after the external circuit has been broken. The probable reactions are:

$$Cu = Cu^{++} + 2e^- \quad \text{(central, anodic sites)}$$

$$H_2O + Cu_2O + 2e^- = 2Cu + 2OH^- \quad \text{(circumferencial, cathodic sites)}$$

Evidence of such local currents was found by Bonhoeffer and Gerischer[55] after the interruption of current during the passive phase of the potential oscillations which occur in hydrochloric acid.

The flattening and polishing of the anode substrate during transpassive dissolution is believed to be the consequence of the large resistance of the thin film to ionic conduction. With the onset of transpassive dissolution, the resistance of the thin film replaces the charge transfer resistance of active dissolution as the controlling impedance for the distribution of current on a microscopic scale. In the thin film is of uniform properties (ionic conductivity and thickness), the current density will be uniform on the surface of any asperity having dimensions which are large compared to the thickness of the film. Continued dissolution under these circumstances will lead to a flattening of an initially rough surface. The mechanism described above is similar to that which is widely held responsible for the electropolishing of copper in, for example, orthophosphoric acid solutions.[120,131]

At cell voltages above V_7, the anode surfaces beneath the precipitate layer appear polished and nearly specular to the unaided eye. With the use of the Metallograph and intense oblique illumination, the surface is seen to be covered with a myriad of diffraction points, as shown in Fig. 4.38c, the surface appears matt, as a consequence of light scattered from the "diffraction points." The individual points could not be clearly resolved with the optical microscope. The appearance of the scattering points may be an initial stage of the

potential breakdown process. We recall from Section IV.A8a, that the cell voltage V_7 markes the minimum potential for cell voltage breakdown at low current densities.

After the fall from peak to trough potentials, the thin film detaches from the metal substrate. The deteched films, appearing in the lower half of Fig. 4.38d, are transparent and resemble crumpled cellophane. Also shown in Fig. 4.38d is a new phase of cuprous oxide, which developes during the active phase of the cycle.

In one experiment current was interrupted during the fraction-of-a-second interval in which the potential was falling from peak to trough levels. A boundary between pre-breakdown and post-breakdown topographies is clearly distinguished in bright and dark field photographs of Figs. 4.39a,b (arrows). With higher magnifications, the film of the post-breakdown surfaces appears split and partially detached from the metal in a number of places. The detachment is complete along a number of meandering paths, although this effect may be consequence of local cell corrosion taking place after current interruption. It is not possible to tell from the microscopic examinations of such electrodes if breakdown occurs as the result of an "activation wave," which sweeps across the surface. There is strong evidence (see below) that reactivation of the entire anode surface generally does not occur after the fall from peak potentials.

The surface topographies produced after prolonged dissolution at higher current densities were also investigated. The anode surfaces appearing in Figs. 4.40a,b were produced by interruption of current

during the trough phase following many oscillation cycles at a current density of 4.0 A/cm^2. Numerous etched patches are distributed with almost geometric regularity on an otherwise polished surface. Details of the etch pattern are shown in Fig. 4.40b. A similar geometric distribution of large pits was produced under certain circumstances during the high current density dissolution of copper in sodium nitrate solutions.

During the high potential phase of the cycle at high current densities, the anode surface is polished on a microscopic scale, but the surface undulates with numerous shallow depressions. The shallow depressions give transpassive surfaces a texture resembling that of an orange peel. The orange peel texture may be the consequence of selective and enhanced dissolution of the etched patches during active phase dissolution.

It is apparent from these photographs that potential breakdown needs not reactivate the entire anode surface. In general, it was found that parts of the thin film from one cycle remained on the surface during the active phase of the succeeding cycle. Incomplete reactivation at high current densities has already been inferred from the large excess of trough cell voltage over that which may be attributed to the ohmic drop in the electrolyte. (See Sections IV.A8c)

D. Electrical Breakdown of Transpassive Thin Films on Copper

1. Introduction

Many electronic insulators and semiconductors are known to undergo an abrupt drop in resistivity upon being subjected to a critical electric field strength. The transition from high to low resistance may be accompanied by the destruction of the material. In such cases the term "breakdown transition" is used. In other cases, called "resistive switching transitions," no readily perceptible material changes occur. The subjects of breakdown and resistive switching phenomena have been thoroughly reviewed in recent articles by N. Klein.[134,135]

Switching and breakdown transitions are known to occur with a wide variety of substances, both amorphous and crystalline, including certain chalcogenic glasses, anodic oxide films of valve metals, and metal halides. Of particular interest to us is the reported occurrance of resistive switching in single- and polycrystalline cuprous oxide samples, which were prepared by the high temperature air oxidation of copper.[136] It is possible that the anodic potential oscillations are intimately connected with a resistive switching of the thin cuprous oxide films produced during transpassive dissolution. A brief discussion of resistive switching and breakdown will be given below, in preparation for the presentation of our experimental results on the resistance transitions in transpassive films produced during anodic dissolution of copper in sodium chlorate solutions.

2. Resistive Switching and Breakdown

Despite the large variety of classes of materials which undergo resistance transitions, the transition events are surprisingly similar when viewed on a phenomenological level. A typical steady state current-voltage characteristic for such substances is shown in Fig. 4.42a. The characteristic consists of a high voltage, low current branch (B) and a low voltage, high current branch (A). The external voltage source (V_s) and series resistance (represented in the figure by a load line) determine the voltages and currents before and after the transition.

The transition is a multistep process, and in general as many as four distinct stages are traversed from the moment of the application of potential to the completion of the event. (1) Initiation Stage. The resistivity drops continuously following the application of potential to a point on the rising portion of the characteristic (B). (2) Instability and Current Runaway. This stage is associated with the portion of the steady state high voltage characteristic showing a negative differential resistance. (3) Voltage Collapse. Energy stored in the electric field is dissipated in the form of heat. If field strengths prior to voltage collapse are sufficiently high ($> 10^5$ V/cm), this stage may be accompanied by local melting and vaporization of the material. (4) Establishment of the Low Voltage Characteristic Branch. With continued passage of current after voltage collapse, a permanent low voltage characteristic is obtained.

The drop in resistance during each stage of the transition may be the consequence of (1) processes which are essentially thermal in nature; (2) processes which are essentially electronic in nature; or (3) thermal processes which are initiated by electronic events. For a given substance, the processes operative depend on the field strength.

It is the third class of processes (called "electronic, modified thermal events") which is widely held responsible for breakdowns and switching in anodic oxide films. A momentary increase in current may be brought about by an electronic event, eg., charge multiplication by impact ionization (avalanching). Semiconductors and insulators have electrical conductivities which increase with temperature. As a consequence of this behavior, local heating along the path of the avalanche may lead to an increase in electrical conductivity and an increase in current. Beyond a certain critical current level, the increase in current and Joule heating will become self-accelerating and will lead to voltage collapse. Mathematical modelling of thermal breakdowns has been persued by Wagner[137] and O'Dwyer.[138]

Electronic, modified thermal events characteristically have the following properties:

(1) Transitions occur over a range of fields, from 10^5 to 10^7 V/cm.

(2) A statistical time lag, T_1, occurs between the application of potential and voltage collapse.

(3) The median time lag decreases rapidly and often exponentially with increasing breakdown field strengths.

(4) The time lag decreases with increasing thickness of the sample.

In switching transitions, the nature of the permanent low resistance state is not fully understood. In general, when a separate low voltage i-V characteristic is obtained, current is conducted through a number of distinct filimentary pathways. The pathways may be the result of a recrystallization and quenching of a high temperature phase of the material. For cuprous oxide, it has been suggested that the pathways consist of copper threads, formed by a high temperature disproportionation of a defect structure of cuprous oxide:[136]

$$(Cu_2O)_{defect} = CuO + Cu$$

3. Experimental Procedures and Apparatus

Experiments were undertaken to determine whether or not the thin cuprous oxide films formed during transpassive dissolution could sustain resistive-conductive transitions at potentials comparable to the amplitudes of the potential oscillations.

Electrodes of the rotating disk system were prepared for dissolution in the manner described in Section IV-C3a. After interruption of current at a point within the transpassive phase of the first oscillation cycle, the electrodes were immediately withdrawn from the electrolyte, washed in distilled water, and allowed to dry.

The anodes were fastened to a movable stage fitted with micrometer screws to allow positioning in two dimensions in the horizontal plane. A testing probe was formed as follows: With the use of a gas flame, a bead was formed on the end of a length of 15 mil copper wire; the

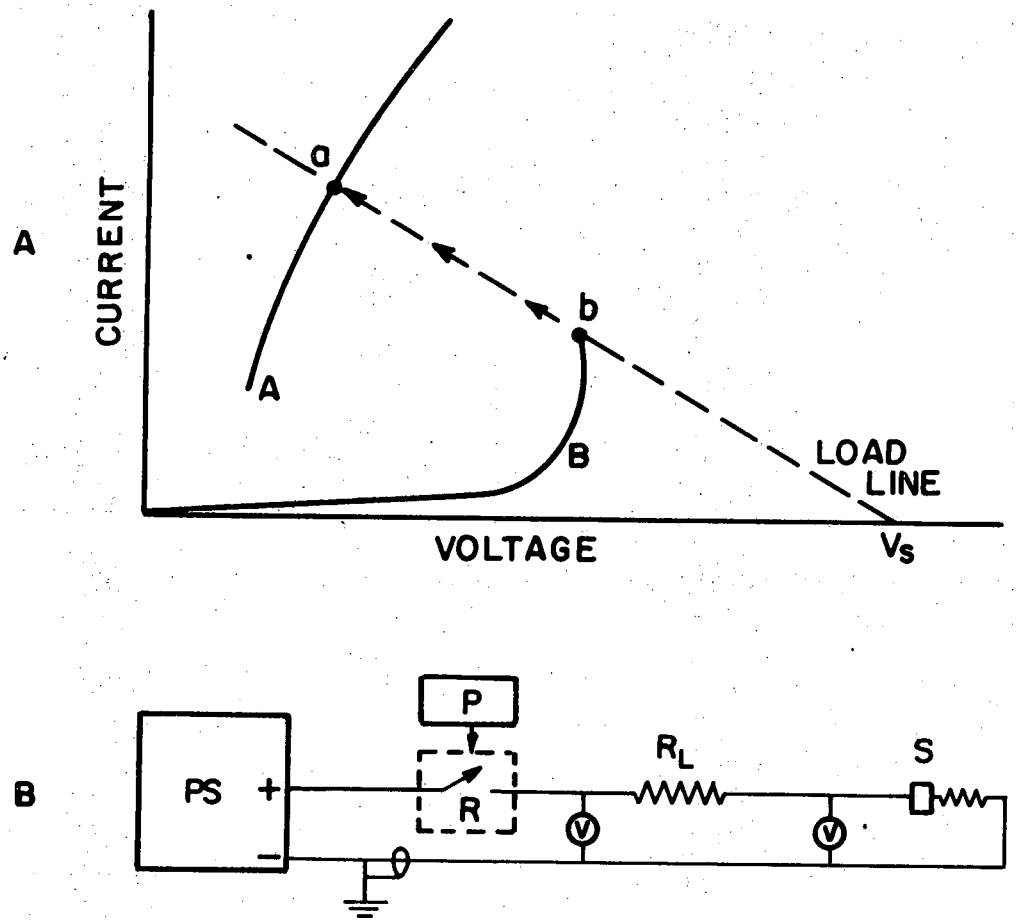

XBL749-7139

Fig. 4.42. (A) Current-voltage characteristic of materials showing resistive-conductive transitions. Low resistance state--A; high resistance state--B; source voltage, V_S. (B) Testing circuit used in breakdown studies of transpassive films. PS, power supply, P, pulse generator; R, mercury-wetted relay; R_L, decade resistance; anode specimen and probe; V, dual beam oscilloscope.

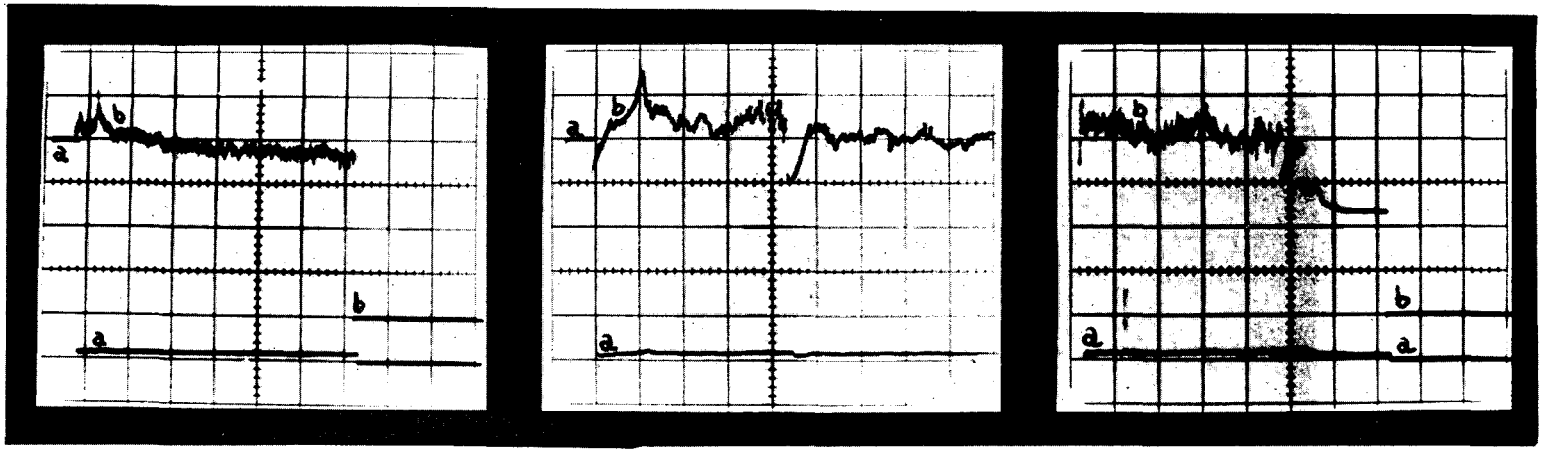

XBB 7410-7511A

Fig. 4.42. (C) Oscilloscope recordings showing time sequence of resistive-conductive transitions in dry transpassive film samples. Breakdown voltage, 10V; R_L=100 ohms. Voltage across film is recorded in traces (a) and (b); traces (a), 2 V/large division; traces (b), 0.1 V/large division. Time scales: 1 ms/large division in photos (1) and (3); 0.1 ms/large division in photo (2)

Samples prepared by interruption of current during dissolution at 0.8 A/cm^2; rotating disk electrode system; 360 r.p.m.; anode potential (relative to trough potential): (1) 8.1V; (2) 9.0 V; (3) 8.0 V.

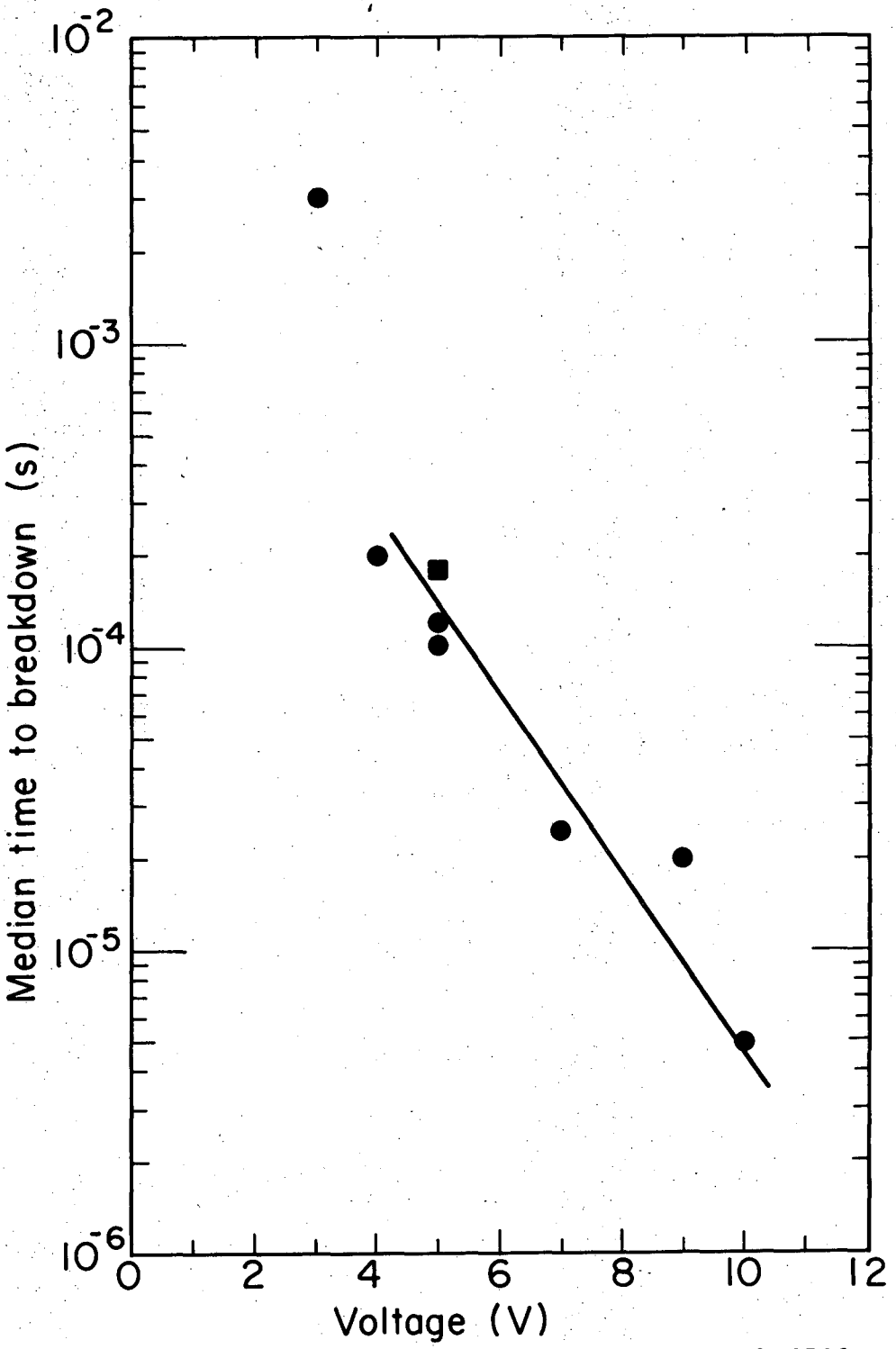

Fig. 4.43. Median time lag to breakdown. Transpassive film produced in 2F $NaClO_3$; current density, 0.8 A/cm^2; rotating disk electrode system, 360 r.p.m.; current interrupted at 5.9 V above trough potential during dissolution; peak potential under these experimental conditions, roughly 9 V.

bead was electropolished in orthophosphoric acid and surface films were subsequently removed in dilute nitric acid. The probe was attached to a lever arm allowing positioning in the vertical axis. The testing set-up allowed the bead to be brought into contact with any point of the anode surface with a minimum of contact pressure. The use of the movable spherical probe is widespread in studies of electrical breakdown.[134]

The testing circuit is shown in Fig. 4.42b. The constant potential source was a Fluke Current/voltage Calibrator.* Current was limited by a series decade resistor (R_L). A mercury-wetted relay switch (R) was closed for a preselected time interval by a square wave pulse generator (P). Voltage drop across the sample or resistor was followed with the use of a Tektronix dual beam oscilloscope. The negative terminal of the power supply was grounded adn shielded cable was used throughout the circuit.

4. Results

Breakdown transitions were found to occur when a potential of 1 to 20 volts was applied across the transpassive films. The occurrance of breakdowns did not depend on the polarity of the probe. After the application of the potential (with a rise time of about 10^{-6} s), the following sequence was observed: (1) the potential remained constant for a time interval of variable length; (2) a rapid fall in potential

*Model 382a; John Fluke Mfg. Co., Inc., Seattle

occurred (fall time about 10^{-6}s); (3) a period of random potential fluctuations followed; and (4) the potential settled to a constant level, which depended on the applied current. The sequence is shown in the oscilloscope photographs in Fig. 4.42c; both traces (labeled a-a, b-b) show voltage drop across the sample on different voltage scales.

Resistance of the anode-probe assembly was measured before and after breakdown with the use of a high impedance electrometer Princeton Applied Research, Model 134; input impedance, 10^{12} ohms). Resistance dropped from 400-600 Mohms to 1-10 ohms. Resistivities could not be computed due to unknown area of conduction pathway, although an effective resistivity change by a factor of 10^7 - 10^8 is evident.

The time lag to breakdown varied widely from specimen to specimen. For a given specimen, median time lag for 20-50 breakdown events was calculated and plotted against applied voltage on a semi-logarithmic plot. The expected linear decrease was obtained. For each voltage, a scatter in time lag of up to one order of magnitude was obtained. The following conditions may be responsible for the considerable scatter of the time lags to breakdown: (1) special inhomogeneities in film properties (conductivity, stoichiometry, and thickness); (2) introduction of weak spots caused by the fracture of the film due to contact probe pressure; or (3) naturally occurring weak spots in the transpassive film (e.g., along grain boundaries).

It can be concluded from these experiments (1) that resistive-conductive transitions occur in dry transpassive films upon the application of voltages comparable to that of the oscillation amplitude; and (2) that the breakdowns are qualitatively similar to those observed in a variety of anodic oxide films. A model for anodic potential oscillations based on anode reactivation following resistive-conductive transitions will be presented in Chapter V.

V. INTERPRETATION OF EXPERIMENTAL RESULTS

In this chapter, we shall endeavor to integrate the experimental results presented in Chapter IV into a comprehensive picture of the periodicity observed during the galvanostatic dissolution of copper in the chlorate electrolyte. In section (A), a model will be presented for the interpretation for the observed alternate growth and breakdown of anode resistance. Section (B) derives the physical basis for the model from the chemical and physical properties of cuprous oxide reported in the literature. In section (C), we shall discuss certain experimental results on the basis of our model. It will not be possible to formulate conclusive explanations for all of our experimental results. Rather, we shall attempt to explain the sequential growth and destruction of the anode surface film in terms of sequential changes in the chemical, electrical, and morphological properties of the anode surface film.

A. A Model for the Interpretation of Periodic Growth and Breakdown of Anode Resistance

The model presented here for the interpretation of periodicity in the galvanostatic dissolution of copper is a relaxation model. (As discussed in Section II-D, relaxation models involve unit cycles wherein continuous processes alternate with abrupt and rapid changes in the electrode state, which occur when the system is subjected to some critical stress.) Three phases of the oscillation cycle are proposed: (1) uniform growth of a cuprous oxide films; (2) resistive breakdown transition of the film; and (3) mixed electrode processes

leading to a restoration of uniform film growth. The phases are depicted schematically in Fig. 5.1.

1. Presentation of the Model

At some point after closing the electrical circuit to the cell, a non-porous cuprous oxide film nucleates and spreads over the anode surface. The film covers the copper substrate and grows in thickness. Film impedance controls current distribution such that growth rate and thickness are independent of position. During growth, the mean field strength (voltage drop divided by film thickness) increases as a consequence of the accumulation of space charge associated with the ionic current carriers. This growth phase is represented by (ab) on each of the schematic diagrams of Fig. 5.1.

At a critical combination of mean field strength and thickness, represented by point (b), the film undergoes a resistive breakdown transition. The transition results in the formation of discrete channels of high electronic conductivity, as described in Section IV-D. As a consequence of low resistance conduction paths, electrode potential and field strength drop to low levels, and ionic current and film growth essentially cease. Electronic current now flows, and current distribution is highly non-uniform on a microscopic scale. The current is consumed in the oxidation of water ($H_2O = \frac{1}{2} O_2 + 2H^+ + 2e^-$). Local Joule heating and electrical discharges occur at the breakdown sites. The cuprous oxide film disintegrates at the breakdown sites by a combintion of dissolution (in the hot, oxidizing acid environment) and the physically disruptive effects of the discharges.

As portions of the copper substrate are uncovered, metal dissolution and film formation resume. Only when the entirety of the low conductivity film has been removed will film repair and sustained film growth occur. The growth of the new cuprous oxide film (segment a'b), spreading from points at the bases of the breakdown channels, will progressively undermine the unbroken remainder of the previous film.

The closed trajectory, a'bca', represents the stable course for all cycles after the first.

2. Inaccessibility of a Stable Electrode State

The relaxation model requires an explanation for the assumed inaccessibility of a stable electrode state giving rise to a uniform and time-independent electrode potential.

No stable electrode states can be reached within each of the three phases of the cycle. First, the growth phase results in a continuous increase of anode potential: anode resistance is roughly proportional to film thickness. Second, the breakdown phase results in a rapid lowering of film resistance: with the passage of current through newly formed low conductivity channels, the resistance of the channels progressively decreases. Third, the restoration phase of the cycle involves an unstable mixed electrode state. Here, electronic conduction resulting in gas evolution, spark discharges, and partial chemical dissolution of the film progressively destroys the originally uniform nature of the anode layer.

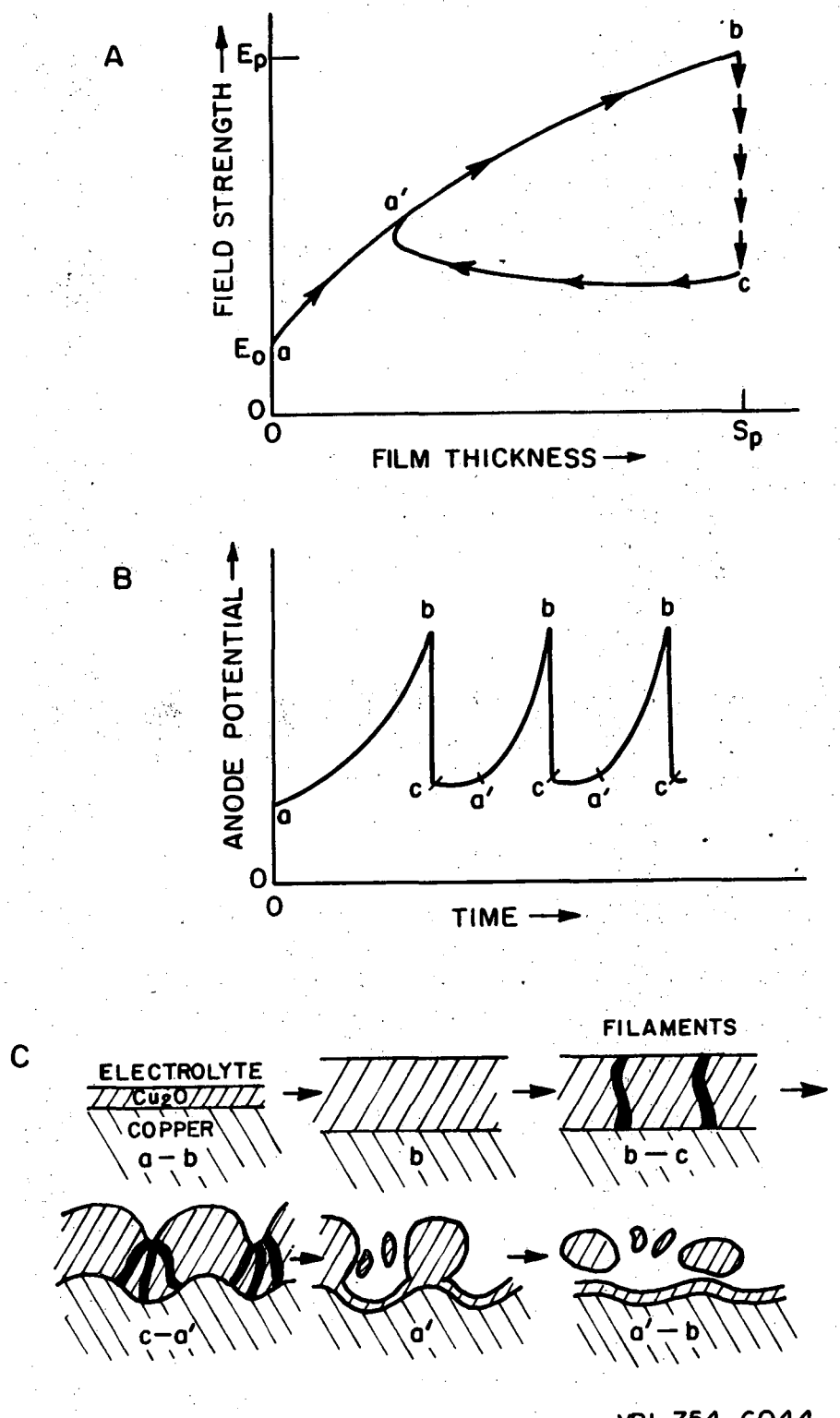

Fig. 5.1 (A). Phase plane diagram of oscillating system. (B) Schematic behavior of anode potential. (C) Schematic behavior of cuprous oxide transpassive film. In each figure, lower case letters refer to equivalent points on the reaction trajectory.

No stable mixed electrode state can arise whereby electronic current flows in breakdown channels and ionic current flows in the unbroken remainder of the film. At the instant of formation of a channel, the potential across the film will drop. Film thickness will remain unchanged. Ionic current (proportional to potential) will fall. As the total current is held constant, the electronic current in the channel will increase, causing a further lowering of channel resistance. In this manner, electrode potential and ionic current will continue to drop until film growth essentially ceases.

A fundamental difference exists between this model and models based on simple dielectric breakdown as discussed in Chapter II. In simple dielectric breakdown, a spark releases electrical energy stored in the electric field and causes local destruction of the film. The current immediately before and after breakdown is ionic and is consumed in respectively the growth or repair of the film. The electrode potential in the case of these models should hover near the breakdown potential while the rate of film growth is balanced by the rate of destruction. In our model, resistive breakdown transitions lead to a permanent lowering of the film resistance and to a temporary shut-off of ionic current and film growth. Film repair is deferred until the volume of solid containing the low conductivity channels is removed.

3. Regularity of the Oscillation Cycles

A relaxation model also requires an explanation for cycle regularity.

Period length and amplitude for all cycles after the first are predicted to be uniform by this model. For a given current density, a critical mean field strength $\bar{E}_{crit}$ will be reached at some critical film thickness, S_{crit}. Breakdowns will occur after the passage of a quantity of charge necessary to form the film. At a constant current, the time interval between film initiation and breakdown will be constant. During the restoration phase the same fraction of the original film must be removed. This will require that the same charge be passed during each restoration phase. The duration of the breakdown phase is negligible compared with the duration of growth and restoration phases. Therefore period length--the sum of the durations of all phases--will be constant for all cycles after the first.

Amplitude is merely the integrated area under the segment a'b in the phase plane diagram and will be constant after the first cycle.

4. Role of the Chloride and Chlorate Ions

This model does not directly indicate the role of the chloride or chlorate ions in the oscillation phenomenon. The chlorate ions may interact with the cuprous oxide surface to establish a high boundary concentration of lattice defects--specifically cation vacancies. This will be discussed further in Section V-B.2.b. The chloride ion may facilitiate the dissolution of the cuprous oxide during the restoration phase by providing soluble reaction products, $CuCl_2^-$ and $CuCl_2$; in addition, chloride is known to catalyze the reduction of ClO_3^- by Cu.[106]

It should be remembered that (1) anode potential oscillations are most uniform and pronounced in chlorate electrolytes; and (2) additions of halides to other electrolytes may give rise to an oscillating anode potential during galvanostatic dissolution of copper. Nevertheless, anode potential oscillations somewhat similar to those in the chlorate and halide electrolytes have been observed during the dissolution of copper in potassium sulfate electrolytes without halide additives.[89]

B. Physical Basis of the Model

We shall now take a closer look at the physical basis of the assumptions of the model presented above.

1. Non-Stoichiometry and Electrical Conductivity of Cuprous Oxide

The oxygen sublattice of the cuprous oxide crystal has a body-centered cubic structure. Each oxygen ion is tetrahedrally surrounded by four cuprous ions such that each cation has two nearest-neighbor anions. The unit cell constant is 4.27Å.

a. Electronic conductivity. Cuprous oxide is a cation-deficient, extrinsic, p-type semiconductor. Both electronic and ionic conductivity are strongly controlled by the deviation from the stoichiometric composition, Cu_2O. The metal deficiency can be expressed as y in the formula, $Cu_{2-y}O$. The value of y varies widely with the conditions under which the samples were prepared, as shown in Table V-1. Non-stoichiometric compositions have the same basic crystal structure, although the lattice is somewhat compressed and distorted for large values of y.

Cuprous oxide has been exhaustively studied under equilibrium conditions in high temperature, low oxygen pressure environments. The subject has been recently reviewed by Kofstad[100] and Jarzebski.[101] Neutral cation vacancies (V_{Cu}^{x})* form by the reaction,

$$(\tfrac{1}{4}\,O_2)_{gas} \rightleftharpoons V_{Cu}^{x} + \tfrac{1}{2}\,O_o\,, \quad \text{equilibrium constant, } K_a \tag{5.1}$$

where O_o represents an oxygen ion (O=) at a site in the oxygen sublattice. Electronic conductivity arises from the dissociation of neutral vacancies into holes ($h^{\cdot}$) and negative cation vacancies (V_{Cu}'):

$$V_{Cu}^{x} \rightleftharpoons h^{\cdot} + V_{Cu}'\,, \quad \text{equilibrium constant, } K_b \tag{5.2}$$

From the equilibrium relations and the assumption of electroneutrality the dependence of electron hole concentration on oxygen partial pressure (p_{O_2}) is calculated:

$$(h^{\cdot}) = (K_a K_b)^{1/2} p_{O_2}^{1/8} \tag{5.3}$$

Electronic conductivity is proportional to hole concentration. A number of experimental studies have confirmed the expected power dependence of conductivity and non-stoichiometry on oxygen pressure.[107,114,117-119]

---

*The Kroger-Vink notation[100,116] is used throughout this chapter. The major symbol indicates the species or defect (V, for vacancy). The subscripts indicate the location of the defect in the crystal lattice. Superscripts refer to the charge of the species relative to the normal charge in the perfect crystal: $'$, $\cdot$, and x for negative, positive, or neutral. For Cu_2O-Cu_{Cu}', Cu_{Cu}^{x} (or Cu_{Cu}), and $Cu_{Cu}^{\cdot}$ refer respectively to Cu, Cu^{+}, and Cu^{++} located at a site in the copper sublattice. Sites in a crystal from which Cu^{+} and Cu had been removed would be indicated respectively by V_{Cu}' and V_{Cu}^{x}.

Table V-1. Deviations from Stoichiometry in Cuprous Oxide.
(Deviation is expressed as y in the formula, $Cu_{2-y}O$)

y	Method of Preparation	Comments	Reference
0.76	Reduction of Cu_2SO_4 in Fehling's solution by glucose, hydrazine, or hydroxylamine	lattice compressed; a=4.2683Å (compare to 4.2700Å in near stoichiometric samples)	King[102]
0.50	oxidation of Cu at p_{O_2}=100 Torr at T=110-200°C.	no CuO present; form identified as gross defect structure of Cu_2O by X-ray, electron, diffraction	Wieder and Czanderna[110]
0.018-0.009	air oxidation of copper; various quenching and ageing procedures	samples contain possible CuO inclusions	Juse and Kurtschatow[111]
10^{-3}-$3\times(10^{-4})$	oxidation of copper in oxygen (0.5-30 Torr) at temperatures 900-1026°C	defect concentration represent equilibrium values under conditions of preparation	Wagner and Hammen[107] O'Keeffe and Moore[114]

One may consider the electronic conductivity of cuprous oxide to arise from a mobile valency: the electron hole is associated with a Cu+ ion to form a Cu++ ion, the excess charge being mobile.

Cuprous oxide is unstable relative to cupric oxide at atmospheric oxygen pressure and at temperatures below 800°C. (See the phase diagram in O'Keeffe[114]). The defect structure of the high temperature form is retained upon quenching, and the electrical and defect properties reflect the conditions during sample formation.

b. Ionic conduction. The high temperature oxidation of copper in oxygen takes place by the movement of ions and electron holes across the growing cuprous oxide film. Wagner elucidated the kinetics of copper oxidation. He accurately predicted the observe parabolic rate law constant from known values of specific electric conductivity, the free energy decrease of the oxidation reaction, and the transport numbers of the ions (the sum, $(t_{Cu} + t_{O})$) and electron holes (t_e). Wagner measured the transport number of copper and found the pressure-independent value of $4(10^{-4})$ at 1000°C.[123,126] The transport number of the electron holes was taken as nearly unity, and that of oxygen was assumed to be negligible. The transport number of oxygen has not been determined.

It is generally assumed that ionic conduction in metal deficient p-type semiconductors occurs by the migration of cations (see p. 28, ref. 115). During the oxidation of copper in oxygen, the transport of the cation involves place exchange of the ion and an adjacent vacancy. It has been determined that the cation concentration decreases

from the metal/oxide interface to the oxide/gas interface, while the vacancy concentration increases in the same direction.[103,112]

c. Anodic oxide films. The thin Cu_2O films formed during the corrosion or anodic oxidation of copper are likewise p-type semiconductors. This has been established by photogalvanic or photovoltaic measurements.[124,125] The degree of nonstoichiometry has not been determined for such films, but there is no reason to assume an origin of semiconduction different from that of samples produced by other means.

2. Origin of a Gradient of Properties in Anodically Formed Cuprous Oxide

a. The driving force for cation movement. The driving force for the transport of a cuprous ion within an anodically formed cuprous oxide film is a gradient of electrochemical potential. The electrochemical potential, $\bar{\mu}$ of a species may be formally decomposed into terms denoting chemical potential (a function of concentration) and electrostatic potential, V.[128] For a cuprous ion in the cuprous oxide film,

$$\bar{\mu} = \mu^{o} + kT \ln a + FV \qquad (5.4)$$

Here μ^{o} is a standard state chemical potential; a is the activity of the cuprous ion; and k, T, and F are respectively the Boltzmann constant, the absolute temperature, and the Faraday constant. If equilibrium of the cuprous oxide ion exists throughout the film, the electrochemical potential will be independent of position and the flux of Cu^{+} will be zero. In an asymmetric system such as Cu/Cu_2O/electrolyte, the chemical potential will differ at the two interfaces and the electrostatic potential will at equilibrium be position dependent. Conversely, with

the imposition of a potential difference across the film by some external voltage source, the establishment of equilibrium would require an adjustment in the concentration profile.

During the anodic oxidation of copper, the concentration profile of the cuprous ion will be determined only in part by the boundary concentrations. For an arbitrary imposed field strength (or potential drop), the concentration profile cannot be expected to adjust to establish equilibrium, and a flux of cuprous ions will result.

In the high rate anodic dissolution of copper through a non-porous surface film, the system is far from an equilibrium state, and a gradient of mobile ion activity can be concluded.

b. Interfacial reactions. With the high temperature oxidation of copper in oxygen gas, the driving force for the formation of the defect structure is the Gibbs free energy decrease associated with the reaction,

$$Cu_2O + n/2\ O_2 = Cu_2O_{1+n}\ , \qquad (5.5)$$

or equivalently,

$$(n/2\ O_2)_{gas} = nV_{Cu}^{x} + nO_o\ .$$

At the cuprous oxide/electrolyte interface, an analogous driving force is associated with the Cu_2O/ClO_3^- redox couple. The oxidation half reaction may be written,

$$Cu_2O = Cu_{2-n}O + n(Cu^{++})_{aq} + 2n\ e^- \qquad (5.6)$$

For the reduction of the chlorate,

$$6H^+ + ClO_3^- + 6\ e^- = Cl^- + 3H_2O \qquad (5.7)$$

The balanced redox reaction is

$$Cu_2O + \frac{n}{3}\ ClO_3^- + 2n\ H^+ = Cu_{2-n}O + nCu^{++} + \frac{n}{3}\ Cl^- + nH_2O \qquad (5.8)$$

Pertinent thermodynamic calculations indicate that chlorate is a sufficiently powerful oxidizing agent to oxidize Cu_2O to the divalent state. For unit activities of ClO_3^-, Cl^-, and Cu^{++} (dissolved species), oxidation will occur at pH below 10.6 according to the reaction,

$$Cu_2O + \frac{1}{3}\ ClO_3^- + 4H^+ = 2Cu^{++} + \frac{1}{3}\ Cl^- + 2H_2O \qquad (5.9)$$

(See Appendix D). We have found that cuprous oxide powder (Baker Reagent Grade) is rapidly dissolved in 2N $NaClO_3$ solutions with simultaneous production of chloride. During anodic dissolution, continuous chemical dissolution of cuprous oxide occurs. We draw the likely conclusion that the oxidation level of the Cu_2O at the film/electrolyte interface approaches some level intermediate between stoichiometric cuprous oxide and CuO. (A stable phase of CuO is not found among the reaction products of copper dissolution in chlorate electrolytes. This is to be expected in the acidic chloride environment at the film/electrolyte interface. Under these conditions, CuO is unstable relative to the basic chloride, $Cu_2Cl(OH)_2$.[105] The basic salt is in fact precipitated during the etching of copper in acidified chloride-chlorate solutions.[106])

In conclusion, any form of cuprous oxide is metastable in the chlorate electrolyte. The concentration of defects is therefore under kinetic control and cannot be calculated from thermodynamic data, but a nonstoichiometric surface composition is expected.

c. Gradient of space charge, conductivity, and field strength. A gradient of properties in the cuprous oxide film has already been predicted from considerations of electrochemical potential as the driving force for cation movement. Various microscopic models for ion transport allow a semi-quantitative derivation of the gradient of electrical properties. At this point the reader is advised to turn to Appendix C. There, kinetic equations describing the dependence of ion flux on field strength will be derived for the case of ion migration at high field strengths through an array of potential energy barriers.

In the model, the oxygen sublattice is pictured as rigid, and conduction occurs by migration of cuprous ions by a "vacancy-cation place exchange" mechanism:

$$Cu^{x}_{Cu_1} + V'_{Cu_2} \rightarrow V'_{Cu_1} + Cu^{x}_{Cu_2} \qquad (5.10)$$

Numbered subscripts refer to specific sites. It is conceptually simpler and equally rigorous to picture the negative vacancies as the charge carriers, as film conductivity is proportional to their concentration.

As discussed in Section V-B.1, negative cuprous ion vacancies arise from the dissociation of neutral cuprous ion vacancies present in nonstoichiometric cuprous oxide. We assume that electron holes migrate to some extent across the film/electrolyte interface--i.e., Cu^{++} ions

Fig. 5.2. Gradient of properties in a growing cuprous oxide film. (A) Defect movement; (B) Profile of absolute value of field strength; (C) Profile of relative electrostatic potential; (D) Profile of defect concentration. Current densities, $i_1 < i_2 < i_3$. Critical field strength, E^*. Broken lines for assumption of thickness independent E^* (light); and for inverse dependence of E^* on total film thickness (heavy). E* is the critical field strength for resistive breakdown transition.

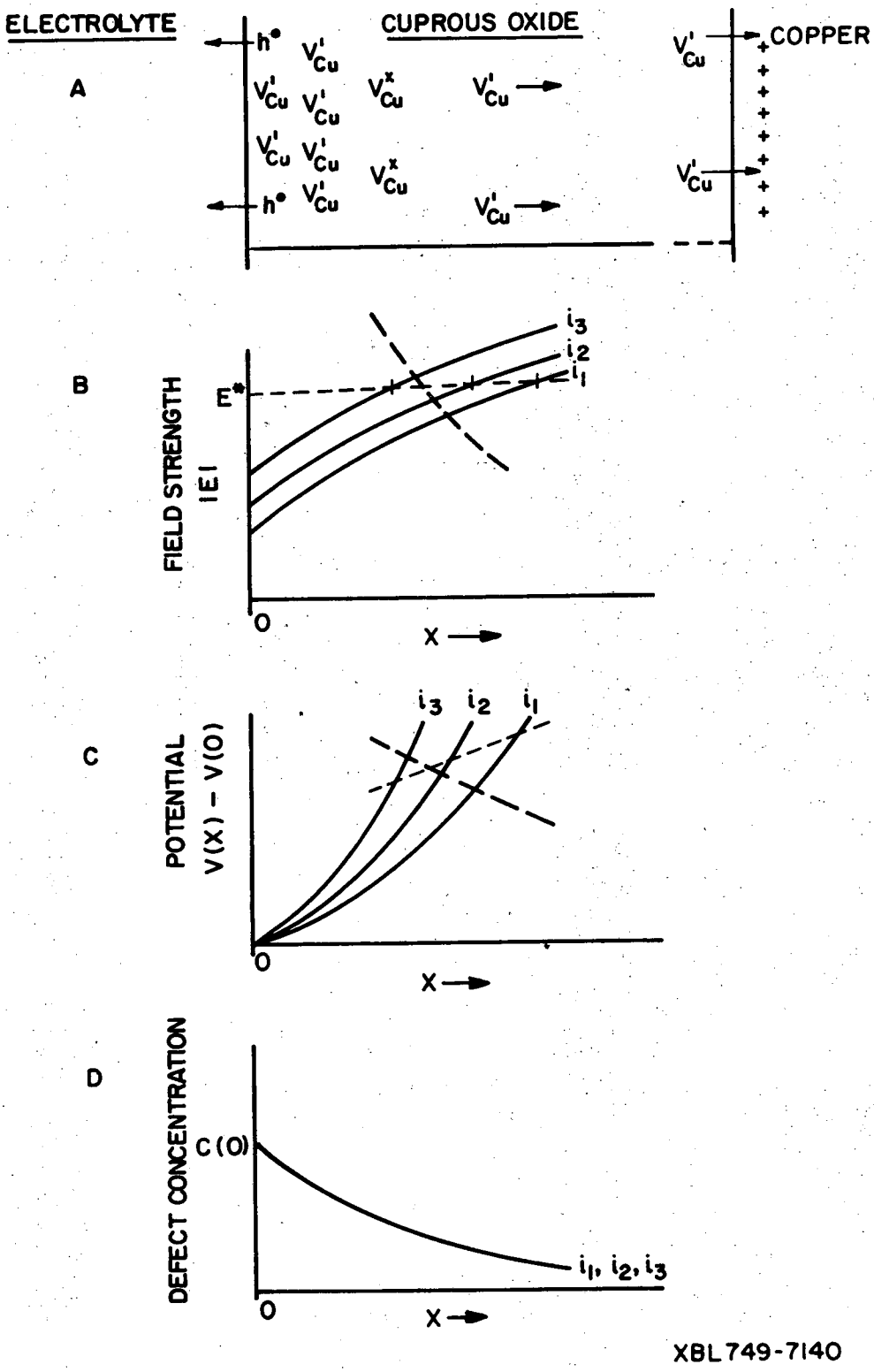
ELECTROLYTE
CUPROUS OXIDE
COPPER
A
B
C
D
FIELD STRENGTH
|E|
POTENTIAL
V(X) - V(0)
DEFECT CONCENTRATION
C(0)
E*
i3
i2
i1
i1, i2, i3
0
X
XBL749-7140

Fig. 5.2.

pass into solution-side complexes. A surface concentration of negative vacancies will therefore be established at the film/electrolyte interface. This situation is shown schematically in Fig. 5.2A.

As treated in Appendix C, the kinetic model predicts that the migration of charged particles away from the interface will give rise to a spatial distribution of space charge, field strength, and electrostatic potential within the bulk of the film. The position dependence of field strength, potential, and defect concentration (proportional to space charge) are plotted in Figs. 5.2B,C, and D, respectively. Note that we have chosen the film/electrolyte interface as the origin of the position variable, X. It should also be remembered that the kinetic model predicts that the electrical properties of the film at any position X are independent of the total thickness of the film. Finally, the situation at the film/copper interface is not indicated. It is shown in Appendix C that, for this model, the electrical properties will be determined by the concentration of defects at the interface where the defects originate and by the microscopic structure of the film substance.

Absolute value of field strength increases with position in the film monotonically; mean field strength therefore increases with film thickness for a fixed current density. For a given film thickness, mean field strength increases with current density. In Fig. 5.2B, field strength profiles are cut by two dashed lines, indicating critical conditions (field, thickness) for breakdown: one line assumes that critical field strength is independent of total film thickness;

the other indicates a critical field strength which is inversely proportional to total film thickness.

In Fig. 5.2C potential is plotted against film position, with critical potentials indicated. The potential at which the critical field strength is attained may either increase or decrease with increasing current density, depending on the assumed relation between critical field strength and film thickness.

Finally, Fig. 5.2D shows that defect concentration decreases monotonically with film position and is independent of current density whenever the boundary concentration is independent of current density. Defect concentration is proportional to space charge, as each mobile defect in our model carries a -1 charge number.

In summary, we have shown that a growing film may be subjected to continuously increasing mean field strengths at a constant current density, because of the accumulation of the space charge associated with mobile charge carriers. It is not possible however to predict even the qualitative dependence of breakdown potential drop on current density without a quantitative knowledge of the relation between critical field strength and total film thickness. More important, resistive switching transitions may be initiated for a critical <u>maximum</u> field strength or a critical <u>mean</u> field strength--such transitions have not been sufficiently characterized for a distinction to be made. Finally, the assumption of a surface defect concentration (C(0)) which is independent of current density is somewhat arbitrary. In the following section, it will nonetheless be shown that this simple kinetic model satisfactorily predicts many aspects of the periodic phenomena.

C. Interpretation of Experimental Results

1. Chemistry of Dissolution

As described in Section IV-C, two distinct phases of cuprous oxide are formed during dissolution: a thick (order of $2(10^{-3})$ cm) porous layer during active dissolution; and a thin (order 10^{-5} to 10^{-4} cm) layer during transpassive dissolution. The formation of either product may be written:

$$2Cu + H_2O = Cu_2O + 2H^+ + 2\ e^-$$

In addition, chloride ion is found and may only be the result of the chemical reduction of chlorate by copper or cuprous species. For example,

$$2H^+ + \frac{1}{2}\ Cu_2O + \frac{1}{6}\ ClO_3^- = Cu^{++} + H_2O + \frac{1}{6}\ Cl^-$$

These observations are consistant with the relevant thermodynamic data. In Fig. 5.3 and 5.4, plots of equilibrium electrode potential against pH (Porbaix diagrams) are shown, indicating the domains of chemical and electrochemical equilibrium among the various possible reaction products. The presence of chloride tends to increase the lower limit pH for the stability of Cu_2O relative to CuCl:

$$Cu_2O + 2H^+ + 2Cl^+ = 2CuCl + H_2O$$

No CuCl is in fact found among the products of dissolution, but its relative solubility in chloride environment via chloride complex formation together with subsequent oxidation by chlorate would render

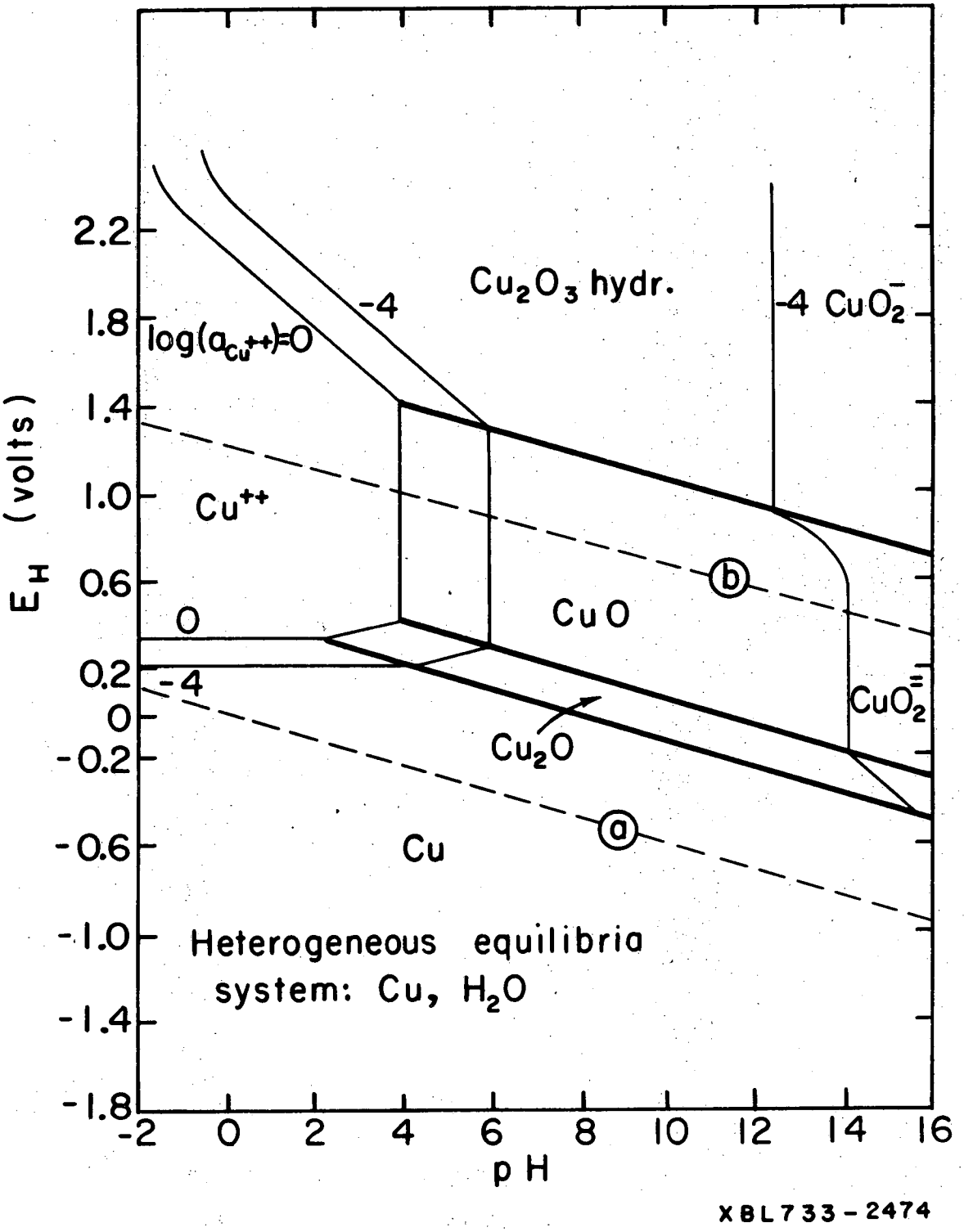

Fig. 5.3. Pourbaix diagram for the system Cu, H_2O.

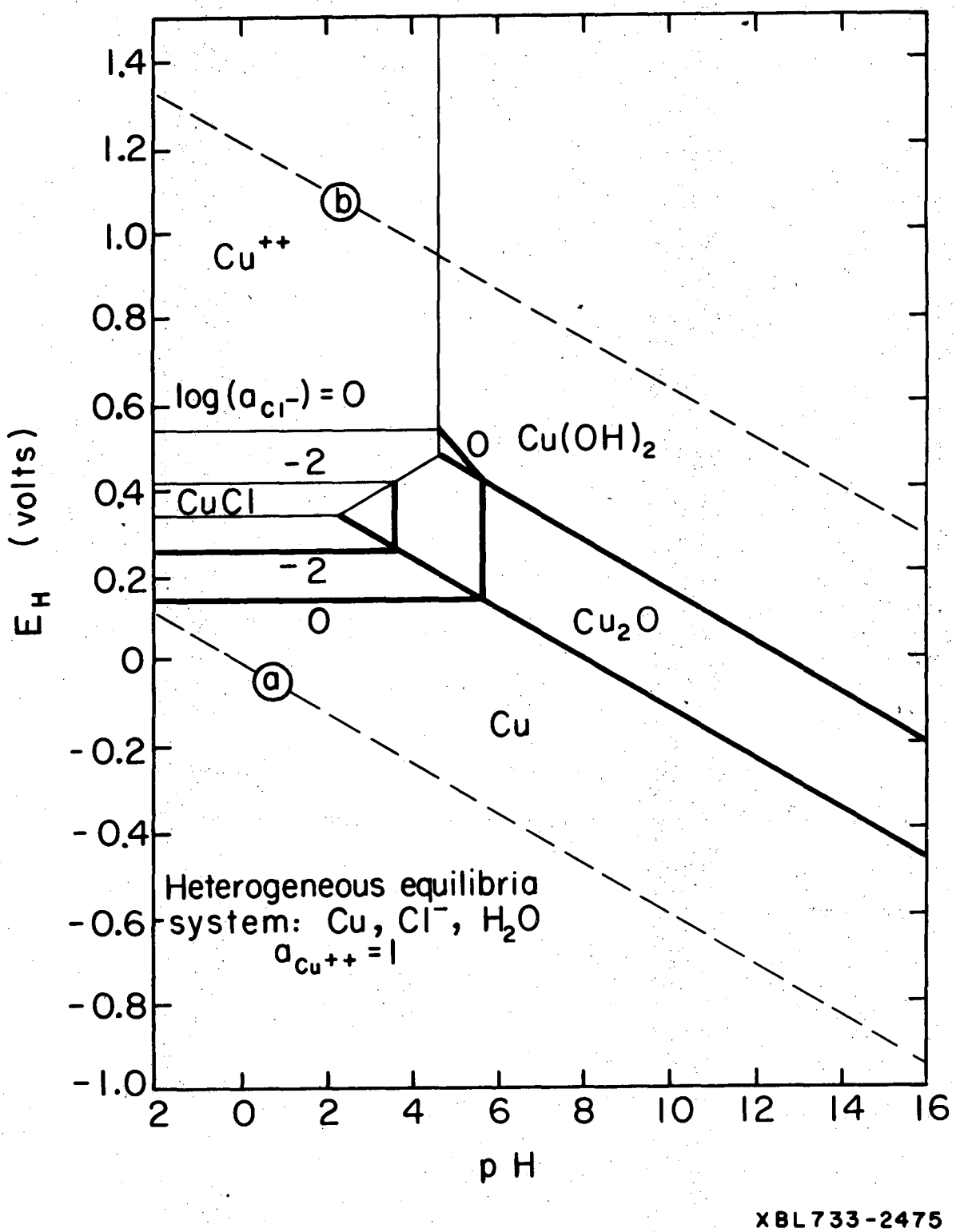

Fig. 5.4. Pourbaix diagram for the system: Cu, Cl^-, H_2O.

cuprous chloride unstable:

$$CuCl + Cl^- = CuCl_2^-$$

$$H^+ + CuCl_2^- + \frac{1}{6} ClO_3^- = Cu^{++} + \frac{13}{6} Cl^- + \frac{1}{2} H_2O$$

The thickness of the active phase cuprous oxide, its porosity, and the etched appearance of the copper substrate are strong indications that this layer is formed by secondary precipitation of Cu_2O from aqueous complexes. The growth of the thin transpassive film is invariably accompanied by a progressive flattening and polishing of the metal substrate. As discussed in Chapter IV-C, electropolishing is an indication of ionic conduction through a thin adherent layer, the impedance of which controls the distribution of current on a microscopic scale.

2. Supportive Evidence for the Migration of Negative Cation Vacancies

The electropolishing effect yields strong supportive evidence to our assumption that charge is carried by the migration of negatively charged cation vacancies. As suggested by Hoar et al.[120] and Novak, et al.,[129] electropolishing results from the spatially random arrival of vacancies at the copper surface. The formation of the vacancies is controlled at the electrolyte/film interface. (See Appendix C). Their random arrival suppresses the effects of nonequal rates of copper ion removal from dissimilar crystallographic sites on the substrate. On the other hand, if transport occurs by the migration of Cu^+ ions by an interstitial mechanism, such that local rates are controlled

at the copper/film interface, the inhomogeneity of the copper surface on a microscopic scale would be expected to produce a non-uniform texture.

3. Dependence of Mean Field Strength on Current Density

The mechanism of ionic conduction can be inferred, in part, from the empirical dependence of mean field strength on current density. We shall compare experimental results with the high field transport equation derived in Appendix C:

$$I = qcA\exp(qBE) \qquad (5.11)$$

$$A \equiv (2a\nu F/N_a)\ \exp -W/kT; \quad B \equiv a/kT$$

Mean field strength, $\bar{E}$, which is directly accessible to experimental determination, is defined as:

$$\bar{E} = \int_0^S E\, dx/S = -(V(S) - V(0))/S \qquad (5.12)$$

where S is film thickness and V is electrostatic potential. At the cycle peaks, the mean field strength is approximately equal to amplitude divided by thickness of the transpassive film. We may compute an upper limit to the film thickness at the cycle peak by assuming that all monovalent copper is retained in the cuprous oxide film and contributed to its growth. Film thickness is then given by,

$$S_p = pITW_e/Fd \qquad (5.13)$$

where I = current density, T = oscillation period, F = Faraday constant, and W_e and d are the equivalent weight and density of Cu_2O. If only Cu^+ and Cu^{++} are produced, the current efficiency for Cu_2O production is $p = (2-n_a)/n_a$. Equation (5.13) is expected to be a good approximation to actual peak thickness only at high current densities (> 10 A/cm^2), where (1) the duration of the active phase is small compared to T; and (2) the rate of chemical dissolution of the film is small compared to the rate of film growth.

Computed values of S_p and $\bar{E}_p$ for current densities from 10 to 75 A/cm^2 appear in Table V-2. Plots of S_p against I, and $\log_{10}I$ against $\bar{E}_p$ are shown in Figs. 5.5 and 5.6. Several observations may be made:

(a). The plot of log(I) against $\bar{E}_p$ is linear. For q=-1, the slope of the plot (cf. Eq. 5.11) yields,

$$B = 6.8\times(10^{-6}) \text{ cm/V} \qquad (5.14)$$

This value is close to that obtained for the thin oxidic films formed during the electropolishing of copper in phosphoric acid solutions. From electrode resistance data and film thicknesses determined by capacitance techniques, Kojima calculated,

$$B = 7.8\times(10^{-6}) \pm 6\times(10^{-6}) \text{ cm/V}.$$

The large error limits arise from the uncertainty in thickness: 13-124 Å.[131] With a probable thickness value of 60Å measured by in situ ellipsometry (Novak, et al.[129]), Kojima calculated a most probable value of B: $6.8\times(10^{-6})$ cm/V. Our value of B is of the same order of magnitude as

Table V.2. Calculation of Transpassive Film Thickness and Mean Field Strength at Peak Cycle Potential

Data from Stagnation Point Flow System					
Flow Rate (cm/s)	Current Density (A/cm^2)	Period (ms)	Amplitude (V)	Thickness* (10^{-4}cm)	Mean Field Strength** (10^5 V/cm)
93	8.5	131	11.3	0.926	1.24
93	10.9	90	12.6	0.816	1.57
93	21.0	33	13.9	0.577	2.45
93	31.5	19.5	15.2	0.511	3.02
94	17.5	40	14	0.582	2.44
94	30.3	19.6	16	0.494	3.29
94	44.8	11.8	17	0.470	3.92
94	59.3	9.31	15	0.459	3.31
94	74.3	5.25	14	0.324	4.34
94	74.3	5.00	14	0.309	4.60
160	8.5	138	13.0	0.976	1.35
160	10.9	91.7	12.2	0.832	1.48
160	31.5	18.4	15.7	0.482	3.30
193	10.9	100	10.4	0.907	1.16
193	15.9	60	14.5	0.794	1.85
193	31.5	19.6	16	0.514	3.16
193	41.5	11.9	16	0.411	3.95
193	53.9	8.3	15	0.372	4.09
193	74.3	6.4	16	0.396	4.10

*Thickness = $S_p = pITW_e/Fd$, where p = current efficiency for Cu_2O production; I = current density; T = oscillation period; W_e = equivalent weight of Cu_2O; F = Faraday constant; and d = density of cuprous oxide.

**Mean field strength is taken as the peak mean field strength $\bar{E}_p$, which is approximated by (amplitude/thickness).

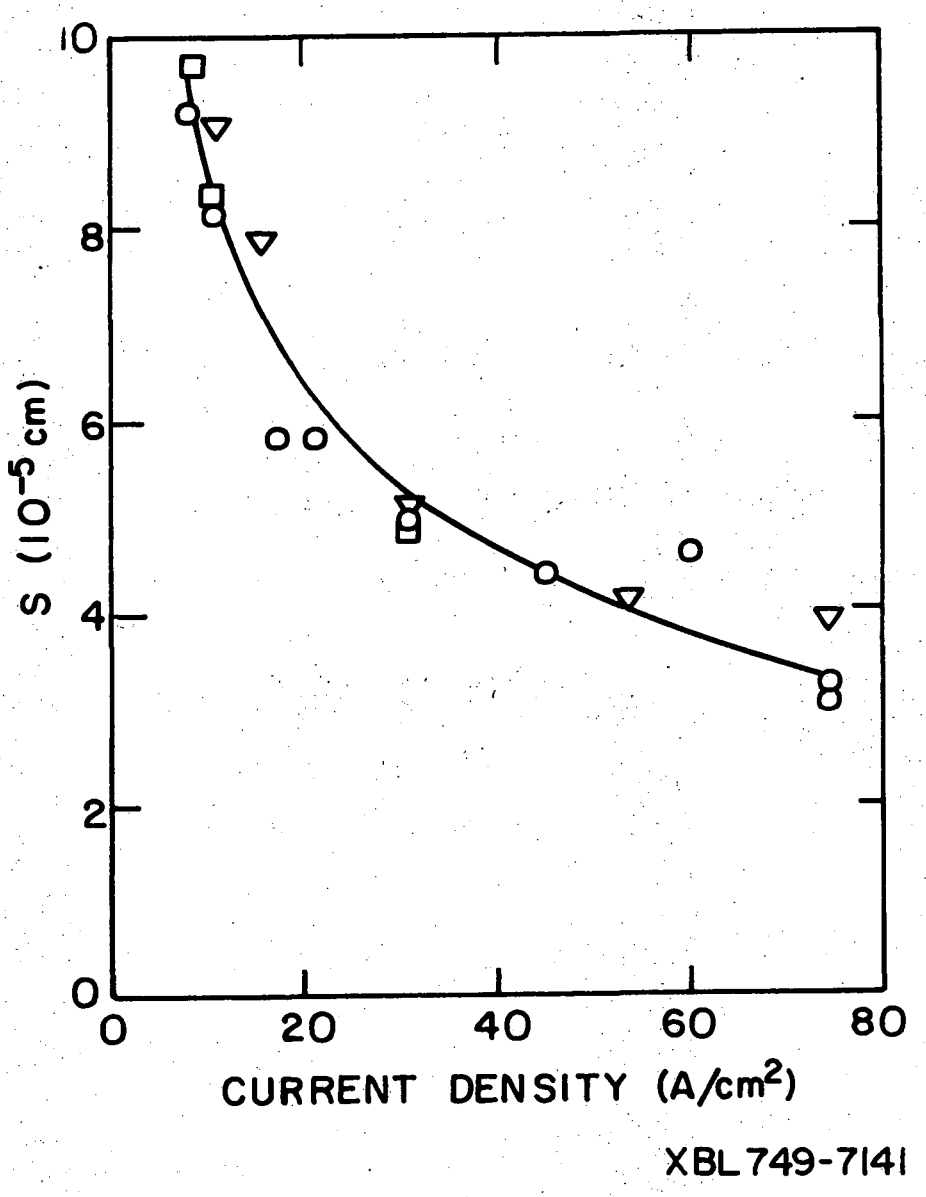

Fig. 5.5. Dependence of Maximum Film Thickness on Current Density. Maximum Film Thickness is calculated from the equation, $S=pITW_e/Fd$, ○, 93-94 cm/s; □, 160 cm/s; △, 193 cm/s.

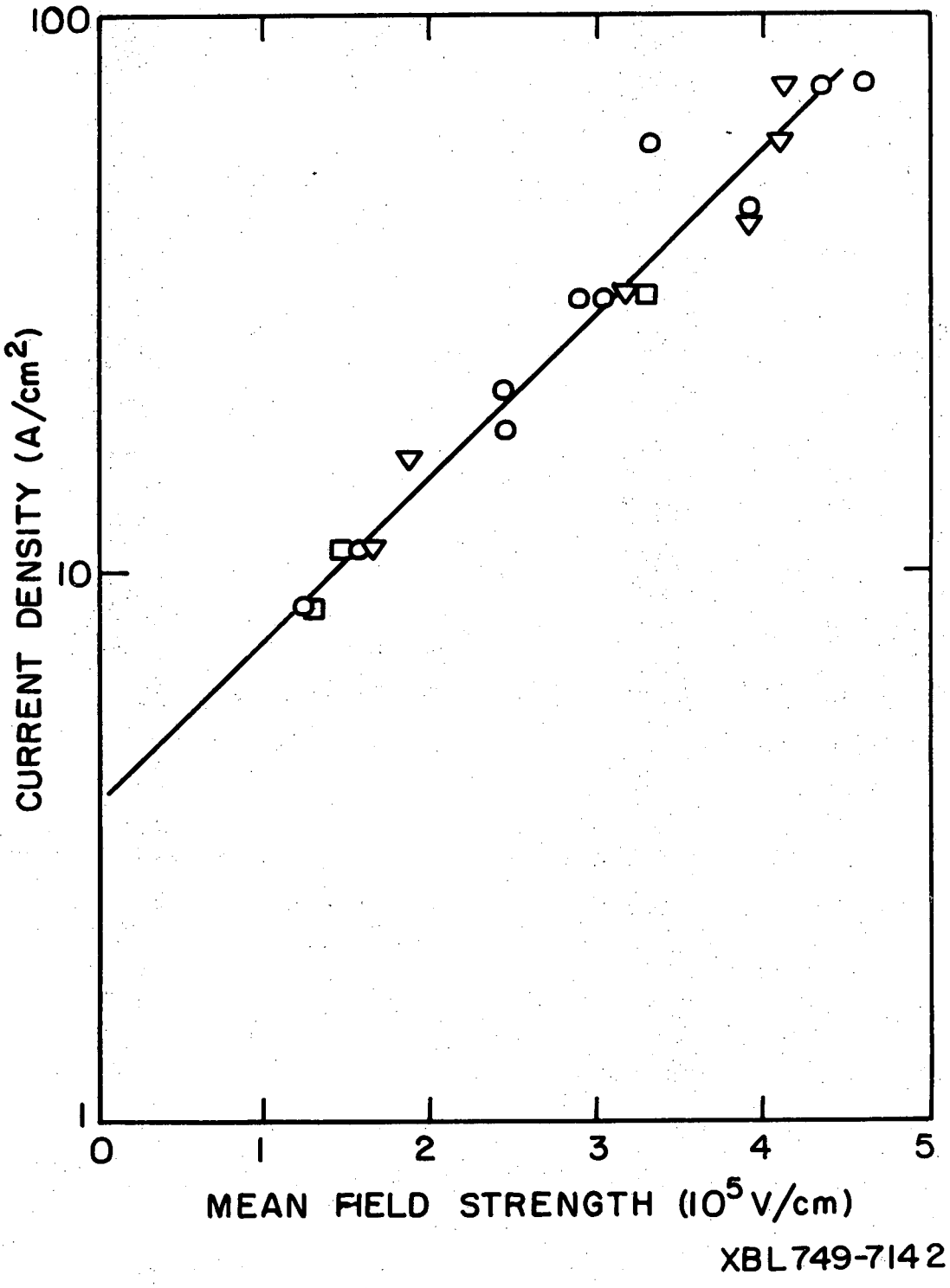

Fig. 5.6. Linear Dependence of Log(current density) on Mean Field Strength, as predicted by high field ionic conduction equation. Stagnation point flow system; ○, 93-94 cm/s; □, 160 cm/s; ▽, 193 cm/s.

for the valve metals (Al, Ta, Hf, Nb, etc.), for which B = (3-10)$\times 10^{-6}$ cm/V. (See Vermilyea,[121] p. 242).

(b). For the linearity of the plot in Fig. 5.6 to imply a high field ionic conduction mechanism, the product qBE must be sufficiently large for the approximation $\sinh(qBE) \sim \frac{1}{2}\exp(qBE)$ to hold. The product qBE ranges from 1 to 3 in the plot; hence, within the limits of experimental scatter, the linearity is consistant with a high field ionic conduction equation.

(c). From Eq. (5.11), B = a/kT. At 25°C, for B = 6.8$\times(10^{-6})$ cm/V, a = 17$\times(10^{-8})$ cm. The parameter (a), the activation distance for ionic transport in the simple model in Appendix C, is an order of magnitude larger than the inter-site spacing in the cuprous oxide lattice. An overestimation of S_p by a factor of ten would have lead to a ten-fold overestimation of (a). However, for the anodic oxide films on the valve metals, experimental values of (a) are consistently two to five times larger than the average cation-cation separation. (Vermilyea,[121] p. 253). The difference is attributed to the dependence of mobile ion concentration or local ionic configuration on field strength, which results in the activation distance losing its simple physical significance. In cuprous oxide, a large apparent activation distance might arise for a grossly nonstoichiometric defect structure, whereby a Cu^+ ion might traverse a number of neutral vacancies before being captured by a negative vacancy.

(d). From Fig. 5.6, we obtain a zero-field intercept of 4 A/cm^2. From Eq.(5.11), we may write:

$$|4/(2aq\nu F/N_a)| = \bar{c} \exp(-W/kT)$$

For q=-1, $a=17\times(10^{-8})$cm, and $\nu=10^{13}$ Hz, a combination of possible values of $\bar{c}$ and W are obtained and tabulated below:

$\bar{c}$ (cm^{-3})	W (eV)	Voltage (V)
10^{19}	0.35	10^3
10^{18}	0.30	10^2
10^{17}	0.24	10^1
10^{16}	0.18	1

The third column gives the voltage of a hypothetical parallel plate condenser (with material of dielectric constant 10) when charged with the same quantity of electricity as in the space charge film. Voltage is calculated from the equation for a parallel plate condenser,[132]

$$V = Q/C = Q/(Ke_oA/d)$$

where we set

$$Q = \bar{c}\ (qF/N_a)(dA) \quad .$$

Here K = dielectric constant, C = capacitance, Q = charge, and A and d are the area and separation of the plates. As the maximum voltage drop across the film is roughly 10 volts, we estimate the mean mobile vacancy concentration to lie between 10^{16} and 10^{18} cm^{-3}, with the corresponding activation energy, W, between 0.18 and 0.3 eV.

The condenser analogy is a crude approximation, which serves only to confirm that the observed voltage drop and dielectric properties of Cu_2O are consistent with combinations of $\bar{c}$ and W derived on the basis of the high field ionic conduction model. A precise calculation of $\bar{c}$ and W would require knowledge of the composition of the layer, including the dependence of K on composition and the dependence of c(0) on time.

It should be noted that the activation energy of roughly 0.25 eV lies midway between activation energies for the valve metal oxides (0.7-1.5 eV) and those for "good" ionic conductors (e.g., Ag_4RbI_5, W = 0.09 eV, ref. 130).

4. The Occurrence of the Resistive Breakdown Transitions

In Chapter IV-D, the nature of resistive switching and breakdown transitions was discussed. The capacity for resistive breakdown transitions in anodically formed cuprous oxide films was demonstrated by this author and by Kosarevich, et al.,[108,109] using dried specimens of transpassive films.

In general, resistive breakdowns occur when field strength exceeds a critical level, which is an inverse function of sample thickness. The thickness dependence is believed to arise from the increased probability of a single electron causing an avalanche of a critical magnitude in thicker films.[127] Experimentally, the dependence of critical field strength on film thickness often takes a quasi-exponential or exponential form:

$$E_{critical} = -G_1 \log S + G_2 \qquad (5.15)$$

where G_1 and G_2 are constants. A relation of the above form was found for aluminum oxide, various forms of mica, and sodium chloride. (See Klein,[134] p. 202). The thickness dependence has not been investigated for cuprous oxide.

In the anodic oxidation of copper in the chlorate electrolyte, a breakdown of anode potential occurs at decreasing film thicknesses for increasing current densities (Fig. 5.5). A plot of log S_p against $\overline{E}_p$ is indeed linear with a negative slope, (Fig. 5.7). Because of the dual dependence of critical field strength on thickness arising from (1) the probability of avalanche and (2) the enhancement of field due to space charge accumulation, the exact dependence of breakdown on experimental variables cannot be predicted with the data at hand. In Fig. 5.2, the behavior of peak potential at different current densities is schematically shown for (1) a single, thickness-independent critical field strength, and (2) a critical field strength which decreases with increasing thickness. It should be noted that either case predicts the observed monotonic decrease of peak film thickness with increasing current density.

The enhancement of field strength during film growth is evidenced by the upward sweeping anode potential (see Figs. 4.2-7) which invariably precedes potential breakdown. The upward sweeping potential cannot be solely attributed to a closing of pores in a hypothetical porous layer of reaction products. With the onset of transpassive dissolution, the metal substrate becomes progressively flattened and polished. This indicates that the metal is already completely covered with a transpassive film prior to the ascent to peak potentials.

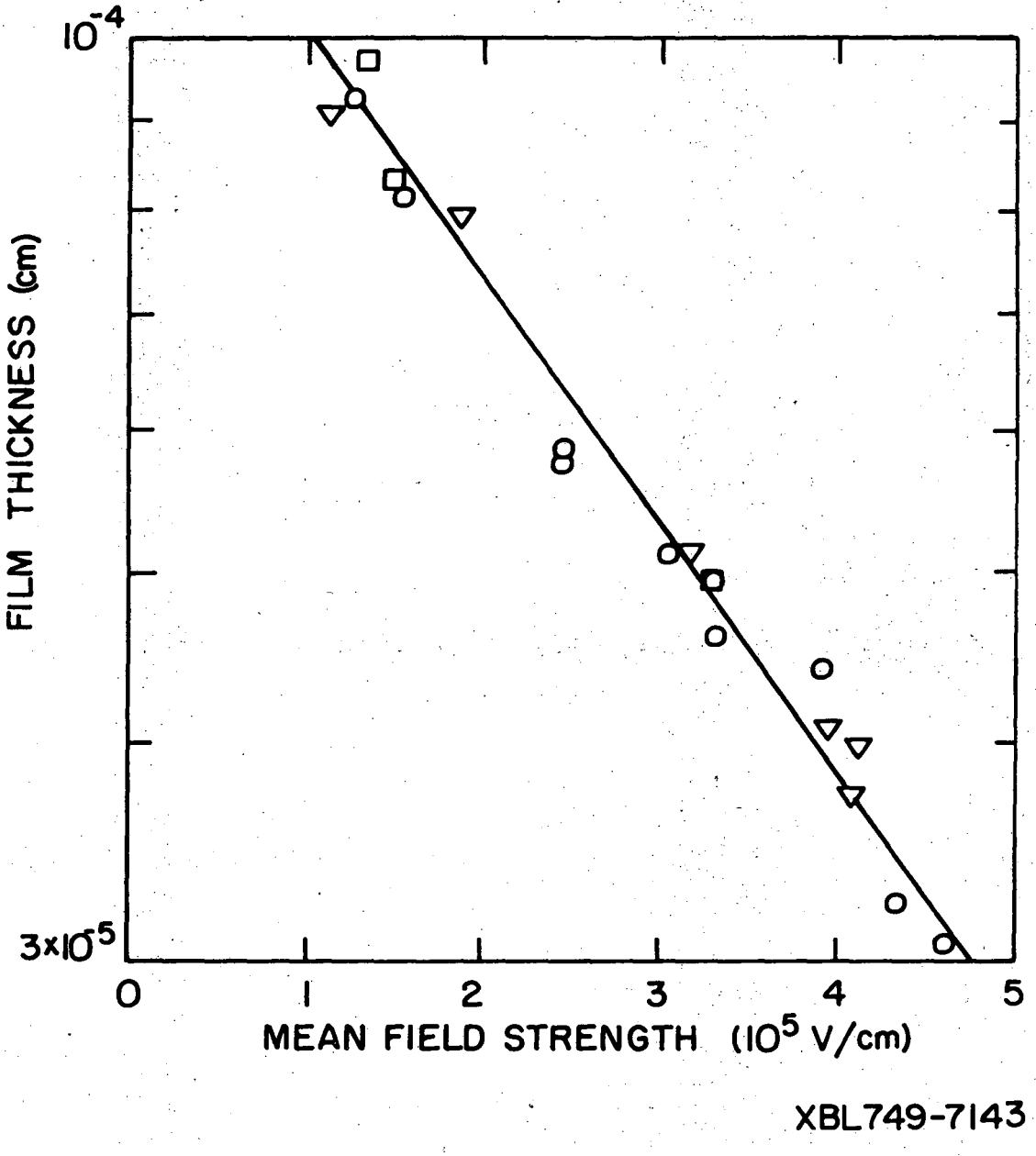

Fig. 5.7. Decrease of Critical Field Strength with Increasing Film Thickness. Stagnation point flow system; ○, 93-94 cm/s; □, 160 cm/s; ▽, 194 cm/s.

The differential field strength, E_d, is given by

$$E_d = E(S) = -dV/dS \qquad (5.16)$$

as shown in Appendix C. As is evident from Fig. 4.2, the slope of anode potential increases by an order of magnitude during film growth. (In contrast to this behavior, the voltage increase is linear for anodic oxide film growth on the valve metals at constant current density.) The increase in slope is consistent with the model of space charge accumulation. It is possible that a change in the chemical nature of the film (for example a partial conversion to CuO) might also lead to an increase in film resistance with increasing thickness. The invariance of instantaneous apparent valence during transpassive dissolution tends to argue against this conclusion.

Finally, it was noted in Chapter IV-D that breakdown on dry specimens occurs at a range of voltages which lies below the voltage attained on the same specimens in situ. This is to be expected whenever space charge accumulation occurs during film growth. Upon breaking the anodizing circuit, the space charge profile will relax, leading to a lower average concentration of negative vacancies. As the concentration of V'_{Cu} subsides, the concentration of holes will increase (Eq. 5.2). Electronic conductivity will therefore be higher in the dried samples than in the in situ films. For a given voltage drop across the dried sample, more current carries are available to initiate a critical avalanche.

5. Dependence of Oscillation Period on Experimental Variables

Oscillation period was found to increase with electrolyte flow rate over the range of current densities employed in the channel flow systems. Increased hydrogen ion concentration prolonged the growth phase of the cycle, the effect being strongest at low current densities. As noted in Section IV-A, increased flow rate and decreased pH effect a lowering in the net rate of transpassive film growth by increasing the rate of its simultaneous chemical dissolution. The rate of chemical dissolution may be expressed as a current density, I_o, which must be subtracted from the applied current density, I, to obtain current available for film growth. The term, $(I-I_o)$, may be entered into the empirical Eq. (4.1), to obtain, $(I-I_o)^a T$ = constant. Increased hydrogen ion concentration and flow rate should increase the minimum current density for film growth, $I=I_o$. For $I \gg I_o$, the effects of these variables on growth rate should be negligible if only chemical dissolution is involved. This was not found. Increasing pH changes the form of the empirical relation by lowering the exponent, a. The plots of log(period) against log(current density) for different flow rates were parallel, not converging.

A complete understanding of pH or mass transport effects would require a knowledge of the dependence of the surface concentration of lattice defects, C(0), on activities of reactants. The surface defect concentration, not film thickness, is the primary factor in controlling the enhancement of space charge, field strength, and ionic conductivity. A quantitative relation between C(0) and reactant concentration is beyond the scope of this research.

D. Summary of Chapter V

(A) A model was presented which interprets the oscillation phenomenon as resulting from sequential phases of film growth (by ionic conduction through a cuprous oxide film; field relaxation (by abrupt resistive switching transitions in the film when a critical combination of field strength and thickness is reached); and restoration of film growth (by destruction and removal of the body of film containing the low resistance breakdown channels). On the basis of the model, it was shown that no stable electrode state is accessible to the system and that the consequent fluctuations should be regularly periodic.

(B) The model makes certain assumptions concerning the physical and chemical nature of the anode surface film, which are shown to be justified by contemporary understanding of cuprous oxide and ionic conduction kinetics.

Cuprous oxide is a cation deficient, p-type semiconductor with a broad range of nonstoichiometry. Ionic conduction occurs by the migration of cuprous ions through the lattice--or equivalently, by the counter-migration of negatively charged cuprous ion vacancies. In a growing film, a gradient of properties was predicted on the basis of electrochemical potential as the driving force for transport. A high concentration of cation vacancies at the film/electrolyte interface was predicted from considerations of the large thermodynamic driving force for the oxidation of cuprous oxide by chlorate.

A classic model for ionic transport in solids, presented in Appendix C, was applied to the case of ionic conduction on negatively

charged cuprous ion vacancies originating at the film/electrolyte interface. Qualitatively, field strength was predicted to increase with current density and with film thickness. The gradient of field strength is a consequence of accumulation of space charge associated with mobile charged defects.

(C) Certain experimental results were interpreted and supportive evidence was adduced for the model.

The formation of cuprous oxide and its subsequent oxidation was shown to be consistent with relevent thermodynamic data. The observed flattening and polishing of the copper substrate indicates that charge is transported by migration of negatively charged defects away from the film/electrolyte interface.

The empirical dependence of mean field strength on current density follows the equation for high field ionic conduction, Eq. (C.5).

An inverse relation between maximum field strength and maximum film thickness was derived from experimental data. The relation was expected on the basis of a similar behavior for a variety of substances undergoing resistive switching breakdowns.

Finally, the predicted increase of field strength with increasing film thickness was evidenced by our observations of order-of-magnitude increases of the time-derivative of anode potential during the growth phase of the cycle.

Further supportive evidence for the model would require:
(1) quantitative knowledge of the dependence of surface defect concentration on electrolyte composition, current density, and film

thickness; (2) a theory of the dependence of breakdown field strength on sample thickness; and (3) characterization of the electrical and chemical properties of the film/metal interface.

APPENDIX A

Large Amplitude Anode Potential Oscillations in Electrolytes Containing Halide Ions*

Table A-I.

Electrode/Electrolyte	Current Density (A/cm^2)	Period (s)	Amplitude (V)	Comments
Cu/5M $NaNO_3$, 0.1M NaCl	20	0.025	20-25	Irregular Waveform
Cu/2M KNO_3, 0.03M KCl	3.1	0.54	8-10	Nearly sinusoidal waveform
Cu/2M KNO_3, 1M KI	3.2	0.24	5	Nearly sinusoidal waveform
Cu/1M K_2SO_4, 1M KCl	9	0.33	25-30	Sharp peaks; O_2 evolution
Cu/2.5M H_3PO_4, 0.03M NaCl	19.6	0.01	25	
Cu/2M HCl	20	0.088	>50	Spark discharge observed during dissolution
	25	0.050		
	30	0.032		
	35	0.020		
	40	0.016		
	45	0.021		
	50	0.009		
Cu/4M NaOH, 1M KCl	9.5	0.046	30-50	Continuous O_2 evolution, spark discharge.
Fe/5M $NaClO_3$	19	0.014	5	Waveform similar to Cu/5M $NaClO_3$ system. Anode metal was SAE-1018 steel

*Investigations conducted by this author.

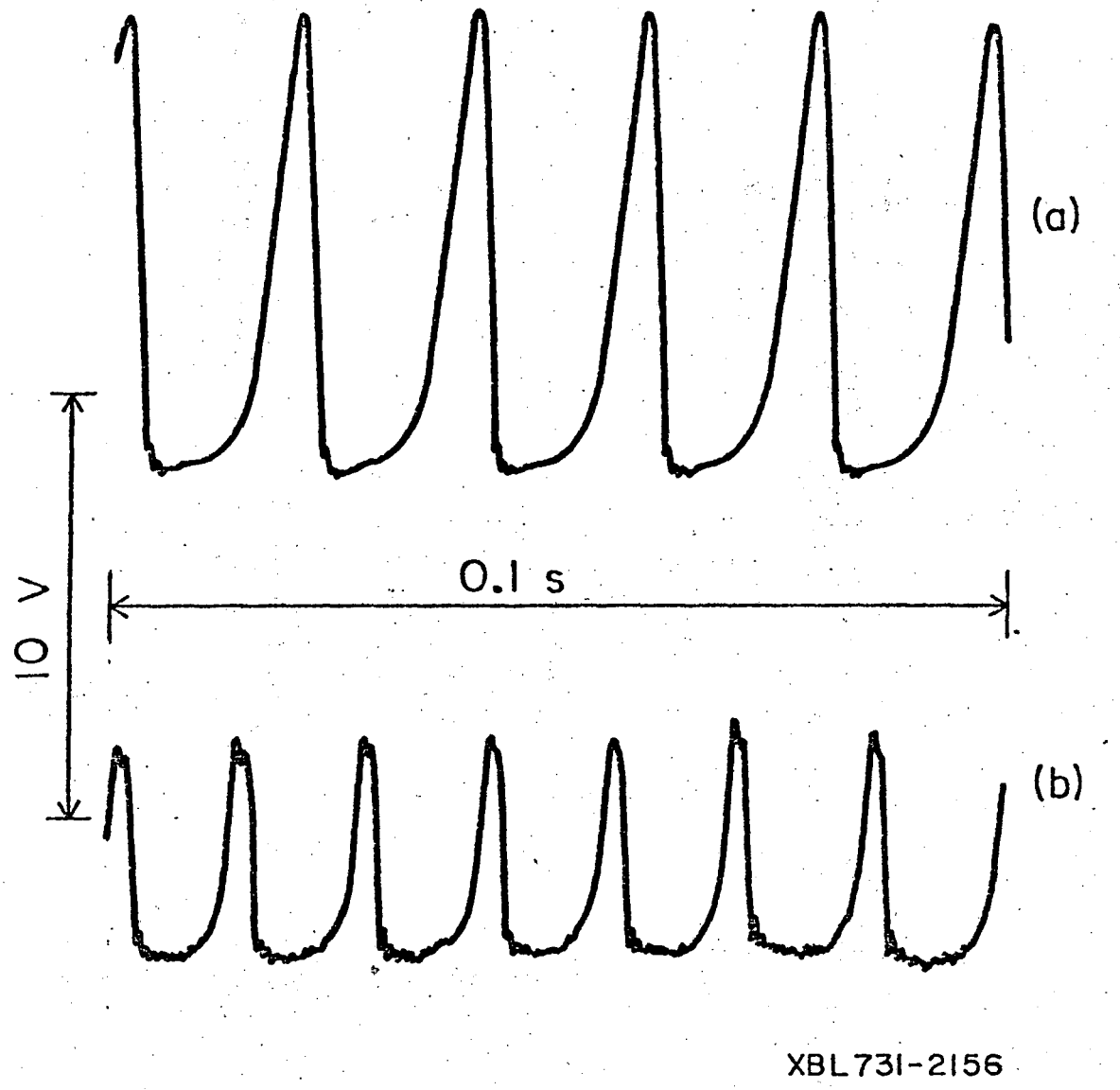

Fig. A.1. Oscillation Waveforms for Dissolution of Cu and Fe: Cell Voltage Tracings. Current Density = 19 A/cm^2; stationary electrolyte. (a) Cu/5F $NaClO_3$; (b) Fe/5F $NaClO_3$; anode metal, SAE 1018 steel.

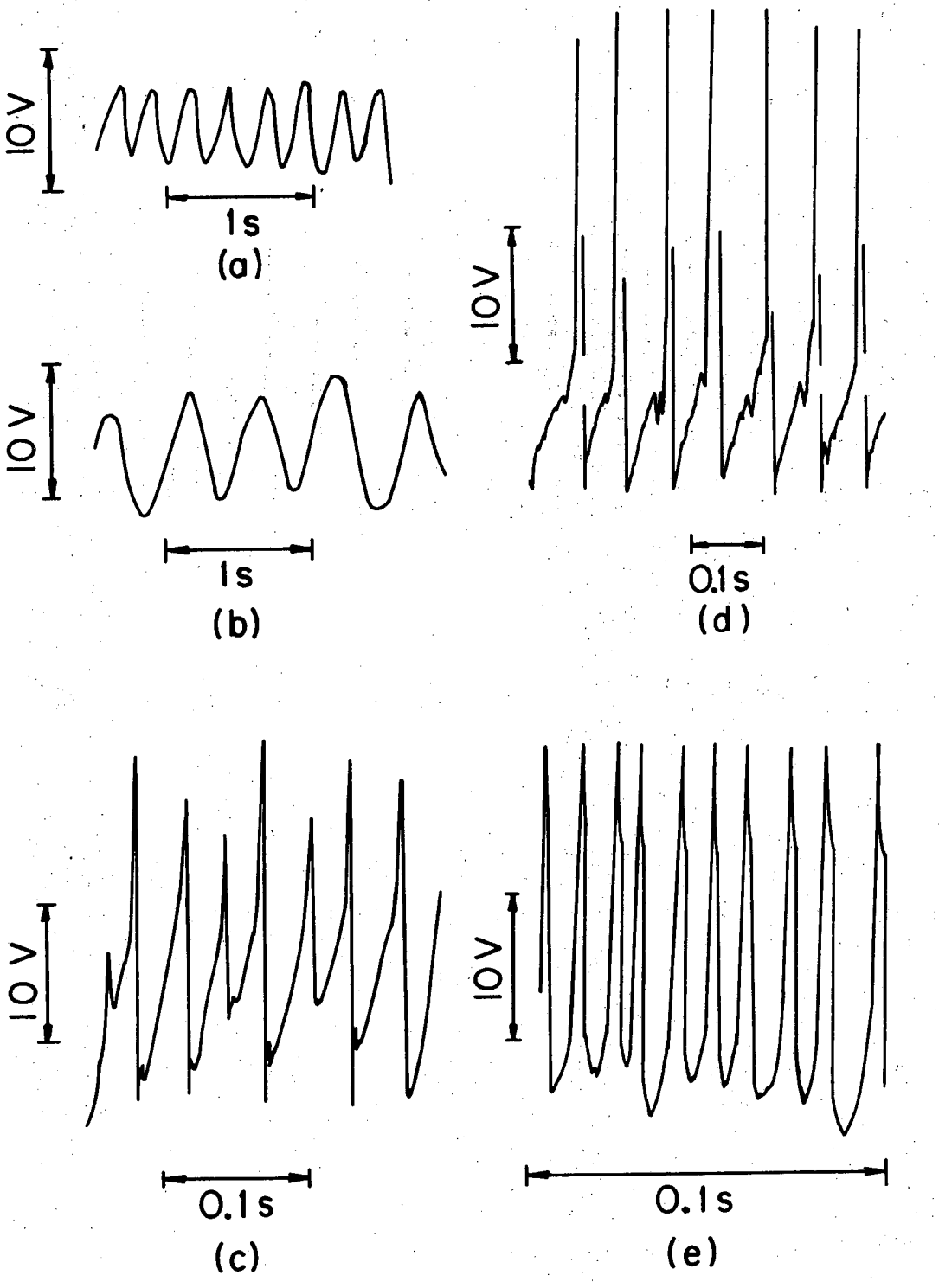

Fig. A.2. Oscillation waveforms in halide-containing electrolytes. Stationary electrolyte; copper anodes. (a) 2M KNO_3, 1M KI; 3.2 A/cm^2; (b) 2M KNO_3, 0.3 MKCl; 3.1 A/cm^2; (c) 5M $NaNO_3$, 0.1 M NaCl; 20 A/cm^2; (d) 4M NaOH, 1M KCl; 9.5 A/cm^2; (e) 2.5 M H_3PO_4, 0.03 M NaCl; 19.6 A/cm^2.

APPENDIX B

Periodic Electrode Phenomena Involving Current-Restricting Surface Layers

Table B-I lists reported observations of periodic electrode phenomena involving the growth and destruction of current-restricting layers of reaction products. Unless otherwise noted, the oscillations in potential or current occur upon anodic polarization of the metal.

The table is intended to show the variety of electrode/electrolyte combinations in which such periodic behavior is observed as well as the variety of models advanced for their interpretation. The listing is not exhaustive; many observations of periodicity reported before 1926 have been excluded. References to earlier work may be found in Hedges and Meyers.[35,76]

Table B-I. Observations of Periodic Electrode Phenomena Involving Current Restricting Surface Layers

No.	Electrode/electrolyte	Observations	Interpretation	Reference
1.	Ag/KCN			
2.	Ag/H_2SO_4	v/i osc.; alternate formation and shedding of solid film		Hedges (77)
3.	Ag/NH_3,$(NH_4)_2SO_4$			
4.	Ag/NH_3,NH_4Cl			
5.	Ag/AgCN,KCN,K_2CO_3	v/i osc.; formation and shedding of film-probably Ag_2O	alternate deposition/ dissolution of AgCN film; formation of $AgCN_2^-$ and AgO_2	Gilbertson (44)
6.	Ag/0.3MAgCN,0.7M	v/i osc.; i=0.3-0.35 A/cm^2; per=0.03 to 0.2 s	alternate deposition/ dissolution of AgCN film to form $AgCN_2^-$	Francis (43)
7.	Ag/0.5 M KCl		Mechanical disruption of AgCl film	Lal (48)
8.	Ag/2-10M HCl	v osc.; galvanostatic 10 mA/cm^2; ampl.=5 v; per.=10^{-5} s; irregular osc.	formation and breakdown of PN junction	Indira (37)
9.	Al/100% H_2SO_4	i/v osc.; i=50 mA/cm^2; amp.=13 V; per.=45 s	---	Hedges (79)
10.	Al/lead laurate, 5 ppm Cl^-	v osc.; galvanostatic; i=0.5 (10^{-6}) A/cm^2; ampl. 0.01-0.1 V; per. 1 min.; irreg. osc.; no osc. without Cl^-.	Field enhancement in oxide film due to Cl^-	Pryor (7)

Table B-I. Observations of Periodic Electrode Phenomena Involving Current Restricting Surface Layers

No.	Electrode/electrolyte	Observations	Interpretation	Reference
11.	Au/4N HCl	i osc.; potentiostatic; E_H=1.8 V; ampl.=2 A/cm^2; per.=5 s	shift in potential of active/passive transition due to alternate depletion/ replenishment of H^+	Franck (40)
12.	Cd/30% H_2SO_4	i&v osc.; ampl.=3-4 V; period=1 min; O_2 evolved at peaks of potential	---	Hedges (78)
13.	Cd/KCN	i&v osc.	---	Hedges (78)
14.	Cd/0.1 F Na_2WO_4	v osc.; galvanostatic, 0.16 A/cm^2 spalling of oxide layer	formation and breakdown of oxidic film; breakdown by electrical discharge	Gruss (61)
15.	Co/1-5% H_2SO_4	v osc.; galvanostatic, 70-250 mA/cm^2; ampl.=1.4 V; per.=1 s	alternate formation/ disruption of film	Hedges (79)
16.	Co/1N HCl, 0.85 M CrO_3	osc. in rest potential; ampl.=0.2 V; per.=1.6 s period depends on electrode size; coupling of two electrodes of different frequencies results in average frequency	Shift in potential of active/passive transition due to alternate depletion/ replenishment of H^+	Franck (26)
17.	Co/HCl,CrO_3	osc. in rest potential		Gougerot (87,86)

Table B-I. Observations of Periodic Electrode Phenomena Involving Current Restricting Surface Layers

No.	Electrode/electrolyte	Observations	Interpretation	Reference
18.	Cu/NHO_3,NCl	osc. in rest potential; Ampl.=0.09 V; per.=6 min.	alternate Cu_2O deposition; dissolution	Hedges (76)
19.	Cu/air sat. HCL	osc. rest potential; per.=several hours; osc. only on cold worked metal	"	"
20.	Cu/5% $CuCl_2$	(same general effects as in HCl system; periodic prec. of Cu_2O film)	"	Hedges (77)
21.	Cu/5% NH_4Cl			
22.	Cu/5% NaCl			
23.	Cu/2.5-10% KCN	i&v osc.; v osc. galvanostatic, 0.06 A/cm^2; Ampl.=1 V; "in every respect this phenomenon is similar to periodic electrolysis of chloride solutions."	"	"
24.	Cu/10-50% HCl	i&v osc.; i(active)= 80-600 mA/cm^2; ampl. depends on external voltage source; period 10-300 s; per. inc. with inc. current density; sudden color changes in Cu_2O film.	alternate CuCl and Cu_2O formation and dissolution; metastable form of Cu_2O suggested;	Hedges (77,81)
25.	Cu/KCl	i&v osc.	periodic film formation/ dissolution	Bartlett (75)

Table B-I. Observations of Periodic Electrode Phenomena Involving Current Restricting Surface Layers

No.	Electrode/electrolyte	Observations	Interpretation	Reference
26.	Cu/1.5-4 N HCl	i&v osc; v osc. in galvanostatic dissolution, 0.1-0.15 A/cm^2; ampl. depends on voltage source; per.=5-100 s; period increases with current density	alternate formation and dissolution of CuCl and Cu_2O; kinetic model	Bonhoeffer (55)
27.	Cu/2F HCl	i&v osc.; osc. found at anode potentials between -.27 and -0.25 V vs 0.1 N calomel; osc. also observed at electrode potentials below those necessary for Cu_2O, Cu^{++}, or O_2 production	alternate formation and dissolution of CuCl porous layer; CuCl dissolves as $CuCl_2$	Cooper (45,46)
28.	Cu/H_3PO_4	i&v osc.; osc. in narrow range of current densities near limiting current plateau (42 mA/cm^2)	alternate formation and breakdown by electrical discharge of Cu/CuO/viscous layer condenser	Pointu (47)
29.	Cu/H_3PO_4	i&v osc.; osc. associated with narrow potential region at low potential end of current plateau for electropolishing: 0.65-0.85 V vs. SCE; per. 0.4-11 s; ampl. 0.2-0.3 V	"unstable intermediate products or adsorbed film"	Dmitriev (66)

Table B-I. Observations of Periodic Electrode Phenomena Involving Current Restricting Surface Layers

No.	Electrode/electrolyte	Observations	Interpretation	Reference
30.	Cu/0.2 M K_2SO_4	v osc.; galvanostatic, 20 A/cm^2; ampl.=15-20 V; per.=0.03-0.05 s	Alternate growth and shedding of surface layers; possibly involving thermal effects.	Landolt (89)
31.	Fe/2-8N H_2SO_4	v&i osc.; low external resistance; per.=5(10^{-4}) to 0.02 s; per. decreases with increasing current	Alternate growth and dissolution of passivating film, associated with shifts in pH.	Bartlett (75,58)
32.	Fe/$KHSO_4$	v&i osc.; no osc. in K_2SO_4 or $FeSO_4$		Bartlett (75)
33.	Fe/1N H_2SO_4	i osc.; potentiostatic E_H=0.49 V; ampl.=0.4 A/cm^2; per.=20 s	Shifts in Flade potential induced by alternate depletion and replenishment of H^+.	Franck (39-41)
34.	Fe/1F H_2SO_4	i/v osc.; damped osc.; per.=10^{-2}-10^{-4} s	alternate deposition/ dissolution of passive layer; "unstable film state."	Torigoe (64)
35.	Fe/H_2SO, 0.002-0.02 M KCl	v osc.; galvanostatic, 0.3-0.8 A/cm^2; ampl.=0.8 V; irreg. osc.	action of local currents following attack on film by Cl^- ions.	Rius (71)
36.	Fe/4N NaCl	v osc.; galvanostatic, 2-4 A/cm^2; ampl.=2V; per.= 0.02 s; per. decreases with increasing current; sawtooth osc. waveform	unstable, porous, non-protective film	Postlethwaite (59)

Table B-I. Observations of Periodic Electrode Phenomena Involving Current Restricting Surface Layers

No.	Electrode/electrolyte	Observations	Interpretation	Reference
37.	Fe/14N HNO_3	v osc.; cathodic polarization; galvanostatic, 0.04 A/cm^2 ampl.=0.6 V; per.=45 s	chemical passivation by HNO_3; reduction by cathodic polarization; kinetic model	Bonhoeffer (18-20)
38.	Stainless Steel (18 Cr-12Ni; 18Cr-9Ni)/0.1N NaCl	v osc.; galvanostatic; i=2 A/cm^2; per.=0.01 s	osc. associated with agresive anion (Cl^-) attack and pitting	Rosenfeld (23,24)
39.	Fe/3.16 N H_2SO_4 0.05 N HCl	osc. in rest potential	Shifts in Flade potential due to alternate depletion	Franck (26)
40.	Fe/CrO_3, HCl	osc. in rest potential		Gougerot (87)
41.	Fe/HCl in Dimethyl-	i&v osc.; osc. at overvoltage of 1.5 V; ampl.=0.5 V; per.=5 s	---	Posadas (72)
42.	Hg/KCN	i&v osc.; alternate formation and breakup of black film; meniscus alternately flattens	---	Hedges (78)
43.	Hg/HNO_3			
44.	Hg/NaSH			
45.	Mg/HCl, $FeSO_4$	i&v osc.; low amplitude	---	Hedges (76)
46.	Mg/H_2SO_4			
47.	Pb/HNO_3	i&v osc.		Hedges (78)
48.	Pb/$LiAlCl_4$ in propylene carbonate	v osc.; galvanostatic, 2.5-7.5 mA/cm^2; ampl.=0.3 V; per.=3-5 s; irregular waveform; unsustained	alternate formation and breakup/dissolution of $PbCl_2$ layer	Bhaskara (73)

Table B-I. Observations of Periodic Electrode Phenomena Involving Current Restricting Surface Layers

No.	Electrode/electrolyte	Observations	Interpretation	Reference
49.	Pd/HCOOK,1M KOH	v osc./galvanostatic, 10^{-5}-10^{-3} A/cm^2; ampl.=1-5 V	reactant depletion; oxide formation; reactant replenishment and oxide reduction	Wojtowicz (20)
50.	Pt/1M $HClO_4$, C_2H_4		"	"
51.	Pt/0.8-2M NaOH, NaS	v&i osc. in three potential regions; ampl.=1V; per.=1-5 s	alternate formation and reduction of Pt-oxide layer during oxidation of S^{-2} to $S_2O_3^{-2}$ or SO_4^{-2}	Gerischer (60)
52.	Pt/1N H_2SO_4, CH_3OH	v osc.; i=320 mA/cm^2; ampl.=0.25 V	alternate formation and reduction of PtO by either methanol, formic acid or formaldehyde; diffusion controlled	Pavela (74)
53.	Pt/1M CH_2O, H_2SO_4	v osc.; galvanostatic 3-100 mA/cm^2; ampl.=0.6 V; per.=20-2.5 s; per. increases with c.d.	coupling of diffusion/ adsorption processes; Pt-oxidic layer formed	Hunger (69)
54.	Pt/H_2SO_4, H_2	v osc.; ampl.=0.4-0.8 V; per.=1000-0.3 s; i=10^{-3} to 1.5 MA/cm^2 per. decreases with increasing c.d.	depletion of H_2 in liquid phase boundary layer; potential rises to oxidize H_2 in metal; replenishment by diffusion of H_2 in liquid phase	Armstrong (83)

Table B-I. Observations of Periodic Electrode Phenomena Involving Current Restricting Surface Layers

No.	Electrode/electrolyte	Observations	Interpretation	Reference
55.	Pr/H_2, 1F H_2SO_4	i/v osc.; i=10-50 micro-A/cm^2; ampl.=0.6-1 V; per.=120-2400 s	alternate formation and reduction (by H_2) of PtO_n film; film formation upon depletion of H_2 from electrolyte	Sawyer (68)
56.	Pt/H_2, 1F HCl			
57.	Pt/HCHO, 9M H_2SO_4 to 10M KOH	v osc.; galvanostatic, 10-40 mA/cm^2; ampl.=0.2-0.4 V; per.=5 s	Formation and Reduction of Pt-oxides by H_2 in metal phase	Buck (29)
58.	Sn/H_2SO_4	i&v osc.	---	Hedges (78)
59.	Sn/HNO_3	i&v osc.	---	"
60.	Sn/0.1-2N NaOH	v osc.; galvanostatic i=1.5-3 mA/cm^2 ampl.=0.1 V per.=seconds	formation of $Sn(OH)_2$; oxidation to $Sn(OH)_4$; dissolution of higher oxide to form stannate;	Shams El Din(42)
61.	Ti/HCOOH	v osc.; galvanostatic, 1-5m Al cm^2; at 45 V overpotential; pitting	pitting; changing ohmic drop in pits due to O_2, CO_2 formatioh	Piggott (85)
62.	Zn/4-16%NaOH	i/v osc.; i=5-130 mA/cm^2 active; ampl.=3V; per.=1 min.	---	Hedges (78)

Table B-I. Observations of Periodic Electrode Phenomena Involving Current Restricting Surface Layers

No.	Electrode/electrolyte	Observations	Interpretation	Reference
63.	Zn-Hg/30-40%H_2SO_4	i/v osc.; i=50 mA/cm^2 active ampl.=1.6 V; per.=30 s	---	Hedges (78)
64.	Zn/4N NaOH	i osc.; potentiostatic E_H=-1.1 V; ampl.=0.3 A/cm^2; per.=3 s	active/passive transitions	Franck (40)
65.	Zn/0.1F $NaAlO_2$ or 0.1F Na_2WO_4	v osc.; galvanostatic, 0.16 A/cm^2; ampl.=50-200 V; per.=100 s	spalling of oxidic layer; breakdown due to electrical discharge through film	Gruss (61)
66.	Zr/0.1 N NaF,0.002M HF, air sat. or 0.004M H_2O_2	osc. in rest potential ampl.=0.9 V per.=4-7 min.	Bonhoeffer kinetic model	Rettig (82)
67.	Zr/0.1N NaF, 0.002M HF	v osc.; galvanostatic, 3.8-1900 µA/cm^2 ampl.=0.9 V per.=60-240 s	"	"

APPENDIX C.

Ionic Transport and Space Charge in Crystalline Solids

1. Fundamental Equations of Ionic Transport

In crystalline solids, ionic conduction occurs through the movement of charged point defects: anion or cation vacancies and interstitial anions or cations. With a simple kinetic model, a transport equation may be derived which expresses the flux of a defect species as a function of field strength and certain physical constants. A simplified derivation will be given below. Detailed derivations and fuller discussion of transport theory in solids are found in Young (Chapter II)[49] and Dignam.[128]

For a solid free of any externally applied field, charged defects are pictured to diffuse through a field of identical potential energy barriers of height W and width 2a. (Solid curve, Fig. C.1). A defect will surmount a barrier if sufficient thermal energy is acquired. From Boltzmann statistics, the probability of a defect possessing at any instant a kinetic energy $\geq W$ is proportional to $\exp(-W/kT)$. When an electrostatic field is applied to the sample in direction x, the energy of the defect will be the sum of thermal energy and energy acquired by movement in the field. This situation gives rise to a skewing of the periodic potential profile such that the effective barrier height for a defect at x will be (W+qaE) for diffusion with or against the direction of the applied field.

From elementary rate theory, the flux in the direction of the field (increasing x) is given by[49]

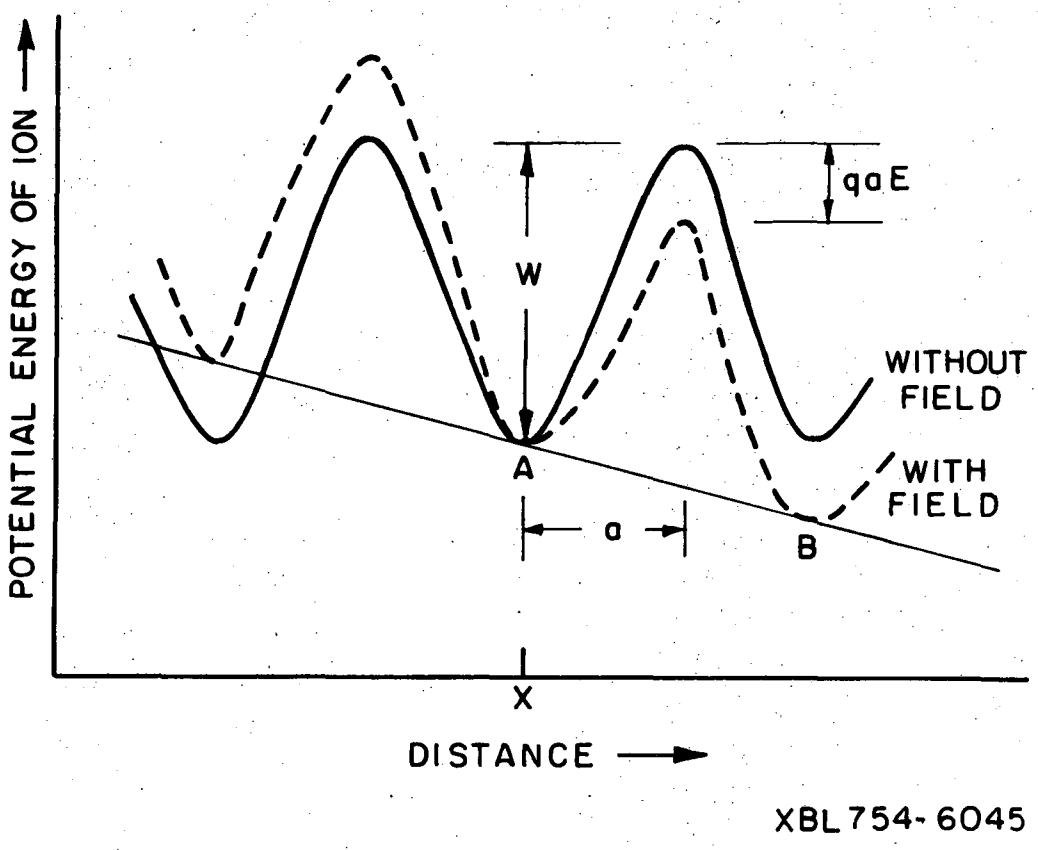

Fig. C.1. Potential energy profile for a crystal lattice with (broken line) and without (solid line) the application of an external field. The directions of current flow and field are to the right. A and B are the positions of a positively charged defect before and after a field assisted jump.

$$\vec{j} = 2ac\nu\exp(-(W-qaE)/kT) \qquad (C.1)$$

The flux against the field is given by,

$$\overleftarrow{j} = 2a(c + 2a(dc/dx))\nu\exp(-(W+qaE)/kT) \qquad (C.2)$$

Here ν is a characteristic vibrational frequency of the defect at a site in the lattice; c is the defect concentration; and q is the charge number. The net flux in the direction of the field is

$$j = \vec{j} - \overleftarrow{j} \qquad (C.3)$$

$$j = 4ac\nu\exp(-W/kT)\sinh(qaE/kT) - 4a^2\nu(dc/dx)\exp(-(W+qaE))/kT)$$

Low Field Approximation. If the field strength is sufficiently low ($qaE \ll kT$; $qaE \ll W$), Eq. (C.3) may be approximated by,

$$j = \left\{\frac{4a^2\nu qc}{kT}\exp(-W/kT)\right\} E - \left\{4a^2\nu\exp(-W/kT)\right\} dc/dx \qquad (C.4)$$

The first quantity in brackets is the ionic conductivity; the second quantity in brackets is a diffusion coefficient.

High Field Approximation. As shown by Dignam[128] (p.142), the diffusion term may be neglected for space charge densities less than about $5\times(10^9)$ e/cm^3 provided $qaE/kT \geq 1$. Under these conditions, Eq. (C.3) takes the simple form,

$$j = 2ac\nu\exp(-W/kT)\exp(qaE/kT) \qquad (C.5)$$

To convert the above expression into units of A/cm^2, we multiply by the factor, qF/N_a, where F is the Faraday constant (96,500 coulombs/equivalent) and N_a is Avogadro's number, $6.023\times(10^{23})$ particles/mole:

$$\begin{aligned} I &= cqA \exp(qBE) \quad (A/cm^2) \\ A &\equiv (2a\nu F/N_a) \exp(-W/kT) \\ B &\equiv a/kT \end{aligned} \tag{C.6}$$

Despite the simplicity of the model, the exponential dependence of current on field strength is well extablished by experiment with anodic oxide films formed on a variety of metals.[49,121,128]

2. Space Charge, Field Strength, and Potential Profiles

The dependence of field strength on space charge concentration is given by Poisson's equation:

$$\nabla E = (F/Ke_oN_a) \sum_i q_i c_i \tag{C.7}$$

Equations (C.7) and (C.6) may be combined to yield the profiles of space charge, field strength, and electrostatic potential within the film.

In this derivation, we make the following assumptions:

(1) Space charge is due exclusively to the negative cation vacancies, V'_{Cu}. The vacancies are the sole current carriers and are injected into the electrolyte/film interface.

(2) Diffusion if considered unimportant relative to migration.

(3) Current is independent of position within the film, i.e., $\partial j/\partial x=0$. This condition will apply whenever the current consumed in the production of space charge is a small fraction of the total current.

(4) The film is of plane parallel geometry. Concentration and field strength vary only in a direction perpendicular to the interfacial planes.

For simplicity, we choose the origin of the position coordinate, x, to coincide with the film/electrolyte interface. The quantity x increases in the direction toward the metal/film interface. The appropriate form of Eq. (C.7) is

$$\partial E/\partial x = qDc \qquad (C.8)$$

$$D \equiv (F/Ke_o N_a)$$

Differentiation of (C.6) yields:

$$\partial E/\partial x = -(1/Bcq)\ \partial c/\partial x \qquad (C.9)$$

Substituting into Eq. (C.8), and integrating gives the concentration profile:

$$c(x) = c(0)/(1 + q^2 BDc(0)x) \qquad (C.10)$$

Substituting c(x) into Eq. (C.8) and integrating, we have the field strength profile,

$$E(x) = E(0) + (1/qB)\ \ln(1 + q^2 BDc(0)x) \qquad (C.11)$$

Electrostatic potential is related to field strength by the equation

$$V(x) = -\int^{x} E\, dx \qquad (C.12)$$

Substituting (C.11) into (C.12) and integrating between limits (0) and (x):

$$V(x)-V(0) = -E(0)x - \frac{(1+q^2BDc(0)x)}{q^3B^2Dc(0)} \ln \left\{ \frac{(1 + (q^2BDc(0)x))}{e} \right\} \qquad (C.13)$$

where e is the base of the Naperian logarithms.

The charge number on the mobile defect is (-1). In this coordinate system, field strength and current are negative quantities for anodic polarization. The absolute magnitude of field strength is seen to increase from the film/electrolyte interface to the metal/film interface, while the concentration of defects falls off monotonically in the same direction. Potential drop within the film is not directly proportional to thickness, but swings upward with increasing thickness.

In this derivation, a boundary condition c(S) at the film/metal interface (x=S) does not appear. Dignam (p.129)[128] showed that the defect concentration at the interface toward which the defects move has no effect on the transport rate (or field distribution), provided that:

$$\Delta\bar{\mu}_i = kT \ln(c(0)/c(S)) + q(V(o)-V(S)) > 4kT$$

and

$$q(V(0) - V(S)) > 4kT$$

In our system $c(0) > c(S)$; at 25°C, 4kT = 0.1 eV. For a potential drop through the film of 0.1 V or greater, Dignam's conditions are met. His derivation was derived for the case of homogeneous field distribution, where transport is controlled only by the concentration of defects at the interface away from which the defects move. The same reasoning should apply when the field is no longer homogeneous, because of space charge accumulation. At the metal/film interface, $c(x)$ will adjust abruptly to the value $c(S)$.

The boundary condition $c(0)$ is related to $E(0)$ by the equation,

$$I = qAc(0) \exp(qBE(0)).$$

At constant current, $c(0)$ will therefore not change with film thickness. The dependence of $c(0)$ on current density and on solution composition is complex and will involve the kinetics of vacancy formation and dissociation. The surface concentration of defects therefore cannot be predicted on the basis of kinetics of transport of defects through the film.

The total potential drop through the film must be added to the potential drops across the two interfaces to obtain the anode potential during film growth. As the metal is completely film-covered for an anode potential increase of only 0.5 V above active dissolution potential, the large subsequent increase of potential may be attributed to the resistance of the growing cuprous oxide film.

APPENDIX D.

Redox Potential of the Cu_2O/ClO_3^- System

We will calculate the redox potential for the net reaction,

$$4H^+ + Cu_2O + \frac{1}{3}\,ClO_3^- = 2Cu^{++} + 2H_2O + \frac{1}{3}\,Cl^- \quad . \qquad (D.1)$$

The associated half reactions are:

$$2H^+ + Cu_2O = 2Cu^{++} + H_2O + 2\,e^-, \quad V_1^o = 0.203\ V \qquad (D.2)$$

and

$$\frac{1}{3}\,Cl^- + 3H_2O = \frac{1}{3}\,ClO_3^- + 2H^+ + 2\,e^-, \quad V_2^o = 1.451\ V \qquad (D.3)$$

where V_1^o and V_2^o are the standard Gibbs electrode potentials. The redox potential may be written;

$$E^o = (V_2^o - V_1^o) - \frac{RT}{nF}\ln\frac{(Cu^{++})^2\,(Cl^-)^{1/3}}{(H^+)^4\,(ClO_3^-)^{1/3}} \qquad (D.4)$$

where quantities in parentheses refer to activities. At 25°C, and using data from Pourbaix (Chapters 14 and 20),[104] we have (after simplification):

$$E^o = 1.248 - 0.1182pH - 0.0591\log_{10}\frac{(Cu^{++})^2\,(Cl^-)^{1/6}}{(ClO_3^-)^{1/6}}\ (\text{volts}) \qquad (D.5)$$

The Gibbs free energy change, ΔF, for reaction (D.1) is related to the redox potential, E^o, by the equation,

$$\Delta F = -nFE^o = -2FE^o \qquad (D.6)$$

At unit activities of Cu^{++}, Cl^{-}, and ClO_3^{-}, the redox potential will be positive below a pH of 10.6. Under the same conditions, the free energy change will be negative, and oxidation of Cu_2O by ClO_3^{-} is thermodynamically feasible.

REFERENCES

1. D. Landolt, R.H. Muller, C.W. Tobias, High Rate Anodic Dissolution of Copper, J. Electrochem. Soc. 116, 1384 (1969).
2. D. Landolt, R. Acosta, R.H. Muller, C.W. Tobias, An Optical Study of the Cathodic Hydrogen Evolution in High-Rate Electrolysis, J. Electrochem. Soc. 117, 839 (1970).
3. D. Landolt, R.H. Muller, C.W. Tobias, Anode Potentials in High-Rate Dissolution of Copper, J. Electrochem. Soc. 118, 40 (1971).
4. Electrochemical Machining, ed. by A.E. de Barr and D.A. Oliver, (American Elsevier, 1968).
5. Kimio Kinoshita, Studies on the Anodic Dissolution of Copper at High Current Densities (Ph.D. Thesis), University of California, Berkeley, September, 1969. (Lawrence Berkeley Laboratory Report No. UCRL-19051).
6. M.A. LaBoda and M.L. McMillan, A New Electrolyte for Electrochemical Machining, Electrochem. Technol. 5, 340 (1967).
7. J. Cooper, R.H. Muller, C.W. Tobias, Periodic Phenomena in Copper Dissolution at Constant Current, (Paper presented at the 138th National Meeting of the Electrochemical Society, Atlantic City, New Jersey, Oct. 1970).
8. A.T. Winfree, Spiral Waves of Chemical Activity, Science 175, 634 (1972).
9. A.T. Winfree, Rotating Chemical Reactions, Scientific American, June (1974).

10. A. Zaikin, A. Zhabotinsky, Concentration Wave Propagation in Two-Dimensional Liquid Phase Self-Oscillating Systems, Nature, 225, 535 (1970).

11. B. Chance, A. Ghosh, J. Higgins, P. Maitra, Cyclic and Oscillatory Responses of Metabolic Pathways involving Chemical Feedback and Their Computer Representations, Ann. N.Y. Acad. Sci. 115, 1010 (1964).

12. A. Zhabotinsky and A. Zaikin, Oscillatory Processes in Biological and Chemical Systems, (Puschino, 1971).

13. R.A. Spengler and F.M. Snell, Sustained Oscillations in a Catalytic Chemical System, Nature 191, no. 1, 457 (1961).

14. A.J. Lotka, Undamped Oscillations Derived from the Law of Mass Action, J. Am. Chem. Soc. 42, 1595 (1920).

15. V. Voltera, Théorie Mathématique de la Lutte pour la Vie, (Gautiers-Villars, Paris, 1931).

16. S. Szpak, Periodic Electrode Reactions Induced by Mass Transport, Electrochim. Acta, 13, 483 (1968).

17. Fechner, Schweigg. J. 53, 141 (1828). (Ref. given by Hedges (76))

18. K. Bonhoeffer, G. Langhammer, Die kathodische Polarisation von Eisen in Salpetersaure, Z. Elektrochem. 51, 29 (1948).

19. K. Bonhoeffer, V. Haase, and G. Langhammer, Der Refraktarzustand frischpassiven Eisens in konzentrierter Salpetersaure, Z. Elektrochem. 51, 60 (1948).

20. K. Bonhoeffer and G. Langhammer, Theorie der kathodischen Polarisation von Eisen in Salpetersaure, Z. Elektrochem. 52, 67 (1948).

21. R. Tamamushi, An Electrochemical Oscillator--An Electrochemical System which Generates Undamped Electric Oscillations, J. Electroanal. Chem. II, 65 (1965).

22. R. De Levie, On the Electrochemical Oscillator, J. Electroanal. Chem. 25, 257 (1970).

23. J. Rosenfeld and I. Danilov, Electrochemical Aspects of Pitting Corrosion, Corrosion Sci. 7, 129 (1967).

24. J. Rosenfeld and V. Maksimtchuk, Uber den passiven Zustand nichtrostenden Legierungen in Gegenwart von Chlorionen, Z. phys. Chem. (Liepzig) 215, 25 (1960).

25. Z. Szklarska-Smialowska and M. Janic-Czachor, Electrochemical Investigation of the Nucleation and Propagation of Pits in Iron-Chromium Alloys, Brit. Corros. J. 4, 138 (1969).

26. U. Franck and L. Meunier, Gekoppelte periodische Elektrodenvorgange, A. Naturforsh. 8b, 396 (1953).

27. J. Wojtowicz, N. Marincic, B. Conway, Oscillatory Kinetics in the Electrochemical Oxidation of Formate and Ethylene, J. Chem. Phys. 48, 4333 (1968).

28. H.F. Hunder, The Mechanism of Oscillatory Behavior During the Anodic Oxidation of Formaldehyde, J. Electrochem. Soc. 115, 492 (1968).

29. R.P. Buck, L.R. Griffith, Voltametric and Chronopotentiometric Study of the Anodic Oxidation of Methanol, Formaldehyde, and Formic Acid, J. Electrochem. Soc. 109, 1005 (1962).

30. H. Degn, Theory of Electrochemical Oscillations, Trans. Faraday Soc. 64, 1348 (1968).

31. A. Katchalsky, R. Spangler, Dynamics of Membrane Processes, Quarterly Review of Biophys. 1, 127 (1968).

32. V.E. Shashoua, Electrically Active Polyelectrolyte Membranes, Nature 215, 846 (1967).

33. H. Drouin, Experimente mit dem Teorellschen Membranoszillator, Ber. Bunsenges. 73, 223 (1969).

35. E.S. Hedges and J.E. Meyers, Problems of Physicochemical Periodicity (Arnold, London, 1926).

36. K. Vetter, Electrochemical Kinetics (Academic Press, New York, 1967).

37. K. Indira, S. Rangarajan, and K. Doss, Further Studies on Periodic Phenomena in Passivating Systems, J. Electroanal. Chem. and Interfac. Electrochem. 21, 49 (1969).

38. J. Wojtowicz, Oscillatory Behavior in Electrochemical Systems (Modern Aspects of Electrochemistry, ed. J. Bockris and B. Conway, Plenum Press, New York; Vol. 8, Chapter 1, 1972).

39. U.F. Franck, Zur Stabilitat von Elektrondenzustanden, Z. Phys. Chem. N.F., 3, 183, (1955).

40. U.F. Franck, Instabilitatserscheinungen an passivierbaren Metallen, Z. Elektrochem. 62, 649 (1958).

41. U.F. Franck and R. Fitzhugh, Periodische Elektrodenprozesse und ihre Beschreibung durch ein mathematisches Modell, Z. Elektrochem. 65, 156 (1961).

42. A Shams el Din and F. Abd el Wahab, On the Anodic Passivity of Tin in Alkaline Solutions, Electrochim. Acta 9, 883 (1964).

43. M.T. Francis and W. H. Colmer, Cyclic Phenomena Observed in Electropolishing of Silver, J. Electrochem. Soc. 97, 237 (1950).

44. L.I. Gilbertson and O.M. Fortner, Electrolytic Polishing of Silver, J. Electrochem. Soc. 81, 199 (1942).

45. L. Stephenson and J.H. Bartlett, Anodic Behavior of Copper in Hydrochloric Acid, J. Electrochem. Soc. 101, 571 (1954).

46. R. Cooper and J. Bartlett, Convection and Film Stability--Copper Anodes in Hydrochloric Acid, J. Electrochem. Soc. 105, 109 (1958).

47. B. Pointu, Oscillations de potentiel au cours du polissage electrolytique d'une anode de cuivre dans l'acide orthophosphorique, Electrochim. Acta 14, 1207 (1969).

48. H. Lal, H.R. Thirsk, and W.F.K. Wynne-Jones, A Study of the Behavior of Polarized Electrodes: The Silver/Silver Halide System, Trans. Faraday Soc. 47, 70, 999 (1951).

49. L. Young, Anodic Oxide Films (Academic Press, London, 1961).

50. K.S. Indira and K.S.G. Doss, A New Approach to Explain the Anodic Passivation and Periodic Phenomena: the PN Junction and SR Mechanisms, Proc. Indian Acad. Sci. A, 66, 69 (1967).

51. A.T. Fromhold, Jr., and J. Kruger, Space-Charge and Concentration-Gradient Effects on Anodic Oxide Film Formation, J. Electrochem. Soc. 120, 722 (1973).

52. J. Higgins, The Theory of Oscillating Reactions, Ind. and Eng. Chem., 59, 18 (1967).

53. D.A. Frank-Kamenetskii, Diffusion and Heat Exchange in Chemical Kinetics (Princeton University Press, Princeton, New Jersey; Chapters 10,11; 1955).

54. K.F. Bonhoeffer, Uber periodische chemische Reaktionen, Z. Elektrochem. 51, 24 (1948).

55. K.F. Bonhoeffer and H. Gerischer, Das anodische Verhalten von Kupfer in Salzsaure, Z. Elektrochem. 52, 149 (1948).

56. W. Boyce and R. DiPrima, Elementary Differential Equations and Boundary Value Problems (John Wiley and Sons, Inc., New York, 1965) p. 29.

57. Wallace Stevens, "Connoisseur of Chaos," (Modern Poetry, ed. by M. Mack, L. Dean, W. Frost; Prentice-Hall, Englewood Cliffs, 1964; p. 293.)

58. J.H. Bartlett and J. Stephenson, Anodic Behavior of Iron in Sulfuric Acid, J. Electrochem. Soc. 99, 504 (1952).

59. J. Postlethwaite and A. Kell, Periodic Phenomena During the Anodic Dissolution of Iron in Sodium Chloride Solutions, J. Electrochem. Soc. 119, 1351 (1972).

60. H. Gerischer, Reaktionen und periodische Vorgange an einer Platinanode in Alkalisulfidlosungen, z. Elektrochem. 54, 540 (1950).

61. L.L. Gruss and W. McNeill, Anodic Spark Reaction Products in Aluminate, Tungstate, and Silicate Solutions, Electrochem. Tech. 1, 283 (1963).

62. J. Osterwald and H.-O. Feller, Zum Stabilitatsverhalten stationarer Elektrodenzustande, Electrochim. Acta 7, 523 (1962).

63. J. Osterwald and U.-O. Feller, Periodic Phenomena at a Nickel Electrode in Sulfuric Acid, J. Electrochem. Soc. 107, 473 (1960).

64. Y. Torigoe, Periodic Oscillations of External Current in Polarization of Iron in Sulfuric Acid Solutions, Denki Kagaku, 35, 206 (1967).

65. T.P. Hoar and J.A.S. Mowat, Mechanism of Electropolishing, Nature 165, 64 (1950).

66. A. Dmitriev and E.V. Rzhevskaya, Periodic Effects in the Anodic Dissolution of Copper in Phosphoric Acid, Russ. J. Phys. Chem. 35, 871 (1961).

67. F. Forster and F. Kruger, Uber das Verhalten von Nidkelanoden, z. Elektrochem. 33, 406 (1927).

68. D.T. Sawyer and E.T. Seo, Electrochemistry of Dissolved Gases--Oxidation of Hydrogen at Platinum Electrodes, J. Electroanal. Chem. 5, 23 (1963).

69. H.F. Hunger, The Mechanism of Oscillatory Behavior During the Anodic Oxidation of Formaldehyde, J. Electrochem. Soc. 115, 429 (1968).

70. M.J. Pryor, Electrode Reactions on Oxide Covered Aluminum, Z. Electrochem. 62, 782 (1958).

71. A. Rius and R. Lizarbe, Study of the Anode Behavior of Iron at High Potentials in Solutions Containing Chloride Ions, Electrochim. Acta 7, 513 (1962).

72. D. Posadas, A.J. Arvia, and J.J. Podesta, The Passivation of Iron in Solutions of Hydrogen Chloride in Dimethylsulphoxide, Electrochim. Acta 16, 1041 (1971).

73. M.L. Bhaskara Rao, Electrochemical Studies on Lead in Organic Electrolytes, J. Electrochem. Soc. 114, 665 (1967).

74. T.O. Pavela, Periodic Process in the Electrolytic Oxidation of Methanol at the Platinum Anode, Suomen Kemistilehti, 30, 138 (1957).

75. J.H. Bartlett, Transient Anode Phenomena, Trans. Electrochem. Soc. 87, 521 (1945).

76. E.S. Hedges and J.E. Meyers, Periodic Electrochemical Phenomena, J. Chem. Soc. (L), 1013 (1925).

77. E.S. Hedges, Periodic Phenomena at Anodes of Copper and Silver, J. Chem. Soc. (L), 1533 (1926).

78. E.S. Hedges, Periodic Phenomena at Anodes of Magnesium, Zinc, Cadmium, Mercury, Tin, and Lead, and at an Unattackable Anode, J. Chem. Soc. (L), 2580 (1926).

79. E.S. Hedges, The Periodic Electrochemical Passivity of Iron Cobalt, Nickel, and Aluminum, J. Chem. Soc. (L), 2878 (1926).

80. E.S. Hedges, The Periodic Electro-deposition of Metals through Secondary Reaction, J. Chem. Soc. (L), 1077 (1927).

81. E.S. Hedges, An Enquiry into the Cause of Periodic Phenomena in Electrolysis, J. Chem. Soc. (L), 1028 (1929).

82. D. Rettig, C. Voight, and K. Schwabe, Untersuchungen über periodische Potentialschwankungen des Zircons in NaF-Losungen, Corrosion Sci. 10, 657 (1970).

83. G. Armstrong and J.A.V. Butler, Electrochemical Periodicity in the Anodic Polarization of Platinum Electrodes in the Presence of Hydrogen and Their Significance, Disc. Faraday Soc. 1, 122 (1947).

84. V.N. Flerov, The Causes of the Maxima and Minima in Electrode Potentials, Russ. J. Phys. Chem. 37, 664 (1963).

85. A.R. Piggott, H. Leckie, and L.L. Shreir, Anodic Polarization of of Ti in Formic Acid--Anodic Behavior of Ti in Relation to Anodizing Conditions, Corrosion Sci. 5, 165 (1965).

86. L. Gougerot and R. Alfieri, Des Variations d'impedance du fer en milieu sulfochromique au cours d'oscillations electrochimiques, J. Chim. Phys. 54, 514 (1957).

87. L. Gougerot and R. Alfieri, Des variation de l'impedance d'une cathode oscillante de cobalt en milieu chlorochromique, J. Chim. Phys. 61, 843 (1964).

88. D. Landolt, R.H. Muller, and C.W. Tobias, Transfer Processes in ECM, (Paper presented at the 138th National Meeting of the Electrochemical Society, Atlantic City, New Jersey, Oct. 1970; Lawrence Berkeley Laboratory Report No. UCRL-19615.)

89. K. Kinoshita, D. Landolt, R.H. Muller, C.W. Tobias, Stoichiometry of Anodic Copper Dissolution at High Current Densities, J. Electrochem. Soc. 117, 1246 (1970).

90. D. Landolt, R.H. Muller, and C.W. Tobias, High Rate Anodic Dissolution of Copper, J. Electrochem. Soc. 116, 1384 (1969).

91. J.S. Newman, Electrochemical Systems (Prentice-Hall, Englewood Cliffs, N.J., 1973).

92. J.S. Newman, Transport Processes in Electrolytic Solutions, (in Advances in Electrochemistry and Electrochemical Engineering, Interscience, New York, 1967; ed. by C.W. Tobias and P. Delahay; Vol. 5).

93. J.R. Selman, Measurement and Interpretation of Limiting Currents, (Ph.D. Thesis, University of California, Berkeley, California, 1971).

94. Der-Tau Chin, Convective Diffusion on a Rotating Spherical Electrode, J. Electrochem. Soc. 118, 1434 (1971).

95. E.C. Potter, Electrochemistry (Cleaver-Hume Press Ltd., London, 1961).

96. P. Von Shaw, L.P. Reiss, T.J. Hanratty, A.I.Ch. Eng. 9, 362 (1963).

97. A.J. Arvia and S.L. Marchiano, Transport Phenomena in Electrochemical Kinetics, (Modern Aspects of Electrochemistry, Plenum Press, New York, 1971; ed. by Bockris and Conway; Chapter 3.)

98. D. Landolt, R.H. Muller, and C.W. Tobias, Anode Potentials in High-Rate Dissolution of Copper, J. Electrochem. Soc. 118, 40 (1971).

99. R.B. Bird, W.E. Stewart, E.N. Lightfoot, Transport Phenomena, (John Wiley & Sons, New York, 1960; p. 47).

100. Per Kofstad, Nonstoichiometry, Diffusion, and Electrical Conductivity in Binary Metal Oxides (Wiley-Interscience, New York, 1972, Ch. 14).

101. Z.M. Jarzebski, Oxide Semiconductors (Pergamon Press, Oxford, 1973, Ch. 13).

102. R.M. King, Deviations from Stoichiometry in Cu_2O, J. Amer. Ceram. Soc. 54, 361 (1971).

103. W.J. Moore and B. Selikson, The Diffusion of Copper in Cuprous Oxide, J. Chem. Phys. 19, 1539 (1951); 20, 927 (1952).

104. M. Pourbaix, Atlas of Electrochemical Equilibria in Aqueous Solutions (Pergamon Press, Oxford, 1966).

105. R. Bartonicek and M. Lukasovska, Completed Potential -pH diagrams for the system Cu-NH_3-Cl^-, Corros. Sci. 11, 111 (1971).

106. B. Miller and T.D. Schlaback, Chlorate etchant systems for copper, Ind. Eng. Chem. 1, 258 (1965).

107. C. Wagner and H. Hammen, Bestimmung des Sauerstoff-Uberschussgehaltes der Kupferoxydulphase, Z. Phys. Chem. B40, 197 (1938).

108. V.P. Severdenko, V.A. Labunov, and E.M. Kosarevich, Switching Effects in Copper Oxide Films, Dokl. Akad. Nauk Beloruss, SSR, 16(1), 21 (1972); 16(6), 497-8 (1972).

109. Kosarevich and Parkun, Switching Effects in Films of Electrolytic Copper Oxides, Vop. Proch. Plast. Metal., Mater. Nauch. Kanf. Molodykh Uch. Akad. Nauk Beloruss. SSR 6th 176-7 (1970); Reference in Chem. Abs. 78:90108d.

110. H. Wieder and A.W. Czanderna, The Oxidation of Copper Films to $CuO_{0.67}$, J. Phys. Chem. 66, 816 (1962).

111. W.P. Juse and B.W. Kurtschatow, Zur Elektrischen Leitfahigkeit von Kupferoxydul, Phys. Z. Sowjetunion 2, 453 (1932).

112. M. O'Keeffe and F.S. Stone, The Magnetochemistry and Stoichiometry of the Copper-oxygen System, Proc. Roy. Soc. A267, 501 (1962).

113. M. O'Keeffe and W.J. Stone, Electrical Conductivity of Monocrystalline Cuprous Oxide, J. Chem. Phys. 35, 1324 (1961).

114. M. O'Keeffe and W.J. Moore, Thermodynamics of the Formation and Migration of Defects in Cuprous Oxide, J. Chem. Phys. 36, 3009 (1962).

115. O. Kubaschewski and B.E. Hopkins, Oxidation of Metals and Alloys, (Butterworths, London (1962)).

116. F.A. Kroger, The Chemistry of Imperfect Crystals, (North-Holland, Amsterdam, 1964).

117. B. Dunwald and C. Wagner, Die Natur der elektrischen Leitfahigkeit von Kupferoxydul, Z. Physik. Chem. B17, 467 (1933).

118. K. Stecker, Conductivity Measurements on Cu_2O in the Region of Stability, Ann. der Physik 3, 70 (1959).

119. R.S. Toth, R. Kilkson, D. Trivich, Electrical Conductivity of Single Crystal Cuprous Oxide at High Temperatures, Phys. Rev. 122, 482 (1961).

120. T.P. Hoar, The Anodic Behavior of Metals (in Modern Aspects of Electrochemistry, Plenum Press, New York, ed. by J. Bockris; Chapter 4, Vol. 2, 1959).

121. D.A. Vermilyea, "Anodic Films," (Chapter 4 in Advances in Electrochemistry and Electrochemical Engineering, 3, p. 211 (1963), ed. by C.W. Tobias).

122. K.E. Johnson, S.J. Sime, J. Dudley, "The Thermal Power of the Solid Electrolytes Ag_4MI_5 and Molten Mixtures of the Same Components," J. Electrochem. Soc. 120, 704 (1973).

123. J. Gundermann and C. Wagner, Uberfuhrungsmessungen an Kupferoxydul, Z. phys. Chem. (Leipzig)(B) 37, 155 (1937).

124. E.K. Oshe and I.L. Rozenfeld, A New Technique for Investigating Superficial Oxides on Metals in Solutions, Soviet Electrochem. 4, 1080 (1968).

125. H. Arbit and K. Nobe, Photopotential Measurements During Corrosion of Copper in Aqueous Solutions, Corrosion 24, 17 (1968); 21, 207 (1965).

126. C. Wagner, Untersuchungen uber Fehlordnungserscheinungen in Kupferoxydul und deren Einfluss auf die elektrischen Eisenschaften, Z. Phys. Chem. (Leipzig) (B) 22, 212 (1933).

127. V.K. Agarwal and V.K. Spivastava, Thickness Dependence of Breakdown in Thin Films, J. Thin Solid Films, 8, 377 (1971).

128. M.J. Dignam, Mechanisms of Ionic Transport through Oxide Films, (in The Anodic Behavior of Metals and Semiconductors Series--Oxides and Oxide Films, Vol. 1, Chapter 2; ed. by J. Diggle, Marcel Dekker, New York 1972).

129. M. Novak, A.K.N. Reddy, and H. Wroblowa, An Ellipsometric Study of Surface Films on Copper Electrodes Undergoing Electropolishing, J. Electrochem. Soc. 117, 733 (1970).

130. K.E. Johnson, S.J. Sime, J. Dudley, The Thermal Power of the Solid Electrolytes Ag_4MI_5 and of Molten Mixtures of the Same Composition, J. Electrochem. Soc. 120, 703 (1973).

131. K. Kojima, A Study of the Mechanism of the Electropolishing of Copper, (Ph.D. Thesis, University of California, Berkeley, California, 1972; pp. 168-171).

132. J. Reitz and F. Milford, Foundations of Electromagnetic Theory (Addison Wesley, Reading, Mass., 1967, p. 114).

133. I. Baker and R.S. Gibbs, Determination of Metallic Copper in Cuprous Oxide, Cupric Oxide Mixtures, Ind. and Eng. Chem. 18, 124 (1946).

134. N. Klein, Electrical Breakdown in Solids, (in Advances in Electronics and Electron Physics, Academic Press, New York; 26, 309 (1969)).

135. N. Klein, Switching and Breakdown in Films, J. Thin Solid Films, 7, 149 (1971).

136. E.L. Cook, Model for the Resistive Conductive Transition in Reversible Resistance-Switching Solids, J. Appl. Phys. 41, 551 (1970).

137. K. Wagner, The Physical Nature of the Electrical Breakdown of Solid Dielectrics, AIEE, 41, 288 (1922).

138. J.J. O'Dwyer, The Theory of Dielectric Breakdown of Solids (Oxford University Press, London, 1964).

139. D. Royer, J. Kleinberg, and A. Davidson, The Anodic Behavior of Copper in Aqueous Solutions, J. Inorg. Nucl. Chem. 4, 115 (1957).

140. Hickling and Salt, Overpotentials for Hydrogen Evolution, Transactions of the Faraday Society, 36, 1226 (1940).

ACKNOWLEDGEMENTS

I would like to express my deep appreciation and gratitude to Professor Charles Tobias for his direction and encouragement throughout my graduate studies. I would also like to thank Dr. Rolf Muller for his many helpful suggestions and critiques during the course of my research. Professor Kurt Spiegler is gratefully acknowledged for his review of this manuscript. Also I would like to thank Alice Ramirez for typing this manuscript.

This work was supported by the U. S. Energy Research and Development Administration.

NOMENCLATURE

Symbol	Definition
A	electrode area (geometric)
A	the quantity, $(2a\ F/N_a)\exp(-W/kT)$--used in kinetic model
B	the quantity, a/kT--used in kinetic model
C	capacitance
D	diffusion coefficient
D	the quantity, (F/Ke_oN_a)--used in kinetic model
D_h	hydraulic diameter (D_h=4(cross section area)/(perimeter))
E	field strength
E	mean field strength
E_d	differential field strength
$\bar{E}_p$	mean field strength at oscillaton peak
E_F	Flade potential
E_H	Gibbs electrode potential
F	Faraday constant
I	current density
K	dielectric constant
L	electrode length in the direction of flow
N	flux
N_a	Avagadro's number
Nu	Nussult number
M	atomic weight
R	radius of entrance tube in stagnation point flow system
Re	Reynolds number

S_i	quantity of reactant, i
S_p	film thickness at oscillation peak
Sc	Schmidt number
T	temperature
T	oscillation period length
T_o	oscillation period length at a reference current density, I_o.
U	potential flow rate in stagnation point hydrodynamics
V	average linear flow rate
V	electrostatic potential
V^o	Standard state reduction potential
V_f	potential drop through anode film.
X	characteristic dimension in mass transfer correlations
W	potential energy barrier for ion migration in crystalline lattice.
W	weight
W_e	equivalent weight
a	slope of double logarithmic plot of period against current density
a	activation distance; half-width of energy barrier in kinetic model.
c	concentration of ionic charge carriers
$\bar{c}$	mean concentration of ionic charge carriers
c_p	heat capacity at constant pressure
d	density
d	plate separation in parallel plate condensor

e	current efficiency for metal removal.
e_o	permittivity of free space
f_{Cu^+}	fraction of charge consumed in the production of Cu^+
i	current
j	ion flux
$\vec{j}$, $\overleftarrow{j}$	forward and reverse ion flux
k	Boltzmann constant
k_e	electrical conductivity
n	instantaneous apparent valence
n_a	average apparent valence
p	current efficiency
q	quantity of charge
q	charge number on a mobile ion
r	rotating disk electrode radius
s	electrode separation (in channel flow systems)
t	time
t	transport number
x	position variable in kinetic model
x,y,x_i	activities of reactants
z	valence
δ	Nernst diffusion layer thickness
η	viscosity
μ^o	standard state chemical potential
$\bar{\mu}$	electrochemical potential
ν	jump frequency
ν	kinematic viscosity

TECHNICAL INFORMATION DIVISION
LAWRENCE BERKELEY LABORATORY
UNIVERSITY OF CALIFORNIA
BERKELEY, CALIFORNIA 94720